Université catholique de Louvain

Louvain Drug Research Institute

Unité de Pharmacologie Cellulaire et Moléculaire

Unité de Pharmacognosie

Membrane interactions of lipopeptides and saponins, two groups of natural amphiphiles

Joseph Lorent

July 2013

Thesis submitted in view to obtain the degree of
"Doctor in Biomedical and Pharmaceutical science"

Supervisor : Professor Marie-Paule Mingeot Leclercq
Co-supervisor : Professor Joëlle Quetin-Leclercq

Committee members

President
Didier Lambert (Louvain Drug Research Institute, Université Catholique de Louvain)

Supervisor
Marie-Paule Mingeot-Leclercq (Louvain Drug Research Institute, Université catholique de Louvain)

Co-supervisor
Joëlle Quetin-Leclercq (Louvain Drug Research Institute, Université catholique de Louvain)

Other members
Marie-Aleth Lacaille-Dubois (Faculté de pharmacie, Université de Bourgogne)
Karl Lohner (Institut für Molekulare Biowissenschaften, Universität Graz)
Marie-Claire Gillet-De Pauw (Département des sciences biomédicales et précliniques, Université de Liège)
Françoise Bontemps (Institut de Duve, Université catholique de Louvain)

Acknowledgment

I wish to thank everyone who contributed to this work and especially :

my supervisor, professor Marie-Paule Mingeot-Leclercq, who accepted me as a PhD student in her laboratory, supported and guided me during these years. Without her help and suggestion, this work would never have been possible,

my co-supervisor, professor Joëlle Quetin-Leclercq, espedially for the confidence she put in me to give the "travaux pratiques" and of course for all the time she invested to make corrections and think about this work,

all the other members of the thesis committee for their positive criticisms and ideas which helped me to advance,

Oscar Domenech who shared a big part of his knowledge about biophysics with me and contributed with important AFM studies to this work,

Cécile Le Duff which made the ^{31}P-NMR studies on multilamellar vesicles and which considerably increased the significance of this thesis,

Claude Poleunis for all the analyses he made for me in Tof-SIMs,

Vincent Duprés, Sylvie Derclaye and the professor Yves Dufrêne for their contributions in AFM and cryodessication,

all the technicians who helped me during this thesis and who explained me all the techniques I had to apply : Martial Vergauwen, Marie-Claire Cambier, Jean-Paul Vanhelleputte, Marie Christine-Fayt, Ramazan Colak, Charlotte Misson, Alfons Brams, Patrick Van Der Smissen and Julie Maron.

Farida Akabi and Marthe Abouzi, the students who were implicated in this work did a great job.

I'm also grateful for all the help and kindness I received from the members of both laboratories I worked with: Cellular and molecular pharmacology (FACM) and Pharmacognosy (GNOS or ex CHAM). I wish to thank explicitely,

Joanne Bero for her neverending encouragements and the funny time we spend together in the "Travaux pratiques" and elsewhere,

Habib Ganfon for his positive spirit, which he passed easily to other members of the lab,

and also Aeçio Diaz da Silva, Emmanuelle Lautié, Eugénie Bassères, Coralie Vallet, Ahalieyah Anantarajah, Mamy Rafamantanana, Aurélie Leverrier, Aurélie Olivier, Isabelle Tytgat, Nathalie Couwenberghe, Martial Vergauwen, Esther Paitre, Marie-France Hérent, Emilie Bony, Salim Hage, Chiara Bacchelli, Katia Santos, Sophie Denamur, Françoise Gelders, Ann Lismond, Marie-Yvonne, Salim Hage, Julien Masquelier, Tamara Milosevic, Pierre Muller, Wafi Siala, Guillaume Sautrey, Hussein, and Nathalie Vandevelde for their daily support and friendship.

Abstract

We study in this work the interaction of some amphiphilic molecules of natural origin with membranes. Two groups of amphiphiles (saponins and lipopeptides) have been selected because they showed interesting activities towards cancer cells and are known to interact with lipid membranes.

Saponins possess a hydrophilic sugar moiety and a hydrophobic triterpenoid or steroid ring structure. They are mainly extracted from plants but can also be found in holotorians and star fish and would constitute defensive molecules. We investigated the membrane interactions of α-hederin, a monodesmosidic pentacyclic triterpenoid saponin, as a representative member of saponins because it has shown some selectivity towards cancer cells (Swamy and Huat, 2003). We also investigated the effects of its aglycone hederagenin, a triterpenic acid, to point out the importance of the sugar chain.

Lipopeptides are composed of a polar polypeptide ring and an apolar acyl chain. They are produced mainly by prokaryotes of the Bacillus species. We investigated the effect of surfactin since it has a strong amphiphilic character, is known to induce membrane lysis and to be active on cancer cells.

Membrane interactions of amphiphiles were investigated by several membrane models and complementary techniques. Large unilamellar (LUV) and multilamellar vesicles (MLV) were used to obtain quantifiable results of the effects induced with regard to the amphiphile/lipid ratio and incubation time. They were used to study binding (ANS affinity), permeabilization (calcein release), membrane order (Laurdan fluorescence), phase separation (Laurdan fluorescence and Förster resonance energy transfer) and formation of new lipid mesophases (^{31}P-NMR, dynamic light scattering). To visualize the effects on a microscopic scale, giant unilamellar vesicles (GUV) were investigated by fluorescence/confocal microscopy. Supported planar bilayers (SPB) were analyzed by atomic force microscopy (AFM) to give information about the effects at a nanoscopic scale. In parallel to the use of membrane models, we also investigated apoptosis and non-apoptotic cell death on cells derived from monocytic leukemiae.

α-hederin was able to interact with sterols in aqueous solution and to form mixed aggregates. In LUV, when no cholesterol was present in the membrane, the molecule inhibited phase separation most probably by a linactant effect. In the presence of cholesterol, α-hederin induced membrane permeabilization and an increase of phospholipid mobility. This was associated with the formation of a non-bilayer mesophase as confirmed by AFM on SPB, and local separation of phospholipids and sterols. In GUV, the effect depended on the critical micellar concentration of the saponin. In its monomeric form, the molecule induced mainly budding, the formation of worm shaped domains and a gradual permeabilization. Above the CMC (critical micellar concentration), budding and domain formation were less important but we observed the appearance of macroscopic pores and instantaneous permeabilization. The presence of a sugar chain at C3 on the triterpenoid ring structure was important for domain formation and rapid permeabilization. We confirmed on cancer cells the cholesterol dependence of cytotoxicity. α-

hederin and hederagenin induced apoptosis and non-apoptotic cell death most probably by formation of membrane defects or induction of the extrinsic apoptotic pathway and activity on lipid rafts.

Surfactin activity was also CMC dependent. In SPB and LUV, at concentrations below its CMC, the molecule inserted at the boundary between gel and fluid lipid domains, inhibited phase separation and stiffened the bilayer. It also induced transient defects and permeabilization of LUV without global morphological changes. At concentrations close to the CMC, surfactin solubilized the fluid phospholipid phase and increased order in the remaining lipid bilayer. At higher concentrations, all bilayer structures were dissolved and transformed most probably into micelles.

On the basis of these results, we develop a new interaction mechanism for α-hederin and hederagenin with lipid membranes which may be applied to other saponins and triterpenic acids as well. We also compare the effects of surfactin, α-hederin and hederagenin on membrane models and discuss possible consequences regarding their effect on cancer cells. Finally, we give some short term perspectives about ongoing and future experiments and explore long term perspectives about the possibility of further pharmacological use of the molecules we used in this work.

List of abbreviations

ANS 6-Anilinonaphthalene
AFM Atomic force microscopy
ATG5, 7 Autophagy protein 5, 7
BAM Brewster angle microscopy
CMC Critical micellar concentration
Cryo-TEM Cryogenic transmission electron microscopy
DHE Dehydroergosterol
DLS Dynamic light scattering
DMAPP Dimethylallylpyrophosphate
DMPC Dimyristoylphosphatidylcholine
DOPC Dioleoylphosphatidylcholine
DOPE Dioleoylphosphatidylethanolamine
DPH Diphenylhexatriene
DPH-PC Diphenylhexatriene-Phosphatidylcholine
DPPC Dipalmitoylphosphatidylcholine
EM Electron microscopy
EPR Electron paramagnetic resonance
FPP Farnesylpyrophosphate
FRAP Fluorescence recovery after photobleaching
FRET Förster resonance energy transfert
GFP-LC3 Green fluorescent protein-LC3
GM1 Oligosaccharide composed of 5 sugars
GPI Glycophosphatidylinositol
GPL Glycerophospholipids
GPP Geranylpyrophosphate
GSL Glycosphingolipids
GUV Giant unilamellar vesicles
HPLC High performance liquid chromatography
IPP Isopentenylpyrophosphate
ISCOMS® Immunostimulating complex (nanoparticles)
Laurdan 6-Dodecanoyl-2-dimethyl-aminonaphthalene
LC3 wild-type human microtubule-associated protein 1 light chain 3; I= cytosolic form; II=membrane bound form
LDH Lactate deshydrogenase
LUV Large unilamellar vesicles
MEP Methylerythritol phosphate pathway
MLV Multilamellar vesicles
MMP Matrix metalloproteinase
MOMP Mitochondrial outer membrane permeabilization
MPT Mitochondrial permeability transition
MVA Mevalonate pathway
NMR Nuclear magnetic resonance
OMM Outer mitochondrial membrane
PC Phosphatidylcholine
POPC Phosphatidyl-oleoyl-phosphatidylcholine
POPG Phosphatidyl-oleoyl-phosphatidylglycerol
Quil-A Saponin extract of *Quillaja saponaria* Molina.
QSAR Quantitative structure activity relationship
RIP1, 2 Receptor interacting protein 1, 2
ROS Reactive oxygen species
SAR Structure activity relationship
SM Sphingomyelin
SPB Supported planar bilayers
SUV Small unilamellar vesicles

TEM Transmission electron microscopy
Th1, Th2 T-helper cell 1, 2
TM Transmembrane proteins
TMA-DPH Trimethylamino-DPH

Lipid phases

L_α,L_d Liquid crystalline/Liquid disordered phase
L_β,S_o,G Gel/solid ordered phase
L_o Liquid ordered phase
P_β Rippled phase
H Hexagonal phase (followed by $_{I}$ = normal phase, $_{II}$ = inverse or reverse phase)
Q, C Cubic phase (followed by $_{I}$ = normal phase, $_{II}$ = inverse or reverse phase)

Table of contents

1. Foreword / Aim of the study

The word “Amphiphile” has its origine in the greek words “αμφις” or “amphis”, which means “double” and “φιλία” or “philia”, meaning “love” or “affinity”. Chemically, it describes a molecule that possesses an amphiphilic character and is composed of both a lipophilic and a hydrophilic part. This amphiphilic character contributes to many interesting physical and chemical properties. Amphiphilic compounds adsorb at interfaces between phases of different polarity and are able to self-aggregate or aggregate with other types of molecules. Self-aggregation of amphiphiles can lead to the formation of a new phase, called mesophase (because it possesses intermediate properties between a solid and a liquid phase). It is often described as fluid-like or “soft” (Israelachvili, 2011). Fluid-like structures are very common in nature and famous examples are lipid membranes. They are composed of self-aggregated phospholipids which form a lamellar mesophase. Because of their amphiphilic nature, membranes are very susceptible to interact with other amphiphiles in the surrounding solution and thought models, illustrating the different types of interactions, have been put forward (Dennis, 1986;Lichtenberg et al., 1983;Bechinger and Lohner, 2006). Especially, the effect of detergents on membranes has drawn much attention because of their capacity to isolate membrane proteins or lipid “rafts” (Kragh-Hansen et al., 1998;London, 2005).

The effects of amphiphiles on membranes are various and include permeabilization, phase changes, induction or disruption of phase separation, changes in membrane dynamics and more. They depend on the nature of the amphiphile, its concentration, the environment and last but not least, the membrane type. Amphiphiles, displaying a certain level of specificity against a special type of membrane are very interesting compounds and ideal candidates for the development of new membrane active drugs. Compounds which act only on the membranes of pathogens and leaving the host cells unchanged would present important antimicrobial potency (Lohner, 2009). Molecules acting selectively on cancer cells or a special type of organelles could provide new pharmacophores for chemotherapy (Riedl et al., 2011). Amphiphiles which act specifically on functional lateral domains (called lipid “rafts”) (Figure 1) could activate membrane receptors in an unspecific way, without acting directly on the protein but rather on the lipid environment.

FIGURE 1

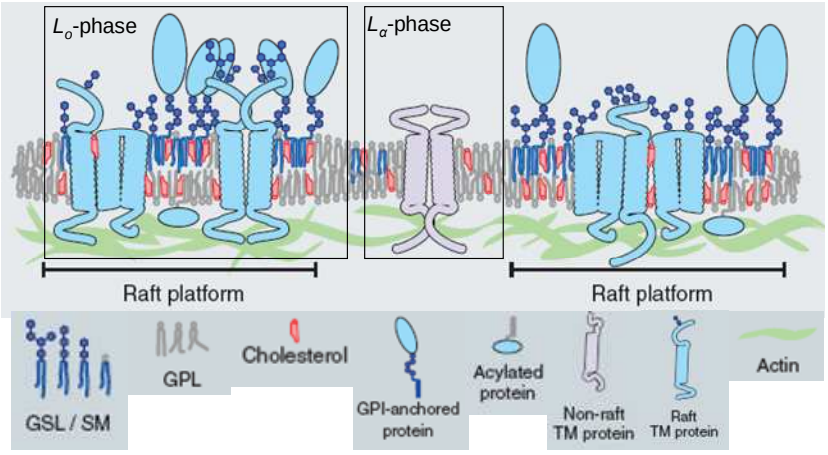

Lipid rafts in biological membranes and the cholesterol enriched associated lamellar organized phase (L_o) and the lamellar crystalline phase (L_α). (Lingwood and Simons, 2010)

Two interesting groups of naturally occurring amphiphiles, which have shown some selectivity towards certain types of membranes are saponins and lipopeptides (Shai et al., 2006;Francis et al., 2002). The aim of this study is to investigate the membrane activity of a representative member of each group: α-hederin, a triterpenoid saponin and surfactin, a cyclic lipopeptide (Figure 2). Both molecules have shown a certain selectivity towards cancer cells and were able to induce membrane lysis and apoptosis (Gauthier et al., 2009;Swamy and Huat, 2003;Cao et al., 2011;Heerklotz and Seelig, 2007). Surfactin has, in addition, antibacterial properties (Carrillo et al., 2003). We will analyze several aspects of their membrane activity towards different membrane models. For α-hederin, we will also investigate the activity of its natural precursor, the triterpenic acid hederagenin (Figure 2), lacking the sugar chain of the saponin and investigate the activity of both compounds against cancer cells in vitro and establish a model which will explain the activity of α-hederin against biological membranes.

FIGURE 2

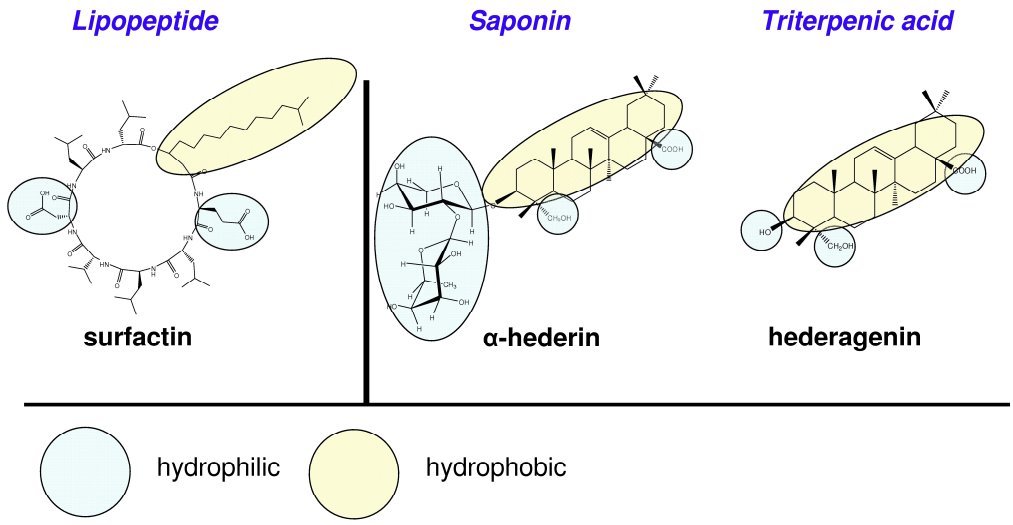

The amphiphilic structures of surfactin, α-hederin and hederagenin

The thesis will be divided into 4 main parts. In the first part, we will introduce notions about physico-chemical properties of amphiphiles, lipid membranes and interactions of amphiphiles with membranes. We will then review what is known in literature about interactions of saponins with different membrane models and cell membranes and their biological consequences. We will also present shortly the molecules whose effects have been analyzed in this thesis: α-hederin, its precursors and surfactin. The second part regroups all results obtained regarding membrane interactions and activities on cancer cells for all compounds. In the third part, we will inteprete these results and develop a mechanism for membrane interaction for each compound. We will also discuss influences of the membrane model and the molecular structure on their activity, the effects on cancer cells and highlight the differences and similarities between surfactin, α-hederin and hederagenin membrane interactions. In the last part we will give some short term perspectives about future and ongoing experiments. We also explore long term perspectives about the possibility of further pharmacological use of the analyzed substances and general lessons which can be taken from this study about further investigations of amphiphiles.

2. Introduction

2.1. Physico-chemical properties of amphiphiles

To understand the activities of amphiphiles on membranes, we first have to describe their physico-chemical properties. Amphiphilic molecules, due to their hydrophilic and lipophilic properties adsorb at interfaces of two immiscible phases of different polarity (Rosen, 1978) and thereby reduce the interfacial energy (or interfacial tension) of both phases (Mehta et al., 2010). The interfacial energy (or tension) is the free energy change which arises from increasing the separating surface by unit area. Mathematically it is expressed in the Dupré equation,

$$\gamma_{12} = \gamma_1 + \gamma_2 - W_{12}$$ **(Equation 1)**

whereby γ_1 and γ_2 are the changes in surface tension (or energy) of media 1 and 2 when both surfaces have been increased by unit area and W_{12} is the adhesion energy between both surfaces. The adhesion energy is the free energy change (or work) when separating two surfaces from contact to infinity in vacuum (Israelachvili, 2011).

The miscibility of two phases depends on the interfacial energy. By reducing the interfacial energy, we increase the miscibility of both phases. Because of this ability, amphiphiles facilitate the formation of foams (liquid-gaseous), emulsions (liquid-liquid) and suspensions (solid-liquid).

2.1.1. Amphiphiles at the air-water interface

The most commonly studied interface is the air-water interface (or water surface). Amphiphiles adsorb at the air-water interface with their hydrophilic part pointing to the water side and the hydrophobic part pointing to the air side. This behaviour will lead to a reduction of surface energy, defined as energy necessary to increase the surface by unit area (J/m^2) or surface tension (γ), defined as force per unit length (mN/m or dyn/cm). The reduction of surface tension at the air-water interface is mainly due to the rupture of hydrogen bonds between water molecules. If amphiphiles are not soluble in water, they will only occupy the air-water interface. This surface can be compared to a two-dimensional reservoir and maybe considered as analogue to a three-dimensional gaz reservoir. It can be described by the two-dimensional Van der Waals equation of state:

$$(\Pi + a / A^2)(A - b) = kT$$ (Equation 2)

Π is called the surface pressure of a monolayer and has the same units than the surface tension γ of a liquid, but in contrary is not constant. It is also the difference between the surface tension of the air water surface (γ_0) without and with amphiphiles adsorbed (γ_a) ($\Pi=\gamma_0-\gamma_a$). A is the area occupied by the amphiphiles, k is the Boltzmann constant and T the absolute temperature. a and b are constants and depend on the amphiphiles (Pallas and Pethica, 1985;Pallas and Pethica, 1987). Similar to a three-dimensional system (gaz), the formula allows us to elaborate a phase diagram of the non-soluble monolayer (Figure 3). We will observe a gaseous state at small amphiphile density (or a high surface area). By increasing the density, we will pass trough a liquid expanded (LE), a liquid compressed or ordered (LC) and a solid state. In several systems, it is possible to observe coexistence of different phases (Knobler and Desai, 1992;Lösche, 1983).
If the amphiphiles are soluble in the solution, they will be submitted to an equilibrium between monomers in the solution and molecules at the air-water interface without changing the surface pressure (Figure 4) (Chang and Franses, 1995;Israelachvili, 2011;Vollhardt and Fainerman, 2006).

FIGURE 3

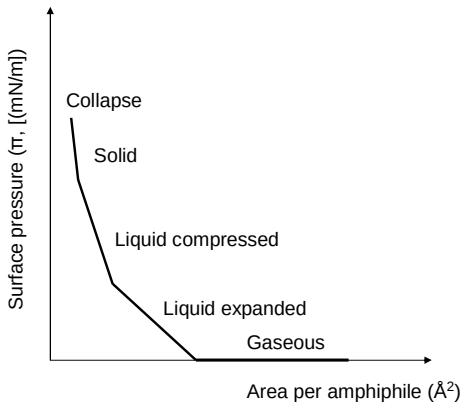

Diagram of surface pressure versus area isotherm

2.1.2. Self-aggregation of amphiphiles

Self-aggregation is one of the most striking properties of amphiphiles. As an example, detergent activity is based on the property to form micelles and mixed micelles in aqueous solution and the formation of bilayers depends on self-aggregation of phospholipids. To

understand the interaction between amphiphiles and bilayers, we have to understand why and how amphiphilic molecules are able to aggregate.

Self-aggregation of amphiphiles leads to the formation of special aggregates and in many cases to the formation of mesophases. Mesophases or “fluid-like” structures are structures which possess intermediate properties between solid and liquid phases. This is simply due to weak intermolecular binding forces between amphiphiles in aggregates which are mostly Van der Waals, hydrophobic, hydrogen bonding and screened electrostatic interactions (Israelachvili, 2011;Israelachvili, 1976;Israelachvili et al., 1977).

In terms of solubility, there exist two types of aggregates. Soluble aggregates have finite sizes (mostly in the nm range) and insoluble aggregates are of infinite size and become visible. Here, the shape of the amphiphile plays an important role (see 2.1.2.3.). Spherical micelles have a finite size (or aggregation number N) and can be considered as soluble (Israelachvili, 2011).

Formation of these aggregates depends on the concentration of the amphiphile in the solution. When it increases above the critical micellar concentration (CMC), monomers will begin to self-aggregate (Figure 4 and Figure 5) and an equilibrium between monomeric amphiphiles and aggregates appears.

Other common mesophases are the hexagonal (H_I), the hexagonal inverted (H_{II}), normal cubic (Q_I), inverted cubic (Q_{II}), or lamellar phases. Besides these “classical” arrangements there exist many other types of aggregates (see 2.1.2.3.) (Israelachvili, 2011).

FIGURE 4

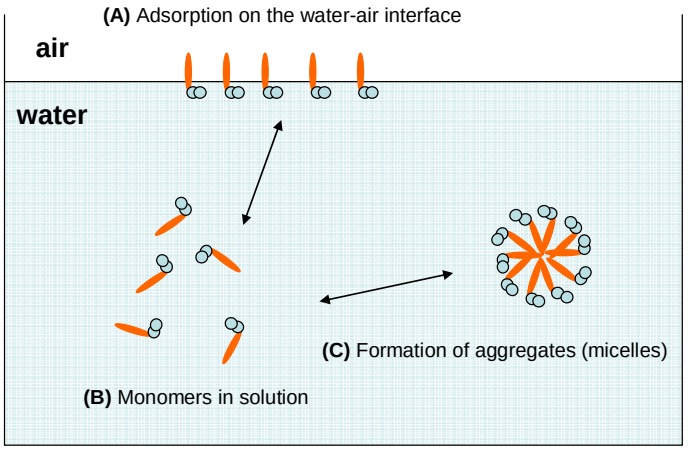

Behaviour of amphiphiles at interfaces (A), in aqueous solution as monomers (B) and aggregates (C)

FIGURE 5

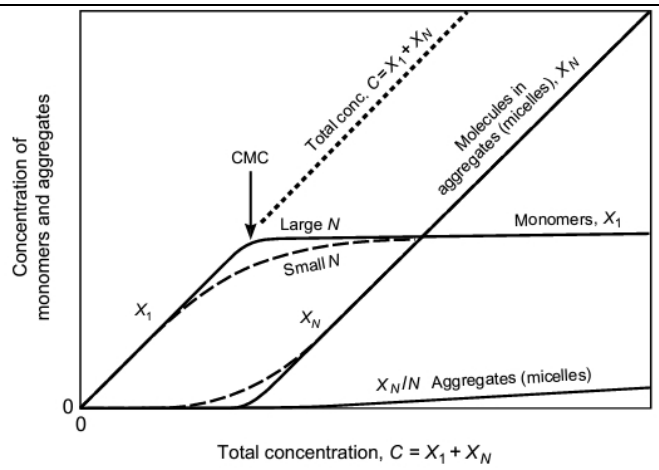

Formation of aggregates (micelles) above the critical micellar concentration (CMC) with increasing concentration of surfactant monomers (X_1).
X_N represents the molar fraction of surfactant molecules in aggregates. N is the aggregation number (Ruckenstein and Bhakta, 1994).

2.1.2.1.Thermodynamics of self-aggregation

To understand the nature of the self-aggregation process in a solution, we have to understand the thermodynamics of the process. Because entropy would lead the system to the formation of many small aggregates or monomers, the interactions between amphiphiles counteract this process. The pioneering work regarding thermodynamics of self-aggregation has been done by Israelacchvili and coworkers. They studied conditions for aggregate formation, the solubility of the aggregate and its CMC.

2.1.2.1.1. Conditions for the aggregate formation

When molecules form aggregates in solution, the chemical potential of all identical molecules in different aggregates has to be equal. It can be expressed as:

$$\mu = \mu_N^0 + \frac{kT}{N}\log\left(\frac{X_N}{N}\right) = \text{constant}$$ **(Equation 3)**

N is the number of molecules in an aggregate (the aggregation number), μ the chemical potential, μ_N^0 the mean chemical potential (mean interaction free energy per molecule) of an aggregate of aggregation number *N*, *k* is the Boltzmann constant, *T* the temperature and X_N is the activity (expressed in volume fraction or mole fraction) of molecules in aggregates of *N* molecules (Israelachvili, 2011).

We can also formulate that the mole or volume fraction of an aggregate of aggregation number N, X_N is equal to :

$$X_N = N.\{X_1 \exp[(\mu_1^0 - \mu_N^0)/kT]\}^N \quad \textbf{(Equation 4)}$$

In this equation, X_1 is the mole fraction of the monomer in solution and μ_1^0 the chemical potential of the monomer. All other parameters have been presented in equation 3.

The condition required to form an aggregate of aggregation number *N* is $\mu_N^0 < \mu_1^0$. In other terms, the free energy of the amphiphiles in the aggregate composed of N amphiphiles has to be smaller than that of the monomer.

2.1.2.1.2. Solubility of aggregates (finite vs. infinite size) and mean aggregation number (M)

The question of aggregate solubility depends very much on the shape of the aggregate. If we consider that αkT is the binding energy in the aggregate relative to the isolated monomers, we can express μ_N^0 as :

$$\mu_N^0 = \mu_\infty^0 + \frac{\alpha kT}{N^p} \quad \textbf{(Equation 5)}$$

α is a positive constant depending on importance of amphiphile interaction, *p* describes the shape or dimensionality of the aggregate (*p*=1 for rod-like aggregates (one-dimensional), *p*=1/2 for discs (two-dimensional) an *p*=1/3 for spheres (three-dimensional)). μ_∞^0 is the mean chemical potential for an aggregate of infinite size.

For rod-like (chain like) or cylinder-like aggregates (*p*=1), the mean aggregation number *M* depends strongly on the concentration of the amphiphile and very polydisperse aggregates of different sizes can be observed.

For disc or spheres $p < 1$ an aggregate of infinite size appears when μ_N^0 decreases upon the aggregation number. In these conditions, we will observe a macroscopic phase separation. Hence, for most amphiphiles, μ_N^0 reaches a minimum value at a mean aggregation value M and therefore spherical aggregates like micelles have monodisperse Gaussian distribution around the mean aggregation number (M) and are of finite size (Israelachvili, 1976).

2.1.2.1.3. The critical micellar concentration (CMC)

The concentration which is needed for aggregate formation (CMC) can be expressed in the following manner.

By combining equation 4 and 5, we can find that

$$X_N = N\left[X_1 e^{\alpha}\right]^N \quad \textbf{(Equation 6)}$$

Since X_N can never exceed unity (it is a molar or volume ratio), X_1 will never exceed 1/exp[(μ_1^0 - μ_N^0)/kT] (equation 4) or exp[-(μ_1^0 - μ_N^0)/kT]. Similarly in equation 6, X_1 can never exceed $e^{-\alpha}$. This concentration is the maximum concentration a monomer can reach and is equal to the critical micellar concentration (CMC) (Israelachvili, 2011;Israelachvili et al., 1977;Israelachvili, 1976) and we can write : CMC = $e^{-\alpha}$

2.1.2.2.Equilibrium between monomeric amphiphiles and aggregates

Amphiphiles in micelles (or other types of aggregates or mesophases) can be considered to be in a permanent equilibrium with their corresponding monomers in the bulk solution. This exchange of molecules can be characterized by the law of mass action and the constants of dissociation (k_D) and association (k_A) of the micelle.

$$\text{N x monomer} \underset{k_D}{\overset{k_A}{\leftrightarrow}} \text{micelle}^N$$

$$K = \frac{k_A}{k_D} = \frac{[micelle]}{[monomer]^N} = \exp[-N(\mu_N^0 - \mu_1^0)/kT] \quad \textbf{(Equation 7)}$$

We can deduce the mean lifetime (or residence time) (τ_R) of a molecule in an aggregate according to its CMC.

$$\tau_R = \tau_0 / e^{-\Delta E / kT} \approx 55\tau_0 / CMC$$ **(Equation 8)**

τ_0 is the typical motional correlation time in an amphiphilic aggregate and is in the range of 10^{-9}-10^{-7} s. ΔE is the activation energy which has to be surmounted by an amphiphile to leave the aggregate.

The CMC (Figure 5) determines therefore the mean lifetime of an amphiphilic molecule in its micelle or mesophase. For bilayer forming amphiphiles, the CMC is smaller (10^{-6}-10^{-10} M) than for micelle forming amphiphiles (10^{-2}-10^{-5} M) and residence time is therefore higher in bilayers (10^4s) than in micelles (10^{-4}s) (Israelachvili, 2011).

2.1.2.3.The molecular shape of amphiphiles and their polymorphic phase behaviour

The resulting form of the aggregate (or mesophase) depends on the molecular shape of the amphiphile, its molecular self-interaction and the environment (Israelachvili, 2011). Several attempts have been made to predict the resulting form of the aggregate by the molecular amphiphilic shape (Marsh, 1996;Kumar, 1991;Israelachvili, 1976). For amphiphiles composed of a lipophilic hydrocarbon chain and a hydrophilic head, Israelachvili et al. defined a molecular packing parameter (Figure 6)

$$S = V / a_0.l_c$$ **(Equation 9),**

where V is the hydrocarbon or lipophilic chain volume, l_c is the critical chain length (corresponds to the fully extended hydrocarbon chain) and a_0 is the optimal headgroup area (corresponding to the area when repulsion and interfacial tension or hydrophobic attraction at the hydrophobic-hydrophilic interface are at equilibrium) (Figure 6,A) (Israelachvili, 1976). This packing parameter is proportional to the Hydrophile-Lipophile Balance (HLB), which designates if amphiphiles form oil in water micelles (O/W, normal) or water in oil micelles (W/O, inverse) in a water-oil-amphiphile mixture (Becher, 1983). According to the self-assembling theory, we consider that amphiphiles presenting a packing parameter smaller than unity possess a cone-shape. In other words, the base of the cone corresponds to a_0.

The packing parameter depends on the charge and the size of the headgroup, the volume of the hydrocarbon chain, the pH, the ionic force and the temperature of the solution (Figure 6,A). It is therefore not astonishing that the same amphiphile can aggregate into different structures in function of the environment. This special character is called polymorphism of amphiphiles. For

example, an anionic amphiphile will rather aggregate into micelles at high pH, because the size of its headgroup (and therefore a_0) increases when ionized. Amphiphiles with packing parameters smaller than one form normal structures in water (Figure 6,B). This means they point their hydrophilic head to the external aqueous phase. Inverse aggregates points their hydrophobic queue to the outside.

The concept of the packing parameter can only be applied to amphiphiles composed of a hydrophobic acyl chain and a hydrophilic head such as phospholipids. For other amphiphilic structures like peptides or lipopeptides, interactions become much more complex because the ternary structure (three dimensional shape) of the peptides is influenced by intrinsic interactions between aminoacids.

The polymorphism of amphiphiles can lead to the formation of numerous different structures of different dimensionality. Rod or cylinder-like structures (one-dimensional), disc-like (or lamellar) structures (two-dimensional) and three-dimensional structures. We summarize there under the most common phases observed.

FIGURE 6

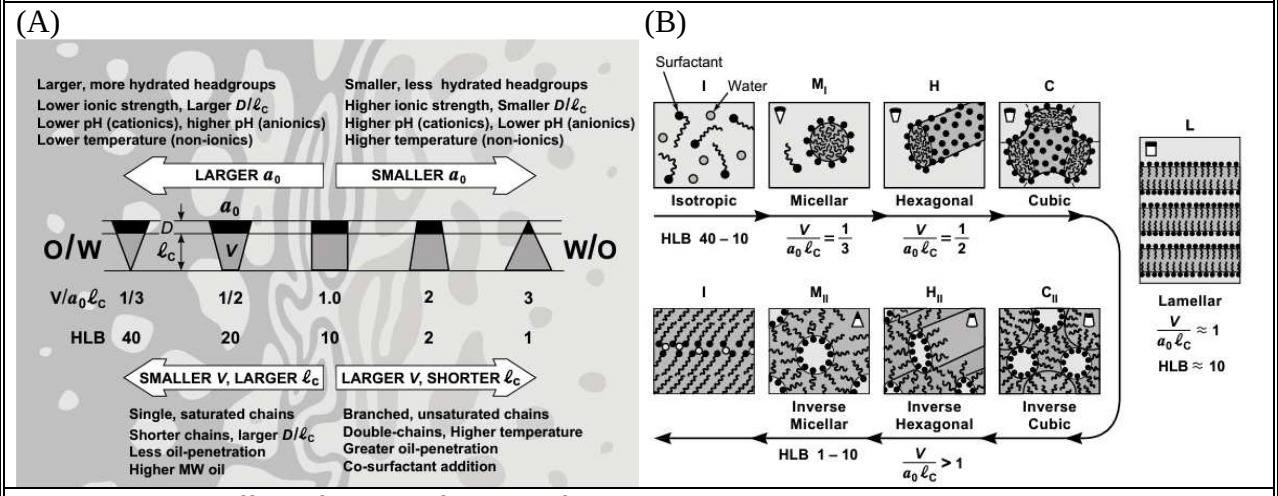

(A) *Effect of various factors influencing the molecular packing parameter and the resulting molecular shape of the amphiphilic aggregate*
(B) *Different phases formed by amphiphiles in function of their molecular packing parameter or hydrophilic-lipophilic balance.*
(Israelachvili, 2011)

2.1.2.3.1. Micellar phases

We can observe the formation of inverse or normal micelles (Figure 6,B). Micellar phases are optically isotropic. Normal micelles are favored by cone-shaped and inverse micelles by inverse cone-shaped amphiphiles. Micelles can be spherical or present other forms and are characterized by a small residence time of amphiphiles (10^{-2}-10^{-5} s) (Israelachvili, 1976). This small residence time makes them "dynamic" structures. The packing parameter of amphiphiles forming spherical micelles has to be smaller than 1/3 (Figure 6,B).

2.1.2.3.2. Lamellar phases or bilayers

Association of amphiphiles with cylindrical shape leads to the formation of lamellar phases or bilayers. There exist several states of lamellar phases. This issue will be discussed in the chapter regarding membrane dynamics. The diffusion of amphiphiles between monolayers (flip-flop) is often in the same range than the residence time of a bilayer (see 2.1.2.2.) (Israelachvili, 2011). Bilayer forming amphiphiles present a packing parameter close to unity (Figure 6,B).

2.1.2.3.3. Hexagonal phases

Hexagonal phases are characterized by long tubular associations of amphiphiles (Figure 7). The normal hexagonal phase is called H_I phase and the inverse phase H_{II} (Seddon, 1990). Transitions between lamellar and hexagonal phases are thought to play an important role in membrane permeabilization ($L_\alpha \rightarrow H_I$ transitions) and membrane fusion ($L_\alpha \rightarrow H_{II}$ transitions) (Seddon, 1990;Hallock et al., 2003). A lot of amphiphilic peptides or proteins are known to promote the H_{II} state when they interact with membrane lipids (Haney et al., 2010). Lipid amphiphiles forming preferentially a hexagonal phase possess a packing parameter in the range of 1/3 till 1/2 (Figure 6,B).

FIGURE 7

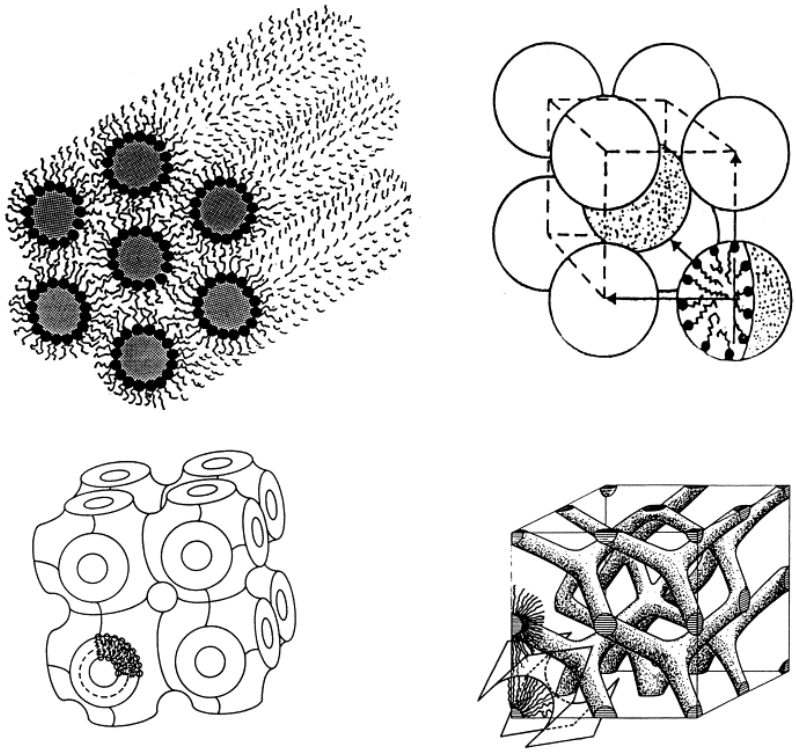

Polymorphism of amphiphiles
Upper left: Inverse hexagonal phase (H_{II}), upper right: micellar or normal cubic phase, lower left: bicontinuous cubic phase of type In3m; lower right: bicontinuous cubic phase of type Pn3m (Seddon, 1990)

2.1.2.3.4. Cubic phases

Cubic phases can present different types of molecular three dimensional arrangements (Figure 7). They can be micellar or bicontinuous. If they are bicontinuous, they are characterized by a space group which defines its three-dimensional arrangements in a cube (for example Pn3m or In3m). They are optically isotropic. They can exist as normal (Q_I or C) or inverse phase (Q_{II} or C_{II}). On a phase diagram, they most often exist between other phase transitions (for example between the hexagonal and lamellar state) (Figure 6,B) (Fontell, 1992;Siegel, 1986). They are favored in systems composed of more than one amphiphile. Cubic phases are thought to be intermediates when fusion promoting peptides act on membrane (Luzzati, 1997).

2.2. Lipid membranes

From a cellular point of view, a membrane is the natural delimitation of a cell. It separates the cells' interior from its exterior and confers therefore protection to the cell. It is also the site of exchange of the cell with its environment. In eukaryotic cells, membranes define also distinct compartments, the organelles.

To discover how different amphiphiles interact with membranes, we have to understand critical membrane properties. We have seen that membranes or bilayers are aggregates of amphiphilic cylinder shaped molecules. However, there exists a big difference between simple bilayer structures composed of some lipids and biological membranes. Biological membranes are composed of hundreds to thousands different lipid species and contain proteins (van Meer, 2005). Moreover, the complete membrane structure is supported by a cytoskeleton, which is very important to the shape of the cell. This complexity confers some interesting properties to the membrane.

2.2.1. Different lipid species in cellular membranes

The variety of lipid species in a cell membrane is enormous. A typical biomembrane contains hundreds to thousand different species of lipids (van Meer, 2005). Three main classes of lipids exist: glycerophospholipids (or phospholipids), sphingolipids, cyclic (sterols) and linear isoprenoids. Glycolipids can be considered as a separate class (van Meer, 2005).

2.2.1.1.Fatty acids

In membranes, free fatty acids are rare. They are mostly esterified. Generally, they possess 10 to 24 carbons and can have one or more insaturations. Their biosynthetic pathway includes the condensation of Acetyl CoA units. That's why natural fatty acids possess only pair numbers of carbons. Dehydration leads to unsaturated fatty acids. In nature, unsaturated fatty acids contain only double bonds in the cis configuration. This cis configuration introduces a kink in the chain. Saturated fatty acids have the property that all carbon-carbon bonds (except the sp2 bond of the carboxylic acid) can freely rotate. The chain is fully extended, when all the torsion angles are 180°. This preferred conformer is called trans or anti. The second most observed form

is the gauche conformer which has a torsion angle of 60°. Free rotation passes through these conformations. The nomenclature of fatty acids implicates most often trivial names. From 12 to 18 carbons the names are: lauric, myristic, palmitic and stearic acid.

2.2.1.2.Phospholipids or glycerophospholipids

The backbone of glycerophospholipids is its glycerol molecule. Two fatty acids (except cardiolipin which contains 4) are bound at the same side of the molecule through an ester linkage at C1 and C2. A phosphatidyl residue is bound to the C3 and points to the opposite side of the acyl chains (*sn*-configuration) (Figure 8,A). If the phospholipid possesses only one acyl chain, it is called lysophospholipid. Glycerophospholipids are the most common lipids in eukaryotic plasmic membranes (van Meer, 2005). Saturated phospholipids are enriched in lipid rafts and in the L_o phase (Figure 10). They have generally a high melting temperature (T_m). Unsaturated phospholipids do not participate in raft formation and have generally a low melting point. Most natural phospholipids possess one saturated and one unsaturated acyl chain.

2.2.1.3.Sphingolipids

Sphingolipids are built of sphingosine, a long chain aminoalcohol bound to a fatty acid by an amide linkage (Figure 8,B). Most of them are sphingomyelins : sphingophospholipids with a phosphocholine or phosphoethanolamine headgroup. Their fatty acids are mostly saturated, which allows them to be closely packed together and to be enriched in lipid rafts (Figure 10).

FIGURE 8

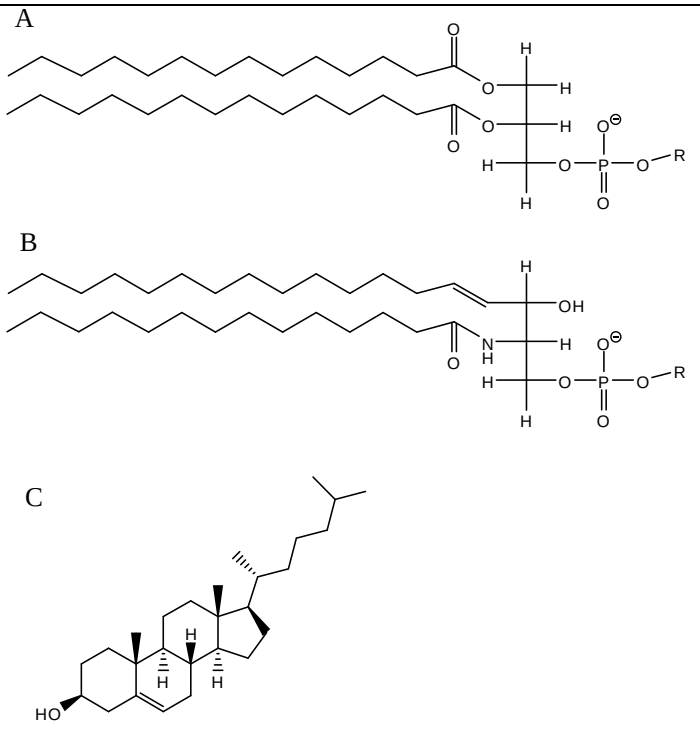

Molecular structures of different lipids

(A) Glycerophospholipid
(B) Sphingolipid
(C) Cholesterol

2.2.1.4.Linear isoprenoids and sterols (terpenes)

Biosynthesis of linear isoprenoids, sterols and triterpenoids is based on the acetate-mevalonate pathway (Figure 9, black panel). First, mevalonate is synthesized via the condensation of three acetyl-CoA units and further reduction of mevalonate-CoA by the enzyme hydroxymethylglutaryl-CoA reductase. Addition of two phosphates and decarboxylation leads to isopentenylpyrophosphate (IPP), a 5 carbon containing molecule. IPP is isomerized into dimethylallylpyrophosphate (DMAPP), a highly reactive molecule. Plants and some parasites have the ability to synthesize IPP and DMAPP by an alternative pathway, the methylerythritolphosphate pathway, in their plastids (Figure 9, green panel) (Lichtenthaler, 1999). Both pathways lead to the addition of IPP on DMAPP to form geranylpyrophosphate (GPP), which contains 10 carbons. Further addition of another IPP unit on GPP leads to farnesylpyrophosphate (FPP) and condensation of two FPP leads to the formation of squalene. Its

cyclization via epoxysqualene leads to the formation of triterpenoids (30 carbons). The further loss of 3 carbon atoms leads to sterols which are composed of 4 rigid cycles and 27 carbons (Figure 8,C) (Nes, 2011;Tchen and Bloch, 1957).

Sterols are only present in eukaryotic cell membranes with exception of some bacterias which might have acquired synthetic capabilities by horizontal gene transfer from eucaryotes (Desmond and Gribaldo, 2009). Vertebrates contain mainly cholesterol, land plants stigmasterol, campesterol and sitosterol and fungi ergosterol. Some eucaryotes like insects have lost the ability to synthesize sterols. For detailed review about the presence of sterols in membranes of living cells, excellent papers have been published (Desmond and Gribaldo, 2009;Nes, 2011). Sterols influence to a large extent the properties of membranes and especially its dynamic and elastic properties (see 2.2.4.) and are a major component of lipid rafts (Figure 10).

FIGURE 9

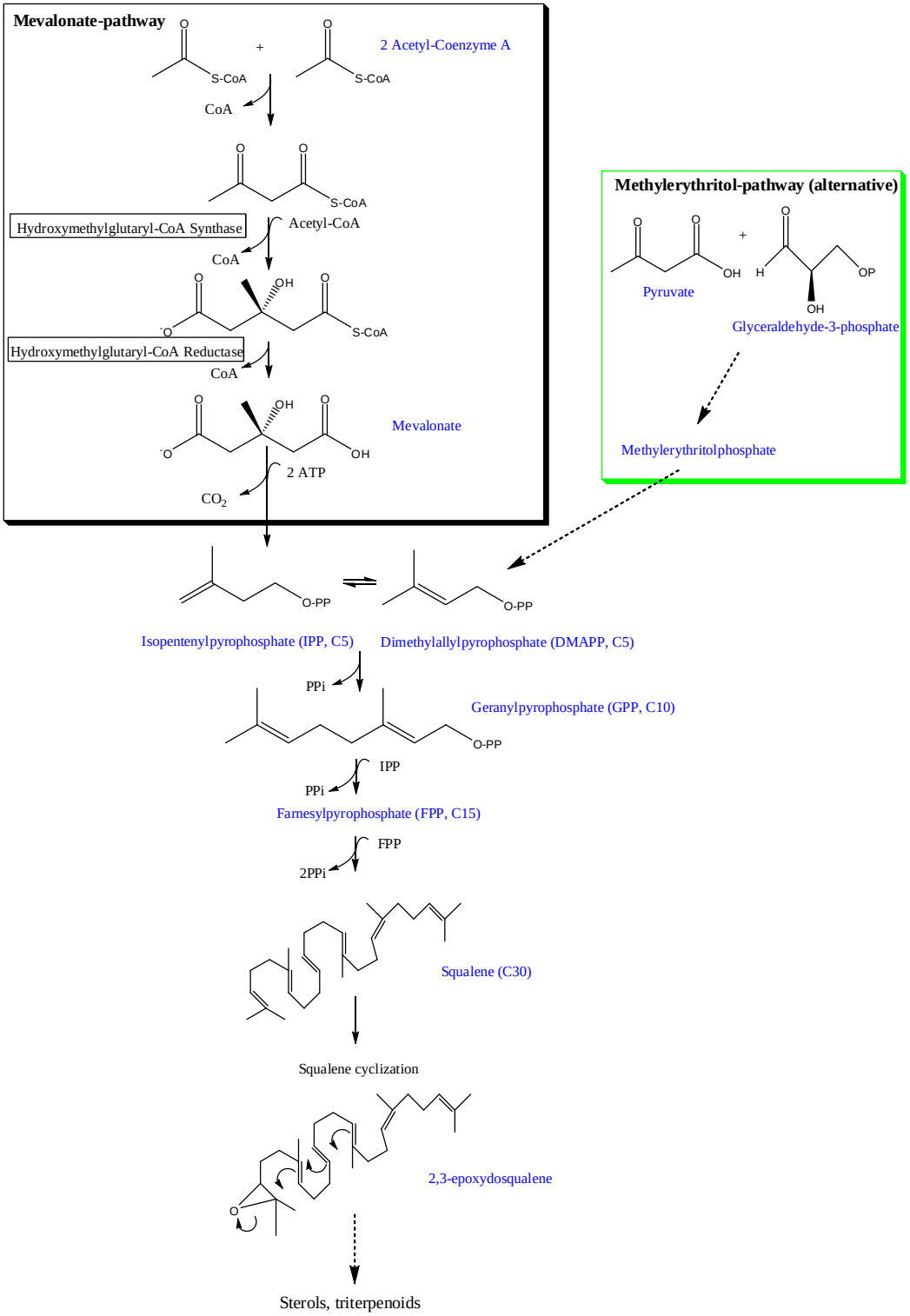

Biosynthesis of sterols and triterpenoids via two different pathways

2.2.1.5.Glycolipids

They are composed of an oligosaccharide and a glycerophospholipid or sphingolipid. Ganglioside GM_2 for example is composed of a sphingolipid and several sugar moieties. Gangliosides are part of lipid rafts (Figure 10). They can also have other functions. Rhamnolipids, glycolipids of *Pseudomonas* are important for quorum sensing and biofilm formation (Desai and Banat, 1997).

2.2.2. Main organization of biological membranes

The understanding of the composition and three-dimensional form of biological membranes was and is a challenging research. In the 20th and 21st century, several scientists developed membrane models describing the reality with accordance to their technical advances.

2.2.2.1.A phospholipid bilayer with "floating" proteins

In 1925, Gorter and Grendel first proposed that erythrocytes would have a membrane in form of a bimolecular leaflet composed of lipids (Gorter and Grendel, 1925). On this basis, the Davson-Danielli model, which suggested that proteins cover the membrane surface, was established (Danielli and Davson, 1935). After numerous findings regarding mainly membrane proteins, the fluid mosaic model was evolved by Singer and Nicolson (Singer and Nicolson, 1972). It assumes that globular proteins can diffuse ("float") freely in a fluid-like phospholipid bilayer. Further studies revealed the existence of different degrees of protein diffusion (Ramadurai et al., 2009).

2.2.2.2.Lateral heterogeneity of mammal membranes, membrane rafts

Already in the eighties, self-association of cholesterol in model membranes (Lentz et al., 1980) and the presence of detergent resistant membranes (Brown and Rose, 1992) led to the assumption that some proteins reside in membrane domains with lower diffusibility. Simons and Ikonen postulated that these domains would form functional "rafts", enriched with cholesterol and sphingolipids (Simons and Ikonen, 1997). Different studies have revealed that rafts have a size between 10-200 nm, a lifetime ranging in the subsecond scale and are enriched with

cholesterol, sphingolipids, glycosylated lipids and GPI-anchored proteins (Figure 10) (Jacobson et al., 2007;London, 2005;Lingwood and Simons, 2010). Rafts should be imagined as lateral nanoscaled domains existing in the subsecond range and which can fuse into a larger, more stable raft phase due to protein-lipid, protein-protein and lipid-lipid interactions (Lingwood et al., 2008;Friedrichson and Kurzchalia, 1998).

By inhibiting interactions of the actin cytoskeleton with the membrane, phase separation into microscopic domains can be observed, which suggest, that the cytoskeleton is able to influence the microheterogeneity (Lenne et al., 2006;Suzuki et al., 2005;Lingwood and Simons, 2010). Questions, as how important lipid interactions influence membrane heterogeneity in cells, have been intensively discussed (Leslie, 2011).

FIGURE 10

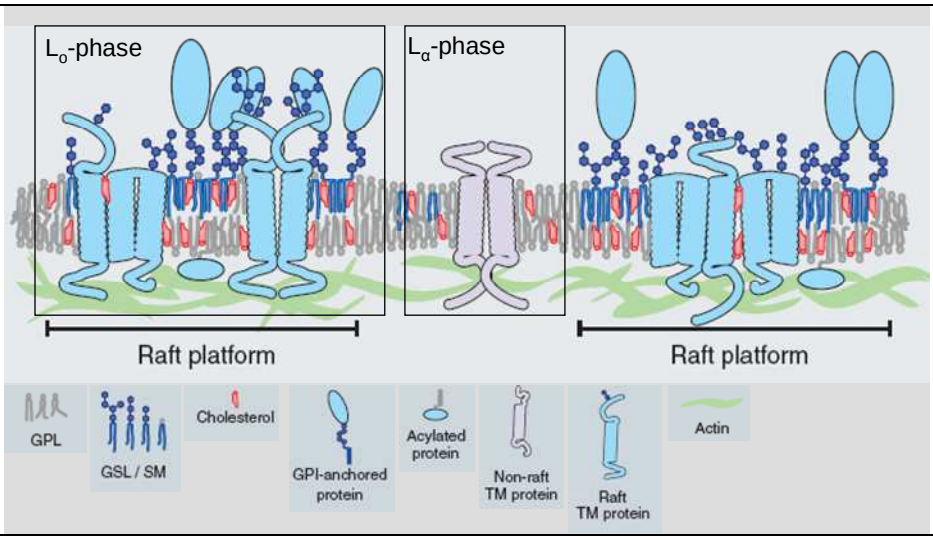

Membrane model showing the formation of raft-platforms in cellular membranes (Lingwood and Simons, 2010).

Rafts are associated with the L_o-phase and are composed of mainly saturated glycerophospholipids (GPL), cholesterol, glycosphingolipids and sphingomyelin (GSL/SM), Glycophosphatidylinositol (GPI) anchored and transmembrane (TM) proteins.

2.2.2.3.Membrane domains in bacteria

Another type of lateral membrane heterogeneity is found in prokaryotic membranes. Liquid/liquid phase coexistence leads to the formation of cardiolipin and phosphatidylethanolamine rich domains. Bacterial membranes do not contain sterols and other types of interactions have to lead to domain formation. Lipid phase separation would here be

guided by hydrogen bonds, Van der Waals and electrostatic interactions (Matsumoto et al., 2006). The domain formation would have a considerable impact on the activitites of antibacterial peptides and especially polycationic peptides (Epand and Epand, 2009;Epand et al., 2008).

2.2.3. Membrane dynamics and lamellar phases

We have seen that membranes are “fluid”-like structures (mesophases) and their components are in constant movement and exchange with the environment. Phospholipids can undergo several types of movements in a membrane which includes rotational and lateral diffusion, flip-flop, protrusion, bond oscillations and trans-gauche isomerizations (Gawrisch, 2005). The membrane itself undergoes undulations (Figure 11). All these oscillations have different correlation times (time periods). We have to be aware that techniques allowing to get informations about lipid “order” like NMR, EPR or fluorescence studies only reflect the order in the time-scales they acquire their information.

FIGURE 11

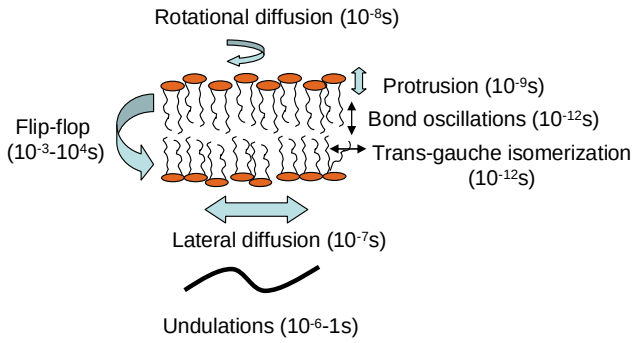

Approximate correlation times of lipid motion in membranes (Gawrisch, 2005).

According to the dynamic state of the membrane, we can distinguish different lamellar phases. At low temperatures, the membrane is in the solid ordered or gel phase state (L_β or S_o). When the temperature is raised beyond its transition temperature the membrane undergoes a phase transition and become fluid crystalline (L_α or L_d). Some membranes composed of pure phospholipids can present intermediate states which are the rippled phase P_β, the pseudocrystalline phase or phases where the chains are tilted (L_β' and P_β').

The gel state is characterized by a high lipid packing and an increased order. When temperature increases, the probability of gauche conformers is raised and at transition temperature (T_m), chain melting occurs. Beyond this temperature, the bilayer will pass into a liquid crystalline state. The membrane in the L_α state is characterized by higher diffusion rates, an increase of the cross-sectional area of each lipid and a thinning of the membrane. Melting temperature decreases with shorter acyl chains and the number of unsaturations. It depends also of the position of the insaturation, the pH, the ionic strength and the size of the headgroup (Lewis and McElhaney, 2005).

2.2.4. The effect of cholesterol on dynamics and the formation of a liquid ordered phase (L_o)

Cholesterol, due to its rigid ring structure inhibits trans-gauche isomerization of acyl chains and favors the trans-conformers in membranes of the liquid crystalline phase (L_α). This leads to an ordering effect of cholesterol. Forcing the acyl chains into a linear conformation leads to thickening and lateral condensing of the membrane. In the gel phase, cholesterol increases the area per lipid molecule and so reduces order because the β-side of the sterol possesses methyl residues which “pushes” phospholipids away (London, 2005;Rog et al., 2009). In other terms, cholesterol rigidifies the liquid crystalline phase and renders the gel phase more liquid. In erythrocytes and most eukaryotic cells which present a high cholesterol concentration, lipid phase transition between the gel and liquid crystalline phase is abolished (Ladbrooke et al., 1968;Parasassi et al., 1993).

If a certain amount of cholesterol in the membrane is reached, we will observe the formation of a new phase, the liquid ordered phase (L_o). The L_o phase will be enriched in saturated phospholipids, sphingomyelin and cholesterol but not in unsaturated lipids. The kink in their acyl chain (because of the cis configuration of the double bond) makes aggregation with cholesterol less favorable and so these lipids will constitute the L_α-phase (London, 2005).

2.2.5. Coexistence of lamellar phases in membranes

In defined conditions, different lamellar phases can coexist in model membranes.

2.2.5.1.The liquid/liquid L_o/L_α phase co-existence

Liquid/liquid phase separation is favored by the line tension which develops at the phase boundaries and inhibited by electrostatic interactions between different domains. Line tension is defined as energy per unit length. To reduce the free energy at the boundary, domains in liquid phase separation are circular (Israelachvili, 2011).

The co-existence between L_o and L_α phases is observed at critical lipid compositions. Most important is the amount of cholesterol in the membrane. In model membranes, this coexistence is thought to mimic the presence of lipid rafts in biological membranes. But on the contrary to lipid rafts, which are unstable structures, L_o/L_d phase coexistence in model membranes is stable upon time (Lingwood and Simons, 2010;London, 2005). The development of phase diagrams allows to define critical lipid compositions and temperatures (Figure 12) (Heberle et al., 2010). The co-existence between L_o/L_α phases in model membranes is mostly observed in ternary systems composed of one unsaturated phospholipid, a saturated phospholipid or sphingomyelin and cholesterol (de Almeida et al., 2003). Nanoscopic domains exist also in binary mixtures of phosphatidylcholines and cholesterol as have shown FRET (Förster energy resonance transfer) and NMR studies (Loura et al., 2001;Heberle et al., 2010).

If a coexistence between L_o and L_α is real, differential scanning calorimetry (DSC) will show the superimposition of two components in the phase transition. A sharp and a broad component reflects the sterol poor and enriched domains respectively (McMullen et al., 1995).

FIGURE 12

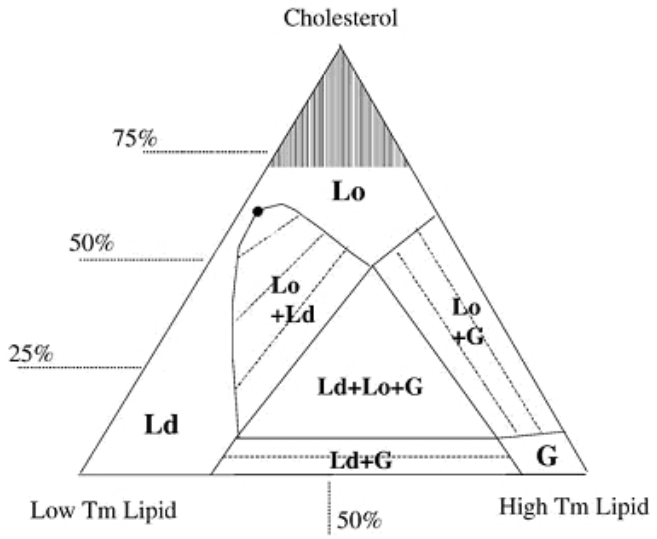

Phase coexistence between liquid crystalline (L_α or L_d), liquid ordered (L_o) and gel phase (G or S_O) at different compositions of a high T_m lipid, cholesterol (Chol) and a low T_m lipid. The striped part represents cholesterol crystals (London, 2005)

2.2.5.2.The solid/liquid (gel/liquid) G,S_o/L_d phase coexistence

In solid/liquid (or gel/liquid) phase separation, domains can have several shapes (Bagatolli et al., 2010). This type of phase coexistence is observed when the membrane is composed of a binary system containing two different lipids, one with a low and another with a high transition temperature (Deleu et al., 2013). It is inhibited at high sterol concentrations (because sterols favor the L_o phase) and is therefore not thought to take place in eukaryotic membranes. This does not exclude that this type of phase coexistence does not happen in other membrane types like bacterias.

2.2.5.3.Cholesterol-phospholipid superlattices in lamellar phases

Other models of lateral heterogeneity in lipid membranes have been put forward. The superlattice model supposes a regular distribution of phospholipid molecules around the sterol.

The arrangement of molecules changes at critical sterol concentrations (Figure 13,A) (Virtanen et al., 1995;Chong, 1994). A new statistical mechanical model, combining superlattices, phase diagrams and condensed complexes of phospholipids and cholesterol describes the membrane as a sludge-like mixture of fluid phase and aggregates of rigid clusters, forming the superlattice (Figure 13,B) (Sugar and Chong, 2012). The superlattice model explains a lot of physical behaviours typical of mixtures between sterols and phospholipids. This model has not been applied to many biological membranes. However, lipid composition of erythrocytes and the platelet plasma membranes could be predicted by the superlattice model (Virtanen et al., 1998). The energy minima observed with the superlattice model and the discrete number of allowed compositions could help to maintain organelle identity in the interests of rapid inter-organelle membrane traffic (Somerharju et al., 2009).

FIGURE 13

(A) (B)

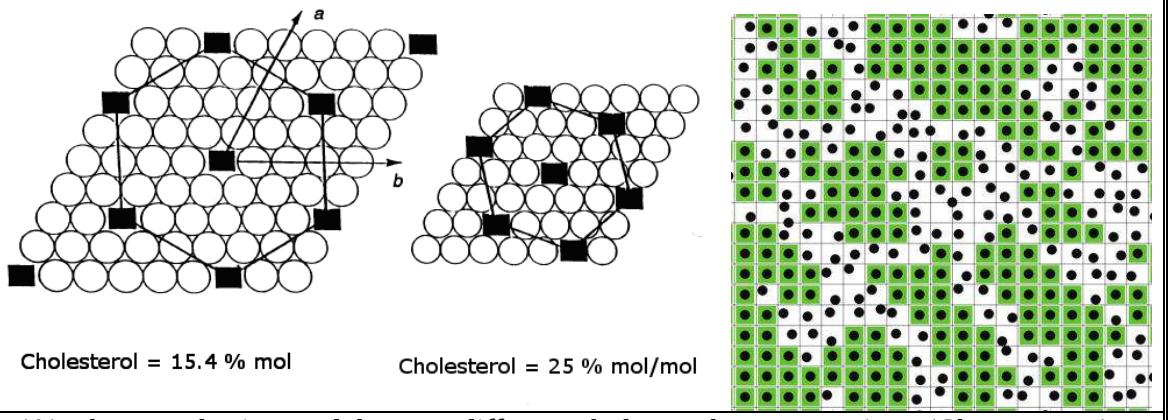

(A) *The superlattice model at two different cholesterol concentrations (Chong, 1994)*
(B) *Sludge-like superlattice (Virtanen et al., 1995)*
Green : rigid clusters of phospholipids and cholesterol (black points)
White : Sludge-like mixture of fluid phase (LG_1)

2.2.6. Spontaneous curvature

According to the shape hypothesis of amphiphiles, aggregation can lead to different phases of different forms (see 2.1.2.3.). Membranes should be mostly composed of cylinder

shaped amphiphiles which favor the formation of lamellar phases or bilayers. This is an oversimplification because in natural membranes a lot of lipids which do not possess a cylinder shape exist (van Meer, 2005). Aggregation of several lipids in lateral membrane domains will also change the local contribution to the membrane form and a flat membrane may develop into a curved structure (Israelachvili, 2011). It is therefore of major importance to understand and quantify the implications of amphiphilic composition to the membrane curvature.

2.2.6.1.Monolayers

The effects of amphiphile composition on a membrane can be most easily understood in a monolayer. The geometric curvature in a point (J) of the monolayer can be defined as the sum of both curvatures C_1 and C_2 (or the inverse radii R_1 and R_2) obtained by the dissection of the layer with two perpendicular planes (Figure 14,A).

$$J = C_1 + C_2 = (1/R_1 + 1/R_2) \quad \textbf{(Equation 10)}$$

The Gaussian curvature (K) is the product of both curvatures and depends on the molecular characteristics of the monolayer (Zimmerberg and Kozlov, 2006).

$$K = C_1.C_2 \quad \textbf{(Equation 11)}$$

The spontaneous curvature of a monolayer (J_s) is the curvature that it tends to adopt if there are no other constraints (pressure, protein activity). It depends on the composition of lipids or amphiphiles (X_i=molar ratio of amphiphiles in the membrane) and their corresponding intrinsic molecular curvature (ς_i).

$$J_s = \Sigma X_i \varsigma_i \quad \textbf{(Equation 12)}$$

The concept of intrinsic molecular curvature is very close to the packing parameter defined by the theory of self assembly (Israelachvili et al., 1977). In contrast to the packing parameter, the intrinsic molecular curvature of an amphiphile is measurable. It is identic to the curvature of a monolayer composed of this amphiphile. The spontaneous curvature of this layer would correspond to the intrinsic molecular curvature of the amphiphile (Figure 14,B). We consider that amphiphiles presenting positive intrinsic molecular curvature possess a cone-shape. In other words, the hydrophilic head presents the base of the cone (Israelachvili, 2011). Unfortunately, there is no mutual agreement about the terms cone or inverse cone-shape.

FIGURE 14

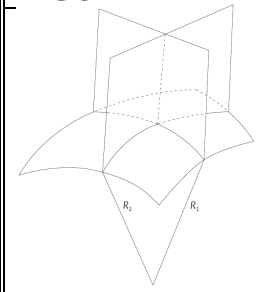

B

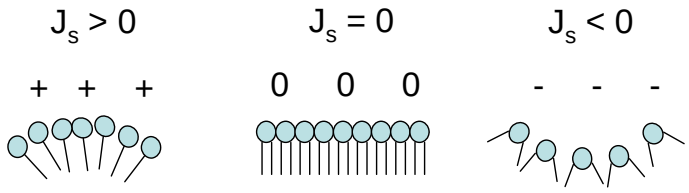

(A) *Total (J) and Gaussian (K) curvature in a point of the membrane*
$J = C_1 + C_2 = (1/R_1 + 1/R_2)$ and $K = C_1.C_2$ (Zimmerberg and Kozlov, 2006)

(B) *Spontaneous curvature in a monolayer*.
Aggregation of cone-shaped amphiphiles promotes positive spontaneous curvature (J_s>0), Cylinder shaped amphiphiles induce no spontaneous curvature (J_s=0) and inverse cone-shaped amphiphiles aggregate into layers of negative spontaneous curvature

2.2.6.2.Bilayers

We have always to keep in mind that a membrane is composed of two monolayers. The induction of positive curvature on one monolayer will have the opposite effect on the other. This is because both monolayers are coupled (Sheetz and Singer, 1974). The shape of a membrane will therefore depend on the spontaneous curvature of the inner and outer monolayer. If we consider a membrane of a vesicle (or a cell) with an outer and inner monolayer of equal bending rigidities (see 2.2.6.1.) we can write:

$$J_S^B = (J_S^{out} - J_S^{in})/2 \quad \textbf{(Equation 13)}$$

where J_S^B is the curvature of the bilayer, J_S^{out} the spontaneous curvature of the outer monolayer and J_S^{in} the spontaneous curvature of the inner layer. The bilayer has a positive curvature when the intrinsic spontaneous curvature of the outer monolayer is larger than that of the inner one (Zimmerberg and Kozlov, 2006).

2.2.7. Mechanical properties of a membrane

If forces are applied on a membrane, resistance against its deformation will raise, due to the elasticity of the membrane. According to Helfrich, there exist three different kinds of membrane elasticity: the shear, the stretching and the bending elasticity (Helfrich, 1973).

The shear elasticity can be in most cases negligible except in membrane-cytoskeleton interactions (Evans and Needham, 1986).

The stretching elasticity opposes the increase or decrease of the membrane surface. It can be quantified by the stretching modulus (Γ) and is approximately 200 mN/m for bilayers. This high value makes the membrane quasi non-compressible and non-stretchable (Meleard et al., 1997;Zimmerberg and Kozlov, 2006).

The third mechanical property of a membrane is its bending resistance (rigidity). This resistance can be quantified by the bending modulus of a membrane (κ_M). In a monolayer, the deviation of curvature from the spontaneous curvature (J-J_S) requires energy. This energy is defined by the Helfrich equation (Helfrich, 1973) for a certain surface area dA,

$$E = \int dA \frac{1}{2} \kappa_m (J - J_S)^2 + \bar{\kappa}_m . K \quad \textbf{(Equation 14)}$$

whereby $\bar{\kappa}_m$ is the Gaussian bending modulus and K the Gaussian curvature. In membranes composed of DMPC and cholesterol, it has been shown, that increasing amounts of cholesterol increase the bending modulus. Normally, values are found in the order of 10^{-19} J (Meleard et al., 1997). The membrane composition influences therefore the rigidity. It depends also strongly on the monolayer thickness (d) ($\kappa_M \sim d^3$) (Zimmerberg and Kozlov, 2006).

2.3. Interactions between membranes and amphiphiles

After having introduced some concepts regarding membrane properties, we will now discuss the general effects that can have amphiphiles on membranes. Interactions between membranes and amphiphiles are numerous and depend on the physico-chemical properties of the amphiphile, its shape, the environment and the membrane itself.

2.3.1. Effect of amphiphiles on membrane dynamics

Many studies treat the effects of amphiphiles (especially surfactants) on membrane order (Schroeder et al., 1998) which depends on the amphiphilic structure, its concentration and on the membrane's composition. We have to be aware that different investigation techniques may show different results regarding the membrane order (see 2.4.5.2.3.).

An interesting study was led by Nazari and coll. who proposed a classification of amphiphiles depending on their perturbing activity on membrane order using DPH anisotropy. They showed that detergents like octyl glycoside, SDS and lauryl maltoside initiated membrane lysis only after reaching a critical amount of disordering. Other types of amphiphiles including lipopeptides and saponins would disrupt the membrane by inducing local effects without general disordering (Nazari et al., 2012).

2.3.2. Induction of membrane curvature by amphiphiles

The induction of membrane curvature in bilayers can be induced by two principal ways.

First, when amphiphiles presenting an intrinsic molecular curvature insert into the outer monolayer, the spontaneous curvature (J_s) of the membrane will be changed because the total composition of one monolayer has changed. The spontaneous curvature of the bilayer depends on the molecular composition of both monolayers (equations 12,13). Cone shaped amphiphiles which insert into the outer monolayer will therefore bend the membrane and induce a positive curvature.

Second, because of the quasi incompressibility of a monolayer, the insertion of high amounts of amphiphiles into the outer monolayer will create an area difference between the outer and inner monolayer (A^{out}-A^{in}), if no flip-flop occurs. This will lead to the bending of the bilayer. The bilayer spontaneous curvature J_S^B created by this asymmetry depends inversely on the monolayer thickness (d).

$$J_S^B = \frac{1}{d}.\frac{A^{out} - A^{in}}{A^{out} + A^{in}} \quad \textbf{(Equation 15)}$$

Normally, the curvature induction produced by the area difference is much more effective than the change of spontaneous curvatures of the monolayers. Hence, when only a small amount of

amphiphiles enters the membrane, and when aggregation of amphiphiles in some spots of the membrane occurs, the contribution of the spontaneous curvature is more important (Zimmerberg and Kozlov, 2006;Sheetz and Singer, 1974).

Beyond these two possibilities of amphiphiles to induce curvature strain in membranes, it is important to be aware about other possible mechanisms. Changes of pH or the ionic force of the solution can influence the size of the headgroup of ionisable phospholipids (or amphiphiles) and therefore change the molecular intrinsic curvature (or the molecular packing parameter). Electrostatic interactions between ionized phospholipids and/or bivalent cations or other charged molecules can also influence the intrinsic curvature of a membrane (Yaghmur et al., 2011;Lewis and McElhaney, 2000). In addition, since an increase in temperature favours trans-gauche isomerizations and increases the molecular volume of the hydrophobic tail of a lipid, this will induces negative curvature in a monolayer (Lafleur et al., 1996).

Large amphiphilic molecules such as peptides or proteins are known to induce curvature strain on the membrane by multiple mechanisms (Riedl et al., 2011;Mizuno et al., 2012). Some proteins are known to regulate membrane curvature in cells. As an example, proteins posseding a BAR-domain (Bin, Amphiphysin, Rvs) wrap around membranes and provide scaffolds for cylindrical curvature. These proteins have a banana shape, coat the membrane and bend it. Amphipathic moities insert between polar headgroups of the membrane and serve as anchors (Zimmerberg and Kozlov, 2006). One other example is dynamin, which is involved in exocytosis by inducing membrane curvature on a GTP (guanisine triphosphate) dependent mechanism (Bashkirov et al., 2008).

2.3.2.1.Bilayer/non-bilayer phase transitions induced by amphiphiles

The changes in spontaneous curvature of a membrane can lead to the formation of a new phase (micellar, hexagonal,…) composed of the amphiphile and membrane lipids or the formation of other curved structures within the membrane such as membrane pores. The induction of positive curvature strain has been associated with the formation of normal phases and the induction of negative curvature with the formation of inverse phases (Van Echteld et al., 1981;Cullis and de Kruijff, 1978). Upon the concentration of the different components (lipids, amphiphiles, solvent), we can establish phase diagrams, which indicate which lipid phase will be observed at a certain amphiphilic/lipid/solvent composition and temperature (Figure 15,A and B)

(Almgren, 2000). An important aspect to consider is the kinetic of the transformation. Metastable structures can coexist with stable phases and their transformation may take several weeks or more, which complicates the construction of a phase diagram (Demana et al., 2004;Almgren, 2000). Another important factor is the ability of the amphiphile to flip from the outer to the inner monolayer. This capacity is reduced if the molecule is charged and the size of the headgroup increased (Sudbrack et al., 2011).

2.3.2.1.1. Transitions due to positive curvature induction

Intensive research has been done regarding the interactions between detergents and membranes (Kragh-Hansen et al., 1998;Lichtenberg et al., 1983). Simple phase diagrams trying to explain the solubilization of lipid vesicles by cone-shaped amphiphiles which do not preferentially interact with one or several lipids have been put forward (Figure 15,A). For a given lipid concentration, there exist an amphiphilic concentration ([amphiphilic]/[lipid] ratio), where solubilization of the vesicle begins ($R_{e(sat)}$). We will observe the formation of mixed micelles composed of lipid and amphiphile molecules. Beyond this ratio, we observe a coexistence of bilayer and micelles until the ratio ($R_{e(sol)}$) where complete transformation of all vesicles into mixed micelles is observed.

FIGURE 15

A

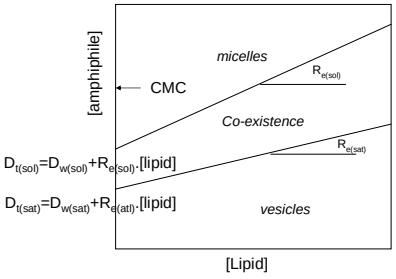

B

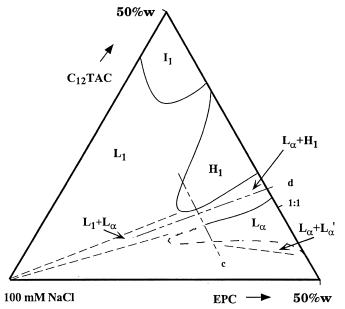

(A) *Binary phase diagram showing the vesicle micelle transition (Lichtenberg et al., 2000).*
(B) *Ternary phase diagram showing the formation of different phases and coexistence of phases at different egg-phosphatidylcholine (EPC), dodecyl-trimethylammonium chloride (C_{12}TAC), NaCl compositions.*
(I_1 = ; L_1 = micellar phase; H_1 = normal hexagonal phase; L_α = liquid crystalline phase; c = NaCl concentration critical for H_1 formation ;d = EPC/C_{12}TAC composition at phase transition between lamellar and hexagonal/micellar phase) (Almgren, 2000)

This simplified model implies that only the ratio between amphiphiles and lipids (the slope of the two straight lines) is important for the phase change (Kragh-Hansen et al., 1998;Lichtenberg et al., 1983). This is not entirely true because the phase behaviour depends also on the absolute concentration of both components and the partition coefficient of the amphiphile (Lichtenberg et al., 2000). The form and temporal stability of the mixed aggregates between surfactant amphiphiles and lipids is very variable. Rod-like, thread-like, lace-like and disk-like aggregates have all been observed along with other phases (Almgren, 2000). The formation of these kind of structures depends on the new molecular arrangements and on the intrinsic curvature of lipids (or packing parameter) and amphiphiles (Stuart and Boekema, 2007).

Formation of the normal H_I phase is observed with mixtures of egg-phosphatidylcholine (EPC) and dodecyl-trimethylammonium chloride (C_{12}TAC) at different salt concentrations and coexistence could be observed at several amphiphiles/lipid ratios (Figure 15,C) (Almgren, 2000). The transformation into normal cubic phases has also been observed. Sometimes vesicles transform first into cubic and later into hexagonal or micellar phases (Van Echteld et al., 1981;Siegel, 1986). Cubic and hexagonal phases are especially induced by amphiphilic peptides (Haney et al., 2010).

The induction of positive curvature on one side on the membrane can also lead to budding and the formation of smaller vesicles (Staneva et al., 2005). In complex biological membrane systems, the transformation depends on the lipid composition and on the presence of proteins (Kragh-Hansen et al., 1998).

2.3.2.1.2. Transitions due to negative curvature induction

The transition mechanisms between lamellar and non-bilayer phases have mainly been focused on the bilayer/H_{II} phase transition. The transition into an H_{II} state has been associated with the induction of negative curvature on the membrane and plays an important role in membrane fusion (Rappolt et al., 2003). This negative curvature can be induced by increasing temperatures (see 2.1.2.3.). If kinetics allow it, the transition may be accompagnied by the formation of a bicontinuus cubic phase (Q_{II}) (Erbes et al., 1996). Coexistence of both lamellar and hexagonal phases has been observed for different systems. The transition is supposed to occur through line defects in the lamellar plane (Siegel and Epand, 1997;Siegel, 1999). A cooperative chain reaction at the transition midpoint was mainly driven by minimizing the

interstitial region and could be explained by the presence of intermediate structures in the membrane (Figure 16) (Rappolt et al., 2003). Typical phospholipids which promote the formation of inverted phases are lipids with negative intrinsic curvature such as ceramides and phosphatidylethanolamines (Kumar, 1991).

FIGURE 16

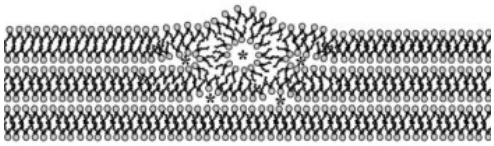

Intermediate between lamellar and hexagonal (H_{II}) phase in a multilamellar vesicle (Rappolt et al., 2003)

2.3.3. Permeabilization of membranes by amphiphiles

Amphiphiles have different ways to permeabilize membranes. It depends mainly on the amphiphilic shape and of its interaction with membrane components. We will summarize the most common mechanisms encountered.

2.3.3.1.Detergent-like mechanism

The detergent like mechanism applies for amphiphiles having a hydrophilic head and a lipophilic tail, displaying positive intrinsic curvature, integrating into the membrane and showing no preferred interaction with one of the membrane constituents. For these amphiphiles, permeabilization of lipid vesicles and erythrocytes occurs often at subsolubilizing concentrations (Ahyayauch et al., 2010;Heerklotz, 2001;Kragh-Hansen et al., 1998). The permeabilization at subsolubilizing concentrations can be due to the formation of nanoscopic transient pores or defects in the membrane. These temporally unstable defects depend on the ability of an amphiphile to diffuse (flip-flop) to the inner monolayer.

If the flip-flop rate of the amphiphile is high (Figure 17,A), the formation of defects would only occur at concentrations where solubilization begins (Sudbrack et al., 2011).
If the flip-flop rate of the amphiphile is low (Figure 17,B), the curvature induced (because of area-asymmetry) between the outer and inner leaflet increases with increasing insertion of the

amphiphile. When a certain amphiphile/lipid ratio is reached, the formation of transient pore is favored. This transient “pore” allows the amphiphile to diffuse from the outer to the inner leaflet and releases the curvature strain (Heerklotz, 2001;Sudbrack et al., 2011).

For some detergents it was shown that the induction of flip-flop, permeabilization and solubilization were different events and occured at different amphiphile/lipid ratios. The model, linking permeabilization to the solubilization of vesicles by amphiphiles cannot explain this behaviour (Ahyayauch et al., 2010).

FIGURE 17

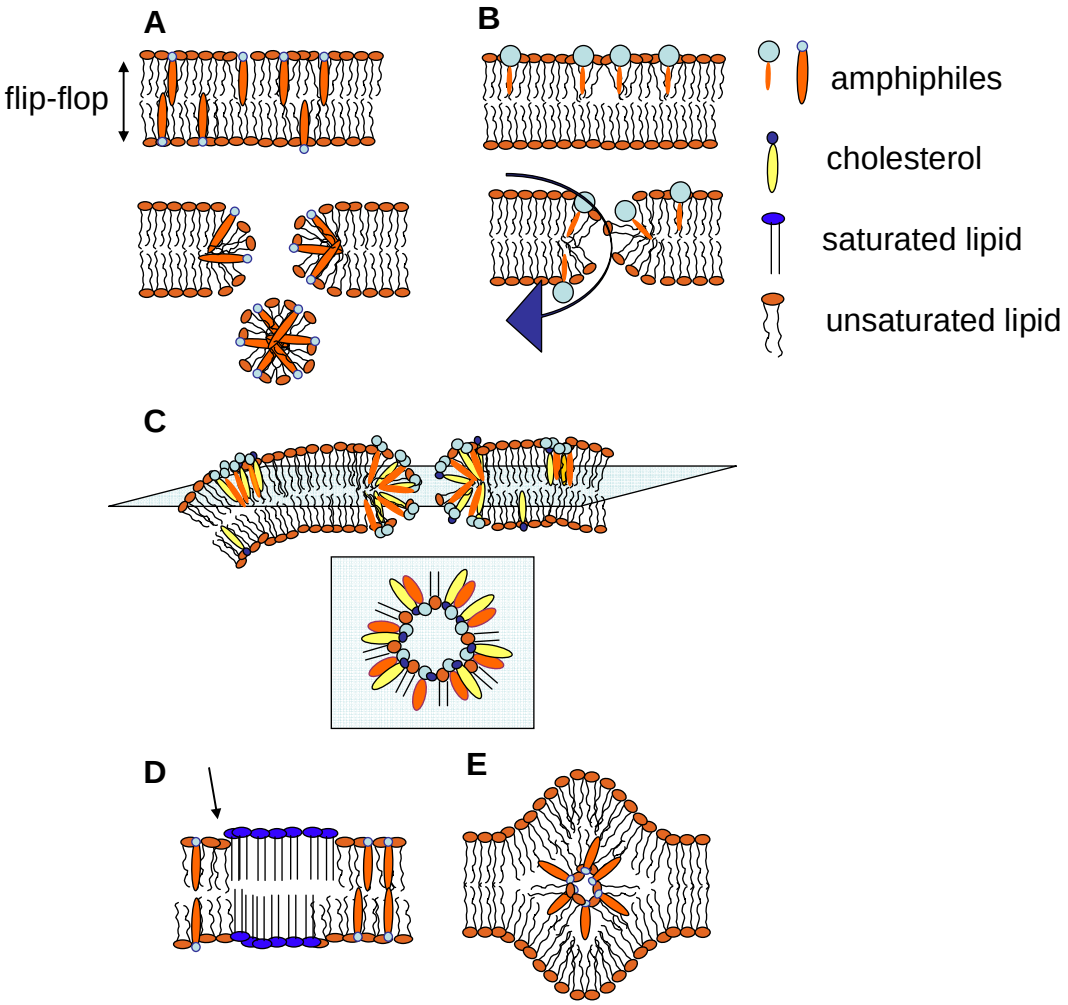

Different models of membrane permeabilization by amphiphiles

(A) Pore formation due to transformation into micelles or other normal structures (solubilization) by detergent with small amphiphilic head and high flip-flop rate (Sudbrack et al., 2011). (B) Transient defects due to the accumulation of an amphiphile with large hydrophilic head on the outer monolayer and subsequent diffusion to the inner monolayer and release of curvature strain (area difference) (Heerklotz, 2001;Sudbrack et al., 2011). (C) Toroidal pore formation due to preferential aggregation with one lipid. Pore showing positive curvature in a transbilayer direction and negative curvature in the membrane plane (Valcarcel et al., 2001). (D) Phase separation due to preferential aggregation of an amphiphile with a lipid. The membrane shows defects at the phase boundaries (arrow) due to packing defects (John et al., 2002). (E) Intermediate structure supposed to exist during the L_α-inverse phase transition and which could increase permeability (Rappolt et al., 2003;Haney et al., 2010).

2.3.3.2.Permeabilization and phase separation

If the amphiphile is able to create domains due to auto-aggregation or aggregation with a membrane component, permeabilization can happen at lower concentrations. This is accompagnied by a lower effect on membrane general order compared to “detergents” showing no preffered interaction for which transition into micelles and permeabilization occurs at the same concentration (see 2.2.3.) (Nazari et al., 2012).

Self-aggregation or aggregation with other lipid components of amphiphiles in 2D monolayers leads to the formation of domains which can be considered as 2D micelles or mixed-micelles respectively (Ruckenstein and Li, 1995;Israelachvili, 2011). This can happen at smaller concentrations than in 3D systems because the CMC at interfaces is generally lower than in the bulk solution (Israelachvili, 2011).

Formation of stable toroidal pores in membranes can be observed when the amphiphile forms separate domains (Figure 17,C) or interacts with one lipid component. Cone-shaped lipids in GUVs and MLVs separated from cylinder shaped lipids and formed stable toroidal pores (Sakuma et al., 2010;Sandstrom et al., 2005). Toroidal pores display positive intrinsic curvature in a transbilayer direction and negative curvature in the direction of a membrane plane (Valcarcel et al., 2001). Stability depends therefore on the amphiphile composition of a pore and on the three dimensional arrangement of the lipids and amphiphiles. It is therefore understandable that the formation of this kind of pore depends very strongly on the lipid composition of the membrane. Cone-shaped amphiphiles which accumulate at the rim of the pore reduce additionally the line-tension and thereby increase the lifetime of a pore considerably. Inverse cone-shaped amphiphiles would increase line tension and inhibit pore formation (Karatekin et al., 2003).

Selective interaction of the amphiphile with one lipid component (Figure 17,D) can lead to phase separation and packing defects. TRITON-X100 showed unfavourable interaction with cholesterol. This led in multicomponent membranes to the separation of palmitoyl-oleanoyl-phosphocholine/TritonX-100 enriched domains from sphingomyelin/cholesterol domains (Tsamaloukas et al., 2006). The formation of domains can induce packing defects at the phase boundaries which would favor increased permeation and lipid diffusion across the membrane (John et al., 2002).

2.3.3.3.Transitions into non-bilayer phases

The solubilization of vesicles can be understood as the transition of a bilayer into another mesophase (mostly micelles). When this transformation is accompagnied by leakage of the inner medium, we have a permeabilization of the vesicle. Permeabilization of vesicles has in general been associated with the transformation into normal phases like the hexagonal (H_I) or cubic (Q_I) phase (Hallock et al., 2003;Teixeira et al., 2012), but the implication of inverse structures should not be excluded. Toroidal pores have also an inverse component in the membrane plane (Figure 17,C) (Prenner et al., 1997).

Permeabilization was mostly observed at concentrations below the phase transitions. This can be due to transient defects induced by the positive curvature strain (see 2.3.3.1.) or intermediate structures (Figure 17,E) created during the phase transitions from bilayer to non bilayer phases (Haney et al., 2010;Prenner et al., 1997).

2.3.3.4.Permeabilizing activity of peptides

Due to their complex structures, peptides can exhibit several mechanisms to permeabilize membranes or form pores. These can be multiple for one type of peptide but can also depend on the membrane. For example, mellitin induced a detergent-like (solubilization) permeabilization in liposomes composed of POPG (Phosphatidyl-oleoyl-phosphatidylglycerol)
but formed stable pores (barrel slave aggregates, Figure 18,A) in POPC vesicles (Phosphatidyl-oleoyl-phosphatidylcholine) (Ladokhin and White, 2001).

All models of permeabilization which have been evoqued for amphiphiles having a lipophilic tail and a hydrophilic head can be applied to peptides having a similar structure (f.ex. lipopeptides). Other types of peptides will not integrate into the bilayer because they are to hydrophilic and the concept that the intrinsic molecular curvature of the amphiphile influences the total membrane curvature cannot be applied. Because we didn’t use such kind of peptides in our study we will only evoke the different permeabilization modes in Figure 18. For further explanations see following reviews (Bechinger and Lohner, 2006;Lohner, 2009;Teixeira et al., 2012).

FIGURE 18

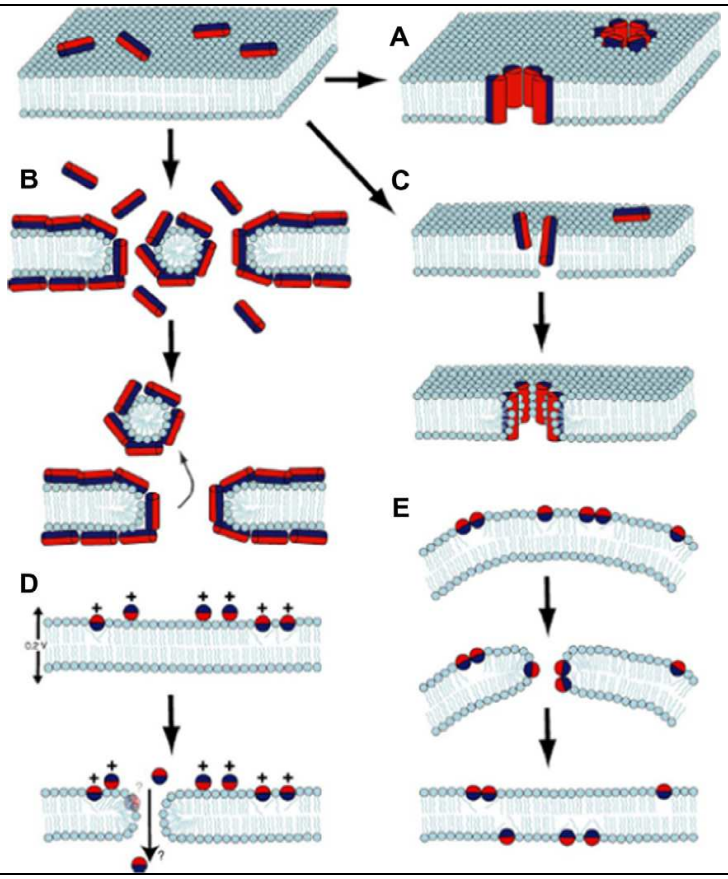

Different models for membrane permeabilization by antimicrobial peptides (Teixeira et al., 2012).

The blue part of the peptide is hydrophobic and the red part of the peptide is hydrophilic.
(A) A barrel slave pore formation, (B) Detergent-like solubilization of the bilayer by the carpet model, (C) the toroidal pore formation, (D) The molecular electroporation model, (E) The sinking raft model

After having reviewed the physico-chemical properties of amphiphiles, lipid membranes and the interaction between amphiphiles and lipid membranes in general, we will focus in the next chapters on main properties of the amphiphilic compounds we selected in this thesis: saponin and α-hederin as well as lipopeptides and surfactin.

2.4. Saponins – amphiphiles of natural origin (article submitted as review)

Saponins originate from plants and some other organisms and have many pharmacological activities (Williams and Gong, 2007). Their name is originated from latin "*sapo*" (soap) and describes the surfactant character and the ability to form foam. A lot of plants containing saponins have therefore been used traditionally as soaps (Bruneton, 2009). Their role in plants is not always clear but they would mainly serve as defensive molecules (Papadopoulou et al., 1999). It has been shown that a lot of saponins are toxic to insects, fish, fungi, bacterias, plants, parasites and mammals (Nielsen et al., 2010;Tadros et al., 2008;Wang et al., 2010;Van Dyck et al., 2011;Okunade et al., 2004;Williams and Gong, 2007;Coleman et al., 2010;Francis et al., 2002). In holothurians and star fish, saponins are repulsive or toxic to predators (Van Dyck et al., 2011;Williams and Gong, 2007).

The term "saponin" is often used in literature and may lead to confusion. It can be used for a specific saponin (for example α-hederin) or it describes a mixture of saponins extracted from a plant. The commercial Merck saponin (saponin pure white, *Saponinum album*) is a crude saponin fraction obtained from roots and rhizomes of *Gypsophyla paniculata* L. Different providers of "saponin" use different plants to extract the saponin fraction and therefore caution has to be taken into account regarding the comparison of results. To prevent confusion we will use the term "saponin®" to designate crude extracts from different providers and the term "saponin" or "saponins" if we refer to one or more different molecules. Quillaja saponins isolated from the *Quillaja saponaria* Molina. bark can be obtained in different degrees of purity. "Quil-A" is a purified aqueous extract of the bark (Myschik et al., 2006;Sun et al., 2009). Other fractions with higher saponin content exist. For example, QS-21 is a fraction of Quil-A, purified by reverse phase chromatography (Pillion et al., 1996). We will refer to all different types of extracts as "Quillaja saponins".

2.4.1. Their amphiphilic structure

Structurally, saponins are amphiphilic compounds composed of one or more hydrophilic sugar parts and a lipophilic steroidal or triterpenic part (sapogenin) (Figure 19). Some substances which are structurally closely related to them such as cardiotonic heterosides or glycoalkaloids are sometimes referred to as saponins and will be treated equally because of their similar structures and effects on membranes. Saponins can be classified into monodesmosidic, bidesmosidic or polydesmosidic saponins, whether they possess one, two or more sugar chains. A large structural variety can be found in nature, due to the presence of different sugars, sugar branchings and sapogenins. The most common sugars are : D-glucose, L-rhamnose, D-galactose, D-glucuronic acid, L-arabinose, D-xylose or D-fucose.

FIGURE 19

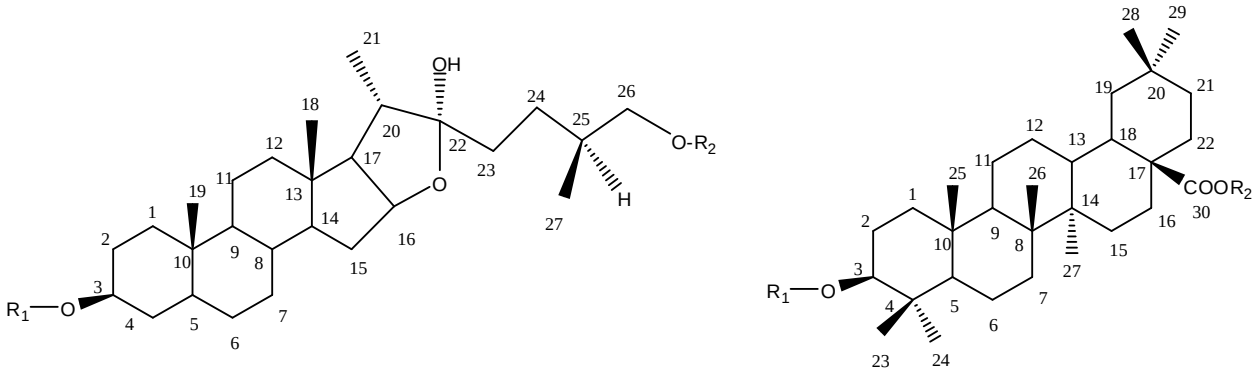

On the left, a steroid pentacyclic saponin (furostanol type) and on the right, a triterpenoid pentacyclic saponin (oleanane type). The saponin will be monodesmosidic or bidesmosidic depending on the number of sugar chains, one or two respectively. R_1 and R_2 are most often ramified sugars, binded via ether or ester link.

2.4.2. Biosynthesis of saponins

Biosynthesis of saponins follows the same pathway than the synthesis of sterols (see 2.2.1.4). The genin is synthesized via the mevalonate route or the pyruvate phosphoglyceraldehyde pathway, an alternative pathway present in plants (Lichtenthaler, 1999). The isoprenoid will further be modified by several enzymes (oxidases, hydroxylases etc.) and

finally a glucosyltransferase will add a sugar moiety via an ether linkage (Bruneton, 2009). For detailed biosynthesis of α-hederin (see 2.5.2.)

2.4.3. Behaviour of saponins at hydrophobic-hydrophilic interfaces

Knowing the structural features of saponins and their amphiphilic character, we will now discuss the physical consequences and the behaviour of these molecules at interfaces.

2.4.3.1.Accumulation at hydrophobic/hydrophilic interfaces

Saponins, like other amphiphiles are able to accumulate at hydrophobic-hydrophilic interfaces and reduce the interfacial tension (see 2.1.). The most common hydrophobic/hydrophilic interface is the air/water interface. The polar sugar part of the saponins makes saponins often soluble in water. According to their solubility, some of them will therefore be dissolved in the solution as monomers and some of them will accumulate at the air/water interface with their hydrophilic part oriented to the water side and their hydrophobic part oriented to the air side (see 2.1.1.). This leads to surfactant activity and the reduction of the surface tension of water. A lot of saponins are known to reduce the surface tension of water (Romussi et al., 1980;Mazzucchelli et al., 2008;Xiong et al., 2008;Pillion et al., 1996;Jian et al., 2011;Bottger et al., 2012). Quillaja saponins were able to build a highly elastic monolayer with its hydrophobic triterpenic part pointing to the air-side (Stanimirova et al., 2011). The effect of saponins on lipid monolayers adsorbed at the air-water interface will be discussed in a later chapter (see 2.4.5.1.).

2.4.3.2.Saponins as surface-active agents

Because of their “biosurfactant” ability, saponins are often used in pharmaceutical, cosmetic or food industry. They are able to stabilize emulsions (emulsifiers) due to their ability to reduce interfacial energy between the different phases (hydrophobic-hydrophilic). Many cosmetics contain saponins as emulsifier (in cremes, lotions, milks…) (Tanaka et al., 1996;Stanimirova et al., 2011). In soaps or shampooings, saponins are used to reduce the surface tension of water and stabilize therefore the formation of foam (Balakrishnan et al., 2006).

Nanosuspensions or –emulsions contain droplets of very small size and which do not exceed 100 nm. They have many interesting pharmacological and pharmaceutical properties. A nanosuspension composed of acetylated aescin was less hemolytic than the original (de Ven et al., 2010). A ginseng based nanoemulsion was able to amplify the immune response towards antigens (Cao et al., 2010).

2.4.4. Formation of amphiphilic aggregates (micelles and other types of nanoscaled objects)

Above their critical micellar concentration (CMC), saponins will form aggregates in solution which stay in equilibrium with monomers whose concentration will not increase further. The complexity of aggregated structures is favored by the number of different amphiphilic species (Israelachvili, 2011). All these structures can be reffered to as nanoobjects as they present a maximum size of 1-100 nm in one or more dimensions. ISCOMS® and micelles are nanoparticles because they are nanoscaled in all three dimensions according to the British standard commission (British standard institute, 2011).

The research on nanoparticles and nanoobjects has become a challenge in pharmaceutical industry and healthcare due to their wide field of applications in cardiovascular diseases, cancer, musculoskeletal, neuro-degenerative and psychiatric disorders, diabetes mellitus and bacterial and viral infections (Raffa et al., 2010). Their shape and chemical composition can be voluntary modified in order to enhance pharmacokinetic and/or -dynamic properties of drugs or imaging agents. They allow the increase of drug concentrations in targeted cells or tissues and thereby enhance efficacy (Schroeder et al., 2012) or reduce toxicity by inhibiting interaction with sensitive tissues (Chu and Sadullah, 2009). Furthermore, an increase of immunogenic responses can also be achieved (Mahapatro and Singh, 2011). The self-aggregating properties of saponins present therefore a most interesting topic and could lead to the formation of completely new nano-objects or -particles.

2.4.4.1.Self-aggregation of saponins

Formation of micelles has been shown for many saponins (Mitra and Dungan, 2001;Sarnthein-Graf and La Mesa, 2004;Balakrishnan et al., 2006;Mitra and Dungan, 2000;Mitra

and Dungan, 1997;Xiong et al., 2008;Bottger et al., 2012;Dai et al., 2013) for example micelles composed of a highly purified fraction of Quillaja saponins have an aggregation number of 65 and form spherical micelles of 3-7 nm of diameter. The CMC increased with temperature and ionic strength and the size of micelles increased with temperature (Sarnthein-Graf and La Mesa, 2004;Mitra and Dungan, 2001;Song et al., 2008;Mitra and Dungan, 2000;Mitra and Dungan, 1997). Other saponins like ginsenoside Ro was able to form vesicles of 30-50 nm and ginsenoside Rb_1 and Rg_1 formed large interaggregate species between micelles because of the hydrophobicity of the sugar chains. Mixtures of saikosaponins and ginsenoside Rb_1 induced the formation of worm-like micelles (Dai et al., 2013).

2.4.4.2.Aggregation of saponins with sterols

2.4.4.2.1. Formation of soluble mixed micelles

Mixed molecular aggregates of finite size and composed of more than one amphiphilic species are mostly mixed micelles. These aggregates are soluble in solution. Some saponins and sterols are known to aggregate and form mixed micelles. *Quillaja* saponins are able to form mixed-micelles with cholesterol and therefore enhance the solubility of the sterol by a factor of 1000. These micelles are bigger in size (10 nm versus 7 nm) than the pure saponin micelles and have a higher aggregation number and CMC. Cholesterol is part of the lipid compartment of the micelle (Mitra and Dungan, 2001;Mitra and Dungan, 2000;Mitra and Dungan, 1997). Demana et al. also observed the formation of worm-like micelles at different saponin/cholesterol proportions (Demana et al., 2004). Saponins of *Saponaria officinalis* L., *Quillaja saponaria* Molina. and *Glycine max* L. are also able to form micelles of rod-, worm- or spherical shape with bile acids (Sidhu and Oakenfull, 1986).

2.4.4.2.2. Formation of insoluble complexes

On the contrary to soluble mixed micelles, insoluble complexes composed of sterols and saponins have also been described. A complex is a molecular entity formed by loose association involving two or more molecular entities (ionic or uncharged). The bonding between components is normally weaker than in a covalent bond. Sterols are able to form water insoluble complexes with digitonin called digitonides. In general, they are stable in ethanol solutions and stability

depends on the sterol structure (Ioffe, 1986;Haslewood, 1947;Haslam and Klyne, 1953). α-tomatine and the α-chaconine/α-solanine mixture were able to form insoluble complexes with sterol. α-tomatine had the ability to form complexes somehow similar to that of digitonides. The formation did not occur with the aglycone tomatidine (Roddick, 1979). Alfalfa saponins (extracted from *Medicago sativa* L.) formed complexes with cholesterol which were dissociable in pyridine (Assa et al., 1973).

2.4.4.2.3. Mixed micelles vs. insoluble complexes

The molecular interactions between components of insoluble complexes and mixed aggregates (micelles) of finite sizes are similar (weak forces). The “solubility” of aggregates depends mainly on their size. If intermolecular forces between both molecules lead to aggregates of infinite size, we will observe a phase separation (precipitation) of the aggregates from the solution (see 2.1.2.1.2.). If the system favors formation of aggregates of finite size and aggregation number, we will observe the formation of mixed micelles. Whether amphiphiles form finite or infinite aggregates depends mainly on the molecular shapes, but the formation of interaggregate species may play an important role towards phase separation (Israelachvili, 2011;Israelachvili, 1976;Israelachvili et al., 1977). The formation of rod-like micelles has been observed with saponins. The polydispersity of such systems is often high because aggregates of different sizes are favored (Israelachvili, 2011). Authors treating with saponin/sterol aggregates should be aware of the nature of the aggregate formed.

2.4.4.2.4. From the formation of saponin/sterol aggregates to the use of saponins as hypocholesterolemiants

Direct interaction of saponins with cholesterol and further complexation or formation of micelles could be interesting for developing drugs against hypercholesterolemia. Hypercholesterolemia increases the risk of cardiovascular diseases. Because of their amphiphilic character, they should be able to influence micelle formation between sterols and bile acids which is necessary to sterol absorption. Digitonin, alfalfa saponins or *Quillaja* saponins (Bruneton, 2009) could form insoluble complexes with cholesterol in the intestinal lumen and therefore reduce cholesterol absorption. *Karaya* root saponins interacted

preferentially with bile salts necessary for micelle formation and reduced therefore cholesterol absorption (Afrose et al., 2009). Some saponins should also be able to transform into phytosterols by hydrolytic enzymes in the lumen. They could therefore act as prodrugs for phytosterols which are well known to reduce cholesterol absorption (Lin et al., 2009;Jones et al., 1997). Tiqueside or pamaqueside would inhibit the active transport of cholesterol from lumen trough the enterocyte brush border membrane (Detmers et al., 2000;Morehouse et al., 1999).

2.4.4.3.Simultaneous aggregation of saponins with sterols and phospholipids

By increasing the number of components of an amphiphilic system, it is possible to obtain large structural varieties of aggregates (nanoobjects or -particles). This is observed when some saponins are incubated simultaneously with phosphatidylcholine and cholesterol. Nanoobjects or -particles appear at special molar ratios and concentrations of the 3 components. The driving forces to obtain these particles are the molecular interactions between these components but their formation depends also on the preparation mode used. Some structures seem to be metastable and transform into other particles after some time (Demana et al., 2007;Demana et al., 2004;Myschik et al., 2006). Repulsive or attractive interactions between aggregates can lead to the formation of ordered nano-structures (Israelachvili, 2011). Because of the multitude of saponins and lipid molecules present in some extracts (especially for *Quillaja* saponins) used to prepare the nanoparticles, it is not always clear which molecules are present in these 3D structures and what are the interactions between them (Demana et al., 2004;Kersten and Crommelin, 1995;Myschik et al., 2006;Ozel et al., 1989;Sun et al., 2009).

2.4.4.3.1. Examples of nanoparticles enhancing immunogenicity, increasing apoptotic responses and decreasing hemolysis

When *Quillaja* saponins, phospholipids and cholesterol are used in different proportions they form multiple types of micelles and nanoparticles: ring-like micelles, worm-like micelles, helices, double-helices, lipid layered structures and ISCOMS® (Figure 20). They can be prepared by the lipid film hydration method (a lipid film is incubated with a saponin solution). Different proportions of reagents used give rise to different nanoparticles (Demana et al., 2007). ISCOMS® are cage-like complexes of 40 nm of diameter. They have a shelf-life of several years

(Hu et al., 2010). Some models have been used to describe the formation of ISCOM. Some seem to derive from multilamellar vesicles (MLV) composed of phospholipids and cholesterol when they are incubated with *Quillaja* saponins. When particles are prepared by the lipid film hydration method, it seems that ring-like micelles aggregate into ISCOMS®. On the other hand, worm-like micelles seem to transform into ring-like micelles. On this basis, Kersten and Crommelin proposed their model for the ISCOM® structure where one building element is equal to one ring-like structure. Helices seem to be formed out of ISCOMS® when they are diluted (Kersten and Crommelin, 1995;Myschik et al., 2006;Demana et al., 2007;Ozel et al., 1989). All structures formed are therefore metastable.

FIGURE 20

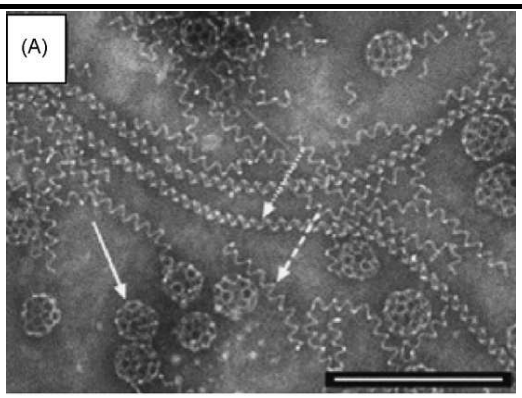

Transmission electron microscopy (negative staining) of cage-like ISCOM matrices (solid arrow), helices (dashed arrow) and double helices (Myschik et al., 2006) (straight line =100 nm)

Modified ISCOMS® (Posintro™) containing DC-Cholesterol (dimethylaminoethane-carbamoyl-cholesterol) in place of cholesterol have a reduced negative particle charge and have been shown to pass through the skin. They could be used to immunize the organism by applying a transdermal patch on the skin (Madsen et al., 2009). Some mannosylated saponins based on oleanolic and glycyrrhizic acids were also able to form nanoparticles. Transmission electron microscopy (TEM) showed the formation of ring-like micelles, rod-like tubular structures, helical and thread-like micelles (Daines et al., 2009). Cucumarioside A2 from marine macrophytes formed tubular nanoparticles (which they called “tubular ISCOMS”) which enhanced immunogenicity by a factor of 4 (Kostetsky et al., 2011). Ginsomes were formed of an ethanol red ginseng root extract incubated with cholesterol and phosphatidylcholine. Spherical

nanoparticles had a diameter of 70-107 nm and were formed of ginsenosides Rb2, Rc, Rb1 and Rd. They were able to enhance the immune response mediated by Th1 and Th2 (Zhang et al., 2012;Song et al., 2009).

Nanoparticles from *Quillaja* saponins induced preferentially apoptosis in cancer cells and less hemolysis compared to the pure extracts (Hu et al., 2010).

2.4.5. Effects on artificial membrane models

We described above how saponins interact with different membrane components in an hydrophilic environment. Membranes provide an amphiphilic environment which can be described by a hydrophobic gradient, which increases from the hydrophilic interfacial domain through the hydrophobic core. The studies of the effects of saponins on artificial membrane models has given a lot of interesting data on how these molecules are able to interact with different membrane components in an amphiphilic environment and give clues about the mechanism of membrane lysis or other types of interactions. Saponins have been tested on different models of different complexity regarding membrane composition and organization.

2.4.5.1.Interaction with supported monolayers

One of the most common ways to investigate the interactions between exogeneous compounds with lipid membranes is to use supported monolayers (Langmuir-Blodget films). A monolayer is a liquid film of water insoluble lipids floating on a water surface pointing their hydrophobic tails to the air side and their hydrophilic heads to the water side (see 2.1.1.). Monolayers are good models to demonstrate integration of saponins and the effect on phase separation or the formation of domains.

2.4.5.1.1. Integration of saponins into monolayers

Some saponins (Table 1) were able to integrate into different types of monolayers when cholesterol was absent (Gogelein and Huby, 1984;Armah et al., 1999;Muhr et al., 1996). In contrast, for α-tomatine, integration into a binary monolayer composed of a saturated phospholipid and cholesterol was only observed in the presence of cholesterol (Stine et al., 2006). This integration was most effective when the hydroxyl function in position 3 of the sterols in the

monolayers was in β (Stine et al., 2006). Surface pressure increased less when pH was low because the protonation of the nitrogen provoques a dissolution in the aqueous phase or a less good integration into the monolayer (Walker et al., 2008). For glycyrrhizin, integration depended upon the surface pressure of the monolayer. Above a critical value (CMC), the saponin accumulated below the monolayer formed (Sakamoto et al., 2013).

2.4.5.1.2. Formation of domains in monolayers containing cholesterol

After integration, formation of domains has been revealed by Brewster angle microscopy in monolayers composed of a binary mixture of a phosphatidylcholine (DMPC) and selected sterols incubated with α-tomatine (Stine et al., 2006;Walker et al., 2008). The authors suggest that these domains are mainly composed of sterol-glycoalkaloid complexes. Domains in monolayers can be considered as 2D micelles but the CMC for domain formation in monolayers would be reduced by a factor of 10 compared to the CMC to form micelles in solution (Ruckenstein and Li, 1995;Israelachvili, 2011). The formation of saponin-sterol aggregates (or even self-aggregation) could therefore be facilitated in a lipid environment.

2.4.5.1.3. Interaction with a raft model

A ternary monolayer raft model composed of DOPC/Palmitoylsphingomyelin/Cholesterol (1:1:1, molar ratio) was used to investigate the effects of glycyrrhizin on macroscopic phase separation. At concentrations below its CMC, glycyrrhizin diminished the size of raft domains. Above the CMC, the appearance of striped regions deprived of phospholipids was observed suggesting the formation of defects in membranes which could be responsible for their permeabilization (Sakamoto et al., 2013).

2.4.5.2.Interaction with bilayer models

Bilayer models are used to mimic the effects of saponins in a biological relevant model (Singer and Nicolson, 1972). Several artificial models of bilayers exist, and saponins have been tested on: supported planar bilayers (SPB), black lipid membranes, liposomes (multilamellar

vesicles [MLV], large unilamellar vesicles [LUV], giant unilamellar vesicles [GUV] and small unilamellar vesicles [SUV]).

2.4.5.2.1. Binding to membranes composed of only phospholipids

Regarding the interaction between saponins and bilayers composed of only phospholipids, a few studies were performed. Digitonin or desglucodigitonin may be bound to membranes by equilibrium binding (no complete integration into the membrane) in membranes composed of only egg yolk phosphatidylcholine (Nishikawa et al., 1984).

2.4.5.2.2. Binding to membranes containing cholesterol

In a model composed of egg yolk phosphatidylcholine and cholesterol, the formation of an equimolar complex would permanently integrate the saponin into the membrane (Nishikawa et al., 1984). A three step model how digitonin binds to membranes containing cholesterol was proposed in a similar model. With increasing digitonin/cholesterol ratio, digitonin and cholesterol would first form “aggregated” species in the membrane. Second, at higher molar ratio, an intermediate complex would be composed of a mixture of equimolecular complexes and aggregated species. Third, an equimolecular complex in the bilayer would be formed (Akiyama et al., 1980). Glycoalkaloids only bound to membranes when cholesterol was present. Results also suggested the formation of an equimolecular complex between sterols and glycoalkaloids (Keukens et al., 1995).

2.4.5.2.3. Effect on dynamic properties and lipid motion

All phospholipids of a membrane are in constant motion (see 2.2.3. and Figure 11). Therefore, by using ^{2}H-NMR, EPR or fluorescence spectroscopy, it is possible to gather information about lipid mobility (order) because these techniques acquire data at different time-scales. Cholesterol has a well known influence on lipid dynamics because of its rigid ring structure (see 2.2.4.). If interaction of saponins with cholesterol in membranes occurs, it should influence the dynamic parameters of a membrane considerably. The saponin itself should also have a significant effect on the membrane without the presence of cholesterol, because the aglycone is mostly composed of a rigid ring structure. In this introduction, we will only mention

studies which have been carried out at temperatures where membranes are in the liquid crystalline state because all mammal membranes are to be considered as “fluid” (Gawrisch, 2005).

When no cholesterol was present in the membranes, a slight reduction of lateral diffusion of fluorescent phosphatidylethanolamine (Armah et al., 1999), an increase of the EPR order parameter of phospholipids (Akiyama et al., 1980;Nishikawa et al., 1984;Fukuda et al., 1987) and a decrease of the ^{2}H-NMR order parameter of marked phospholipids when vesicles have been incubated with different saponins was observed (Akiyama et al., 1980).

In the presence of cholesterol, the anisotropy of fluorescently labeled lipids and the EPR and the ^{2}H-NMR order parameter of labeled phospholipids and cholesterol were generally reduced (Akiyama et al., 1980;Nishikawa et al., 1984).

The differences obtained by EPR or fluorescence spectroscopy and NMR can be explained by the time-scale difference by which the three methods work (Figure 11). EPR and fluorescence spectroscopy work at 10^{-9}-10^{-8} s. On this time-scale we observe especially gauche-trans isomerization (10^{-10}s) and rotational diffusion (10^{-8}s), which are obviously reduced by saponins when no cholesterol is present, and increased by saponins when cholesterol is present. The ordering effect of cholesterol seems to be inhibited by saponins. ^{2}H-NMR works at 10^{-5}s. A reduction of the order parameter means that lipid motions corresponding to correlation times form 10 ns-10 µs are increased independent of the cholesterol content.

2.4.5.2.4. Effect on lateral organization of membrane lipids

Lateral organization of lipids into domains has become a founded concept in cell membrane biology and depends mainly on the presence of sterols in eukaryotic cells (see 2.2.2.2.) (Lingwood and Simons, 2010). Because some saponins are able to form aggregates with cholesterol in 3D and 2D systems (see 2.4.5.1.2. and 2.4.5.2.2.), it seems evident that they act on lateral organization of the membrane. Saponin allowed the solubilization of alkaline phosphatase, a protein known to be present in domains, by Triton X-100 in liposomes enriched with cholesterol but not in liposomes enriched with sphingolipid, which is an indication of cholesterol domain disruption (Schroeder et al., 1998). The cofactor for acrosome reaction-inducing substance (Co-ARIS), a steroidal monodesmosidic saponin, was able to co-localize and provoque expansion of ganglioside-GM1 clusters (Naruse et al., 2010).

2.4.5.2.5. Permeabilizing activity

As previously described, saponins were able to interact with phospholipids and/or cholesterol. In parallel, numerous studies showed that cholesterol is a key factor for membrane permeabilization induced by saponins. For most saponins (Table 1) it was an enhancing or necessary factor for permeabilization (Armah et al., 1999;Li et al., 2005;Gogelein and Huby, 1984;Keukens et al., 1995;Nishikawa et al., 1984). However, for some saponins (Table 1), especially bidesmosides, cholesterol presented an inhibiting or a not necessary factor for membrane permeabilization (Hu et al., 1996;Li et al., 2005). We can therefore assume that different saponins may permeabilize by different ways. Regarding the different mode of action between monodesmosidic and bidesmosidic saponins, the data published can be summarized as follows.

2.4.5.2.5.1.Models of permeabilization by saponins

A first model of permeabilization was established in 1962. Bangham et al. observed the hexagonal structures only in cholesterol containing planar membranes (lecithin/cholesterol) incubated with saponin®. They proposed a micellar arrangement of saponins and cholesterol in the membrane which would lead to the formation of a pore and correspond to the hexagonal structures observed (Figure 21) (Bangham et al., 1962).

FIGURE 21

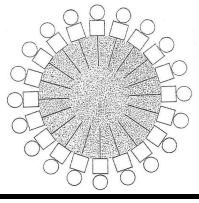

Micellar rearrangement of saponin with cholesterol in the membrane as proposed by Bangham et al. Cholesterol (⬭), saponin (——□). The central speckled area represents the pore
(Bangham et al., 1962)

A model for monodesmosidic glycoalkaloids (presenting sugar residues at C_3) was proposed. Interaction with sterols would lead to equimolecular complexes in the membrane.

When these complexes reach a certain density, hydrophilic interactions between sugars would induce the formation of a stable new lipid phase and the three-dimensional shape of the sterol/glycoalkaloid complex would be determinant for the formation of spherical buds or tubules. The rearangement of the membrane would have as consequence its disruption (Keukens et al., 1995). Tubular aggregates with glycoalkaloids have also been observed by others (Elias et al., 1979).

A different model for avenacin A1, a monodesmosidic triterpenoid saponin, was established (Figure 22) in a POPC:DOPE:Chol model. Hydrophilic interaction between the sugar moieties and interaction with cholesterol would lead first to aggregation of these compounds and further to the formation of pores (Armah et al., 1999).

FIGURE 22

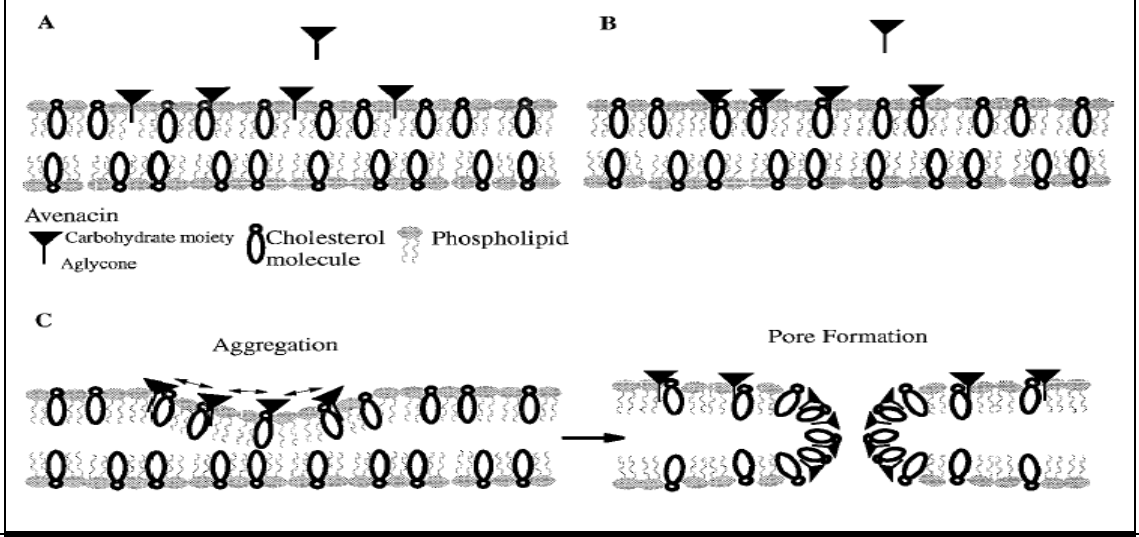

Pore formation by Avenacin A1 proposed by (Armah et al., 1999)

For avicin G, a bidesmosidic saponin, the formed pores showed a certain selectivity regarding the charge of ions and were stable (~1.1 nm). This selectivity was dependent on the phospholipids present in the membranes. Cholesterol was not thought to be necessary for membrane permeabilization, which suggests, that for this saponin, interaction with phospholipids induces pore formation. The hydrophobic side chain of avicin G could probably play an important role in pore formation (Li et al., 2005).

2.4.5.2.5.2.Structure-activity relationships (SAR) studies

It is difficult to establish a structure-activity relationship of the membrane permeabilizing activity of saponins because of their different modes of action (see previous paragraph). Most of SAR studies describe hemolysis and the lytic effect on living cells.

For monodesmosidic saponins, interaction with sterols was crucial for their permeabilizing activity. This was not true for bidesmosidic saponins. It seems also, that for monodesmosidic saponins, a special headgroup in C3 is necessary to induce curvature and consequent pore formation. Regarding the membrane sterol, some SAR studies regarding the important structural features for membrane permeabilization induced by monodesmosidic saponins have been made. Several chemical functions are important for membrane permeabilisation for at least three different monodesmosidic saponins (Table 1). The hydroxyl function at position C3 in beta, the alkene function in C5,6 and the side chain at C17, until a limited number of carbons, enhanced the membrane permeabilizing activity (Keukens et al., 1995;Popov, 2003).

2.4.5.3.From membrane interacting compounds to therapeutic agents

We have seen, that saponins exert various activities on artificial membrane models. Their interaction with membrane dynamics and lateral organization could lead to the activation of membrane receptors or proteins known to be influenced by their lipophilic environment (Legembre et al., 2005;Naruse et al., 2010;Liu et al., 2011).

Cholesterol dependent permeabilization of membranes may be interesting in cancer therapy because some resistant cancers have shown increased amounts of cholesterol in membranes and especially in the outer mitochondrial membrane (see 2.4.8.3.4.1.) (Montero et al., 2008).

SAR studies could lead to the development of saponins which would interact with specific sterols. Ergosterol is mainly present in funghi (Desmond and Gribaldo, 2009). Saponins interacting specifically with this sterol would be good candidates for antimycotic treatment.

Some bidesmosidic saponins would probably be interesting compounds for antibacterial activity as some of them specifically permeabilize membranes without cholesterol and prokaryotic membranes do not contain sterols.

The concentration dependent switch in the permeabilizing ability, which has been observed between aggregated and non-aggregated α-hederin could lead to some interesting molecules which are able to induce phase separation without membrane permeabilization. These molecules could have many interesting effects on biological membranes.

2.4.6. In silico models of saponin/cholesterol and saponin/membrane interactions

In silico models are very interesting approaches to study molecular interactions and effects on membranes. Several studies try to point out the interactions of saponins with sterols (Keukens et al., 1995;Oftedal et al., 2012), whereby other studies focus on saponin membrane interactions (Lin and Wang, 2010).

Dioscin, a monodesmosidic saponin, would bind preferentially to cholesterol in a hydrophobic environment. Extraction of cholesterol from the membrane seems therefore unlikely with dioscin. The most probable interaction was between the hydroxyl of cholesterol and the sugar of dioscin, but a “head to tail” interaction could not be excluded (Lin and Wang, 2010).

Aggregation was most likely by superposing hydrophobic rings of saponin and cholesterol (Keukens et al., 1995;Oftedal et al., 2012). A ternary structure of phospholipids, saponin and cholesterol was suggested for glycoalkaloids (Keukens et al., 1995).

Molecular dynamics simulation showed that dioscin preferentially binds to membrane rafts and increases the curvature of these. This curvature would be the reason for the membrane disruption (Lin and Wang, 2010).

2.4.7. Effects on red blood cells

Taking into account the critical role of cholesterol for membrane permeabilization, red blood cells present an ideal model since they are characterized by a high cholesterol amount in

the plasma membrane (Ashworth and Green, 1966;Heiner et al., 2008). They are further deprived of a nucleus and other organelles and are therefore simpler models than other eukaryotic cells.

Many saponins are known for their hemolytic effect and a high amount of studies regarding the lysis of red blood cells was made (Assa et al., 1973;Arias et al., 2010;Chwalek et al., 2006;Baumann et al., 2000;Hase et al., 1981;Levin and Korenstein, 1991;Lin and Wang, 2010;Meyer Bodansky, 1929;Liu et al., 2002;Muhr et al., 1996;Ponder, 1953;Romussi et al., 1980;Seeman et al., 1973;Segal et al., 1966;Seeman, 1967;Segal et al., 1974;Segal et al., 1977;Segal and Milo-Goldzweig, 1978;Takechi et al., 1992;Takechi and Tanaka, 1995;Takechi et al., 1996;Voutquenne et al., 2002;Gauthier et al., 2009;Wang et al., 2007c;Segal and Milo-Goldzweig, 1975;Segal and Schlosser, 1975).

2.4.7.1.Saponin induced hemolysis

Some issues of saponin induced hemolysis are still unanswered despite the number of studies available. We give here a morphological description of saponin hemolysis and some controversial topics open to discussion.

2.4.7.1.1. Morphological features of hemolysis

Morphological description of saponin induced hemolysis is often lacking, which is a pity because it could give information about saponins activity. Levin and Korenstein described that erythrocytes treated with saponin® transformed into “ghost” cells. These erythrocytes lost their biconcave shape and became spherical. This process could not be reversed by adenosyl triphosphate (ATP) (Levin and Korenstein, 1991). This irreversible transformation of shape, which was not accompanied by important changes in membrane elasticity, could be due to a disturbance of membrane cytoskeleton interactions (Sleep et al., 1999;Baumann et al., 2000). At a nanoscopic level, transmission electron microscopy revealed the presence of long-lasting holes or pits in red blood cells incubated with saponins and the formation of multilamellar stacks, composed of crystallized lipids out of the membrane (Baumann et al., 2000;Shany et al., 1974). Pits were uniformly distributed and possessed a diameter of 4-5 nm. The authors suggest the consequent developpment of bigger “holes” or larger defects (Seeman et al., 1973). Larger pores

would be consistent with the release of proteins from the cytoplasm induced by saponins (Baumann et al., 2000;Seeman, 1967).

2.4.7.1.2. Correlation with surfactant activity

Many studies showed that for some saponins a correlation between their surfactant and hemolytic activities exist (Bottger et al., 2012). Nevertheless, no clear correlation could be established (Romussi et al., 1980;Segal et al., 1966;Hase et al., 1981;Voutquenne et al., 2002), which excludes that hemolysis is driven only by a detergent-like mechanism.

2.4.7.1.3. Aggregation with cholesterol

The importance of cholesterol for hemolysis is subject to discussion. Some studies showed indirectly that saponins aggregate with cholesterol. Several amphipaths would be able to displace cholesterol from phospholipids and therefore increase the hemolytic potency of *Quillaja* saponins (Lange et al., 2009;Lange et al., 2005). Cholesterol was able to inhibit hemolysis when added to the media (Takechi et al., 1992). However, this was not in agreement with studies led by Segal et al. who proposed that cholesterol does not serve as specific binding site for saponins because no clear relationship between cholesterol amount in cells and hemolysis was established (Segal and Milo-Goldzweig, 1978;Segal and Milo-Goldzweig, 1975).

2.4.7.1.4. Activation through membrane glycosidases

Segal et al. found for monodesmosidic saponins containing a glucose residue, that the aglycones had similar hemolytic activity as their corresponding saponin. They concluded that the saponins are firstly cleaved into their sapogenin by glycosidases (glucosidases or galactosidases) before getting effective (Segal et al., 1974). Conversely to these results, some sapogenins (oleanolic acid, gitogenin, hederagenin and others) had no hemolytic effect. In fact, preincubation of red blood cells with sapogenins inhibited even saponin induced hemolysis. Inhibition of saponin induced hemolysis could also be achieved when erythrocytes were preincubated with other non-hemolytic saponins (Chwalek et al., 2006;Gauthier et al., 2009;Wang et al., 2007c;Takechi et al., 1996;Hase et al., 1981).

Some sapogenins are able to disrupt the membrane, but it is not likely that glycosidases are needed to “activate” the hemolytic power of all saponins. It should be kept in mind that for monodesmosidic saponins, the sugar residues were a prerequisite for their permeabilizing activity in model membranes, erythrocytes and cancer cells (Keukens et al., 1995;Chwalek et al., 2006;Gauthier et al., 2009).

2.4.7.1.5. Structure activity relationships

There exist many SAR studies on hemolytic activity of saponins but unfortunately different protocols or different types of erythrocytes are used. So it is tricky to compare the activities of different studies. We summarized some studies which tested a huge number of saponins under the same conditions. Results for monodesmosidic saponins are shown in Figure 23. Some studies comparing the activities of steroid versus triterpenoid saponins showed that steroid saponins induced a faster hemolysis (Takechi and Tanaka, 1995).

FIGURE 23

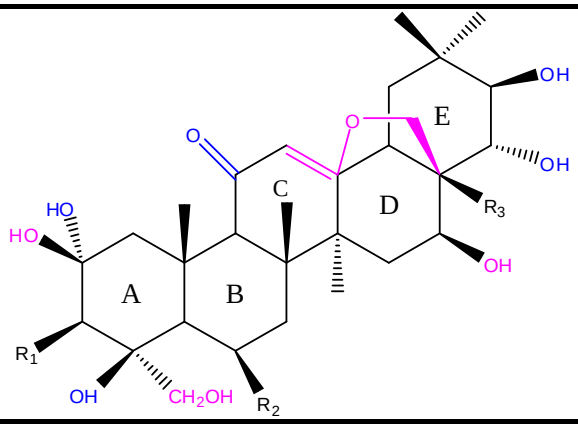

SAR studies on hemolytic activity of monodesmosidic saponins

(Please be aware that some chemical functions exclude the presence of others.)

Magenta : structural features which enhance hemolytic activity

Blue: inhibit hemolytic activity

R_1: Sugars are necessary for hemolytic activity,
The residue (α-L-Rha(1→2)-α-L-Ara) is very active
For some genins, activity rises with number of sugars (n)
Activity changes, when sugar branching changes
If the number of sugars = constant ⇔ α-L-Rha → β-D-Glc (1→2), (1→4) and (1→6) is more active than (1→3)

R_2: Triterpenoid saponins (-OH enhances activity)
Steroid saponins, diosgenin (-OH and alcane chains reduce activity, except -COC_5)

R_3: Triterpenoid saponins (-COOH enhances activity, esterification of COOH also enhances activity)

(Voutquenne et al., 2002;Gauthier et al., 2009;Chwalek et al., 2006;Wang et al., 2007c;Takechi et al., 1996)

Bidesmosidic (residue at C3 and C28) triterpenoid or steroid saponins were in most cases less hemolytic than monodesmosidic saponins, even if the surfactant activity increased (Romussi et al., 1980;Hase et al., 1981;Wang et al., 2007c;Voutquenne et al., 2002). Some general enhancing properties are summarized in Figure 24.

FIGURE 24

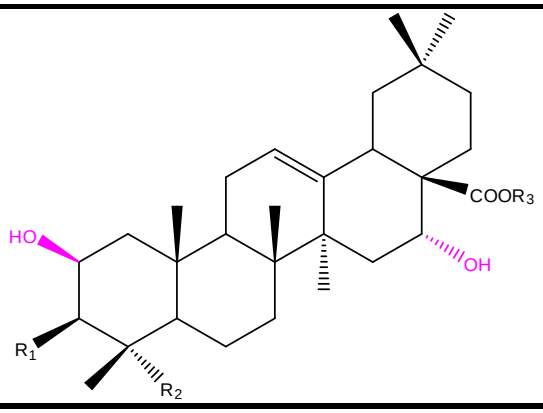

SAR studies on hemolytic activity of bidesmosidic saponins

Magenta : structure features which enhances hemolytic activity
- R1 = at least 1 sugar (needed)
- R2 = COOH, CH_2OH (needed)
- R3 = if 1 sugar ➔ R1 = at least 3 sugars
  Best activity ⇔ 4 sugars and R1 = 1 sugar

(Voutquenne et al., 2002;Wang et al., 2007c)

2.4.7.2.Pharmacological implications of hemolysis

Excessive hemolyis induced by saponins can lead to anemia and further death (Stohlman and Smith, 1934). Saponins can only be used pharmacologically if they don't induce important hemolysis or if they do not pass into the blood stream. The synthesis or research of saponins which are not hemolytic is therefore very challenging. The understanding of the mechanisms involved in saponin hemolysis and implications of molecular structural features can lead to synthesis of compounds which will have a high activity and low toxicity. Gauthier et al. showed that lupane saponins have a very low tendency to induce hemolysis, but an increased ability to induce apoptosis in cancer cells compared to the oleanane type saponins (Gauthier et al., 2009). As seen before (see 2.4.4.3.1.), the formation of saponin nanoparticles can also be an interesting approach to reduce the hemolytic activity of saponins by keeping or increasing their activity towards cancer cells. The effect of saponins on cancer cells will be developed in the next chapter.

2.4.8. Effect on cancer cells

Compared to red blood cells, other eucaryotic cells possess a nucleus and different types of organelles. These cellular compartments are separated from the cytoplasm by membranes which have different compositions in lipids and proteins. The cholesterol content of different organelles is very variable (van Meer, 2005;Wassler et al., 1987) so the activity on eukaryotic cells is much more complex as a saponin could act specifically on a certain type of organelle. As we have shown in (2.4.5.), the effects of saponins are not only restricted to membrane lysis. They can influence the dynamics of the membrane or their lateral organization. All these effects can lead to activation or inhibition of membrane proteins or even cascades which lead to programmed cell death (Chaigne-Delalande et al., 2008;George and Wu, 2012;Legembre et al., 2005;Li et al., 2006;Xu et al., 2009;Park et al., 2010;Yi et al., 2009).

2.4.8.1.Effect on dynamic properties of the membrane

We already discussed the effects of saponins on the dynamic properties of artificial membrane models and the corresponding time-scales of these effects. Cellular membranes of mammals are always in a fluid state (Gawrisch, 2005). Results on membrane dynamics should be therefore comparable to the effect of saponins on artificial membranes in the liquid crystalline (or liquid ordered) state. Furthermore, the modulation of dynamic membrane properties in cells can have multiple effects on membrane proteins and cell metabolism (Kwon et al., 2008;Ishida et al., 1993;Harada, 2005).

The effects of saponins on dynamic properties of artificial membranes often depended on the cholesterol content. As cholesterol content varies a lot between cell types or organelles, modulation of order parameters may vary from one cell type to another. As an example, ginsenoside Rg3 reduced the fluorescence anisotropy of DPH and TMA-DPH only in multidrug resistant cells. This decrease was correlated to a decrease of resistance towards adriamycin (Kwon et al., 2008). Other saponins increased or decreased different order parameters in different cell types independently of their lytic potential (Harada, 2005;Ishida et al., 1993;Ota et al., 1987;Jiang et al., 2010). Ginsenoside Re significantly reduced microviscosity (DPH) in mitochondria isolated from rat brain. This could probably explain its protective effect against

cerebral-ischemia injury as mitochondria play an important role in ROS production and subsequent lipid peroxidation (Zhou et al., 2006).

2.4.8.2.Effect on lateral organization (interaction with rafts)

We have seen that rafts in cell membranes are nanoscopic functional lateral domains (see 2.2.2.2.). Their disruption or aggregation may induce pathways leading to programmed cell death or have other effects (Jacobson et al., 2007;Lingwood and Simons, 2010).

An earlier technique to prove association of proteins with rafts is based on the fact that these domains were resistant to triton X-100 extraction (Lingwood and Simons, 2010). This technique is obsolete because association with detergent resitant membranes might result from an artifact due to the treatment with Triton-X (McMullen et al., 2004). Nevertheless, some saponins were able to render proteins known to be insensible to triton X-100 extraction soluble, meaning that the rafts were disrupted by saponin treatment. This disruption would have various effects on cell membranes like receptor activation or changing ion channel permeability (Ilangumaran and Hoessli, 1998;Heffer-Lauc et al., 2007;Taverna et al., 2004;Nanjundan and Possmayer, 2001;Cerneus et al., 1993;Schroeder et al., 1998;Becher et al., 2001;Sehgal et al., 2002;Zhuang et al., 2002). Using confocal or biphoton microscopy, other studies showed the translocation of some receptors or membrane proteins from rafts or the disruption of rafts upon treatment with different saponins. Ginsenoside Rh2 and Avicin D proved such an effect which would lead to the activation of apoptosis by the extrinsic pathway (Figure 28, blue pathway) (Yi et al., 2009;Xu et al., 2009;Jiang et al., 2010;Park et al., 2010).

2.4.8.3.Cell death induced by saponins

Different kinds of cell death have been induced by saponins including cell lysis, necrosis, apoptosis and autophagy. Cell lysis and necrosis both include the destruction of the plasma membrane. Apoptosis and autophagy are both programmed cell deaths and are induced via various stimuli and executed trough specific pathways. It is of major importance to describe morphological changes and provide biochemical evidence to classify the induced cell deaths by saponins (Galluzzi et al., 2012;Kroemer et al., 2009).

2.4.8.3.1. Morphological features of saponin induced cell death

Ehrlich ascites tumor cells showed various manifestations when treated with different saikosaponins (Figure 25). Only minor changes in the structures provoqued major changes in morphological appearences, which shows that there is not only one process involved (Abe et al., 1981). The main morphological features induced by saponins are (i) the formation of “blebs” (Gao et al., 2011;Abe et al., 1981), which could be classical hallmarks of necrosis and apoptosis (Barros et al., 2003;Kroemer et al., 2009) but could also be direct consequences of saponin membrane interactions (Keukens et al., 1995), (ii) the disappearance of microvilii or other changes of membrane topology like the formation of a granular surface (Mazzucchelli et al., 2008;Sung et al., 1995;Gao et al., 2011;Jian et al., 2011), (iii) the formation of intracellular vesicles (Sung et al., 1995). These vesicles could correspond to autophagic vacuoles, hallmarks of autophagy or to a direct effect on the membrane (King et al., 2009;Ellington et al., 2005).

FIGURE 25

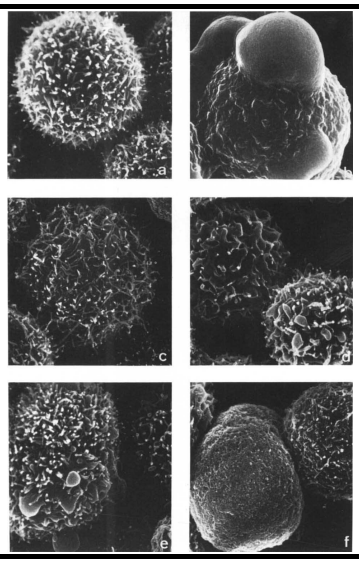

Scanning electron microscopy of Ehrlich ascites tumor cells.
a. Control, b. Cells treated with saikosaponin a (large protrusions: blebs), c. Saikosaponin b1 treated (longer microvilii than in control), d. Coral reef like surface when treated with saikosaponin b2, e. Appearance of blebs and microvilii saikosaponin c, f. Disappearence of microvilii with saikosaponin d.(Abe et al., 1981)

2.4.8.3.2. Cell lysis or necrosis

It is difficult to distinguish between direct permeabilization of the plasma membrane and secondary permeabilization due to necrosis. Necrosis is characterized by the increase of cellular volume, formation of blebs, destruction of the plasma membrane and release of the cytoplasm to the sourrounding environment. It is accompagnied by the activation of Ca^{2+}-dependent enzymes which are able to lyse the cytoskeleton (Figure 28, grey pathway) (Kroemer et al., 2009;Trump and Berezesky, 1995;Barros et al., 2003). Cell lysis or the formation of pores by saponins would also produce osmotic swelling and further rupture of the membrane (Figure 28, magenta pathway). Both cell deaths are interconnected and it is very difficult to say whether one or another is induced. Recently, regulated necrosis or necroptosis has become a widely accepted term. It is characterized by the activation of the kinases RIP1 and RIP2 (receptor interacting protein 1 and 2), which should be investigated to discern between cell deaths (Galluzzi et al., 2012). Unfortunately, effects of saponins on this marker have not yet been published.

Cell lysis provoqued by saponins can be very fast at high saponin concentrations (Mazzucchelli et al., 2008). Electron microscopy revealed the formation of holes larger than 1 µm only after 2 minutes of incubation with 10 µM hederacolchiside A1 (Figure 26). Tof-SIMS analysis of cells revealed no colocalization of cholesterol and hederacolchiside A1 after 2 min of treatment. After 30 min hederacolchiside, phospholipids and cholesterol seemed to aggregate (Mazzucchelli et al., 2008).

FIGURE 26

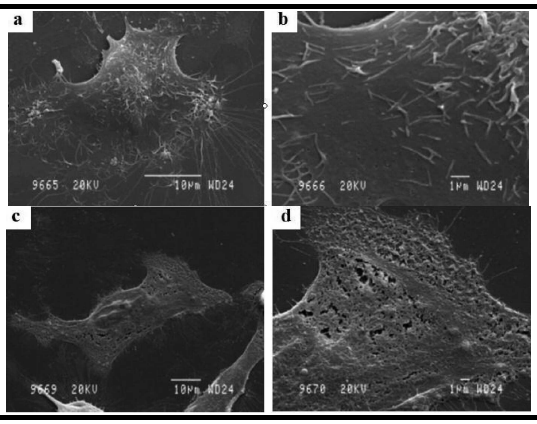

Scanning electron microscopy
Control MEL-5 cells (a,b)
Appearance of holes after 2 min of treatment with hederacolchiside A1 (c,d)
(Mazzucchelli et al., 2008)

Oleanane type saponins induced the permeation of cancer cells to small hydrophilic molecules like calcein and propidium iodide (Gauthier et al., 2009;Gilabert-Oriol et al., 2013). *Gypsophila* saponins induced pores whose size increased with concentration and time (Wassler et al., 1987) or pores large enough to induce fast release of LDH or other proteins (Mazzucchelli et al., 2008;Gerkens et al., 2007;Guan et al., 2011;Wassler et al., 1990). Therefore, saponins are used to permeabilize cellular membranes for immunohistochemistry of intracellular proteins (Ohsaki et al., 2005;Verdier et al., 2000;Mazzucchelli et al., 2008). AFM allowed to vizualize pores induced by saponin® in fibroblasts (Figure 27) (Lee et al., 2006). An increase of permeability to larger molecules was observed when tetrandine (a bisbenzylisoquinoleine) was coincubated with *Quillaja* saponins. This enhancement was not observed with digitonin nor ginseng saponins, so we can suppose that tetrandrine interacts specifically with the pore formed by *Quillaja* saponin (Leung et al., 1997).

FIGURE 27

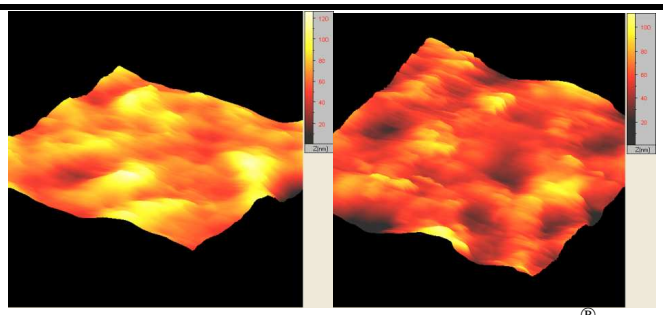

Control Treated with saponin®

Membrane surface of fibroblasts (AFM)
(Lee et al., 2006)

2.4.8.3.3. Lysis of cell organelles

Saponins showed some specificity regarding lysis of different organelles. Brain microsomes derived from plasma membrane treated with saponin® showed ring-like micellar structures. It was not observed in cardiac sarcoplasmic reticulum. Microsomes derived from the endoplasmic reticulum were more resistant to saponin® lysis than vesicles derived from plasma membranes (Inamitsu and Ohtsuki, 1984). In muscle cells, β-escin and saponin® were able to permeabilize the traverse tubular system (Launikonis and Stephenson, 1999). Avicins were able to perforate the outer mitochondrial membrane and so to induce the release of cytochrome c. This would lead to an inhibition of respiration and the induction of apoptosis (Lemeshko et al., 2006).

The susceptibility of different organelles to *Gypsophila* saponins could be correlated to the cholesterol/phospholipid ratio of their membranes. The order of sensitivity to permeabilization was the plasma membrane > the lysosomal membrane > the golgi membrane > the outer mitochondrial membrane > the inner mitochondrial membrane > the endoplasmic reticulum (parallel with cholesterol content) (Wassler et al., 1987).

2.4.8.3.4. Apoptosis

Morphologically, apoptosis will lead to the condensation of chromatin, fragmentation of the nucleus, formation of membrane blebs and apoptotic bodies (Barros et al., 2003;Kroemer et al., 2009). Apoptosis is mediated by two major pathways, the intrinsic and the extrinsic pathway (Jin and El Deiry, 2005). Many saponins were able to induce apoptosis (Zhang et al., 2007;Zhang

et al., 2008;Yi et al., 2009;Xu et al., 2007;Xu et al., 2009;Xiao et al., 2009;Xiao et al., 2007a;Xiao et al., 2007b;Wang et al., 2006;Tin et al., 2007;Swamy and Huat, 2003;Shin et al., 2009;Raju and Bird, 2007;Niu et al., 2008;Park et al., 2010;Liu et al., 2009;Liu et al., 2007;Lin et al., 2008;Li et al., 2006;Li et al., 2005;Lemeshko et al., 2006;Lee et al., 2009;Kumar et al., 2009;King et al., 2009;Kim et al., 2008b;Kim et al., 2008a;Kim et al., 2009;Jin et al., 2009;Jeong et al., 2008;Ham et al., 2006;Guo et al., 2009;Gerkens et al., 2007;Choi et al., 2008;Cheng et al., 2006). The description of each pathway would pass the limits of this work. However, we wanted to point out studies where apoptosis is in direct relationship with membrane interaction.

2.4.8.3.4.1.The intrinsic pathway

The intrinsic pathway depends primary on the disruption of the external mitochondrial membrane and the release of proapoptotic proteins present in the intermembrane space. This can be achieved by permeabilization of the outer mitochondrial membrane (OMM). The external mitochondrial membrane presents a high content in cholesterol on the contrary to the internal membrane which lacks cholesterol. Some avicins were shown to induce the intrinsic pathway most probably by direct pore formation of the OMM (Figure 28, green pathway) (Lemeshko et al., 2006;Li et al., 2005;Haridas et al., 2007). Reactive oxygen species (ROS) and Ca^{2+} are able to activate the mitochondrial permeability transition pore (MPT-pore). This also leads to the release of proapoptotic proteins into the cytoplasm (Kowaltowski et al., 1996;Hunter and Haworth, 1979a;Hunter and Haworth, 1979b;Haworth and Hunter, 1979). α-Hederin and macranthoside B provoqued the increase of cytosolic ROS species and extracellular Ca^{2+}-influx which led to apoptosis (Choi et al., 2008;Swamy and Huat, 2003;Guan et al., 2011). ROS production can also be a consequence of a direct activity on the mitochondrial membrane and acts as amplificator of apoptosis (Wang et al., 2007a).

2.4.8.3.4.2.The extrinsic pathway

The extrinsic pathway is activated by membrane death receptors (Dickens et al., 2012). Death receptors are present in lipid rafts (George and Wu, 2012). Disorganization of these rafts can therefore lead to activation of membrane death receptors, which has been proven for Avicin D

and ginsenoside Rh2 (Figure 28, blue pathway) (Xu et al., 2009;Yi et al., 2009;Jiang et al., 2010;Park et al., 2010).

FIGURE 28

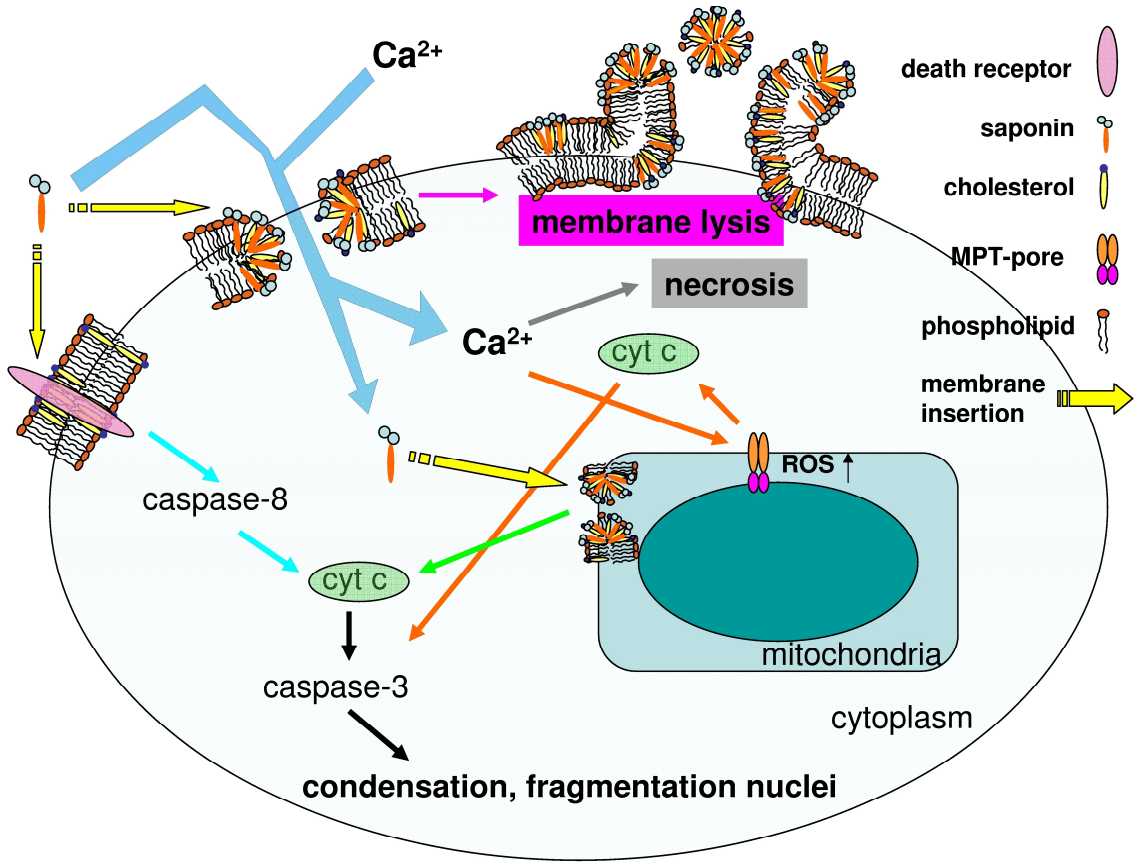

Pathways of known saponin induced cancer cell membrane lysis, necrosis and apoptosis in relation with their membrane activity
Magenta pathway: membrane lysis induced by direct pore formation of the membrane. (Mazzucchelli et al., 2008;Gerkens et al., 2007;Guan et al., 2011;Ohsaki et al., 2005;Wassler et al., 1990;Gauthier et al., 2009;Verdier et al., 2000;Gilabert-Oriol et al., 2013).
Grey pathway: necrosis induced by increased Ca^{2+} influx (Trump and Berezesky, 1995).
Green pathway: apoptosis induced by direct permeabilization of the outer mitochondrial membrane (Lemeshko et al., 2006;Li et al., 2005;Haridas et al., 2007).
Orange pathway: apoptosis induced by the increase of intracellular calcium, ROS production and the triggering of the mitochondrial permeability transition (MPT) (Choi et al., 2008;Swamy and Huat, 2003).
Blue pathway: apoptosis induced by the activity on rafts and activation of death receptors (Xu et al., 2009;Yi et al., 2009;Jiang et al., 2010;Park et al., 2010).

2.4.8.3.5. Autophagy

Autophagic cell death is accompanied by cytoplasmic vacuolization which leads the cell to its autodigestion. Some major proteins involved are beclin 1, ATG5 or LC3. The latest meeting of the committee of classification of cell death stated that inhibition of at least 2 of these essential proteins is needed to prove autophagic cell death because autophagy would be mainly a cell protecting mechanism (Galluzzi et al., 2012). Saponin® can cause formation of structures which ressembled GFP-LC3 puncta (a hallmark of autophagy) in HeLa cells. Puncta formation was not due to autophagy but protein aggregation and presented an artifact. Puncta are obviously not a good hallmark for saponin induced autophagy (Ciechomska and Tolkovsky, 2007).
Autophagy was induced by some saponins (Table 1) as a protective mechanism towards apoptosis (Sy et al., 2008;Ko et al., 2009). Avicin D on the contrary induced autophagic cell death when apoptosis was inhibited (Xu et al., 2007).

2.4.8.3.6. Cancer treatment by saponins

Some saponins could be suitable candidates for cancer treatment research because they are specifically cytotoxic towards cancer cells (King et al., 2009;Swamy and Huat, 2003;Man et al., 2010).

As we have seen, the formation of saponin containing nanoparticles can enhance the selectivity towards cancer cells and reduce their hemolytic potential. This couls lead to an increased therapeutic index (Hu et al., 2010).

Another advantage is that several saponins induce cell death via multiple mechanisms (apoptosis, necrosis, membrane lysis or autophagic cell death) and pathways (ROS, activity on organelles, mitochondrial outer membrane permeabilization [MOMP]). This could prevent the occurrence of resistances and increase efficiency of treatment.

Membrane cholesterol is known to be largely involved in cancer progression and resistance (Montero et al., 2008;Patra, 2008). Cholesterol rafts are known to promote cancer and cholesterol enrichment in mitochondria leads to chemotherapeutic resistance (Montero et al., 2008). The specific interaction of some saponins with cholesterol and the disruption of lipid rafts led to apoptosis in cancer cells (Gajate and Mollinedo, 2011;Patra, 2008;Yi et al., 2009).

It has also been shown for ginsenosides and other saponins, that they are able to reduce the cell growth by inhibiting proteins involved in the cell cycle (cyclins or cyclin dependent kinases) or inhibit other important cancer promoting pathways (Nag et al., 2012). Saponins could be therefore ideal candidates to act on resistant cancer cells and to reduce resistance toward other therapeutic agents.

2.4.9. Conclusions on saponin activities on membrane models

We put together studies using several techniques to analyse different aspects of saponins.

Their amphiphilic character gives them the ability to self aggregate, reduce the interfacial tension between phases and stabilize emulsions or foams.

They are also able to interact with other amphiphilic molecules like phospholipids and cholesterol. This can lead to the formation of micelles or other nanoobjects, which could be used in vaccination or cancer therapy.

Interaction with membrane components of bilayers has enormous repercussions on cell homeostasis. Saponins can activate membrane receptors via changes of membrane dynamics or interaction with membrane rafts, rich in cholesterol. The modulation of protein activity by saponins could lead to the development of interesting compounds with various pharmacological activities.

The interaction with cholesterol was also very important for pore formation in several membrane models, especially for monodesmosides with a sugar chain in C_3. Some bidesmosides were able to permeabilize membranes independently of cholesterol which suggests that their mechanism is different.

Hence, cell death induced by saponins is very complex and several mechanisms can be induced simultaneously. Besides direct pore formation, apoptosis and autophagy play an important role. Permeabilization of organelles might also play a crucial role for saponin induced cell death.

Saponins which were able to permeabilize membrane models were usually hemolytic and also active on cancer cells. The artificial membrane models used showed that the basic lytic activity does not depend on membrane proteins even if it is not excluded that activity can be enhanced or inhibited.

But not only interactions of saponins with membranes are responsible for cell death. For example, several saponins have shown specific activity on proteins involved in the cell cycle (Guo et al., 2009).

All in one, saponins have unique activities and properties which could be very useful in the development of future therapeutic agents.

Table 1 : Physico-chemical activities of saponins and interaction with membranes

Model	Effect	Techniques	Type of interaction	Cholesterol presence in model	Consequences	Cholesterol dependency	Saponin	References
Hydrophobic / hydrophilic interfaces	Adsorption at air-water interface	Tensiometry	Saponin/air-water surface	No	Reduction of surface tension of water, foam forming ability	No	Soyasaponins, Anchusosides, Glycyrrhizin, Digitonin, Hederacolchiside, α-hederin, Hederacoside C β-escin, Ginsenoside RG2, Glycyrrhizinic acid, Primulic acid	(Romussi et al., 1980;Mazzucchelli et al., 2008;Bottger et al., 2012;Xiong et al., 2008;Pillion et al., 1996;Jian et al., 2011)
	Adsorption at other interfaces	Tensiometry, viscosity measurements, miscibility tests, quasi-elasitc light scattering	Saponin/interface	No	Reduction of interfacial tension, stabilization of emulsions or suspensions	No	*Quillaja* saponins, *Yucca* saponins, Ginsenosides, Acetylated aescin, Extract of *Sapindus mukorossi*	(Tanaka et al., 1996;Cao et al., 2010;Stanimirova et al., 2011;de Ven et al., 2010;Balakrishnan et al., 2006)

Aqueous solution	Self-aggregation	DLS, tensiometry, solubilization of fluorescent probes, NMR, TEM, dielectric permittivity	Saponin/saponin	No	Formation of spherical micelles or other types of amphiphilic aggregates	No	*Quillaja* saponins, Digitonin, Hederacolchiside, α-hederin, Hederacoside C, β-escin, Ginsenoside Ro, Rg2, Rb1, Rg1 Glycyrrhizinic acid, Primulic acid	(Balakrishnan et al., 2006;Sarnthein-Graf and La Mesa, 2004;Mitra and Dungan, 2001;Mitra and Dungan, 2000;Mitra and Dungan, 1997;Xiong et al., 2008;Bottger et al., 2012;Dai et al., 2013)
	Aggregation with cholesterol	DLS, tensiometry, TEM	Saponin/Cholesterol	Yes	Formation of soluble mixed micelles or other types of aggregates (composed of cholesterol and saponins)	Yes	*Quillaja* saponins	(Demana et al., 2004;Mitra and Dungan, 2001;Mitra and Dungan, 2000;Mitra and Dungan, 1997;Sidhu and Oakenfull, 1986)
		Observation, light microscopy, TEM, solubility product, stoichiometric reaction	Saponin/Cholesterol	Yes	Formation of insoluble cholesterol/saponin complexes	Yes	Digitonin, α-tomatine, α-chaconine Alfalfa saponins	(Ioffe, 1986;Assa et al., 1973;Roddick, 1979;Haslewood, 1947;Haslam and Klyne, 1953)

Aqueous solution	Aggregation with cholesterol and phospholipids	TEM	Saponin/phospholipid/cholesterol	Yes	Formation of ISCOMS®	Yes	*Quillaja* saponins	(Kersten and Crommelin, 1995;Myschik et al., 2006;Demana et al., 2007;Ozel et al., 1989;Hu et al., 2010)
		TEM	Saponin/phospholipid/cholesterol		Formation of ginsomes	Yes	Ginsenosides Rb2, Rc, Rb1, Rd	(Song et al., 2009)
		TEM	Saponin/phospholipid/cholesterol		Formation of "tubular ISCOMs"	Yes	Cucumarioside A2	(Kostetsky et al., 2011)
		TEM	Saponin/phospholipid/cholesterol		Ring-like micelles, rod-like tubular structures, helical, thread-like micelles	Yes	Mannosylatyed saponins of oleanolic and glycyrrhizic acid	(Daines et al., 2009)
	Aggregation with DC-Cholesterol and phospholipids	TEM,	Saponin/phospholipid/DC-cholesterol	No	Posintro™	No	*Quillaja* saponins	(Madsen et al., 2009)
Monolayers	Binding	Lateral pressure measurements	Saponin/cholesterol	Yes	Increasing lateral pressure	Yes	α-tomatine	(Stine et al., 2006;Walker et al., 2008)
		Lateral pressure and surface tension measurements, fluorescence of avenacin A1	Saponin/Phospholipid	Yes/No	Increasing lateral pressure, reduction of surface tension, Avenacin A1 insertion	No	Digitonin, Merck saponin®, Avenacin A1	(Gogelein and Huby, 1984;Armah et al., 1999;Nishikawa et al., 1984)

Monolayers	Binding	Lateral pressure measurements	Saponin/rafts	Yes	Binding until certain lateral pressure. Above critical value→ accumulation below monolayer (formation of stripes)	?	Glycyrrhizin	(Sakamoto et al., 2013)
	Aggregation of cholesterol and saponin	BAM	Saponin/cholesterol	Yes	Domain formation	Yes	α-tomatine	(Stine et al., 2006;Walker et al., 2008)
	Interaction with rafts	BAM, fluorescence microscopy	Saponin/Cholesterol	Yes	Decrease of raft size below CMC and formation of striped regions above CMC	Yes	Glycyrrhizin	(Sakamoto et al., 2013)
Bilayers	Binding	Binding to LUV	Saponin/phospholipid	Yes/No	Reduction of surface potential/equilibrium binding	No	Digitonin, desglucodigitonin	(Nishikawa et al., 1984)
		Binding to LUV, HPLC	Saponin/Cholesterol	Yes/No	Cholesterol dependent binding	Yes	α-tomatine/ α-chaconine	(Keukens et al., 1995)
		^{2}H-NMR, scintillation counting	Saponin/cholesterol	Yes	Permanent binding and formation of complexes with cholesterol	Yes	Digitonin, Desglucodigitonin	(Akiyama et al., 1980;Nishikawa et al., 1984)
	Effect on dynamic properties	EPR, fluorescence spectroscopy of order sensitive probes	Saponin/phospholipid	No	Reduction of trans-gauche isomerizations and rotational diffusion	No	Digitonin, Ginsenoside, Avenacin A1	(Akiyama et al., 1980;Fukuda et al., 1987;Armah et al., 1999;Nishikawa et al., 1984)

Bilayers	Effect on dynamic properties	EPR, fluorescence spectroscopy of Laurdan and DPH	Saponin/cholesterol	Yes	Increase of trans-gauche isomerizations and rotational diffusion	Yes	Digitonin	(Akiyama et al., 1980;Nishikawa et al., 1984)
		^{2}H-NMR	Saponin/cholesterol	Yes/No	Increase of motions in the µs timescale	No	Ginsenoside, Digitonin	(Akiyama et al., 1980;Fukuda et al., 1987)
	Effect on lateral organization	AFM	Saponin/Cholesterol-Ganglioside	Yes/No	Co-localization with ganglioside GM1-clusters and expansion of clusters	Yes	Co-ARIS	(Naruse et al., 2010)
	Permeabilization/ Pore formation	Electron microscopy	Saponin/Cholesterol	Yes/No	Micellar arrangement of saponins and cholesterol in membrane	Yes	Saponin®	(Bangham et al., 1962)
		Freeze-fracturing, release of fluorescent probes, SAR, ^{31}P-NMR, HPLC, molecular modeling	Saponin/sterol/phospholipid	Yes/No	Permeabilization, spherical and tubular budding due to formation of irreversible glycoalkaloid/sterol matrix	Yes	α-tomatine, α-chaconine, (glycoalkaloids)	(Keukens et al., 1995;Elias et al., 1979)
		Calcein release, QSAR	Saponin/Phospholipid	Yes/No	Cholesterol independent membrane disruption	No	Bidesmosidic triterpenoid saponins	(Hu et al., 1996)
		Conductivity measurements, FRAP	Saponin/cholesterol	Yes/No	Pore formation due to hydrophilic sugar interactions	Yes	Avenacin A1	(Armah et al., 1999)

Bilayers	Permeabilization/ Pore formation	Conductance measurements, molecular modeling	Saponin/Cholesterol/phospholipid	Yes/No	Pore formation due to interaction with phospholipids and importance of the side chain of Avicin D and G	Yes (avicin G), No (Avicin D)	Bidesmosides (Avicin G, Avicin D)	(Li et al., 2005)
In Silico	Cholesterol/saponin/phospholipid interaction	Molecular modeling	Saponin/ Cholesterol	Yes	Most probably head to head binding	Yes	Dioscin	(Lin and Wang, 2010)
			Saponin/Cholesterol/Phospholipid	Yes	Possible ternary complex	Yes	Glycoalkaloids	(Keukens et al., 1995;Oftedal et al., 2012)
	Pore formation in bilayer	Molecular dynamics simulation	Saponin/Cholesterol/phospholipid	Yes	Induction of curvature in rafts	Yes	Dioscin	(Lin and Wang, 2010)
Effect on red blood cells	Hemolysis	TEM, freeze-fracture EM, ferritin labeling, Hemoglobin release	Saponin/ ?	Yes	Increasing defects, protein release	?	Merck pure saponin, Alfalfa saponins	(Seeman et al., 1973;Shany et al., 1974;Baumann et al., 2000;Seeman, 1967)
		Hemoglobin release, Tensiometry	Surfactant activity	Yes	No clear correlation between surfactant and hemolytic activity	?	Monodesmosides and Bidesmosides	(Romussi et al., 1980;Segal et al., 1966;Hase et al., 1981;Voutquenne et al., 2002;Bottger et al., 2012)

Effect on red blood cells	Hemolysis	Amphipaths cholesterol activation, variation of cholesterol content of erythrocytes	Saponin/Cholesterol	Yes	Aggregation with cholesterol leads to hemolytic activity	Yes	*Quillaja* saponins, α-hederin, dioscin, timosaponin A-III, β-escin, saikosaponin d, holotoxin A	(Lange et al., 2009;Takechi et al., 1992;Lange et al., 2005)
		Cholesterol depletion of erythrocytes	Saponin/Cholesterol	Yes	No clear correlation between cholesterol amount and hemolytic activity	No	Digitonin, Styrax saponin A Aescin, Smilagenyl-β-maltoside, Tigogenyl-β-maltoside, Styrax sapogenin-A	(Segal and Milo-Goldzweig, 1978;Segal and Milo-Goldzweig, 1975)
		Microscopy, measurements of membrane fluctuation	Saponin/cytoskeleton-membrane	Yes	ATP independent shape transformation into ghosts	?	Saponin® (pure white)	(Sleep et al., 1999;Levin and Korenstein, 1991;Baumann et al., 2000)
		Inhibitors of glycosidases, saponin extraction from lysed cells	Saponin/membrane glycosidases	Yes	Hydrolysis of saponin into sapogenin by contact with erythrocytes	No	Digitonin, Tomatin, Solanin, Styrax saponin-B, Glycyrrhizin	(Segal et al., 1974;Segal and Milo-Goldzweig, 1975)
Effect on cancer cells	Effect on dynamic properties	Fluorescence anisotropy DPH, TMA-DPH	Saponin/?	Yes	Decrease of resistance toward adriamycin in multidrug resistant cells	?	Ginsenoside Rg3	(Kwon et al., 2008)

Effect on cancer cells		DPH fluorescence anisotropy	Saponin/?	Yes	Reduced microviscosity in mitochondria	?	Ginsenoside Re	(Zhou et al., 2006)
	Effect on lateral organization	Sensibility of rafts to Triton X-100 extraction	Saponin/cholesterol	Yes	Disruption of domains containing cholesterol/redistribution of raft associated proteins	Yes	Saponin®, Digitonin, Saponin (Sigma)	(Ilangumaran and Hoessli, 1998;Heffer-Lauc et al., 2007;Tavernna et al., 2004;Nanjundan and Possmayer, 2001;Cerneus et al., 1993;Schroeder et al., 1998;Becher et al., 2001;Sehgal et al., 2002;Zhuang et al., 2002)
		Confocal microscopy	Domain (raft) interaction	Yes	Caspase-8 Activation	Yes	Ginsenoside Rh2, Avicin D	(Yi et al., 2009;Xu et al., 2009;Jiang et al., 2010;Park et al., 2010)
		Fluorescence microscopy, scintillation of radiolabeled saponin	Co-ARIS/Cholesterol	Yes	Change in domain (raft) structure and composition, induction of acrosome receptor	Yes	Co-ARIS (monodesmosidic steroid)	(Naruse et al., 2010)

Effect on cancer cells	Necrosis/Lysis	Cell death assays, calcein-AM release, light and electron microscopy, flow cytometry, LDH release, PI influx	Saponin/plasma membrane	Yes	Necrosis like cell death	Yes	Oleanane type monodesmosidic saponins, macranthoside B, digitonin, *Quillaja* saponins, *Gypsophila* saponins	(Gauthier et al., 2009;Mazzucchelli et al., 2008;Guan et al., 2011;Verdier et al., 2000;Leung et al., 1997;Ohsaki et al., 2005;Gerkens et al., 2007;Lee et al., 2006;Wassler et al., 1987;Wassler et al., 1990;Gilabert-Oriol et al., 2013)
		Detection of mitochondrial permeabilization, isolation of mitochondria	Saponin/ outer mitochondrial membrane	Yes	Outer mitochondrial membrane, ER, traverse tubular system	Yes	Avicins, saponin®, β-escin	(Lemeshko et al., 2006;Inamitsu and Ohtsuki, 1984;Launikonis and Stephenson, 1999)
		Differential centrifugation, enzyme markers	Saponin/organelles	Yes/No	Lysis of organelles increases with cholesterol content	Yes	*Gypsophila* saponin	(Wassler et al., 1987)

Effect on cancer cells	Apoptosis	Markers intrinsic apoptotic pathway (release proapoptotic proteins,…)	Saponin/mitochondria	Yes	Activation mitochondrial pathway (intrinsic)	?	Avicins	(Li et al., 2005;Haridas et al., 2007;Lemeshko et al., 2006)
		Extracellular calcium influx (Ca^{2+}), ROS activation	Saponin/ plasmatic membrane	Yes	Permeabilization plasma membrane, activation mitochondrial pathway (intrinsic)	Yes	α-hederin, macranthoside B	(Choi et al., 2008;Swamy and Huat, 2003;Guan et al., 2011;Danloy et al., 1994)
		Markers extrinsic apoptotic pathway, caspase-8 activation, Fas activation, raft desorganization	Saponin/rafts	Yes	Activation death receptor pathway (extrinsic)	Yes/No	Ginsenoside Rh2, Avicin D	(Yi et al., 2009;Jiang et al., 2010;Xu et al., 2009;Park et al., 2010)
	Autophagy	LC3-I→LC3-II transformation, autophagic vacuoles	Saponin / ?	Yes	Protection towards apoptosis	?	Timosapopnin AIII, Ginsenoside Rk1	(Sy et al., 2008;Ko et al., 2009)
		LC3-I→LC3-II transformation, autophagic vacuoles, Atg5, Atg 7 activation	Saponin / ?	Yes	Activation of autophagy, when apoptosis is inhibited	?	Avicin D	(Xu et al., 2007)

2.5. The monodesmosidic triterpenoid saponin α-hederin

The interesting properties of saponins have led us to the investigation of the monodesmosidic saponin α-hederin, which has shown interesting activities towards cancer cells (Choi et al., 2008). α-Hederin or Kalopanaxsaponin A was first isolated from the leaves of common ivy or *Hedera helix* L. (Araliaceae) (Figure 30,A) along with its aglycone hederagenin (van der Haar, 1912). It has been further isolated in the seeds of *Nigella sativa* L. (Kumara and Huat, 2001), the stem of *Clematis parviloba* Gardner&Champ. (Yan et al., 2009), the aerial parts of *Clematis tangutica* Korsh. and *Patrinia scabiosaefolia* Fisch. (Kim, 1997;Zhong et al., 2001), the root bark of *Smelophyllum capense* Radlk. (Lavaud et al., 1995) and the bark of *Kalopanax pictus* Nakai. (Sano et al., 1991).

2.5.1. Molecular structure

FIGURE 29

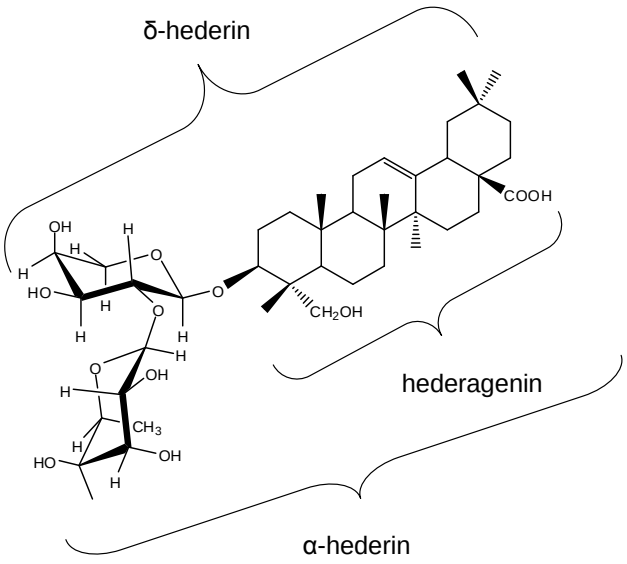

α-Hederin, δ-hederin and hederagenin

2.5.2. Biosynthesis

Biosynthesis of α-hederin is linked to the synthesis of δ-hederin and hederagenin which are its precursors and which lack one or two sugar units. It has been investigated in several plants and especially in *Nigella sativa* (Figure 30,B). The triterpenoid structure of all triterpenoid saponins is biosynthesized before the addition of sugars (see 2.2.1.4., Figure 9). For the synthesis of hederagenin, 2,3-epoxidosqualene is further cyclized by β-amyrin synthethase leading to the formation of β-amyrin (oleanane series), a triterpenoid pentacyclic ring structure. Oxidations of carbons in C23 and C28 lead to the formation of hederagenin. Glycosyltransferases add further the arabinose residue to to the C3 hydroxyl to give δ-hederin and finally the addition of the rhamnose sugar leads to the formation of α-hederin (Scholz et al., 2009;Bruneton, 2009).

FIGURE 30

Common ivy (Hedera Helix L.) (Thome, 1885)

2.5.3. Biological activity

α-Hederin has shown important induction of hemolysis and cytotoxic activity especially towards cancer cells. Cytotoxic activity would be mainly due to the induction of membrane lysis and apoptosis (Swamy and Huat, 2003;Chwalek et al., 2006). The α-L-rhamnopyranosyl-(1→2)-

α-L-arabinopyranose moiety at C3 seems to confer increased cytotoxicity to the molecule compared to similar oleanane type saponins (Jung et al., 2004;Chwalek et al., 2006;Gauthier et al., 2009).

In vivo, it showed antitumor activity and increased the survival in mice affected by colon 26- or 3LL Lewis lung carcinoma, being as effective as cisplatin (Park et al., 2001). The compound would not only have antitumor activity because of its cytotoxicity but would also be an antiproliferative agent (Danloy et al., 1994). Reduction of metalloproteinase-9 m-RNA stability would inhibit the invasion of tissues by cancer cells (Hwang et al., 2012). So, the molecule attacks cancer via different targets, which makes it interesting for the use against resistant cancer cell lines. It also potentiated the cytotoxic activity of antitumor agents like 5-fluorouracil which shows its interest in combined chemotherapy (Bun et al., 2008).

Besides its cytotoxic activity against cancer cells, it was also antimycotic against human pathogenic fungi most probably because of its interaction with the membranes (Moulin-Traffort et al., 1998;Kim et al., 1998).

α-Hederin, δ-hederin and hederagenin showed leishmanicidic activity. Interestingly, hederagenin was the only compound that was active against the amastigote form. The corresponding bidesmoside of α-hederin showed no activity (Majester-Savornin et al., 1991).

At concentrations below its cytotoxic activity, α-hederin (and also hederagenin) was antimutagenic (Lee et al., 2000). It inhibited mutations induced by tobacco derived substances and chemotherapeutic agents like doxorubicin (Amara-Mokrane et al., 1996). This special property in addition to its antioxidant activity (Gulcin et al., 2004) makes it an excellent chemopreventive agent against cancer.

The antioxidant activity combined with the induction of metallothionein (oxygene radicals captor) in hepatic cells, provides hepatoprotective capacities to α-hederin (Kim et al., 2005). α-Hederin also possessed anti-inflammatory properties *in vitro* but the effect was not confirmed *in vivo* (Li et al., 2003;Gepdiremen et al., 2005).

2.6. Lipopeptides

Besides saponins, we also wanted to investigate the activities of peptide based amphiphiles and especially lipopeptides which have a strong amphiphilic character and have been subject to a growing attention in the last years. An interesting subject to the closer investigation of lipopeptides was surfactin, which was easily accessible for our laboratory and has shown interesting activities on cancer cells (see 2.7.).

Two main classes of lipopeptides exist. Cyclic and linear lipopeptides. Both classes have been isolated from bacteria and fungi (Mandal et al., 2013).

Because we will study the effect of surfactin, a cyclic lipopeptide extracted from *Bacillus subtilis*, we will only focus on cyclic lipopeptides. These amphiphilic compounds have been found in marine cyanobacterias and other prokaryotes but especially in the *Bacillus* and *Pseudomonas* species (Smyth et al., 2010;Jokela et al., 2012;Desai and Banat, 1997). They can't be found in higher eukaryotes because they do not have the necessary enzymatic machinery to produce them. The most popular lipopeptides are daptomycin and polymyxin, produced by *Bacillus brevis* and *Bacillus polymyxa* (Figure 31). These two antibiotics are nowadays used in clinics against resistant bacterial infections (Desai and Banat, 1997).

FIGURE 31

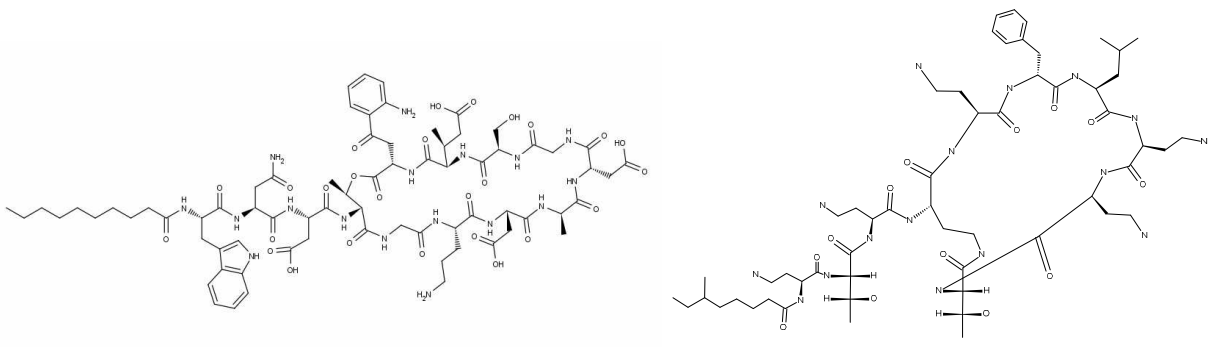

Daptomycin *Polymyxin*

2.6.1. Molecular Structure

Cyclic lipopeptides are composed of an amino acid cycle which is closed by an ester or peptide bond. These cycles are linked to acyl chains in different manners (Figure 31, Figure 32). The fatty acid linked to the polyamine cycle gives the molecules the amphiphilic character. The charge of the peptide groups is very important for their specific activity. Cationic lipopeptides like polymyxin have shown to be specifically active on bacteria (Clausell et al., 2007), whereby anionic lipopeptides seem to have a broader spectrum of activity (Straus and Hancock, 2006;Cao et al., 2011). Because of these different structural features, there exists a high structural variety of lipopeptides. This makes them very interesting compounds for the discovery of new pharmacophores.

2.6.2. Biosynthesis

Synthesis of peptides does not always rely on the ribosome. Lipopeptides are generally assembled by non-ribosomal peptide synthethases (NRPs). They work as assemblies where each module is responsible for the incorporation of a single monomer. The amino acids used are not the same as for protein synthesis. Cyclization can be achieved by an ester or peptide bond and results in the formation of lactams or lactones respectively (Giessen and Marahiel, 2012). Non ribosomal peptide synthethases are lacking in higher eukaryotes but are present in fungi (Hur et al., 2012).

2.6.3. Biological activity

Lipopeptides have surfactant properties and reduce the interfacial energy and surface tension of water. That’s why they could be used as “biosurfactants” (Desai and Banat, 1997). Some of them are also able to self-aggregate in aqueous solution and form oligomers (Straus and Hancock, 2006). Their surfactant properties seem to increase the ability of bacteria secreting lipopeptides to form biofilms (Raaijmakers et al., 2010).

Many lipopeptides have antibacterial activity especially against resistant strains. For example, daptomycin has been shown to be very efficient against MRSA (methicilline resistant *Staphylococcus aureus*) strains. Antibiotic activity is mostly due to the interaction with membranes. This interaction is strengthened by the lipid acyl tail (Straus and Hancock, 2006). The antibacterial activity is not only interesting to treat human or animal infections. Bacterial strains producing lipopeptides have been used successfully to protect plants from infections (Stein, 2005).

The ability to interact with membranes gives lipopeptides additionally anticancer, antimycotic, antihelminthic and antimycoplasmic activities (Raaijmakers et al., 2010).

2.7. Surfactin

Surfactin is one of three major lipopeptide groups produced by the *Bacillus* species. The two other peptide families are fengycin and iturin (Smyth et al., 2010). The most common producer of surfactine is *Bacillus subtilis* (Figure 32,A), the bacteria where the lipopeptide has first been isolated (Arima et al., 1968). The surfactin family is composed of 8 analogs (Kanatomo et al., 1995). Their structures are made of a cycle of seven amino acids linked to a C13-C16 β-hydroxyl fatty acid (Figure 32B). The carboxyl of the fatty acid is connected to the N-terminus of the peptide by a peptide bond and the β-hydroxyl group to the C-terminus by an ester link (Smyth et al., 2010). We have to be aware that the peptide loop is very flexible and can adopt different conformations in different environments (Gang et al., 2011).

FIGURE 32

(A) (B)

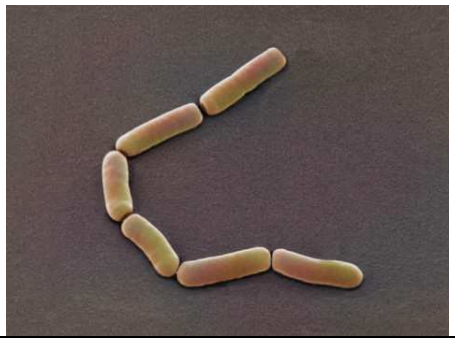

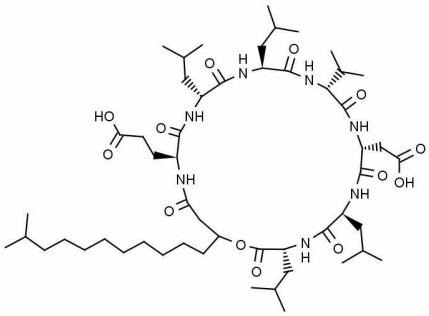

(A) *Colored Scanning electron micrograph (17000x) of Bacillus subtilis (Stanley Flegler)®*
(B) *Chemical structure of the Surfactin family*

Surfactin has strong surfactant activity and reduces the surface tension of water from 72 to 27 mN/m (Desai and Banat, 1997). Interestingly, the reduction of surface tension of the air water interface due to surfactin enhanced the spreading and aeral biofilm formation of *Bacillus subtilis* conferring an enormous evolutionary advantage to the bacteria (Angelini et al., 2009).

Surfactin was further able to induce ion-channels in lipid bilayer membranes and cause hemolysis (Dufour et al., 2005). It induced a detergent-like membrane lysis (Arima et al., 1968;Heerklotz and Seelig, 2001). The molecule showed a very broad spectrum of lytic activities including fungi, bacteria (including MRSA), mycoplasma, cancer and virus (Sen, 2010;Kracht et al., 1999).

Beyond this lytic activity, surfactin induced apoptosis in different kinds of cancer cells and was able via different mechanisms to inhibit proliferation of cancer. Surfactin induced apoptosis via the intrinsic apoptotic pathway. An increase of intracellular Ca^{2+} and ROS and the activation of the MPT was implicated (Cao et al., 2011). It diminished replication of cancer cells trough inhibition of the cell cycle at G(2)/M. Most probably because of the inhibition of a G(2) specific kinase (cdc2) (Cao et al., 2009;Kim et al., 2007). Surfactin would also decrease invasion of cancer cells via inhibition of Matrix metalloproteinase 9 (MMP-9) (Park et al., 2013). This pleiotropic activity of surfactin on cancer cells should make of it an interesting candidate to overcome multidrug resistance.

3. Results

This chapter contains the most important results I obtained during my thesis in FACM and GNOS. It is divided into two parts. In the first part, I will assemble all data in relation with α-hederin, δ-hederin and hederagenin. The second part will handle the results obtained with surfactin. I will reprint the articles in their original form, as they have been submitted, accepted or published. For studies which haven't been integrated into articles yet, I will give the purpose of the study, a brief introduction of the subject, describe materials and methods, comment the results and open a short discussion.

3.1. Activities of α-hederin and hederagenin on different membrane models and cancer cells

To explore the effects of α-hederin, δ-hederin and hederagenin on membranes and the consequences for cells, we studied the effects of both molecules on several artificial membrane models and cancer cells. We used α-hederin as example to explore membrane lysis induced by monodesmosidic saponins, because it had shown a hemolytic and cytolytic potential in the past (Gauthier et al., 2009). We were also interested in a possible relation between membrane interactions and apoptosis induction by α-hederin.

The results were divided into four main studies. The first study explores the lytic potential of α-hederin, δ-hederin and hederagenin on different membrane models and cancer cells. In the second study, we observe the effects of α-hederin on a membrane model which displays macroscopic phase separation. The third study describes the potential activity of α-hederin and hederagenin on membrane rafts and adds further information on the lytic potential of the saponin. Finally, we explored the lytic and apoptotic activities of α-hederin and hederagenin on cancer cells *in vitro*.

3.1.1. Induction of highly curved structures in relation with membrane permeabilization and budding by the triterpenoid saponins, α-hederin and δ-hederin (**article 1, J. Biol. Chem. 288, 2013**)

Authors : Joseph Lorent[1,2], Cécile S. Le Duff[3], Joelle Quetin-Leclercq[2] and Marie-Paule Mingeot-Leclercq[1]

[1]Université catholique de Louvain, Louvain Drug Research Institute, Cellular and Molecular Pharmacology, Avenue E. Mounier 73, UCL B1.73.05, B-1200 Bruxelles, Belgium.

[2]Université catholique de Louvain, Louvain Drug Research Institute, Pharmacognosy, Avenue E. Mounier 72, UCL B1.72.03, B-1200 Bruxelles, Belgium.

[3]Université catholique de Louvain, - Institute of Condensed Matter and Nanosciences, Molecules, Solids and Reactivity, Place Louis Pasteur 1, UCL L4.01.04, B-1348 Louvain-la-Neuve, Belgium.

Subject and background : The aim of this study was to better understand the permeabilizing activity displayed by many monodesmosidic triterpenoid saponins. The article deals with the permeabilizing activity of α-hederin, δ-hederin and hederagenin, two monodesmosidic triterpenoid saponins and a triterpenic acid, on model membranes. To our knowledge, this is the first study which investigates this well known activity of saponins on GUVs (Giant unilamellar vesicles containing fluorescent lipid probes, a membrane model which I recently introduced into the FACM laboratory), which have the size of eukaryotic cells and can therefore be observed in light microscopy. The results obtained on GUVs, in combination with ^{31}P-NMR and other techniques allowed new conclusions regarding the membrane lytic activity of monodesmosidic saponins.

THE JOURNAL OF BIOLOGICAL CHEMISTRY VOL. 288, NO. 20, pp. 14000–14017, May 17, 2013

Induction of Highly Curved Structures in Relation to Membrane Permeabilization and Budding by the Triterpenoid Saponins, α- and δ-Hederin[S]

Received for publication, August 9, 2012, and in revised form, March 19, 2013 Published, JBC Papers in Press, March 25, 2013, DOI 10.1074/jbc.M112.407635

Joseph Lorent[‡§], **Cécile S. Le Duff**[¶], **Joelle Quetin-Leclercq**[§], **and Marie-Paule Mingeot-Leclercq**[‡1]

From [‡]*Cellular and Molecular Pharmacology and* [§]*Pharmacognosy, Louvain Drug Research Institute, Université Catholique de Louvain, B-1200 Bruxelles and* [¶]*Molecules, Solids and Reactivity, Institute of Condensed Matter and Nanosciences, Université Catholique de Louvain, B-1348 Louvain-la-Neuve, Belgium*

Background: The triterpenoid monodesmosidic saponins, α- and δ-hederin, induced membrane permeabilization.
Results: The membranous cholesterol and the sugars branched on the aglycone, hederagenin, are critical for membrane permeabilization, budding, and the change in lipid phase.
Conclusion: Permeabilization and budding are dependent on the interaction of saponin with cholesterol and the molecular shape of the saponin.
Significance: Induction of curvature by saponins is responsible for permeabilization and budding.

The interactions of triterpenoid monodesmosidic saponins, α-hederin and δ-hederin, with lipid membranes are involved in their permeabilizing effect. Unfortunately, the interactions of these saponins with lipid membranes are largely unknown, as are the roles of cholesterol or the branched sugar moieties (two for α-hederin and one for δ-hederin) on the aglycone backbone, hederagenin. The differences in sugar moieties are responsible for differences in the molecular shape of the saponins and the effects on membrane curvature that should be the most positive for α-hederin in a transbilayer direction. In large unilamellar vesicles and monocyte cells, we showed that membrane permeabilization was dependent on the presence of membrane cholesterol and saponin sugar chains, being largest for α-hederin and smallest for hederagenin. In the presence of cholesterol, α-hederin induced the formation of nonbilayer phases with a higher rate of Brownian tumbling or lateral diffusion. A reduction of Laurdan's generalized polarization in relation to change in order of the polar heads of phospholipids was observed. Using giant unilamellar vesicles, we visualized the formation of wrinkled borders, the decrease in liposome size, budding, and the formation of macroscopic pores. All these processes are highly dependent on the sugars linked to the aglycone, with α-hederin showing a greater ability to induce pore formation and δ-hederin being more efficient in inducing budding. Hederagenin induced intravesicular budding but no pore formation. Based on these results, a curvature-driven permeabilization mechanism dependent on the interaction between saponin and sterols and on the molecular shape of the saponin and its ability to induce local spontaneous curvature is proposed.

Saponins are widely distributed in nature and are known for their physiological, immunological, and pharmacological properties (1). All of these properties have led to considerable clinical interest in these substances. Currently, however, the mechanisms of action involved in these effects are not completely understood.

Saponins can be classified as either monodesmosidic or bidesmosidic, based on the number of branched sugar chains on the aglycone, as well as into steroid or triterpenoid saponins, depending on the carbon numbers on the aglycone backbone. α-Hederin (also called kalopanaxsaponin A) (2) is a monodesmosidic triterpenoid compound with an α-L-rhamnose-(1→2)-α-L-arabinose sugar chain attached at C3 of the aglycone, hederagenin (Fig. 1). α-hederin was first isolated from the leaves of *Hedera helix* (3). This molecule possesses strong hemolytic activity (4, 5) and cytotoxicity against *in vivo* tumors; in addition, it has *in vitro* effects on various cancer cell lines, which could result from apoptosis (2, 6, 7) and/or membrane alterations (5, 8).

The potential of saponins to interact with biological membranes has drawn much attention. In particular, the interaction with cholesterol has been suggested to be involved in the membrane permeabilization by monodesmosidic saponins with a sugar moiety at C3 (9, 10).

Sterols are essential components of eukaryotic membranes. They enable the cells to modulate the physical properties of membranes in relation to their biological functions (11), including the dynamics and regulation of metabotropic receptors (12). In the mammalian plasma membrane, cholesterol is the most abundant sterol (20–40% mol/mol).

This work aimed to study the interactions of α-hederin and its derivatives that lack one or two sugars (δ-hederin (hederagenin 3-*O*-α-L-arabinopyranoside) and hederagenin) (Fig. 1) with cholesterol and to identify their membrane permeabilizing ability. To understand the molecular mechanism involved and to establish a model explaining their ability to induce membrane permeabilization, we used complementary information afforded by lipid models of mem-

[S] This article contains supplemental Materials and Methods, Results, and Figs. 1–3.

[1] To whom correspondence should be addressed. Tel.: 32-2-764-73-74; Fax: 32-2-764-73-63; E-mail: marie-paule.mingeot@uclouvain.be.

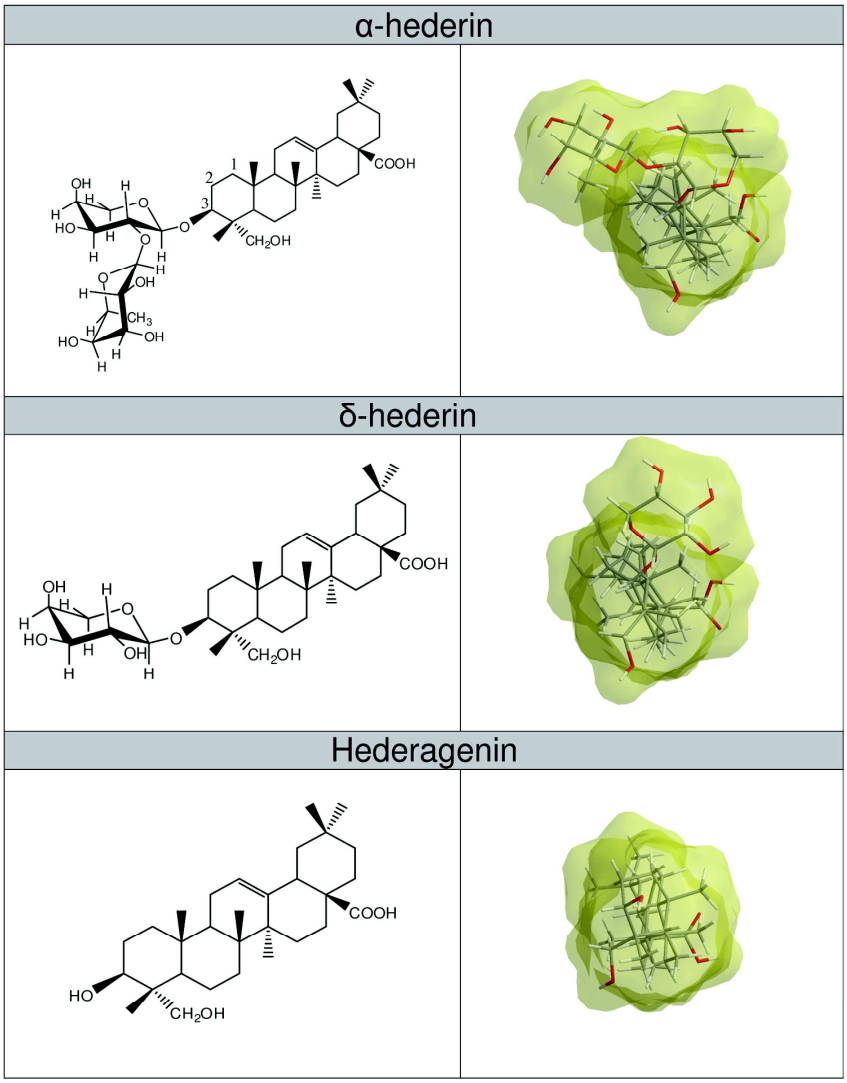

FIGURE 1. *Left panels*, two-dimensional chemical structures of α-hederin, δ-hederin, and hederagenin. *Right panels*, three-dimensional structures and molecular shape of minimized energy (view on the C3 residue of the molecule).

branes (large unilamellar vesicles (LUV),[2] multilamellar vesicles (MLV), and giant unilamellar vesicles (GUV)) (13–16). The biological relevance of our study and the importance of membrane cholesterol for cytotoxicity were ascertained by monitoring the effect of α-hederin on a human monocytic cell line depleted or not for cholesterol.

Using LUVs, we measured membrane permeabilization (calcein release), liposome size (dynamic light scattering), and variations in membrane potential (1-anilinonaphthalene-8-sulfonic acid (ANS)). To obtain further information on the ability of α-hederin to interact with the polar head group region of the membrane, we determined the excitation generalized polarization (GP_{ex}) upon increasing temperature using 6-dodecanoyl-2-dimethylaminonaphthalene (laurdan), which resides at the interfacial region of the bilayer (17–20). The consequences of the interaction of α-hederin with cholesterol on lipid phases were studied by one-dimensional ^{31}P NMR on MLVs.

We took advantage of the size of GUVs to visualize the effects of α-hederin on lipid membrane deformation, budding, and pore formation, and we related these effects to the membrane permeabilization induced by this saponin. To our knowledge, this is the first study investigating the effects of triterpenoid saponins on GUVs.

[2] The abbreviations used are: LUV, large unilamellar vesicle; MLV, multilamellar vesicle; GUV, giant unilamellar vesicle; DMPC, phosphatidylinositol 1,2-dimyristoyl-*sn*-glycero-3-phosphocholine; Chol, cholesterol; DHE, dehydroergosterol; TR-DPPE, Texas-Red 1,2-dipalmitoyl-*sn*-glycero-3-phosphoethanolamine; DPH, 6-diphenyl-1,3,5-hexatriene; PI, phosphatidylinositol; PC, phosphatidylcholine; SM, sphingomyelin; ANOVA, analysis of variance; ANS, 1-anilinonaphthalene-8-sulfonic acid.

Membrane Permeabilization and Budding by α- and δ-Hederin

We showed that α-hederin binds to model lipid membranes (LUVs) and to cholesterol, alters the thermotropic behavior of lipids, and forms pores in a cholesterol-dependent fashion. The role of cholesterol and of the branched sugars on the aglycone backbone (α-hederin > δ-hederin > hederagenin) in membrane permeabilization was highlighted. Using GUVs, we visualized potential differences in the permeabilization and deformation of membranes (α-hederin > δ-hederin) or in the production of buds (δ-hederin > α-hederin) in relation to the molecular shape of the saponin and its ability to induce local spontaneous curvature, as we demonstrated using ^{31}P NMR spectroscopy. On a monocyte model, we showed that cell death induced by α-hederin is dependent on the cellular cholesterol content.

This work provides new insights regarding possible molecular mechanisms involved in the pharmacological effects of α-hederin or its derivatives, and this study may renew the clinical interest in saponins, in general.

EXPERIMENTAL PROCEDURES

α-Hederin and hederagenin (HPLC quality) were purchased from Extrasynthèse, (Genay, France). δ-Hederin was kindly provided by Prof. Voutquenne-Nazabadioko (CNRS FRE 2715, IFR 53, Reims, France). The compounds were dissolved in ethanol. After evaporation of the solvent, the residue was resolubilized in a buffer solution (10 mM Tris-HCl adjusted to pH 7.4 with NaOH) in an ultrasonic bath for 1 min. Depending upon the experiments performed, DMSO (maximum 1%) was used for a complete solubilization of α-hederin, δ-hederin, or hederagenin, and the corresponding controls were used. Cells were purchased from ATCC. RPMI 1640 medium was ordered by Invitrogen. Egg phosphatidylcholine, sphingomyelin, phosphatidylinositol 1,2-dimyristoyl-*sn*-glycero-3-phosphocholine (DMPC), and cholesterol were ordered from Avanti Polar Lipids (Birmingham, AL). The bicinchoninic (BCA) protein assay was purchased from Thermo Scientific. Methyl-β-cyclodextrin (MβCD), calcein, FITC-dextran (4 and 250 kDa), and dehydroergosterol (DHE; Δ5,7,9(11),22-ergostatetraen-3β-ol) were ordered from Sigma. Calcein was purified as described previously (21). 1,8-ANS, 6-dodecanoyl-2-dimethyl-aminonaphthalene (laurdan), Texas-Red 1,2-dipalmitoyl-*sn*-glycero-3-phosphoethanolamine (TR-DPPE), and the Amplex® red cholesterol assay kit were purchased from Invitrogen. Polydimethylsiloxane was kindly provided by Henri Burhin and Christian Bailly (Université Catholique de Louvain/Science and Technology Sector/Institute of Condensed Matter and Nanosciences, Louvain-la-Neuve, Belgium). All other reagents were purchased from Merck.

Molecular Modeling of α-Hederin, δ-Hederin, and Hederagenin—Molecules were drawn in ChemDraw Ultra 10.0 and then visualized in three-dimensions by Chem three-dimensional Ultra 10.0. A minimized energy structure was calculated, and the molecular surface shape was displayed using the "Connolly molecular" mode.

Incubation with α-Hederin of THP-1 Monocytes Depleted or Not in Cholesterol—Cells were cultivated in RMPI 1640 medium supplemented with 10% fetal calf serum in 95% air and 5% CO_2.

For cholesterol depletion, cells (10^6 cells/ml) were harvested and incubated for 2.5 h in fresh RPMI 1640 medium supplemented with 1 mg/ml BSA and 5 mM methyl-β-cyclodextrin (MβCD) (22). Cell counting was performed in a Burker chamber. After this incubation, cells were washed three times with RPMI 1640 medium. At this time, part of the cells was quantified for the cholesterol and protein content with the Amplex® Red cholesterol assay and BCA protein assay kit, respectively. The other part was incubated with increasing concentrations of α-hederin. Cell death was quantified by the trypan blue assay and given in percent of total cells.

Preparation of MLVs and LUVs—DMPC or DMPC/Chol (3:1) MLVs were prepared according to the freeze-thawing method as described previously (23) in a buffer solution (10 mM Tris-HCl, pH 7.4).

LUVs composed of PC/SM/PI/Chol (4:4:3:0, 4:4:3:2.25, or 4:4:3:5.5), DMPC, or DMPC/Chol (3:1) were prepared by the extrusion technique (24), using a 10-ml Thermobarrel extruder (Lipex Biomembranes, Vancouver, Canada). The MLVs were extruded at 45 °C, 10 times through two superimposed track-etch polycarbonate membranes (pore size = 100 nm; Whatman Nucleopore, Corning Costar Corp., Badhoevedorp, The Netherlands) to obtain LUVs. The lipid concentration of the liposomal suspension was measured by phosphorous quantification (25) and adjusted according to the experimental protocol used.

Release of Calcein Entrapped at Self-quenching Concentration within LUVs—The leakage of entrapped self-quenched calcein from LUVs induced by a permeabilizing agent can be monitored by the fluorescence increase caused by its dilution (26).

For these permeability studies, the lipid film was resuspended in a purified calcein solution (72 mM calcein and 10 mM Tris-HCl) adjusted to pH 7.4 and 400 mosm/liter (measured by the freezing point technique (Knauer osmometer automatic, Berlin, Germany)). The unencapsulated calcein was removed using the minicolumn centrifugation technique (27).

The calcein-filled liposomes (5 μM lipids) were incubated with α-hederin at 37 °C for increasing periods of time. The percentage of calcein released was determined as described previously (28). The excitation and emission wavelengths were 472 and 512 nm, respectively. All steady-state fluorescence experiments were performed on an LS55 luminescence spectrometer (PerkinElmer Life Sciences).

DHE Steady-state Spectroscopy—The ability of α-hederin to bind to cholesterol was investigated using DHE fluorescence spectroscopy. DHE is a structurally close cholesterol analog presenting a similar behavior in aqueous solution and biological membranes as cholesterol (29–31).

When DHE is excited at 310 nm in aqueous solution, it presents a low intensity monomeric peak at 375 nm and a high intensity maximum of structured emission at 395 and 424 nm due to the presence of microcrystals in buffer solution. Therefore, the ratio between fluorescence intensities at 375 *versus* 395 or 424 nm (I_{375}/I_{395} or I_{375}/I_{424}) reflects the ratio of monomers *versus* microcrystals in aqueous solution. Moreover, a decrease in the dielectric constant of the microenvironment of DHE induces a blue shift of λ_{max} emission (29).

DHE was solubilized at 4 μg/ml in buffer solution containing 0.1% DMSO. Increasing α-hederin concentrations were added. The emission spectrum was taken at excitation wavelength of 310 nm. To confirm formation of aggregates composed of α-hederin and cholesterol, we incubated both compounds at equimolar concentration (500 μM) in buffer solution at 1% DMSO and looked for the formation of a macroscopic precipitate.

DHE was also incorporated in MLVs composed of DMPC/Chol/DHE (75:24:1) to probe the effect of α-hederin on cholesterol in a lipid environment. Maximal emission of DHE was observed around 355, 375, and 390 nm, as described previously in membrane systems. Seras *et al.* (32) observed no spectral shift during the transformation of bilayers into micelles but reported a decrease in fluorescence lifetime and intensity. The MLVs were incubated for 3 h at 25 °C at increasing α-hederin/total lipid ratios.

Dynamic Light Scattering and ANS Fluorescence—The apparent average diameter of LUVs was determined by dynamic light scattering spectroscopy using a Malvern Zetasizer Nano ZS® (Malvern Instruments, Ltd., Worcestershire, UK). The fluctuation of light scattering was measured at an angle of 90° with monodisperse latex particles with diameters of 100 and 800 nm as controls. The data were collected using the size distribution analysis mode to determine the full size distribution profile of the liposomes incubated with α-hederin. The membrane potential differential was assessed with ANS, a probe that fluoresces when it is bound to lipid membranes (33, 34) and characterized by its sensitivity to superficial charges on the membrane surface. An ANS stock solution of 5 mM in methanol was prepared. The fraction of ANS bound to the membrane and the variation of surface potential of the liposomes caused by α-hederin were determined as described previously (35).

One-dimensional ^{31}P NMR Spectroscopy on MLVs—MLVs (30 mg of total lipid in Tris-HCl, pH 7.4) were prepared according to the freeze-thaw method. Because ^{31}P NMR spectroscopy requires high amounts of products, we avoided the solubility problem by inserting compounds during the formation of the lipid film. As a positive control, we used SDS, which is known to be cone shaped and to induce positive curvature (36).

0.3 ml of D_2O was added for deuterium lock to 2.5 ml of sample. This sample was placed in a 10-mm Wilmad 513-pp NMR tube that rotated at 20 rpm in the NMR spectrometer.

NMR spectra were acquired on a Bruker Avance DRX500 spectrometer operating at 500.13 MHz for ^{1}H (202.47 MHz for ^{31}P) and equipped with a 10-mm Bruker broad band observe probe.

The temperature in the probe was regulated at 37 or 60 °C for the duration of the experiments. All ^{31}P spectra were referenced to the ^{31}P peak from an 85% solution of phosphoric acid (H_3PO_4) measured at 25 °C (set at 0 ppm).

One-dimensional ^{1}H spectra were recorded prior to ^{31}P experiments to ensure the best field homogeneity was attained for each sample. 114,688 points and an acquisition time of 0.7 s using power-gated Waltz16 ^{1}H decoupling were used, and 26,000 scans per ^{31}P experiment with a sweep width of 83.1 kHz were acquired with a delay of 1.5 s between scans. The signal was Fourier-transformed using an exponential multiplication function with a line broadening of 50 Hz and zero-filled to a final spectral resolution of 0.6 Hz per point.

Laurdan Generalized Polarization—Using LUVs, the effect of the drugs on the mobility of phospholipids and the polarity at the level of the glycerol backbone were determined by monitoring the Laurdan excitation generalized polarization (GP_{ex}) (17, 37). Upon excitation, the dipole moment of laurdan increases noticeably, and water molecules in the vicinity of the probe reorient around this new dipole. When the membrane is in a fluid phase, the reorientation rate is faster than the emission process, and consequently, a red-shift is observed in the emission spectrum of laurdan. When the bilayer packing increases, some of the water molecules are excluded from the bilayer, and the dipolar relaxation rate of the remaining water molecules is slower, leading to an emission spectrum that is significantly less red-shifted. The GP_{ex} allows quantification of this red-shift from the emission spectra.

The lipid concentration of the liposome solution was adjusted to 25 or 50 μM with 10 mM Tris-HCl at a pH of 7.4. Laurdan (5×10^{-3} M stock solution in tetrahydrofuran) was added to the lipid film to obtain a lipid/probe ratio of 300. Then α-hederin or hederagenin was added to the liposomes at a final concentration of 30 or 60 μM and incubated under continuous agitation at 37 °C in the dark for 60 min. The generalized polarization values from the emission spectra were calculated using Equation 1,

$$GP_{ex} = \frac{I_{440} - I_{490}}{I_{440} + I_{490}} \quad \text{(Eq. 1)}$$

where I_{440} and I_{490} are the fluorescence intensities at emission wavelengths of 440 nm (gel phase) and 490 nm (liquid crystalline phase), respectively, at a fixed excitation wavelength of 340 nm. The generalized polarization was determined as a function of temperature.

Depending on the shape of the curves, the best adjustment was selected. For DMPC/Chol and DMPC, GP_{ex} values as a function of temperature were adjusted using the Hill equation or a five-parameter Richards function, respectively (38).

Preparation of GUVs—GUVs were prepared by electroformation (39). Briefly, 1 μl of a chloroform solution of DMPC/Chol (3:1; 5 mg/ml), was spread on an indium tin oxide-covered glass. The fluorescent probes were added to the chloroform solution at a concentration of 0.1% mol/mol. The solution was dried in a vacuum chamber for 2 h. An electroformation chamber was constructed using another indium tin oxide-covered glass slide, with the conducting face pointed toward the interior of the electroformation chamber, which was filled with a 0.1 M saccharose solution. Polydimethylsiloxane containing 5% fumed silica was used to separate the two glass slides. The GUVs were grown by applying a sinusoidal alternating current of 10 Hz and 1 V for 2 h at 60 °C.

Fluorescence and Confocal Microscopy of GUVs—The GUVs were labeled with TR-DPPE (40), which was excited at 561 nm and recorded at 617 nm. In the fluorescence microscopy experiments, we used an Axioskop 40 microscope (Carl Zeiss, Jena, Germany) with a 40×/0.75 Zeiss EC Plan-Neofluar® objective,

Membrane Permeabilization and Budding by α- and δ-Hederin

and the images were recorded with a Nikon digital sight DS-5 M camera (Nikon, Tokyo, Japan).

For the confocal microscopy experiments, an Axio-observer spinning disk inverted microscope Z.1 (Carl Zeiss, Jena, Germany) was utilized. The spinning disk was a CSU-X1 model (Yokogawa Electric Corp., Tokyo, Japan). The objectives used included an LD LCI Plan-Apochromat 25×/0.8 Imm Korr DIC M27, an EC Plan-Neofluar 40×/1.30 Oil DIC M27, an LCI Plan-Neofluar 63×/1.30 Imm Korr DIC M27, and a Plan-Apochromat 100×/1.40 Oil DIC M27. The images were recorded with an AxioCamMR3 camera using the Carl Zeiss AxioVision 4.8.2 software.

Permeability of Dextran through Membranes of GUVs—After electroformation, 10 μl of GUVs were added to a solution containing 20 μM FITC-dextran (mean molecular weight of 4 or 250 kDa) and 40 μM α-hederin, δ-hederin, or hederagenin. As positive control, we used 30 mM SDS. The FITC-dextran was excited at 488 nm, and the emission was recorded with a 520/35-nm emission filter and visualized as described previously (41). We chose GUVs that presented typical deformation features and followed one GUV with fluorescence microscopy at corresponding time points. The difference in fluorescence intensity between the outside and inside of one GUV reflects the membrane integrity. In contrast, similar fluorescence intensities indicate the penetration of the fluorescent probe. The difference in fluorescence intensity outside and inside the vesicle was calculated by dividing the fluorescence values by the highest intensity recorded and multiplying by a factor of 1000. The difference of the mean of 20 normalized values taken from inside and outside the vesicle was then determined. The significant difference was calculated using a Student's *t* test.

Deformation, Pore Formation, and Budding of GUVs—After electroformation, 30 μl of the GUVs were added to a saccharose solution (0.1 M; DMSO 0.1%) containing 40 μM α-hederin, δ-hederin, or hederagenin. As positive control, we used 400 μM, 4 mM, and 30 mM SDS. The deformation of the vesicles was followed for at least 50 min (except for 30 mM SDS where complete dissolution occurred after several minutes). An initial image was captured immediately after the vesicles were added to the solution containing one of the three compounds. Subsequent images were taken at regular intervals thereafter. Because photobleaching reduced the visibility of the vesicle, the luminosity and contrast were enhanced by the acquisition software (NIS-Elements D 3.10, Nikon, Tokyo, Japan). Selected images were used to visualize by fluorescence and confocal microscopy the pore formation and budding of vesicles upon increasing times of exposure. In the confocal microscopy experiments, we chose a cross-section that passed through the middle of the vesicle. Three-dimensional images represented the superimposition of all of the cross-sections obtained from one vesicle. The quantification of vesicles presenting different features (wrinkled membrane deformation, pore formation, budding, or aggregation) was achieved by counting a total of 200 vesicles after 0.5 or 1 h of incubation with the compounds.

Statistical Analysis—All statistical analyses were performed using GraphPad Prism version 4.00 for Windows (GraphPad Software, San Diego) with a two-way ANOVA using all data points to compare plots or a Student's test when dextran fluorescence intensities inside and outside the vesicles were compared. For the nonlinear regression of laurdan GP_{ex} in the DMPC LUVs, we used a five-parameter Richard's function in JMP 8.01.

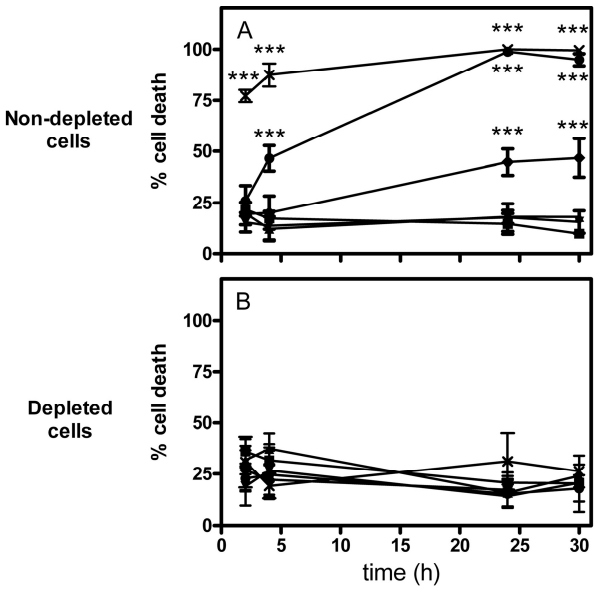

FIGURE 2. **Trypan blue assay of nondepleted and cholesterol-depleted THP-1 cells incubated for 2, 4, 24, and 30 h with increasing α-hederin concentrations.** Control (■), 10 (▲), 15 (▼), 20 (♦), 25 (●), and 30 μM (×). Each value is the mean of four independent assays ± S.D. Statistical analysis: two-way ANOVA comparing each data point for normal *versus* depleted cells. ***, $p < 0.001$.

RESULTS

Cell Death Induced by α-Hederin in Cells Depleted or Not in Cholesterol—Using trypan blue assay, we investigated the cytotoxicity of α-hederin on a human leukemic monocytic cell line (THP-1) and the role of membrane cholesterol (Fig. 2). Cell membranes were depleted in cholesterol by MβCD (22), and cholesterol content was quantified after incubation. Nondepleted THP-1 cells had a free cholesterol amount of 12.55 ± 0.68 μg of cholesterol/mg of protein whereby depleted cells showed 6.80 ± 1.17 μg/mg. We can assume that this depletion is mainly due to the depletion of the plasma membrane because 90% of the total cholesterol content of the cell is found in the plasma membrane (42). Results show that on nondepleted cells, the cytotoxicity induced by α-hederin in THP-1 was concentration- and time-dependent (Fig. 2*A*). In contrast, when cells were depleted in cholesterol, almost any cytotoxicity was observed (Fig. 2*B*). Hederagenin at 30 μM did not significantly increase cell death for at least 24 h of incubation regardless of the cholesterol content (data not shown).

Membrane Permeabilization Induced by α-Hederin, δ-Hederin, and Hederagegin on LUVs and GUVs—To investigate the effect of α-hederin and its derivatives on lipid membrane permeability, we determined the ability of α-hederin, δ-hederin, and hederagenin to induce release of calcein from LUVs and permeation of dextran of 4 and 250 kDa through GUV mem-

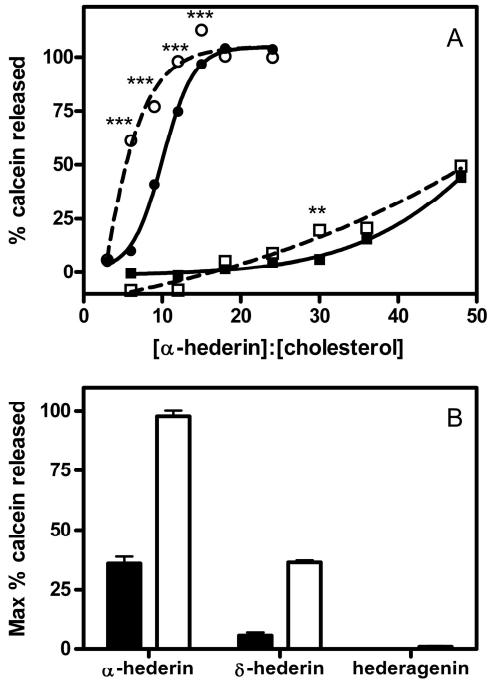

FIGURE 3. *A,* release of calcein from liposomes (5 μM of total lipids) upon exposure at 37 °C for 30 min (*solid lines; filled symbols*) or 18 h (*dashed lines; open symbols*), upon increasing α-hederin/cholesterol ratios. The liposomes were made of PC/SM/PI/Chol (4:4:3:5.5) (*circles*), PC/SM/PI/Chol (4:4:3:2.25) (*squares*). The *graph* shows the functions obtained by fitting a one-phase exponential association function to the data by nonlinear regression. *B,* maximal release of calcein from liposomes composed of DMPC/Chol (3:1) upon exposure at 37 °C to α-hederin, δ-hederin, or hederagenin at a compound/cholesterol molar ratio of 16 (*closed histogram*) or 48 (*open histogram*). Because of the partial insolubility of α-hederin, δ-hederin, and hederagenin, the three compounds were dissolved in DMSO (final solution 0.5% DMSO). The *ordinate* shows the percentage of calcein released compared with what was observed after addition of 2% Triton X-100. Each value is the mean of triplicate ± S.D. (when not visible, the *bars* are smaller than the symbols). Statistical analysis: two-way ANOVA comparing each data point for 30-min and 18-h incubations: **, $p < 0.01$; ***, $p < 0.001$).

branes. Using LUVs, we also questioned the roles of cholesterol for membrane permeabilization induced by α-hederin.

We first used LUVs containing PC/SM/PI/Chol, a lipid mixture mimicking the lipid composition of the plasma membranes (43), to characterize the effect of α-hederin and hederagenin on membrane permeability. To investigate the importance of cholesterol, we prepared liposomes with varying contents of cholesterol (PC/SM/PI/Chol, 4:4:3:0, 4:4:3:2.25, or 4:4:3:5.5). With increasing cholesterol content (from 0 to 33.3%), α-hederin induced a greater release of calcein, even at an equal α-hederin/cholesterol ratio (Fig. 3*A*). In the absence of cholesterol, no release of calcein was observed (data not shown). At the highest cholesterol composition (PC/SM/PI/Chol, 4:4:3:5.5) and after 18 h of incubation, the release of calcein reached more than 50% at an α-hederin/cholesterol ratio of 6 and reached 100% at a ratio of 12 (Fig. 3*A*). Under these conditions, the duration of incubation was also a critical parameter because the release of calcein increased with the time of incubation (18 h *versus* 30 min) (Fig. 3*A*). Upon addition of hederagenin, no release of calcein was observed regardless of the cholesterol content, the time, or the hederagenin/lipid molar ratio (data not shown).

The role of the branched carbohydrate chain on hederagenin in membrane permeabilization was confirmed using binary liposomes composed of DMPC/Chol (3:1) (Fig. 3*B*). At both compound/cholesterol ratios of 16 and 48, there is a clear relationship between the number of sugars and the release of calcein, with α-hederin inducing the greatest release, followed by δ-hederin and hederagenin.

To decipher the mechanism involved, we also performed permeabilization experiments using GUVs. We therefore visualized by confocal microscopy the evolution of the concentration profile of FITC-dextran (Fig. 4) at molecular masses of 4 kDa (Fig. 4, *A, C,* and *E*) and 250 kDa (Fig. 4, *B* and *D*) outside and inside the vesicle. We followed the effect induced by α-hederin (Fig. 4, *A* and *B*), δ-hederin (Fig. 4, *C* and *D*), and hederagenin (Fig. 4*E*) at corresponding stages of membrane deformation. The control images were obtained by adding GUVs to an equimolar sucrose solution containing FITC-dextran.

In the control solutions, FITC-dextran was located outside the vesicle, and a large difference in fluorescence intensities between the outside and inside of the GUVs was observed for the whole duration of the incubation. Upon addition of GUVs to the α-hederin solution, the difference between FITC-dextran (4 kDa) concentration located outside and inside was quickly suppressed as a result of the penetration of FITC-dextran through α-hederin-induced pores in the lipid membrane (Fig. 4*A*). The permeabilization was observed before any deformation of the vesicle was visible. A permeabilization was also observed with the higher molecular weight FITC-dextran (250 kDa), but the rate was slower (Fig. 4*B*).

Regarding the effect of δ-hederin when FITC-dextran 4 kDa was used, we also observed a decrease in the difference in fluorescence intensities outside and inside the vesicle, but which appeared later as observed with α-hederin (Fig. 4*C*). When FITC-dextran of 250 kDa was used, almost no effect was observed after over 2 h of incubation for δ-hederin (Fig. 4*D*).

Our results suggested that both α-hederin and δ-hederin have the ability to induce a time-dependent growth of pore size, with α-hederin being more efficient. In contrast, hederagenin was unable to induce permeation of FITC-dextran (4 kDa) even after 24 h of incubation (Fig. 4*E*).

SDS, a cone-shaped detergent, was used as a positive control. It induced a fast suppression of the dextran gradients at 30 mM (supplemental Fig. S1). Micrometer sized pores appeared nearly simultaneous to the permeabilization (supplemental Fig. S2, pores).

All these results suggest that membrane permeabilization induced by α-hederin was increased by the following: (i) the cholesterol content of the liposomes; (ii) the time of incubation; (iii) the α-hederin/cholesterol ratio, and (iv) the number of sugars attached to the C3 residue. Pore size seemed to increase with time. Moreover, permeation to a low size dextran (4 kDa) was faster than to the large size dextran (250 kDa) and was higher for α-hederin when compared with δ-hederin.

Binding of α-Hederin to Sterols and Membranes—Because cholesterol plays a critical role in membrane permeabilization induced by α-hederin, we explored the ability of the latter to

Membrane Permeabilization and Budding by α- and δ-Hederin

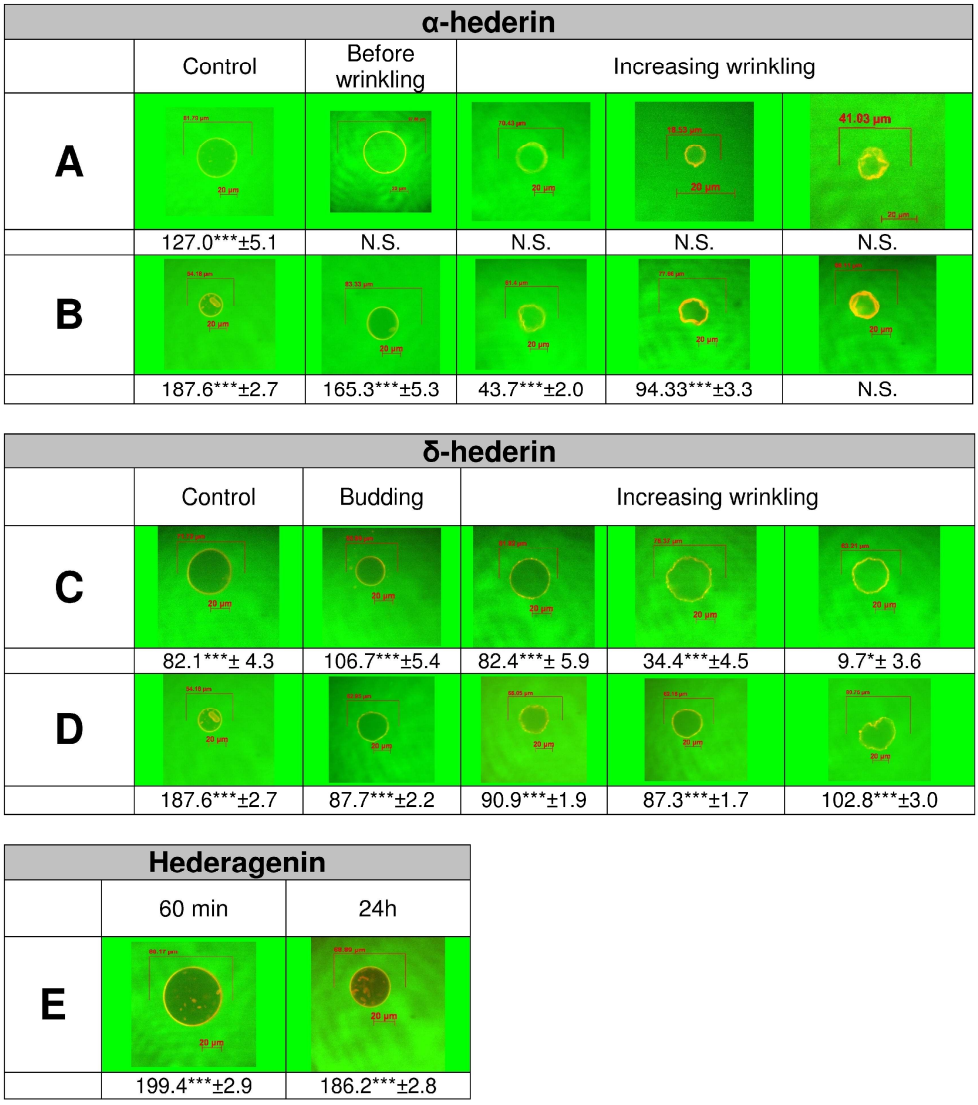

FIGURE 4. **Effect of α-hederin, δ-hederin, or hederagenin on the permeability to FITC-dextran 4 kDa (*A*, *C*, and *E*) or 250 kDa (*B* and *D*) of GUVs composed of DMPC/Chol (3:1) and labeled with TR-DPPE, at different stages of deformation.** For each stage, the difference of normalized fluorescence between inside and outside of the vesicle was quantified. For hederagenin, no deformation was observed. Statistical analysis (*t* test): ***, $p < 0.001$. *N.S.* means no significant difference.

bind to dehydroergosterol (DHE), a fluorescent analog of cholesterol (29–32), or to change membrane surface potential of DMPC/cholesterol vesicles as compared with DMPC liposomes. To address these questions, we used fluorescence spectroscopy of DHE and ANS, respectively.

In an aqueous environment, and upon increasing α-hederin/DHE ratios, we observed a global increase of fluorescence intensities and specifically an increase of the intensity ratio (I_{375}/I_{395}) (Fig. 5*A*). This ratio reached 0.63 ± 0.05 in control solution and 0.90 ± 0.03 with a α-hederin/DHE molar ratio set at 4. Moreover, the maximum of the structured emission was undergoing a blue shift from 424 to 419 nm, reflecting a more hydrophobic environment for DHE (29, 31). Both results indicate the formation of dehydroergosterol/α-hederin micelles or aggregates, which clearly points out the affinity of α-hederin for DHE. The formation of macroscopic aggregates was observed when α-hederin and cholesterol were co-incubated at equimolar concentrations (500 μM).

In MLVs, upon increasing concentrations of α-hederin, we observed an important decrease of DHE fluorescence intensity after 3 h of incubation (Fig. 5*B*). In contrast, the intensity ratio did not change significantly, and we observed no shift of the maxima. The same behavior of DHE was observed with octyl glycoside (32) and could be related, as suggested by the authors, to a reduction of fluorescence lifetime of DHE in mixed micellar lipid aggregates. Therefore, the results

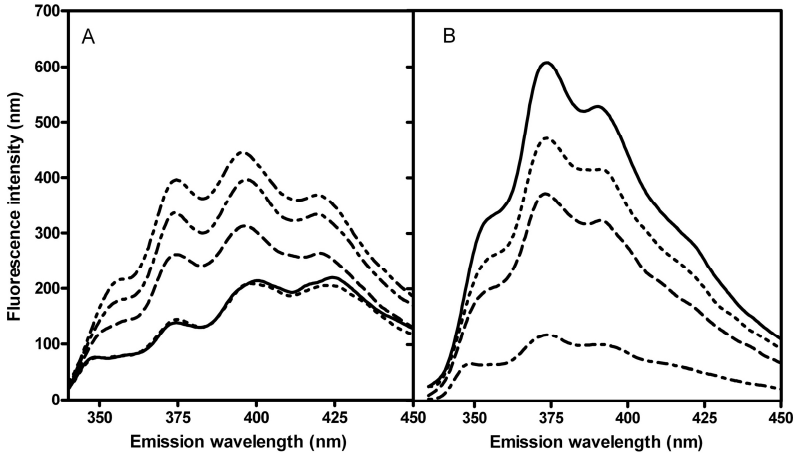

FIGURE 5. **Fluorescence emission spectra of DHE (*A*) in aqueous solution (4 μg/ml and 0.1% DMSO) and MLV (*B*) composed of DMPC/Chol/DHE (75:24:1).** Excitation wavelength was set at 310 nm. In aqueous solution, spectra were recorded upon increasing α-hederin/DHE ratios. Control (*solid line*), 0.5 (*dotted line*), 1.5 (*dashed line*), 2 (*dash dot line*), and 4 (*dash dot dot line*). In MLV after incubation for 3 h (25 °C) at increasing α-hederin/total lipids ratios, spectra were taken. Control (*solid line*), 0.1 (*dotted line*), 0.3 (*dashed line*), and 0.6 (*dash dot line*).

TABLE 1
Variation of membrane surface potential (Δψ and corresponding intervals of confidence) of LUVs incubated with α-hederin or hederagenin

Compound/ lipid ratio	10 min, α-hederin		60 min			
			α-Hederin		Hederagenin	
	DMPC	DMPC/Chol	DMPC	DMPC/Chol	DMPC	DMPC/Chol
1.2	−1.89 (−5.33; 1.70)	−1.43 (−5.39; −2.72)	−14.75 (−17.53; −12.01)	+0.53 (−7.09; 7.28)	−5.09 (−9.58; −0.97)	−6.00 (−9.81; −2.15)
2.4	−14.78 (−21.74; −8.63)	−11.41 (−16.04; −6.66)	−16.09 (−19.31; −12.99)	−3.27 (−7.00; 0.31)	−8.56 (−11.16; −5.99)	−9.29 (−16.06; −3.42)

strongly suggest that α-hederin induces nonbilayer mixed lipid aggregates.

Second, the critical role of cholesterol for binding of α-hederin to liposomes was ascertained by determining the ΔΨ of liposomes (Table 1) of DMPC or DMPC/Chol (3:1) upon increasing incubation times and α-hederin/lipid molar ratios. After an incubation time of 10 min, with α-hederin/lipid ratios of 1.2 and 2.4, ΔΨ decreased in DMPC and DMPC/Chol liposomes. When the liposomes were incubated with α-hederin for 1 h, the surface potential of the DMPC liposomes reached more negative values, whereas ΔΨ showed slightly positive or negative values when α-hederin was incubated with DMPC/Chol (3:1) liposomes. In contrast, upon addition of hederagenin, the decrease in ΔΨ was similar for liposomes with or without cholesterol after 60 min of incubation.

At a glance, cholesterol was probably critical for the interaction of α-hederin with lipid membranes as suggested by the change in fluorescent properties of DHE and the formation of a precipitate when α-hederin and cholesterol were co-incubated in aqueous solution. In a bilayer environment, α-hederin interacts with DHE (and most probably with cholesterol) and forces it into mixed nonbilayer lipid aggregates.

The reduction of membrane surface potential of liposomes incubated with α-hederin suggests that the saponin binds independently of the presence of cholesterol to the membrane. However, at longer incubation periods, the presence of cholesterol reversed the decrease of the surface potential, indicating its important role for membrane interaction.

Changes in Liposome Size and Appearance of New Structures Induced by α-Hederin—To decipher if the interaction between α-hederin and cholesterol results in variations of liposome size and changes in lipid organization, we determined the size of DMPC and DMPC/Chol LUVs upon increasing α-hederin/cholesterol ratios, using dynamic light scattering. We also characterized the phospholipid organization in MLVs where α-hederin had been integrated within the lipid film, using one-dimensional ^{31}P NMR spectroscopy.

First, we showed the effect of α-hederin on the size of LUVs composed of DMPC (Fig. 6, *A* and *B*) or DMPC/cholesterol (3:1 molar ratio; Fig. 6, *C* and *D*) after 1 h (Fig. 6, *A* and *C*) and 24 h (Fig. 6, *B* and *D*) of incubation at 37 °C with increasing amounts of α-hederin. In the absence of cholesterol, regardless of the duration of incubation or the concentration of saponin, no change in the mean size of the liposomes was observed (Fig. 6, *A* and *B*). This lack of effect was in strict contrast to what was observed when the liposomes contained cholesterol. In such samples, two main populations of liposomes emerged (Fig. 6, *C* and *D*). One was centered at smaller sizes and the other at higher sizes than the original (100 nm). For example, at an α-hederin/lipid ratio of 8, one population was centered at ~70 nm and the other at ~255 nm. At higher ratios, the samples presented a high polydispersity index, making the results unreliable. α-Hederin had a similar effect on LUVs composed of PC/SM/PI/Chol (4:4:3:5.5) (data not shown).

Second, to gain information about the newly formed structures determined by dynamic light scattering, we used one-

Membrane Permeabilization and Budding by α- and δ-Hederin

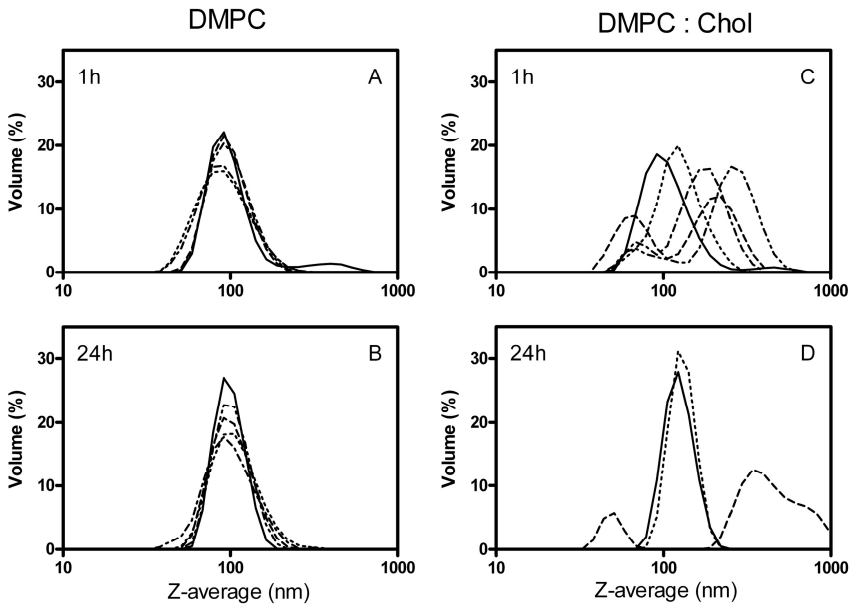

FIGURE 6. ***Z*-average of liposomes upon exposure with α-hederin as determined by dynamic light scattering at high resolution in multimodal analysis.** Vesicles composed of DMPC (*A* and *B*) or DMPC/Chol (3:1) (*C* and *D*) were incubated for 1 h (*A* and *C*) or 24 h (*B* and *D*) without (*solid line*) or with α-hederin at a molar ratio of α-hederin/lipids of 1.2 (*dotted line*), 2.4 (*dashed line*), 4 (*dash dot line*), and 8 (*dash dot dot line*). For DMPC/Chol (3:1) vesicles, these ratios also correspond to α-hederin/cholesterol ratios of 4.8, 9.6, 16, and 32, respectively. For *D*, at α-hederin/lipid ratios higher than 2.4, the polydispersity index values became too high to have confident measures. The diameters of the particles are presented in nm, and the ordinate shows the volume of the population associated with a size expressed in %.

dimensional ^{31}P NMR spectroscopy. Fig. 7 shows the spectra of MLVs prepared with α-hederin (Fig. 7, *C–F*) and hederagenin (Fig. 7, *G–J*) at 10 (Fig. 7, *C, D, G,* and *H*) and 20% (Fig. 7, *E, F, I,* and *J*) mol/mol and at both 37 °C (*left column*) and 60 °C (*right column*).

DMPC/Chol (3:1) MLVs showed at 37 and 60 °C (Fig. 7, *A* and *B*) typical spectra of a bilayer organization displaying an asymmetric pattern with a low field shoulder and a high field peak. The chemical shift anisotropy (Δσ) was 40 and 39 ± 1 ppm. α-Hederin (10% mol/mol), at 37 °C (Fig. 7*C*), clearly disrupted the bilayer organization. The spectra showed a broad peak centered at 0 ppm superimposed to the bilayer shape. Δσ decreased from 40 ± 1 to 34.5 ± 1 ppm reflecting the presence of structures with higher mobility or diffusibility. At 60 °C, a sharp peak overlapping with a wide peak centered on 0 ppm became more pronounced, and a hexagonal phase pattern became noticeable (Fig. 7*D*). The Δσ reduction was similar to that observed at 37 °C (from 39 ± 1 to 33.5 ± 1 ppm). Macroscopically, for both temperatures, a phase separation was observed in the NMR tube as described in a system composed of bilayer/cubic and bilayer/hexagonal phases (44, 45). By increasing the α-hederin concentration to 20% mol/mol, at 37 °C, the bilayer structure was heavily disrupted because its characteristic asymmetrical peak has completely disappeared (Fig. 7*E*). A broad peak (over 10 ppm) centered at 0 ppm was observed in these conditions, which could correspond to structures larger than micelles like buds or small unilamellar vesicles, for example (46–48). By increasing the temperature to 60 °C (Fig. 7*F*), the one-dimensional ^{31}P NMR spectrum clearly showed a hexagonal pattern (highlighted by an *arrow* in Fig. 7*F′*). Macroscopically, the phase separation disappeared at high α-hederin concentration. The effects are critically dependent upon the presence of cholesterol because we did not observe any change in spectra, except a small increase of Δσ (39 to 42.5 ppm), when α-hederin (10%) was inserted in bilayers lacking cholesterol at 37 °C.

Hederagenin, at 10% mol/mol affected the bilayer signal to a lower extent compared with α-hederin. At 37 °C, the Δσ only decreased from 40 ± 1 to about 36.5 ± 1 ppm (Fig. 7*G*). As for α-hederin, a broad peak centered at 0 ppm was observed at 60 °C (Fig. 7*H*), and this peak increased with a concomitant decrease of the intensity of the bilayer signal. At a higher concentration (20% mol/mol) and both at 37 and 60 °C (Fig. 7, *I* and *J*), hederagenin induced a sharp isotropic peak at 0.4 ppm even though the bilayer signal was always present (Δσ = 38 ± 1 and 37 ± 1 ppm at 37 and 60 °C, respectively). We observed neither a significant change of Δσ nor a macroscopic phase separation regardless the concentrations tested.

This is in strict contrast with what was observed when SDS was used as a positive control. In these conditions, a reduction of Δσ to values to 29 and 26.5 ± 1 ppm at 37 and 60 °C, respectively, was observed with the appearance of a small isotropic peak at 0 ppm (see supplemental Fig. S3). This effect could be related to the size reduction of the vesicles induced by this detergent even though the bilayer structure is maintained (47). This mode of action is different from the one of α-hederin that deeply modifies the structure of the cholesterol containing MLVs.

In a nutshell, α-hederin did not change the mean diameter of the liposomes lacking cholesterol. When liposomes contained

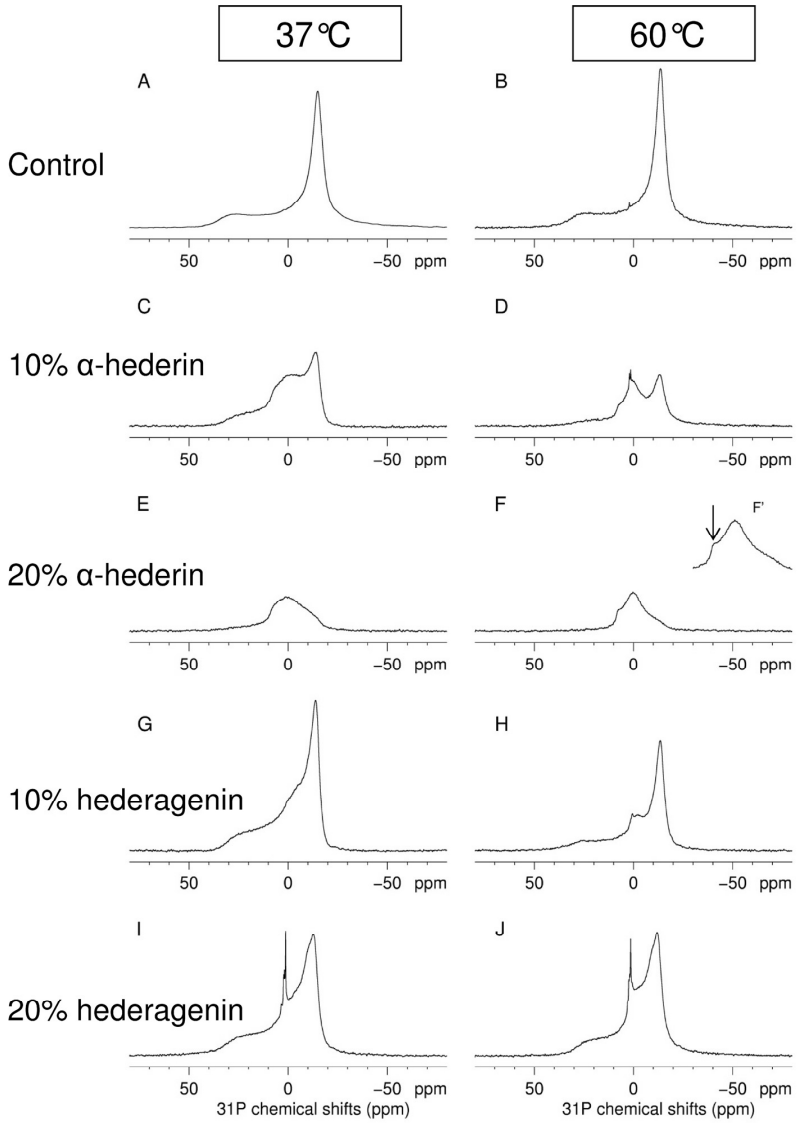

FIGURE 7. **^{31}P NMR spectra of MLVs composed of DMPC/cholesterol (3:1) at 37 °C (*left column*) or 60 °C (*right column*).** Control (*A* and *B*), 10% mol/mol α-hederin (*C* and *D*); 20% mol/mol α-hederin (*E–F′*); 10% mol/mol hederagenin (*G* and *H*), and 20% mol/mol hederagenin (*I* and *J*). 10 or 20% α-hederin or hederagenin corresponds to a molar ratio of compound/total lipids ratio = 0.1 or 0.2, respectively.

cholesterol, the saponin induced two new populations of different sizes most probably due to the formation of new lipid structures composed of a mixture of bilayers, isotropic and hexagonal phases. At higher α-hederin concentrations and temperatures, the hexagonal pattern was favored (see Fig. 7*F′*).

Packing at the Interfacial and Hydrophobic Regions of the Lipid Bilayer—To characterize the binding of α-hederin at the molecular level and particularly the consequences of its interaction within the interfacial domain, we determined GP_{ex}. A high GP_{ex} value is usually associated with a high bilayer packing and a low polarity and a low GP_{ex} value with the opposite (37). This was illustrated by changes in the decreasing GP_{ex} values upon increasing temperatures (Fig. 8). At physiological and high temperatures, α-hederin and hederagenin induced a marked increase in GP_{ex} values on DMPC vesicles (Fig. 8, *A* and *B*).

When cholesterol was present in the liposomes (3:1), the trend of the curves was modified (Fig. 8, *C* and *D*) in accordance with other studies (49, 50). We observed a slight reduction of GP_{ex} values at low temperatures that became important at physiological temperatures (Fig. 8*C*). At higher temperatures, GP_{ex} increased as compared with the control situation, especially at the highest α-hederin/lipid ratio investigated. Hederagenin (Fig. 8*D*) had no effect at physiological temperature, but it induced a small decrease of the GP_{ex} below 40 °C and a slight increase above this temperature.

Membrane Permeabilization and Budding by α- and δ-Hederin

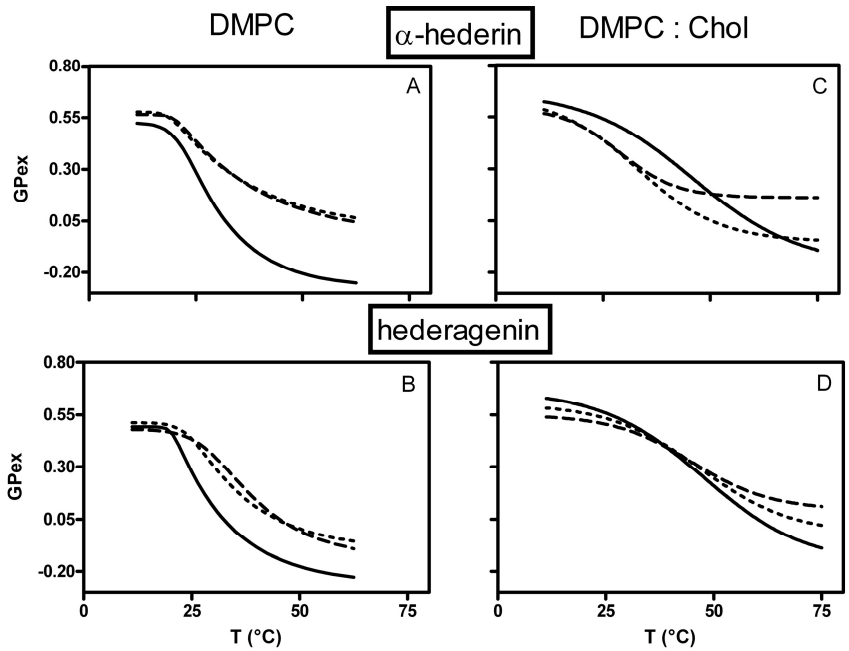

FIGURE 8. **Effect of α-hederin (*A* and *C*) and hederagenin (*B* and *D*) on the generalized polarization (GP_{ex}) values for laurdan in liposomes made of DMPC (*A* and *B*) or DMPC/Chol (3:1) (*C* and *D*) as a function of temperature.** The *lines* refer to data obtained in absence (*solid line*) or presence of α-hederin or hederagenin at drug/lipid molar ratios of 1.2 (*dotted line*) or 2.4 (*dashed line*). For DMPC/Chol (3:1) vesicles, these ratios correspond to a drug/cholesterol ratio of 4.8 and 9.6, respectively. The excitation wavelength was fixed at 340 nm and emission intensities at 440 nm (gel phase) and 490 nm (liquid crystalline phase). Each value is the average of three experiments. Statistical analysis was performed with Graph Pad Prism 4.0 (two-way ANOVA, comparing three data points at the beginning, physiological temperature, and the end of the curves).

Thus, at physiological conditions, and if cholesterol is present, only α-hederin induced a decrease of the GP_{ex} values. At the highest temperatures investigated, both α-hederin and hederagenin increased GP_{ex} values regardless of the presence of cholesterol. The same general observations for Laurdan GP_{ex} have been made for DPH fluorescence anisotropy (*r*), a probe integrated into the hydrophobic core (data not shown).

Appearance of Membrane Deformations, Micrometric Pore Formation, and Budding—To ascertain the critical role of the sugars branched on the genin, we aimed to visualize the earliest alterations induced by α-hederin, δ-hederin, and hederagenin and their ability to promote shape deformations on GUVs containing cholesterol (16). An initial image was captured immediately after the addition of GUVs to the solution containing the compound. One GUV was followed over 60 min, and pictures were taken at regular time intervals. Images, presenting time intervals with important features, are shown in Fig. 9 upon addition of GUVs to a control solution (Fig. 9*A*) or to a solution containing α-hederin (Fig. 9*B*), δ-hederin (Fig. 9*C*), or hederagenin (Fig. 9*D*). The mean size diameter of GUVs at all times points was also monitored.

Just after their addition to a solution containing α-hederin (Fig. 9*B*), the GUVs possessed a spherical shape with no detectable membrane fluctuations. Then a rapid decrease in the mean diameter of the liposomes was observed (Fig. 9*E*), and after 30 min of incubation, wrinkled borders appeared. These wrinkles were more pronounced after 40 min (Fig. 9*B*, *white arrow*). Deformation was visible until 50 min but reversed to a spherical shape at 60 min. Quantification of wrinkled borders induced by α-hederin is shown in Fig. 11 (85.2 ± 2.2% after 30 min (Fig. 11*A*) and 72.0 ± 17.2% after 1 h (Fig. 11*B*) of incubation).

With δ-hederin (Fig. 9*C*), wrinkled borders were much less present (4.7 ± 1.2% after 30 min (Fig. 11*C*) and 13.4 ± 6.2% after 1 h (Fig. 11*D*)). A marked decrease of the size of GUVs was observed but later (40 min), as compared with α-hederin (Fig. 9*E*).

Hederagenin induced neither membrane deformation (Fig. 9*D*) nor reduction in the size (Fig. 9*E*) of the GUVs, but sometimes it induced the formation of intravesicular buds (Fig. 9*D*).

After longer incubation periods of GUVs with α-hederin and δ-hederin, we observed the formation of visible pores (Fig. 10, *A–D*). We took advantage of confocal microscopy (Fig. 10*B*) and three-dimensional image reconstruction (Fig. 10*C*) to visualize the pore formation induced by α-hederin. Sometimes more than one pore was visible on one GUV. These pores expanded with time. The rim of the pore rolled itself up through the external side of the membrane (Fig. 10, *A–C*), resulting in the rolled rim shape as described by Sakuma *et al.* (16). When the complete vesicle had been "rolled up," the resulting form often resembled an angulated torus (Fig. 10, *complete transformation*). The appearance of micrometer-sized pores increased with incubation time (2.2 ± 2.3% after 30 min (Fig. 11*A*) and 4.3 ± 1.5% after 1 h (Fig. 11*B*)). For δ-hederin (Fig. 11*D*), this transformation was also visible but less frequent. No pore formation was observed with hederagenin. SDS at 30 mM induced the fast formation of macroscopic pores (supplemental Fig. S2, pores) and subsequent dissolution of the vesicle into small vesicles (supplemental Fig. S2, dissolution).

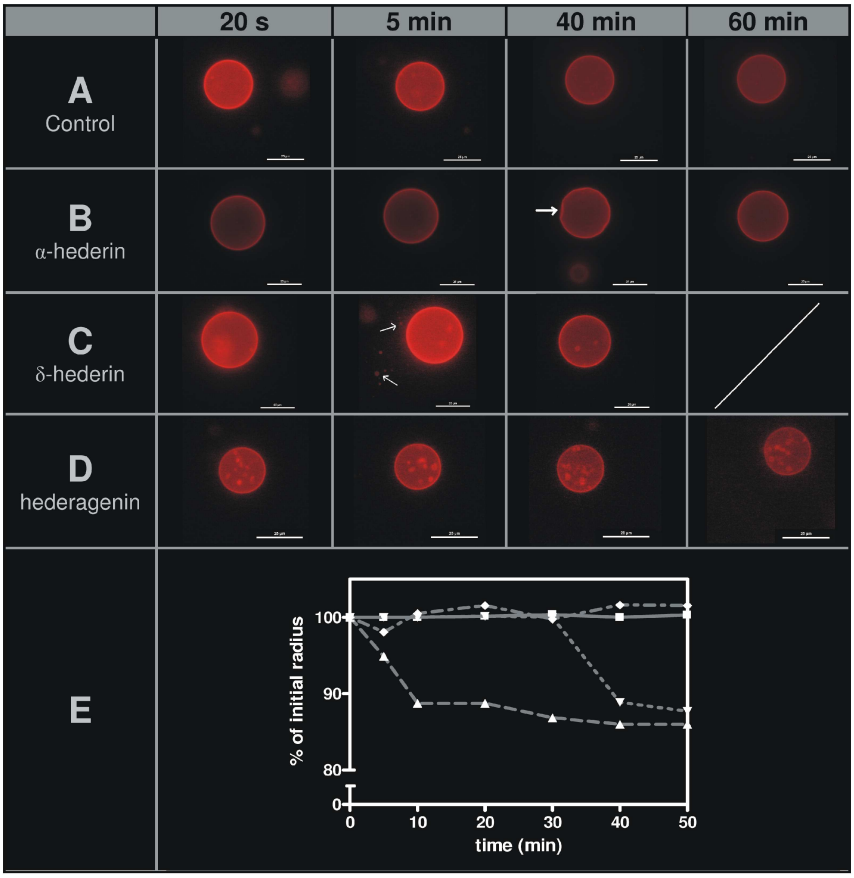

FIGURE 9. **Fluorescence microscopy of GUVs composed of DMPC/Chol (3:1) and labeled with TR-DPPE.** One GUV was followed, and pictures were taken at different incubation times. *A*, control; *B*, 40 μM α-hederin; *C*, 40 μM δ-hederin, and *D*, 40 μM hederagenin. One scale bar represents 25 μm. *E*, percentage of initial radius of one GUV as a function of incubation time with the compounds. The percentage was obtained by dividing the radius of a GUV at one time point by its radius measured when the incubation started. The ratio was multiplied by 100. Control liposomes (■), α-hederin (▲), δ-hederin (▼), and hederagenin (♦). The radius was determined using the acquisition software (see under "Experimental Procedures"). The experiment was performed three times at 25 °C. *Arrows* indicate deformation of the GUV for α-hederin and budding for δ-hederin.

Because the slight area difference between the two monolayer leaflets of the membrane or a change in the vesicle area-to-volume ratio may lead to budding (51), we investigated the ability of α-hederin, δ-hederin, and hederagenin to induce budding again by using fluorescence (Fig. 10*E*) and confocal microscopy (Fig. 10*F*).

Because this process was mostly induced by δ-hederin, it has only been illustrated for this saponin (Fig. 10, *E* and *F*). Two different kinds of buddings were observed. First, immediate budding led to complete fission of the newly formed vesicle. Small fluorescent spheres were formed several minutes after incubation (Figs. 10, *immediate budding*, and 9*C*, *white arrows*). These spheres detached from the membrane, and a decrease in the mean diameter was observed after 40 min of incubation (Fig. 9*E*). Second, later budding, leading to incomplete fission, was produced at longer incubation periods, with the formation of larger vesicles, which were interconnected by nanotubes and did not detach from the membrane (Fig. 10, *later budding*). With α-hederin, budding was occasionally only observed after 1 h of incubation (2.2 ± 1.4%; Fig. 11*B*), but with δ-hederin this process was much more frequent (23.4 ± 3.5% after 30 min (Fig. 11*C*) and 20.1 ± 5.3% after 1 h (Fig. 11*D*)). SDS (supplemental Fig. S2, budding) was also able to induce budding at concentrations of 400 μM, 4 mM, and 30 mM. The size of the buds decreased with increasing concentrations of SDS.

The possible effect of osmotic stress on this process is excluded because of the significantly low concentration of the compounds (~40 μM), which is orders of magnitude lower than the concentration of salt (a few millimolars) that has been reported to induce vesicle budding (52).

DISCUSSION

α-Hederin, a triterpenoid saponin, induced membrane permeabilization in relation to its biological activity. Despite numerous studies, the molecular mechanism involved remains unknown.

The results we obtained highlighted the role of a curvature-driven process (see Fig. 12), characterized by a three-step mechanism as follows: (i) cholesterol-independent binding to the membrane; (ii) interaction with cholesterol and asymmetric lateral distribution of α-hederin, and (iii) induction of curva-

Membrane Permeabilization and Budding by α- and δ-Hederin

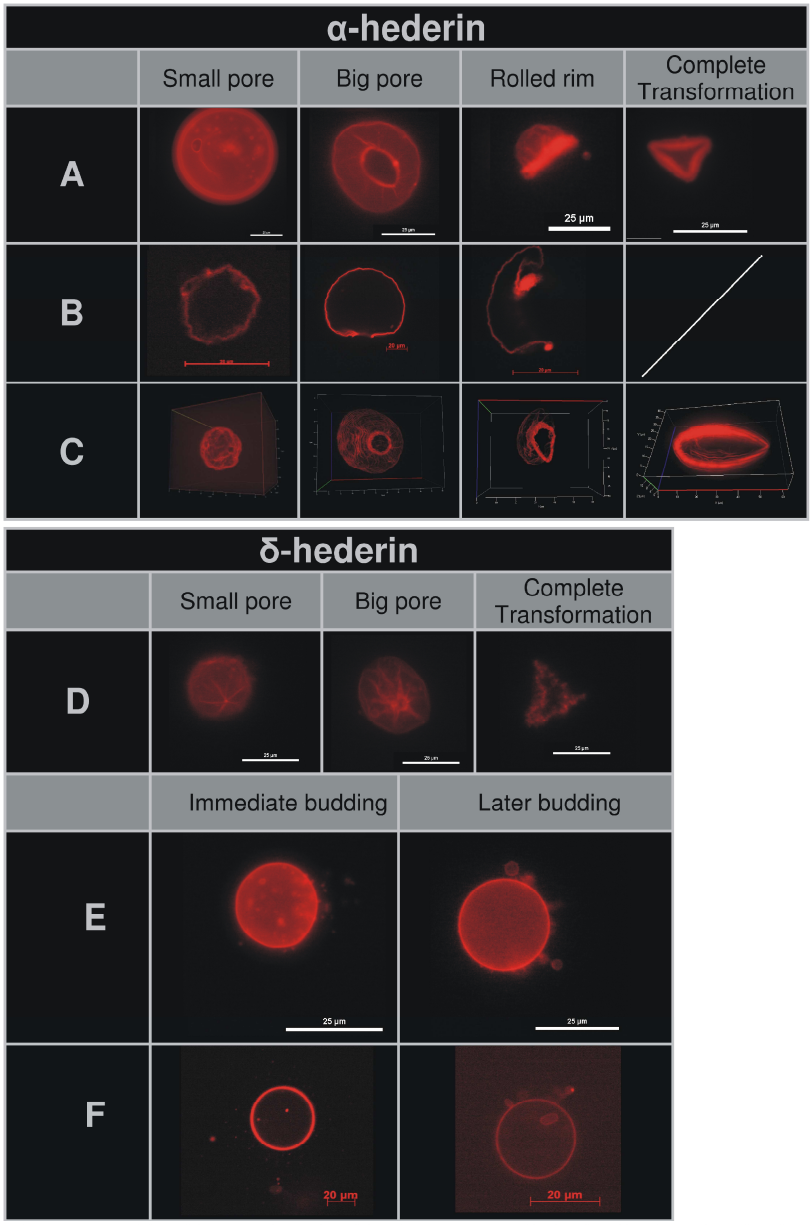

FIGURE 10. **Stages of pore formation (*A–D*) and budding (*E* and *F*) of GUVs composed of DMPC/Chol (3:1) incubated with 40 μM of α-hederin (*A–C*) or δ-hederin (*D–F*).** *A*, *D*, and *E*, fluorescence microscopy images of vesicles; *one bar* represents 25 μm. *B* and *F*, confocal microscopy, cross-section of the middle of one vesicle, *one bar* represents 20 μm. *C*, confocal microscopy, three-dimensional view of all cross-sections taken from one vesicle.

ture stress, resulting in membrane permeabilization and pore formation, as well as budding and the formation of a new lipid phase containing cholesterol, α-hederin, and phospholipids.

First, the cholesterol-independent binding of α-hederin and hederagenin to DMPC liposomes was suggested by the decrease in the membrane potential of lipid bilayers that could result from the negatively charged carboxylic function of the genin interacting with the positively charged choline head group of DMPC. Such interaction of α-hederin with the phospholipids results in an increase of the GP_{ex} of laurdan, especially at physiological and high temperatures. This suggests an increase in the microviscosity at the level of the polar heads of DMPC. A similar effect was observed for α-hederin when the hydrophobic membrane core was investigated. Condensing and acyl chain ordering effects on the phospholipids in their liquid disordered (L_d) state are similar to the effects that have been well described for cholesterol and assigned to the rigid ring structure of the sterol limiting trans → gauche isomerization of vicinal phospholipid acyl chains (53). Thus, the rigid triterpenoid structure of the genin could explain our results because both α-hederin and hederagenin are able to increase the GP_{ex} in the absence of cholesterol.

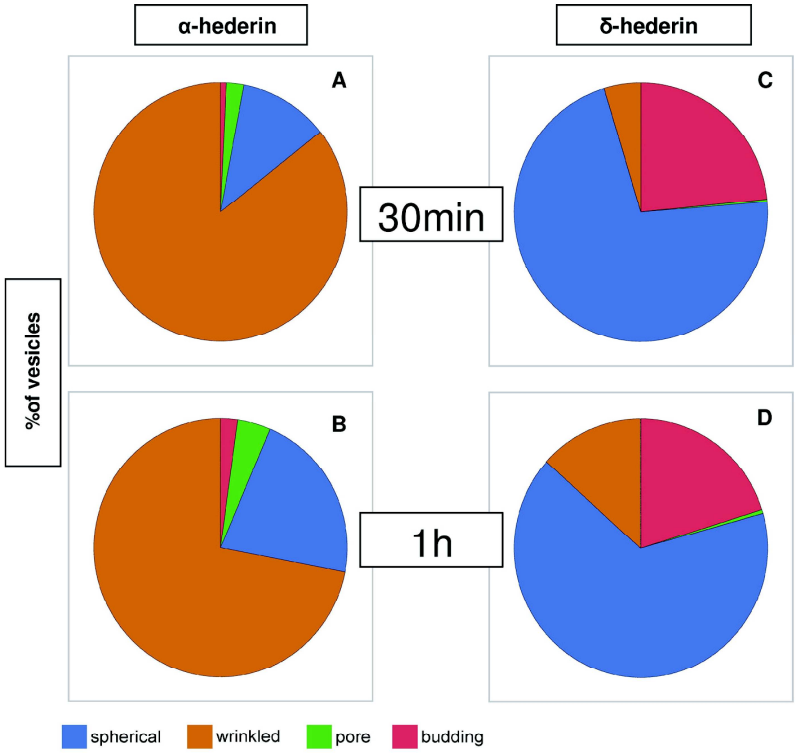

FIGURE 11. **Quantification of vesicles presenting different features (spherical, wrinkled, pores, or budding) after 30 min of incubation (*A* and *C*) or 1 h of incubation (*B* and *D*) with 40 μM of α-hederin (*A* and *B*) or δ-hederin (*C* and *D*).** A total of 200 vesicles were counted.

Second, after the initial binding to lipid membranes (Fig. 12*B*), α-hederin would interact with cholesterol, inducing a marked decrease of GP_{ex} values at physiological temperatures in DMPC/Chol (3:1). The formation of equimolecular complexes or aggregates composed of cholesterol and saponins could disorganize the phospholipid/cholesterol matrix and change the thermotropic behavior of membranes (54, 55). Our results from DHE spectroscopy support such interaction between cholesterol and α-hederin. Hederagenin only slightly influenced GP_{ex}, leading to the assumption that the decrease of GP_{ex} is mainly dependent on the sugar residues. The glycoside residues could act like "umbrellas," shielding the nonpolar part of cholesterol from water (56), and thereby enhancing the interaction between the saponin and the sterol (Fig. 12*B*) and inhibiting polar interactions of the phospholipids with the sterols.

Third, α- and δ-hederin would induce permeabilization of LUVs and GUVs, as well as the formation of wrinkles, micrometer-sized pores and buds in GUV, as well as the formation of a new lipid phase in MLVs. All these effects are highly dependent upon the nature of the saponin (α-hederin, δ-hederin, or hederagenin).

The appearance of GUVs presenting a flaccid shape and wrinkling would most likely result from the inhomogeneous insertion of saponin molecules and the release of the intravesicular Laplace pressure and internal water after permeabilization (57). The flaccid-shaped vesicles sometimes redeveloped into a spherical vesicle, with a smaller radius, suggesting a loss of membrane material, which could be related to the formation of the new isotropic lipid phase as evidenced by ^{31}P NMR spectroscopy and suggested by DHE spectroscopy on MLVs. This new phase would most probably be composed of cholesterol, α-hederin, and DMPC.

Budding and permeabilization have been previously associated with changes in surface area and spontaneous curvature (58–63). At first glance, the effects of the area asymmetry resulting from the bending of the inner monolayer after the insertion of molecules in the outer monolayer and an increase in the surface area (62–63) should be stronger than the effects of the spontaneous curvatures. However, with compounds characterized by a cone shape (like for α-hederin) or an inverted cone shape, which are locally accumulated, the opposite takes place, with the effects of spontaneous curvature being stronger than those of the area asymmetry. Thus, relative changes in the local lipid composition would result in the variation of the bilayer spontaneous curvature in the same location, making this mechanism more effective than that based on the area difference averaged over the entire membrane surface (60).

The induction of spontaneous curvature induced by α-hederin is supported by the following: (i) nonbilayer structures with a higher rate of Brownian tumbling or lateral diffusion around the vesicle observed by ^{31}P NMR (64, 65) in accordance with the reduction of the chemical shift anisotropy; (ii) the new structures of different sizes evidenced by dynamic light scattering; (iii) the decrease of GP_{ex} and DPH fluorescence anisotropy values observed at 37 °C (42, 63); (iv) the formation of macroscopic pores (16), and (v) budding (66).

Membrane Permeabilization and Budding by α- and δ-Hederin

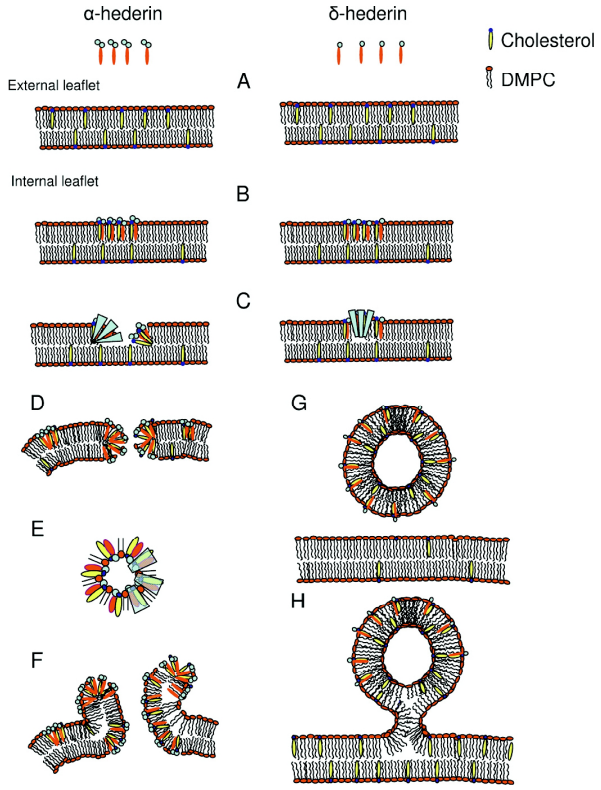

FIGURE 12. **Model proposed for the interaction of α-hederin and δ-hederin with GUVs.** *A,* α-hederin binds independently of cholesterol to the membrane and integrates into the outer leaflet. *B,* interaction between saponins and cholesterol leads to the formation of regions with a higher α- and δ-hederin/cholesterol concentration. *C,* increase of spontaneous curvature in a transbilayer direction due to the sugar moiety of the saponin in these regions leads to permeabilization (*D*) or budding (*G* and *H*). *D,* pore is stabilized by the sugar moieties pointing to the exterior of the membrane and reducing line tension, and a slight negative curvature in the direction of the membrane plane (*E*). *F,* diffusion of α-hederin at the rim toward the interior of the vesicle leads to inhomogeneous distribution of α-hederin molecules between the inner and outer leaflet and the rolled rim shape. *G* and *H,* intermediate curvature of δ-hederin is responsible for the immediate budding with complete fission from the GUVs at the beginning of incubation (*G*) and for the later budding with the bud still connected to the GUV at longer incubation times (*H*).

The nature of the formed nonbilayer structures is unknown, and electron or atomic force microscopy would have to be performed to fully characterize the structures. Among the more mobile structures, which could be induced by α-hederin, cubic phases or structures larger than micelles, like *e.g.* buds or small unilamellar vesicles (46–48, 67), are the most likely. The hexagonal pattern observed at the highest temperature and α-hederin concentration could probably be associated with tubular structures as it has been suggested for glycoalkaloids (10).

The enhancement of curved structures in relation to membrane permeabilization appears clearly related to the nature of the saponin (α-hederin, δ-hederin, and hederagenin). In agreement with the self-assembly theory established by Israelachvili *et al.* (68), amphiphiles are approximated by rigid bodies of defined three-dimensional shape (Fig. 1). α-Hederin has two sugar units, which confer to the molecule a large hydrophilic headgroup compared with its lipophilic, rigid triterpenic pentacyclic ring structure, which results in a positive spontaneous curvature, as it adopts a cone shape. The sugar moiety points in the direction perpendicular to the genin, giving the molecule the form of an axe. The formation of a normal hexagonal phase (H_I) (or tubular structures) would be in accordance with the three-dimensional shape proposed for α-hederin (very slight curvature in one direction and positive curvature into the other) (60). In this context, toroidal pore formation has been associated with a positive spontaneous curvature applied to the transbilayer direction and negative curvature regarding the rim of the pore in the membrane plane (69, 70). Aggregation of cholesterol and α-hederin could lead to a complex presenting positive curvature (cone shape) in a transbilayer direction and slight negative curvature (inverted truncated cone shape) in the membrane plane (Fig. 12, *D* and *E*).

δ-Hederin has only one sugar at C3. Its hydrophilic headgroup is smaller and the positive spontaneous curvature applied should decrease relative to α-hederin. δ-Hederin would induce smaller positive curvatures into the transbilayer direction. Hederagenin has a structure that resembles cholesterol, and its spontaneous curvature should therefore be negative, as has been observed for cholesterol (57), explaining its lower ability to induce pore formation.

SDS, a molecule with a single acyl chain and an ionized sulfate group, would rather induce positive curvature in all directions of the membrane plane. This would lead to the formation of pores, small buds, and/or micelles, which is in accordance with our results. The critical role of a three-dimensional molecular shape and the ability to induce curvature have also been proposed to explain membrane permeabilization induced by the following: (i) dioscin (71); (ii) glycoalkaloids (10); (iii) cone-shaped amphiphiles (57), and (iv) cone-shaped lipids (16).

Regarding the kinetics of pore formation, the permeabilization to 4-kDa FITC-dextran was faster than to 250-kDa FITC-dextran. Moreover, an increase in the time to reach micrometer-sized pores was observed, as reported when hepatocytes were treated with saponins extracted from *Gypsophila* plants (72). Therefore, permeabilization appeared to be a graded process, characterized by the appearance of wrinkled borders and the continuing shape deformations, as well as the formation of pores with increasing size. For influx to occur, the pores should be equal to or larger than the Stokes-Einstein radii of FITC-dextran molecules (73) (1.83 and 11.1 nm for 4- and 250-kDa FITC-dextran, respectively). With time, the pores were stabilized, and the formation of the so-called rolled-rim shape was observed (16). The segregated cone-shaped amphiphilic α-hederin molecules could cap the edge of the bilayer at the rim of the pore, decreasing line tension and thereby stabilizing the pore (16, 57). The membrane at the rim was rolled to the outside of the vesicle after pore formation (Fig. 10, *rolled rim*; Fig. 12*F*), which could result from a time-dependent inhomogeneous distribution of saponin molecules between the inner and outer leaflet, a model that has been recently established for cone-shaped amphiphiles (16).

As membrane permeabilization, budding is favored by molecules that induce positive curvature to the external monolayer (Fig. 12, *C*, *G*, and *H*). Immediate budding (Figs. 9 and 10) occurred just after the GUVs had been added to the δ-hederin

solution. At this stage, we observed no permeabilization of the GUV to dextran. GUVs behaved in exactly the same manner in a SDS solution. Because of its hydrophilic sugar moiety, we can assume that δ-hederin will not flip to the internal monolayer and only induce positive curvature to the external leaflet that would result mostly in budding. The buds were variable in size, suggesting differences in concentrations of δ-hederin in the external monolayer of the vesicles. These buds detached from the membrane and created independent spheres or, upon increasing incubation time, formed pearled structures (buds connected through necks (Fig. 10*H*), later budding) as observed with low concentrations of detergents or lysophosphatidylcholines (66, 74). GUVs in the presence of hederagenin formed intravesicular buds, which is in accordance with the inverted cone shape and resulting negative curvature of this molecule.

In addition to the mechanism of permeabilization induced by α-hederin, the importance of cholesterol concentration within the membrane must be discussed. Calcein release from LUV demonstrated that α-hederin induced no permeabilization in membranes lacking cholesterol, even at a concentration reaching its solubility limit (data not shown). It appears that a certain cholesterol density in the liposomes is required to allow α-hederin to induce pores. The importance of this threshold for pore formation by other saponins agrees with observations reported by others (9, 10, 75, 76). On cells, THP-1 macrophages depleted in cholesterol were protected against cytotoxicity induced by α-hederin. This ascertained the physiological relevance of our work, and the high amounts of cholesterol especially in resistant cancer cell lines could confer some specificity to α-hederin derivatives or similar saponins toward these cells (77, 78). Very rapid cell death was obtained at high concentrations of α-hederin. Gauthier *et al.* (5) showed that α-hederin would induce cancer cell death to a large extent by membrane permeabilization, and similar to our results, they showed that α-hederin was more effective in inducing membrane permeabilization than δ-hederin, whereas hederagenin had no effect on three different cancer cell lines.

In conclusion, this work contributes to the understanding of the mechanism involved in membrane disruption induced by α-hederin and δ-hederin, and other monodesmosidic saponins. It demonstrates the role of cholesterol in this process and shows the effect of the sugar moieties branched on the genin on permeabilization. Understanding the molecular mechanism involved in membrane permeabilization is critical and can be exploited for therapeutic applications, such as the development of pore-forming proteins or peptide-based antibiotics and the design of membrane-permeabilizing drugs that selectively kill cancer cells (79).

Acknowledgments—We thank Henri Burhin and Christian Bailly for suggestions about polymers and providing the polydimethylsiloxane for the electroformation chamber. We are thankful for suggestions in NMR experiments made by Professor A. Schank. δ-Hederin was kindly provided by Prof. Voutquenne-Nazabadioko (CNRS FRE 2715, IFR 53, Reims, France). We also thank the members of the Laboratory of Genetic Development (Institute of Neurosciences, Université Catholique de Louvain, Brussels, Belgium) for access to the fluorescent microscope.

REFERENCES

1. Francis, G., Kerem, Z., Makkar, H. P., and Becker, K. (2002) The biological action of saponins in animal systems: a review. *Br. J. Nutr.* **88,** 587–605
2. Choi, J. H., Lee, H. W., Park, H. J., Kim, S. H., and Lee, K. T. (2008) Kalopanaxsaponin A induces apoptosis in human leukemia U937 cells through extracellular Ca^{2+} influx and caspase-8 dependent pathways. *Food Chem. Toxicol.* **46,** 3486–3492
3. van der Haar, A. W. (1912) Phytochemische untersuchungen in der familie der Araliaceae. I. Saponinartige glykoside aus den blättern von polyscias nodosa und hedera helix. *Arch. Pharm.* **250,** 560
4. Chwalek, M., Lalun, N., Bobichon, H., Plé, K., and Voutquenne-Nazabadioko, L. (2006) Structure-activity relationships of some hederagenin diglycosides: haemolysis, cytotoxicity, and apoptosis induction. *Biochim. Biophys. Acta* **1760,** 1418–1427
5. Gauthier, C., Legault, J., Girard-Lalancette, K., Mshvildadze, V., and Pichette, A. (2009) Haemolytic activity, cytotoxicity, and membrane cell permeabilization of semi-synthetic and natural lupane- and oleanane-type saponins. *Bioorg. Med. Chem.* **17,** 2002–2008
6. Swamy, S. M., and Huat, B. T. (2003) Intracellular glutathione depletion and reactive oxygen species generation are important in α-hederin-induced apoptosis of P388 cells. *Mol. Cell. Biochem.* **245,** 127–139
7. Kumara, S. S., and Huat, B. T. (2001) Extraction, isolation, and characterisation of antitumor principle, α-hederin, from the seeds of *Nigella sativa*. *Planta Med.* **67,** 29–32
8. Danloy, S., Quetin-Leclercq, J., Coucke, P., De Pauw-Gillet, M. C., Elias, R., Balansard, G., Angenot, L., and Bassleer, R. (1994) Effects of α-hederin, a saponin extracted from hedera helix, on cells cultured in vitro. *Planta Med.* **60,** 45–49
9. Armah, C. N., Mackie, A. R., Roy, C., Price, K., Osbourn, A. E., Bowyer, P., and Ladha, S. (1999) The membrane-permeabilizing effect of avenacin A-1 involves the reorganization of bilayer cholesterol. *Biophys. J.* **76,** 281–290
10. Keukens, E. A., de Vrije, T., van den Boom, C., de Waard, P., Plasman, H. H., Thiel, Γ., Chupin, V., Jongen, W. M., and de Kruijff, B. (1995) Molecular basis of glycoalkaloid-induced membrane disruption. *Biochim. Biophys. Acta* **1240,** 216–228
11. Mouritsen, O. G., and Zuckermann, M. J. (2004) What's so special about cholesterol? *Lipids* **39,** 1101–1113
12. Sieben, A., Prenner, L., Sorkalla, T., Wolf, A., Jakobs, D., Runkel, F., and Häberlein, H. (2009) α-Hederin, but not hederacoside C and hederagenin from hedera helix, affects the binding behavior, dynamics, and regulation of β2-adrenergic receptors. *Biochemistry* **48,** 3477–3482
13. Kerdous, R., Heuvingh, J., and Bonneau, S. (2011) Photo-dynamic induction of oxidative stress within cholesterol-containing membranes: shape transitions and permeabilization. *Biochim. Biophys. Acta* **1808,** 2965–2972
14. Tamba, Y., Ariyama, H., Levadny, V., and Yamazaki, M. (2010) Kinetic pathway of antimicrobial peptide magainin 2 induced pore formation in lipid membranes. *J. Phys. Chem. B* **114,** 12018–12026
15. Wesołowska, O., Michalak, K., Maniewska, J., and Hendrich, A. B. (2009) Giant unilamellar vesicles–a perfect tool to visualize phase separation and lipid rafts in model systems. *Acta Biochim. Pol.* **56,** 33–39
16. Sakuma, Y., Taniguchi, T., and Imai, M. (2010) Pore formation in a binary giant vesicle induced by cone-shaped lipids. *Biophys. J.* **99,** 472–479
17. Chong, P. L., and Wong, P. T. (1993) Interactions of Laurdan with phosphatidylcholine liposomes: a high pressure FTIR study. *Biochim. Biophys. Acta* **1149,** 260–266
18. Kaiser, R. D., and London, E. (1998) Location of diphenylhexatriene (DPH) and its derivatives within membranes: comparison of different fluorescence quenching analyses of membrane depth. *Biochemistry* **37,** 8180–8190
19. Lentz, B. R. (1993) Use of fluorescent probes to monitor molecular order and motions within liposome bilayers. *Chem. Phys. Lipids* **64,** 99–116
20. Shinitzky, M., and Barenholz, Y. (1978) Fluidity parameters of lipid regions determined by fluorescence polarization. *Biochim. Biophys. Acta* **515,** 367–394
21. Van Bambeke, F., Mingeot-Leclercq, M. P., Schanck, A., Brasseur, R., and

Tulkens, P. M. (1993) Alterations in membrane permeability induced by aminoglycoside antibiotics–Studies on liposomes and cultured cells. *Eur. J. Pharmacol.* **247,** 155–168
22. Christian, A. E., Haynes, M. P., Phillips, M. C., and Rothblat, G. H. (1997) Use of cyclodextrins for manipulating cellular cholesterol content. *J. Lipid Res.* **38,** 2264–2272
23. Bensikaddour, H., Snoussi, K., Lins, L., Van Bambeke, F., Tulkens, P. M., Brasseur, R., Goormaghtigh, E., and Mingeot-Leclercq, M. P. (2008) Interactions of ciprofloxacin with DPPC and DPPG: fluorescence anisotropy, ATR-FTIR, and ^{31}P NMR spectroscopies and conformational analysis. *Biochim. Biophys. Acta* **1778,** 2535–2543
24. Hope, M. J., Bally, M. B., Webb, G., and Cullis, P. R. (1985) Production of large unilamellar vesicles by a rapid extrusion procedure–Characterization of size distribution, trapped volume, and ability to maintain a membrane potential. *Biochim. Biophys. Acta* **812,** 55–65
25. Bartlett, G. R. (1959) Phosphorus assay in column chromatography. *J. Biol. Chem.* **234,** 466–468
26. Weinstein, J. N., Yoshikami, S., Henkart, P., Blumenthal, R., and Hagins, W. A. (1977) Liposome-cell interaction: transfer and intracellular release of a trapped fluorescent marker. *Science* **195,** 489–492
27. Lelkes, P. I. (1984) in *Liposome Technology* (Gregoriadis, G., ed) Vol. 3, p. 225, CRC Press, Inc., Boca Raton, FL
28. Domenech, O., Francius, G., Tulkens, P. M., Van Bambeke, F., Dufrêne, Y., and Mingeot-Leclercq, M. P. (2009) Interactions of oritavancin, a new lipoglycopeptide derived from vancomycin, with phospholipid bilayers: Effect on membrane permeability and nanoscale lipid membrane organization. *Biochim. Biophys. Acta* **1788,** 1832–1840
29. Loura, L. M., and Prieto, M. (1997) Dehydroergosterol structural organization in aqueous medium and in a model system of membranes. *Biophys. J.* **72,** 2226–2236
30. Wüstner D. (2007) Fluorescent sterols as tools in membrane biophysics and cell biology. *Chem. Phys. Lipids* **146,** 1–25
31. Cheng, K. H., Virtanen, J., and Somerharju, P. (1999) Fluorescence studies of dehydroergosterol in phosphatidylethanolamine/phosphatidylcholine bilayers. *Biophys. J.* **77,** 3108–3119
32. Seras, M., Gallay, J., Vinvent, M., Ollivon, M., and Lesieur, S. (1994) Micelle-vesicle transition of nonionic surfactant-cholesterol assemblies induced by octyl glucoside: a time-resolved fluorescence study of dehydroergosterol. *J. Colloid Interface Sci.* **167,** 159–171
33. Ma, J. Y., Ma, J. K., and Weber, K. C. (1985) Fluorescence studies of the binding of amphiphilic amines with phospholipids. *J. Lipid Res.* **26,** 735–744
34. Montero, M. T., Pijoan, M., Merino-Montero, S., Vinuesa, T., and Hernández-Borrell, J. (2006) Interfacial membrane effects of fluoroquinolones as revealed by a combination of fluorescence binding experiments and atomic force microscopy observations. *Langmuir* **22,** 7574–7578
35. Domenech, O., Dufrêne, Y. F., Van Bambeke, F., Tukens, P. M., and Mingeot-Leclercq, M. P. (2010) Interactions of oritavancin, a new semi-synthetic lipoglycopeptide, with lipids extracted from *Staphylococcus aureus*. *Biochim. Biophys. Acta.* **1798,** 1876–1885
36. Nazari, M., Kurdi, M., and Heerklotz, H. (2012) Classifying surfactants with respect to their effect on lipid membrane order. *Biophys. J.* **102,** 498–506
37. Parasassi, T., De Stasio, G., d'Ubaldo, A., and Gratton, E. (1990) Phase fluctuation in phospholipid membranes revealed by Laurdan fluorescence. *Biophys. J.* **57,** 1179–1186
38. Giraldo, J., Vivas, N. M., Vila, E., and Badia, A. (2002) Assessing the (a)symmetry of concentration-effect curves: empirical versus mechanistic models. *Pharmacol. Ther.* **95,** 21–45
39. Angelova, M. I., Soléau, S., Méléard, P., Faucon, J. F., and Bothorel, P. (1992) Preparation of giant vesicles by external AC electric fields. Kinetics and applications. *Prog. Colloid Polymer Sci.* **89,** 127–131
40. Juhasz, J., Davis, J. H., and Sharom, F. J. (2010) Fluorescent probe partitioning in giant unilamellar vesicles of "lipid raft" mixtures. *Biochem. J.* **430,** 415–423
41. Praper, T., Sonnen, A., Viero, G., Kladnik, A., Froelich, C. J., Anderluh, G., Dalla Serra, M., and Gilbert, R. J. (2011) Human perforin employs different avenues to damage membranes. *J. Biol. Chem.* **286,** 2946–2955
42. Luckey, M. (2008) *Structural Biology: With Biochemical and Biophysical Foundations*, pp. 13–41, Cambridge University Press, New York
43. van Meer, G. (2005) Cellular lipidomics. *EMBO J.* **24,** 3159–3165
44. Lohner, K., and Prenner, E. J. (1999) Differential scanning calorimetry and x-ray diffraction studies of the specificity of the interaction of antimicrobial peptides with membrane-mimetic systems. *Biochim. Biophys. Acta.* **1462,** 141–156
45. Kleinschmidt, J. H., and Tamm, L. K. (2002) Structural transitions in short-chain lipid assemblies studied by ^{31}P NMR spectroscopy. *Biophys. J.* **83,** 994–1003
46. Viseu, M. I., Correia, R. F., and Fernandes, A. C. (2010) Time evolution of the thermotropic behavior of spontaneous liposomes and disks of the DMPC-DTAC aqueous system. *J. Colloid Interface Sci.* **351,** 156–165
47. King, M. D., and Marsh, D. (1989) Polymorphic phase behavior of lysopalmitoylphosphatidylcholine in poly(ethylene glycol)-water mixtures. *Biochemistry* **28,** 5643–5647
48. Nezil, F. A., Bayerl, S., and Bloom, M. (1992) Temperature-reversible eruptions of vesicles in model membranes studied by NMR. *Biophys. J.* **61,** 1413–1426
49. Parasassi, T., De Stasio, G., Ravagnan, G., Rusch, R. M., and Gratton, E. (1991) Quantitation of lipid phases in phospholipid vesicles by the generalized polarization of Laurdan fluorescence. *Biophys. J.* **60,** 179–189
50. Parasassi, T., Giusti, A. M., Raimondi, M., and Gratton, E. (1995) Abrupt modifications of phospholipid-bilayer properties at critical cholesterol concentrations. *Biophys. J.* **68,** 1895–1902
51. Käs, J., and Sackmann, E. (1991) Shape transitions and shape stability of giant phospholipid vesicles in pure water induced by area-to-volume changes. *Biophys. J.* **60,** 825–844
52. Hamada, T., Miura, Y., Ishii, K., Araki, S., Yoshikawa, K., Vestergaard, M., and Takagi, M. (2007) Dynamic processes in endocytic transformation of a raft-exhibiting giant liposome. *J. Phys. Chem. B* **111,** 10853–10857
53. Róg, T., Pasenkiewicz-Gierula, M., Vattulainen, I., and Karttunen, M. (2009) Ordering effects of cholesterol and its analogues. *Biochim. Biophys. Acta* **1788,** 97–121
54. Nishikawa, M., Nojima, S., Akiyama, T., Sankawa, U., and Inoue, K. (1984) Interaction of digitonin and its analogs with membrane cholesterol. *J. Biochem.* **96,** 1231–1239
55. Bangham, A. D., Horne, R. W., Glauert, A. M., Dingle, J. T., and Lucy, J. A. (1962) Action of saponin on biological cell membranes. *Nature* **196,** 952–955
56. Huang, J., and Feigenson, G. W. (1999) A microscopic interaction model of maximum solubility of cholesterol in lipid bilayers. *Biophys. J.* **76,** 2142–2157
57. Karatekin, E., Sandre, O., Guitouni, H., Borghi, N., Puech, P. H., and Brochard-Wyart, F. (2003) Cascades of transient pores in giant vesicles: line tension and transport. *Biophys. J.* **84,** 1734–1749
58. Lee, M. T., Hung, W. C., Chen, F. Y., and Huang, H. W. (2008) Mechanism and kinetics of pore formation in membranes by water-soluble amphipathic peptides. *Proc. Natl. Acad. Sci. U.S.A.* **105,** 5087–5092
59. Sudbrack, T. P., Archilha, N. L., Itri, R., and Riske, K. A. (2011) Observing the solubilization of lipid bilayers by detergents with optical microscopy of GUVs. *J. Phys. Chem. B* **115,** 269–277
60. Zimmerberg, J., and Kozlov, M. M. (2006) How proteins produce cellular membrane curvature. *Nat. Rev. Mol. Cell Biol.* **7,** 9–19
61. van Duyl, B. Y., Meeldijk, H., Verkleij, A. J., Rijkers, D. T., Chupin, V., de Kruijff, B., and Killian, J. A. (2005) A synergistic effect between cholesterol and tryptophan-flanked transmembrane helices modulates membrane curvature. *Biochemistry* **44,** 4526–4532
62. Heinrich, V. V., Svetina, S., and Zeks, B. (1993) Nonaxisymmetric vesicle shapes in a generalized bilayer-couple model and the transition between oblate and prolate axisymmetric shapes. *Phys. Rev. E. Stat. Phys. Plasmas Fluids Relat. Interdiscip. Topics* **48,** 3112–3123
63. Sheetz, M. P., and Singer, S. J. (1974) Biological membranes as bilayer couples. A molecular mechanism of drug-erythrocyte interactions. *Proc. Natl. Acad. Sci. U.S.A.* **71,** 4457–4461
64. McLaughlin, A. C., Cullis, P. R., Hemminga, M. A., Hoult, D. I., Radda, G. K., Ritchie, G. A., Seeley, P. J., and Richards, R. E. (1975) Application of ^{31}P NMR to model and biological membrane systems. *FEBS Lett.* **57,**

213–218
65. Cullis, P. R., De Kruyff, B., and Richards, R. E. (1976) Factors affecting the motion of the polar headgroup in phospholipid bilayers. A ^{31}P NMR study of unsonicated phosphatidylcholine liposomes. *Biochim. Biophys. Acta* **426,** 433–446
66. Allain, J. M., and Ben Amar, M. (2006) Budding and fission of a multiphase vesicle. *Eur. Phys. J. E. Soft. Matter* **20,** 409–420
67. Alves, I. D., Goasdoué, N., Correia, I., Aubry, S., Galanth, C., Sagan, S., Lavielle, S., Chassaing, G. (2008) Membrane interaction and perturbation mechanisms induced by two cationic cell penetrating peptides with distinct charge distribution. *Biochim. Biophys. Acta* **1780,** 948–959
68. Israelachvili, J. N., Mitchell, D. J., and Ninham, B. W. (1977) Theory of self-assembly of lipid bilayers and vesicles. *Biochim. Biophys. Acta* **470,** 185–201
69. Matsuzaki, K., and Horikiri, C. (1999) Interactions of amyloid β-peptide (1–40) with ganglioside-containing membranes. *Biochemistry* **38,** 4137–4142
70. Valcarcel, C. A., Dalla Serra, M., Potrich, C., Bernhart, I., Tejuca, M., Martinez, D., Pazos, F., Lanio, M. E., and Menestrina, G. (2001) Effects of lipid composition on membrane permeabilization by sticholysin I and II, two cytolysins of the sea anemone *Stichodactyla helianthus*. *Biophys. J.* **80,** 2761–2774
71. Lin, F., and Wang, R. (2010) Hemolytic mechanism of dioscin proposed by molecular dynamics simulations. *J. Mol. Model* **16,** 107–118
72. Wassler, M., Jonasson, I., Persson, R., and Fries, E. (1987) Differential permeabilization of membranes by saponin treatment of isolated rat hepatocytes. Release of secretory proteins. *Biochem. J.* **247,** 407–415
73. Venturoli, D., and Rippe, B. (2005) Ficoll and dextran *vs.* globular proteins as probes for testing glomerular permselectivity: effects of molecular size, shape, charge, and deformability. *Am. J. Physiol. Renal Physiol.* **288,** F605–F613
74. Tanaka, T., Sano, R., Yamashita, Y., and Yamazaki, M. (2004) Shape changes and vesicle fission of giant unilamellar vesicles of liquid-ordered phase membrane induced by lysophosphatidylcholine. *Langmuir* **20,** 9526–9534
75. Akiyama, T., Takagi, S., Sankawa, U., Inari, S., and Saitô, H. (1980) Saponin-cholesterol interaction in the multibilayers of egg-yolk lecithin as studied by deuterium nuclear magnetic resonance–digitonin and its analogs. *Biochemistry* **19,** 1904–1911
76. Li, X. X., Davis, B., Haridas, V., Gutterman, J. U., and Colombini, M. (2005) Proapoptotic triterpene electrophiles (avicins) form channels in membranes: cholesterol dependence. *Biophys. J.* **88,** 2577–2584
77. Todor, I. N., Lukyanova, N. Y., and Chekhun, V. F. (2012) The lipid content of cisplatin- and doxorubicin-resistant MCF-7 human breast cancer cells. *Exp. Oncol.* **34,** 97–100
78. Gayet, L., Dayan, G., Barakat, S., Labialle, S., Michaud, M., Cogne, S., Mazane, A., Coleman, A. W., Rigal, D., and Baggetto, L. G. (2005) Control of P-glycoprotein activity by membrane cholesterol amounts and their relation to multidrug resistance in human CEM leukemia cells. *Biochemistry* **44,** 4499–4509
79. Pálffy, R., Gardlík, R., Behuliak, M., Kadasi, L., Turna, J., and Celec, P. (2009) On the physiology and pathophysiology of antimicrobial peptides. *Mol. Med.* **15,** 51–59

3.1.2. Phase separation and permeabilization induced by the saponin α-hederin and its aglycone hederagenin in a raft mimicking bilayer (**article 2, submitted**)

Authors: Joseph Lorent[1,4], Laurence Lins[2], Domenech Òscar[3], Joelle Quetin-Leclercq[4], Robert Brasseur[2] and Marie-Paule Mingeot-Leclercq[1]

[1]Université catholique de Louvain, Louvain Drug Research Institute, Cellular and Molecular Pharmacology, UCL B1.73.05, avenue E. Mounier 73, B-1200 Brussels, Belgium.
[2]ULg, Centre de Biophysique Moléculaire Numérique, Agro-BioTech Gembloux, Passage des Déportés, 2, B- 5030 Gembloux, Belgium.
[3]University of Barcelona, Departament de Fisicoquímica, Facultat de Farmàcia, UB and Institut de Nanociència i Nanotecnologia IN, 08028 Barcelona, Spain.
[4]Université catholique de Louvain, Louvain Drug Research Institute, Pharmacognosy, B1.72.03, avenue E. Mounier 72, B-1200 Brussels, Belgium.

Subject and background : In addition to the immediate permeabilization and macroscopic pore formation induced by α-hederin on GUVs at relatively high concentrations (40 µM) (see 3.1.1.), we analyzed the effect of lower concentrations of α-hederin (10 µM) but also hederagenin on GUVs. This article will give insights into a new striking phenomenon observed with both compounds which might have major implications for saponin and triterpenoid activity.

INTRODUCTION

Lipid phase separation has become an important concept in membrane organization and has been associated with the formation of lateral functional domains in cells, also called lipid rafts. Rafts are temporary domains having a nanoscopic size of about 10-200 nm. Their fusion into larger domains would provide platforms for protein signaling (Lingwood and Simons, 2010). Some of the proteins located in lipid rafts are involved in cancerogenesis and apoptosis (Staubach and Hanisch, 2011). Disruption or fusion of lipid rafts can lead to the activation or inhibition of these proteins which makes them a potential target in cancer therapy (George and Wu, 2012). Cholesterol is an essential component of these lipid rafts (Lingwood and Simons, 2010). Due to its rigid planar steroid ring system, it induces a high conformational order of the lipid acyl chains. This results in a condensing effect with a decrease of the area occupied by the other lipids as well as an increase of the bilayer thickness. It also modifies the thermotropic phase transition between the liquid-disordered, often termed fluid phase (L_d or L_α), and the solid-ordered, also called gel phase (S_o) by inducing an intermediate liquid-ordered (L_o or L_β) phase (Simons and Vaz, 2004). In model membranes, the L_o phase is laterally separated from the L_d phase and is thought to mimic lipid rafts in cells.

In specific situations, we can observe the coexistence of bilayer phases with non-lamellar lipid mesophases (hexagonal, cubic, isotropic). In biological membranes, some of these non-bilayer phases are thought to be important for protein/membrane interactions and fusion (de Kruijff, 1997;Luzzati, 1997). Besides their biological function, non-lamellar phases can be induced when amphiphilic drugs or peptides come into contact with membranes. The formation of the normal isotropic or hexagonal (H_I) phase has been put in relationship with the permeabilization of membranes (Hallock et al., 2003;Correia et al., 2012). At intermediate amphiphiles/phospholipids ratios, the bilayer phase can coexist with the newly formed phase (Almgren, 2000). Sometimes, even macroscopic phase separation becomes visible in the sample (Kleinschmidt and Tamm, 2002;Lohner et al., 1999).

Several saponins, amphiphilic compounds of natural origin, are kown for their ability to interact with cholesterol, a major component of rafts (Yi et al., 2009;Bangham et al., 1962). Among them, avicin D, ginsenoside Rh2 and glycyrrhizin alter membrane permeability and interact with lipid rafts (Xu et al., 2009;Sakamoto et al., 2013;Yi et al., 2009). Some triterpenic acids, lacking the sugar chains of saponins, have shown the same potential (Bayer et al., 2011). In a recent study (Lorent et al., 2013), we demonstrated that α-hederin, a triterpenoid monodesmosidic saponin, but not hederagenin, its triterpenic aglycone, induced cholesterol dependent permeabilization and budding. Both molecules induced the formation of a new lipid mesophase, whenever this effect was much more important with α-hederin. In addition, new tubular structures presenting high curvature grew out of membranes when they have been put in contact with glycoalkaloids (Keukens et al., 1995) and digitonin (Elias et al., 1978). The formation of the new lipid phase depends upon interaction of the compound with the sterol, its molecular shape and the presence of the sugar chain at C3 on the aglycone (Armah et al., 1999). In parallel, we reported that α-hederin induced toroidal pores which supposed saponin enriched spots with increased transbilayer curvature in the bilayer (Lorent et al., 2013). Nevertheless, for α-hederin or hederagenin, the formation of lateral domains has never been shown. Understanding this mechanism should give interesting clues on how saponins and triterpenic acids are able to interact with membranes and especially membrane rafts.

For this purpose, we investigated the ability of α-hederin (3-*O*-α-L-rhamnopyranosyl-(1→2)-α-L-arabinopyranoside) and hederagenin, its aglycone lacking the sugar chain, to induce lateral phase separation in a dimyristoylphosphatidylcholine (DMPC)/cholesterol (chol) (3:1, mol/mol) model. This binary membrane model has the advantages to be composed of a phospholipid which is in the fluid state at ambient temperature and to present a nanoscopic L_o phase enriched in cholesterol. This is similar to what has been observed for lipid rafts in cells even if lipid composition in biological membranes is much more complex (Loura et al., 2001;de Almeida et al., 2009;Meinhardt et al., 2013;Lorent et al., 2013;van Meer, 2005). The same binary model has also been used to show domain formation induced by glycalkaloids in monolayers (Stine et al., 2006;Walker et al., 2008) and to investigate the mechanism of permeabilization induced by α-hederin (Lorent et al., 2013), which facilitated comparison with other published results.

We selected complementary investigation techniques to understand the membrane activity of α-hederin and hederagenin. By molecular modeling and fluorescence spectroscopy of dehydroergosterol (DHE), a fluorescent cholesterol analogue (Wustner, 2007), we demonstrated the ability of α-hederin and hederagenin to interact with sterols. Using Förster resonance energy transfer (FRET) of DHE and diphenylhexatriene-phosphatidylcholine (DPH-PC) inserted into Multilamellar Vesicles (MLVs), we monitored quantitative and temporal aspects of lipid phase separation. Using Giant Unilamelar Vesicles (GUVs), we visualized the effect of α-hederin and hederagenin on lipid phase separation by fluorescence and confocal microscopy using Texas-Red-dipalmitoylphosphoethanolamine (TR-DPPE) and 2-dipalmitoyl-*sn*-glycero-3-phosphoethanolamine-*N*-7-nitro-2-1 3-benzoxadiazol-4-yl (NBD-DPPE), located in L_d and L_o phases respectively (Juhasz et al., 2010). In parallel, we determined the effect of α-hederin on Supported Planar Bilayers (SPBs) by Atomic Force Microscopy (AFM) to gain insights into the nanoscopic aspects of phase separation.

This study shows how α-hederin and hederagenin are able to promote the formation of macroscopic domains in a nanoscopic raft model. It gives some insights on how saponins and triterpenic acids could be able to interact with rafts in cellular membranes and induce membrane permeabilization.

MATERIAL AND METHODS

Material

α-Hederin and hederagenin (HPLC quality) were purchased from Extrasynthese, (Genay, France) and dissolved in ethanol. After evaporation of the solvent, the residue was dissolved in buffer solution (10 mM Tris.HCl adjusted at pH=7.4 with NaOH) containing 0.1% DMSO to prevent solubility problems. DMPC (dimyristoyl-*sn*-glycero-3-phosphocholine) and cholesterol were purchased from Avanti Polar Lipids. TR-DPPE (Texas-Red 1,2-dipalmitoyl-*sn*-glycero-3-phosphoethanolamine), NBD-DPPE (*N*-(7-nitrobenz-2-oxa-1,3-diazol-4-yl)-1,2-dihexadecanoyl-*sn*-glycero-3-phosphoethanolamine), DPH-PC (Diphenylhexatriene Phosphatidylcholine) and R18 (octadecylrhodamine) were purchased from Invitrogen (Paisley, Scotland, UK). DHE (dehydroergosterol) and FITC-dextran (4-kDa) was purchased by Sigma-Aldrich (St. Louis, MO).

PDMS (Polydimethylsiloxane) was kindly provided by Henri Burhin and Christian Bailly (SST/Institute of Condensed Matter and Nanosciences, Bio and soft matter, Université catholique de Louvain, Louvain-la-Neuve). All other reagents were from E. Merck AG (Darmstadt, Germany).

Preparation of MLVs

Multilamellar vesicles (MLVs) composed of DMPC:Chol (3:1) were prepared by the extrusion technique(Hope et al., 1985), using a 10 ml thermobarrel extruder (Lipex Biomembranes, Vancouver, Canada). A dry lipid film was formed by evaporating a lipid solution of 10 mg/ml of total lipid, in $CHCl_3$:CH_3OH (2:1 v/v) using a rotavapor R-210 (Buchi Labortechnik AG, Flawil, Switzerland). The film was resuspended in a buffer solution (Tris-HCl 10 mM at pH=7.4). This buffer solution was used troughout all experiments. The suspension was submitted to five cycles of freezing/thawing to obtain multilamellar vesicles (MLVs). The lipid concentration of the liposomal suspension was measured by phosphorous quantification(Bartlett, 1985) and adjusted according to the experimental protocol used.

Molecular modeling and assembly of α-hederin and hederagenin with lipids

The assembly of α-hederin or hederagenin with DMPC or cholesterol was studied by molecular modeling and the Big Layer Method. This method proceeds in two steps (i) calculation of paired interactions between the molecules and (ii) construction of a grid of 600 x 600 molecules, taking the molar ratios account.

The first step was derived from the hypermatrix method described elsewhere (Brasseur et al., 1987;Lins et al., 1999). The molecules (α-hederin, hederagenin, cholesterol and DMPC) were first oriented at the interface, taking their hydrophobic and hydrophilic centers into account (Brasseur, 1990). For each pair of molecules (α-hederin/ α-hederin, α-hederin/Chol, α-hederin/DMPC, hederagenin/hederagenin, hederagenin/Chol and hederagenin/DMPC), the interaction energies (sum of electrostatic, Van der Waals, hydrophobic energies) were calculated for a large number of positions, resulting from translations and rotations of one molecule toward the other. In this study, molecules underwent 36 rotations around themselves with a precision of 10°. For each of these positions, horizontal and vertical translations were carried out on a distance of 10 and 5 Å with a step of 0.5 and 0.25 Å, respectively. For all those positions, an

additional tilt of -10° to +10° by step of 0.5° was further applied. The total number of relative positions tested was thus more than 23 400 000 000 (36x36x21x21x41). For each pair of molecules, the statistical Boltzmann energy was considered. The latter was calculated taking into account a Boltzmann statistics corresponding to the sum of the interaction energy of each relative position tested multiplied by the probability of the position. This interaction energy matrix was then used in the second step.

The second step consisted in the construction and minimization of the system using the interaction matrix calculated in the first step. A grid of 40 000 (200x200) molecules, initially positioned at random, was constructed and the energy of the system was calculated. The energy of one molecule was equal to the average of the interaction energies with its 24 closest neighbors in the grid. Random permutations were made and the energy of the new configuration was calculated. By a Monte Carlo procedure, this new configuration was kept or not, as a function of the energy difference between the two states. For a grid of 360 000 molecules, one calculation step consists in 360 000 permutations. 100 000 steps were carried out. For the molecules at the border of the grid, the molecules at the opposite border were considered as their closest neighbours, avoiding border limits.

Graphically, each molecule type was represented by a colored point and all the points were represented on the grid. This allowed us to visualize preferential interactions and phase separation between the molecules studied.

Steady-state fluorescence measurements

Fluorescence spectra were performed at 25°C using a LS55 luminescence spectrometer (Perkin Elmer Ltd., Beaconsfield, UK). FRET measurements of DHE and DPH-PC were done on a Spectramax M3 (Molecular Devices, Sunnyvale, USA).

Dehydroergosterol (DHE) spectroscopy

Spectral features of DHE in media of different polarities and lipid membranes have been extensively studied (Loura and Prieto, 1997;Schroeder, 1984). Emission spectra of DHE in aqueous medium give insights on the ratio between monomer and the aggregated form of the sterol. When DHE is excited at 310 nm in aqueous solution, it presents a low intensity monomeric peak at 375 nm and a high intensity maximum of structured emission at 395 and 424

nm due to the presence of microcrystals in buffer solution. The ratio between fluorescence intensities at 375 vs 395 or 424 nm (I_{375}/I_{395} or I_{375}/I_{424}) reflects the ratio of monomers vs. microscrystals in aqueous solution(Loura and Prieto, 1997). Moreover, a decrease in the dielectric constant of the microenvironment of DHE induces a blue shift of λ_{max} emission (Cheng et al., 1999).

The aqueous dispersions of DHE (10 µM) were prepared by evaporation of an ethanol solution in which the DHE was dissolved. DHE was resuspended with 1 µl of DMSO and 1 ml of buffer (10 mM Tris.HCl; pH=7.4) to obtain DHE in a final 0.1% DMS0 solution. Fluorescence emission spectra of DHE in buffer solution were taken at increasing concentrations of α-hederin and hederagenin and the intensity of the monomeric vs microcrystalline peak ratio was put upon concentration. The influence of DMSO and DHE concentration was checked. Excitation monochromator was set to 310 nm (slit = 4.5) and the emission spectra was recorded from 335 to 445 nm (Cheng et al., 1999;Schroeder et al., 1987).

FRET between DHE and DPH-PC

FRET provides a measure of the average distance between an array of donor and acceptor molecules. If the probes (DHE and DPH-PC e.g.) show varying partition coefficients between two phases (e.g. L_o and L_d phases) the assay can be used to detect membrane heterogeneities (Parker et al., 2004). MLVs were composed of DMPC:Chol:DHE:DPH-PC (75/24/1/0.1 [mol/mol]) and were adjusted to 50 µM of total lipid concentration in buffer solution. FRET of DHE (donor) and DPH-PC (acceptor) in lipid bilayers was determined by exciting DHE at 310 nm (slit = 4 nm) and taking emission intensities at 371 nm (DHE emission peak) and 430 nm (DPH-PC emission peak). The fluorescence intensity ratio (I_{430}/I_{371}) was taken as a measure of the energy transfer efficiency. Use of the intensity ratio largely eliminated the noise introduced by variations in lipid and probe concentrations between samples.

Electroformation of Giant Unilamellar Vesicles (GUVs)

DMPC:Chol (3:1) giant unilamellar vesicles were prepared by electroformation as described previously (Angelova et al., 1992;Lorent et al., 2013). Briefly, 1µl of a chloroform solution of DMPC:Chol (5mg/ml), was spread on an indium thin oxide (ITO) covered glass. All fluorescent probes used were added to the chloroform solution at 0.1% mol/mol.The solution was

dried in a vacuum chamber during 2h. An electroformation chamber was constructed using another ITO covered glass slide, were the conducting face pointed to the interior of the electroformation chamber. Polydimethylsiloxane containing 5% aerosol was used to separate both glass slides. The lipid film was hydrated with a sucrose solution of 0,1M. GUVs were grown by applying a sinusoidal alternative current of 10 Hz and 1V for 2h at 60°C.

Fluorescence microscopy

Developments in fluorescence microscopy, combined with the ability to produce giant unilamellar vesicles, allowed direct visualization of liquid-liquid phase separation in DMPC/cholesterol mixtures. The probes TR-DPPE and NBD-DPPE were used to visualize the potential of α-hederin (10 µM) and hederagenin (40 µM) to induce phase separation, budding, vesicle deformation and macroscopic pore formation. TR-DPPE is a fluorescent probe which partitions into the L_d phase and NBD-DPPE into the L_o phase (Juhasz et al., 2010). We used a fluorescent microscope (Axioskop 40, Carl Zeiss, Jena, Germany) and signals were recorded with a Nikon digital sight DS-5M (Nikon, Tokyo, Japan). The acquisition software used was NIS-Elements v. 2.11. All observations were made in an observation chamber of 400 µl filled with a sucrose solution of 0.1 M and α-hederin and hederagenin. One GUV was followed for at least 4h (with hederagenin phase separation was much slower, and therefore we showed a typical example of a GUV presenting phase separation after 4 and 48h). Three independent experiments were performed.

A movie showing phase separation in a GUV marked by TR-DPPE was recorded. Speed is accelerated 4 times (one second in the movie represents 4 real seconds) and contrast was slightly enhanced.

Quantification of different features (budding, deformation, phase separation, pore formation and spherical vesicles) was made for a total number of 200 vesicles.

Confocal microscopy of domain formation

Confocal microscopy was performed by using an Axioobserver spinning disk inverted microscope Z.1 (Carl Zeiss, Jena, Germany). The spinning disk model was a CSU-X1 (Yokogawa Electric corporation, Tokyo, Japan). We used an EC Plan-Neofluar 40x/1.30 Oil DIC M27, a LCI Plan-Neofluar 63x/1.30 Imm Korr DIC M27 or a Plan-Apochromat 100x/1.40 Oil

DIC M27 objective. Images were recorded with an AxioCamMR3 using the software of Carl Zeiss AxioVision 4.8.2. GUVs were incubated in an artificial chamber containing ~150 µl of sucrose solution (0.1M) and 10 µM of α-hederin or 40 µM of hederagenin. Those presenting typical stages of phase separation were recorded. TR-DPPE and NBD-DPPE were excited at 561 and 488 nm and emission was recorded at 617/73 and 520/35 nm, respectively.

Permeability of dextran through membranes of GUVs

After electroformation, 20 µl of GUVs were added to the artificial chamber (see above) containing in addition to 10µM of α-hederin or 40 µM of hederagenin, 20 µM of FITC-dextran (mean molecular weight of 4-kDa). The FITC-dextran was excited at 488 nm, and the emission was recorded with a 520/35 nm emission filter. TR-DPPE was visualized as described in confocal microscopy. The difference in fluorescence intensity between the outside and inside of one GUV reflects the membrane integrity. We chose GUVs that presented typical features (budding, phase separation) which developed during incubation time.

We normalized the difference in fluorescence intensity outside and inside the vesicle by dividing the fluorescence values by the highest intensity recorded and multiplying by a factor of 1000. The difference of the mean of 20 normalized values taken from inside and outside the vesicle was then determined. The significant difference was calculated using a Student's t-test.

AFM of supported planar bilayers (SPBs)

SPBs were prepared on mica as previously described(Domenech et al., 2009). Briefly, 50 µL of LUVs at 500 µM of DMPC:Chol (3:1, mol/mol) in buffer containing 20 mM of $CaCl_2$ were deposited onto freshly cleaved mica mounted on a teflon disk. Samples were incubated at 65ºC for 2h in an oven preventing water evaporation. After this period, non-adsorbed liposomes and calcium were eliminated by gentle washing with buffer (10 mM Tris, 150 mM NaCl, pH 7.40).

Liquid AFM imaging was performed using a multimode microscope controlled by Nanoscope V electronics (Bruker AXS Corporation, Santa Barbara, CA) in contact mode (CMAFM). To perform AFM imaging it was necessary to drift equilibrate and thermally stabilize the cantilever for no less than 30 min in the presence of buffer. To minimize the applied force on the sample, the set point was continuously adjusted during imaging. V-shaped Si_3N_4 cantilevers (MLCT-AUNM, Veeco) with a nominal constant of 0.01 $N \cdot m^{-1}$ were used. Images were acquired

at 0º scan angle with a scan rate of 2 Hz. All images were processed through commercial NanoScope Analysis Software (Bruker AXS Corporation, Santa Barbara, CA).

3D reconstruction, texture profile and grain size analysis of AFM raw data

For 3D reconstruction of AFM sheets (Gwyddion 2.26, GNU [General Public License]), we corrected for horizontal scars, and leveled the image by a mean plane subtraction. We used the full z-scale for representation which is shown at the right side of each sheet. 3D reconstruction parameters were φ=40°, θ=-61°, scale=2.3 and value scale=0.1.

Texture profiles of AFM raw data were made using the same processing methods as for 3D reconstruction. The texture profile was extracted from a straight line at y=9.48 µm (red line, Fig 10A). We used this line because it passes through a small hole of the SPB present before injection of α-hederin and therefore indicating the thickness of the bilayer ~ 4nm.

Results

Formation of mixed micelles between DHE and α-hederin

We analyzed the effects of α-hederin (Fig 1A,C) and hederagenin (Fig. 1B,D) on DHE in aqueous solution to understand interactions of the saponin/triterpenic acid with sterols. DHE forms mainly microcrystals in aqueous solution(Loura and Prieto, 1997) and exhibits fluorescence properties which give information on the molecular organization. By monitoring the fluorescence emission spectrum of DHE at excitation wavelength of 310 nm, the fluorescence maxima were near 375 nm, 402 nm and 424 nm (Fig. 1A,B). This agrees with previously obtained results (Schroeder et al., 1987;Loura and Prieto, 1997).

By adding α-hederin at increasing concentrations, we observed (i) a shift of emission maxima from 402 nm to 396 nm and (ii) an increase of the intensity ratio between the monomeric peak and the structured emission (Fig. 1C). The blue shift represents a reduction of the dielectric constant or polarity of the DHE environment, which could correspond to the formation of DHE /α-hederin aggregates as it has been previously suggested (Lorent et al., 2013). The increase of the ratio between the monomeric peak (first maximum at 375 nm) and the structured emission (second and third maxima around 395 and 424 nm) (I_{375}/I_{395} or I_{375}/I_{424}) reflects the separation of DHE molecules from the microcrystals and their preferential interaction with saponin molecules. Hederagenin was more efficient than α-hederin regarding the blue shift of the structured peak (402 to 391 nm) (Fig. 1B) and the increase of the intensity ratio (Fig. 1D). This means that hederagenin induced a more hydrophobic environment for DHE than α-hederin most probably due to the lack of a sugar chain at C3.

When the intensity ratio was plotted upon the logarithmus of α-hederin/hederagenin concentration (Fig. 1C,D), we obtained a sigmoidal relation. For α-hederin, we found an inflexion point of 12.33 ± 3.21 µM which corresponded closely to its CMC value previously reported (13 µM in water) (Bottger et al., 2012). For hederagenin, the inflexion point was 14.33 ± 8.46 µM. To our knowledge, the CMC of hederagenin hasn't been reported in literature but asiatic acid, which structure is only slightly different from hederagenin, possesses a CMC of 15 ± 2 µM (in PBS at pH of 7.2) (Rafat et al., 2008).

At a glance, these results suggest that α-hederin and hederagenin are able to form mixed micelles (or aggregates) in aqueous solution with sterols above a critical concentration of 12 and 14 µM, respectively.

FIGURE 1

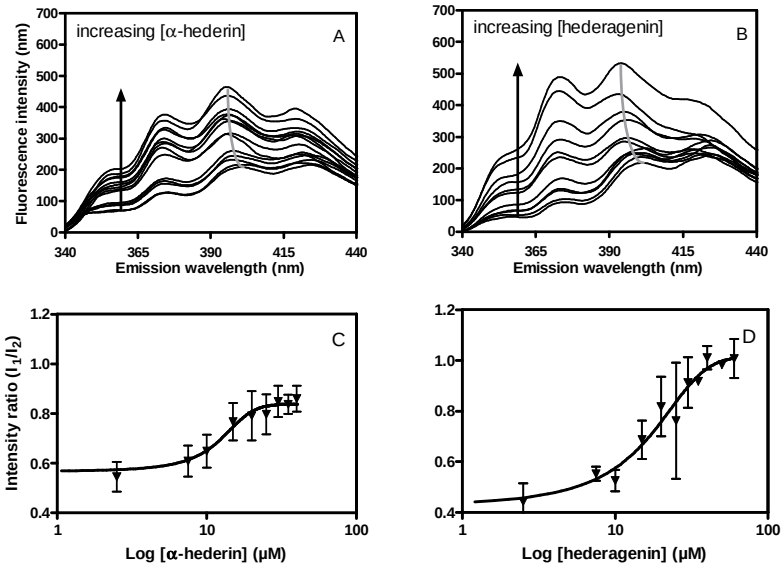

Fluorescence emission spectra of DHE in aqueous solution (0.1% DMSO, λ_{exc}=310 nm) (A,B). Increasing concentrations (arrow) of α-hederin (A) and hederagenin (B) (from 0 to 60 µM) were used. DHE concentration was set up at 4 µg/ml. The fluorescence intensity ratio I_{375}/I_{395} upon the $\log_{10}$ of α-hederin (C) and hederagenin (D) concentration is shown and inflexion point was determined making a non-linear regression (Hill function) of data values. The grey line represents the blue shift of the maxima at 395 nm.

Molecular interaction and simulation of domain formation

To gain information about the preferential orientation of α-hederin/hederagenin in membranes and their molecular interaction with DMPC/Cholesterol, we used molecular modeling.

α-Hederin inserted into the membrane by pointing its sugar moiety to the membrane exterior (Fig. 2). This sugar moiety was placed in the hydrophilic part of the membrane. In contrast, the triterpenic part was located such as cholesterol in the lipophilic portion of the membrane. When interacting with cholesterol, α-hederin pointed its carboxylic function (its beta side) towards the beta side of the cholesterol molecule. In contrast, when α-hederin interacted with DMPC, it pointed its carboxylic function away from the phospholipid. The interaction mostly involved the sugar moiety of the saponin as the hydrophilic head of DMPC. A ternary

structure composed of cholesterol, α-hederin and DMPC as cholesterol bond to the side of the carboxylic function and DMPC to the other could therefore be possible. This is similar to what has been proposed for glycoalkaloids (Keukens et al., 1995).

The triterpenic acid hederagenin was less profoundly inserted into the hydrophobic core than the aglycone of its corresponding saponin. The sugar chain could therefore play an important role and forcing the saponin deep into the membrane by interacting with the hydrophilic heads of the surrounding molecules. Hederagenin bound in a different manner to cholesterol than to DMPC which does not exclude the formation of a ternary complex.

FIGURE 2

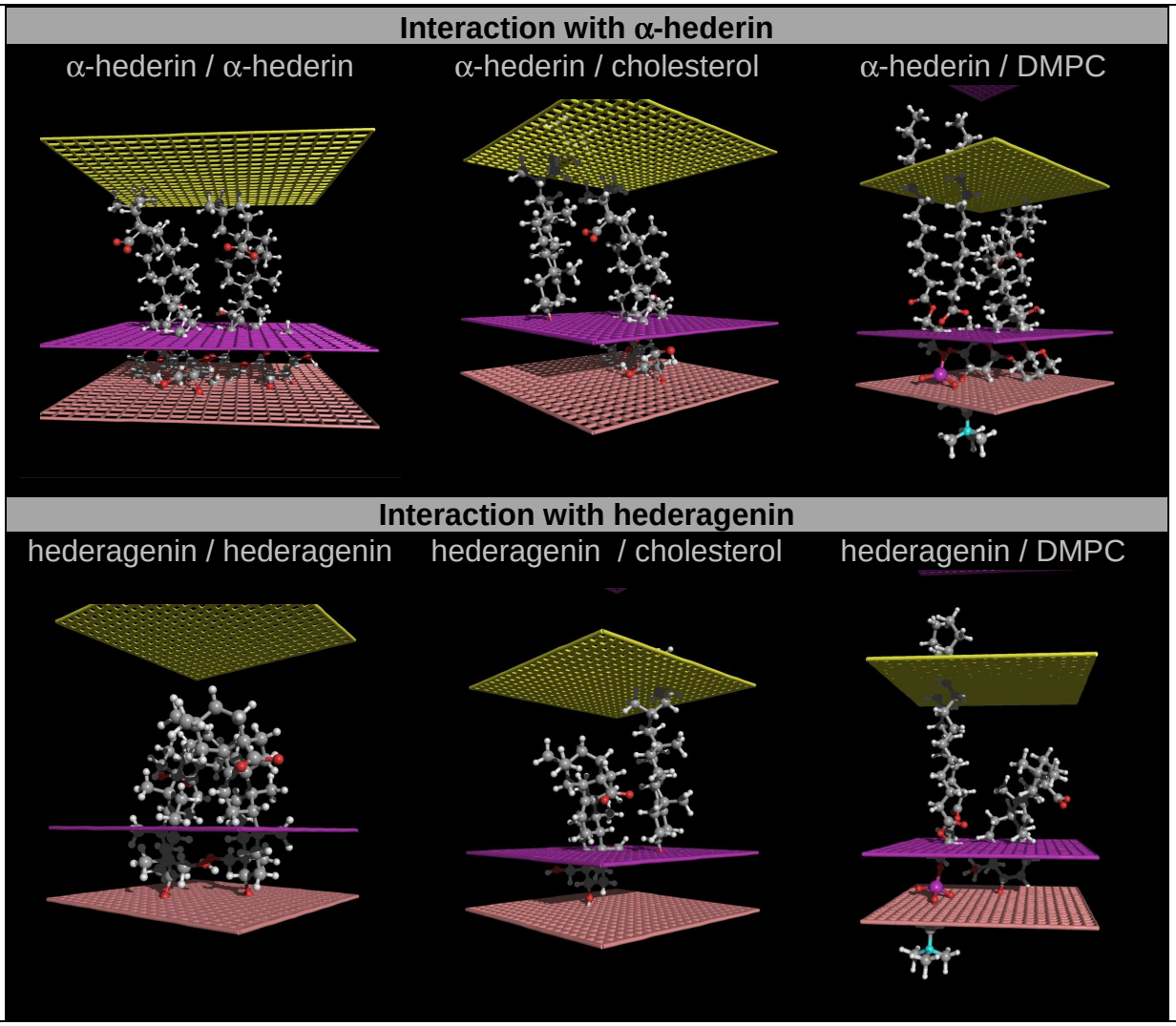

The formation of molecular complexes of α-hederin and hederagenin with themselves, cholesterol and DMPC in a lipid membrane (as determined by molecular modeling). The yellow grid represents the hydrophobic middle of the monolayer. The violet grid separates the hydrophobic core from the hydrophilic membrane part and the rose grid reflects the interfacial area separating the layer from the aqueous environment.

After establishing the most probable interaction conformers, we wanted to know how α-hederin and hederagenin would partition laterally into a membrane composed of DMPC and cholesterol and if they would be able to induce a phase separation. For this purpose, we took benefit from Monte-Carlo simulations which simulated monolayers of different compositions. In monolayers containing 25% cholesterol, small cholesterol domains were obtained (Fig. 3A). This

is in agreement with domains observed in Langmuir monolayers composed of DMPC and cholesterol(Seul and Sammon, 1990). By adding α-hederin, we observed a sequestration of cholesterol molecules into larger domains (Fig. 3B). α-Hederin was located between cholesterol and DMPC molecules and "forced" the cholesterol molecules together.

Hederagenin was mostly colocalized with cholesterol and induced the formation of domains with a ramified shape. These domains were smaller and more numerous than those induced by α-hederin (Fig. 3C).

FIGURE 3

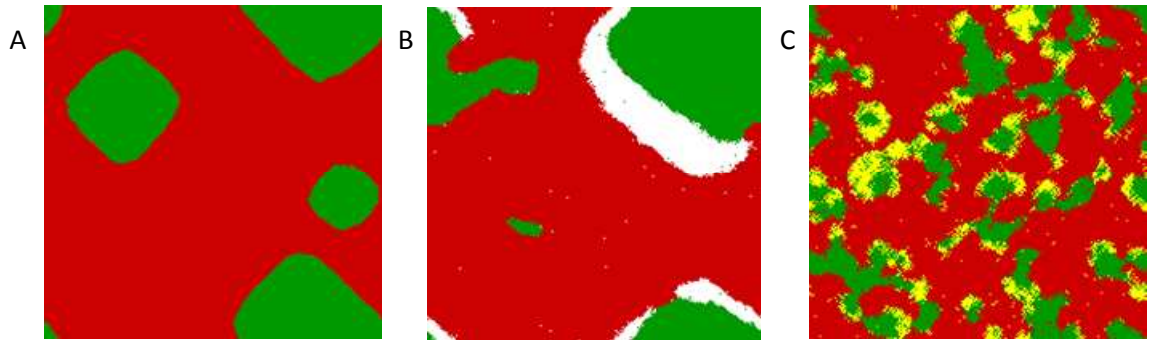

Monolayer grid of 200X200 molecules calculated by the Big Layer Method. Each pixel represents a molecule. Red: DMPC molecules; green: cholesterol molecules; white: α hederin molecules and yellow : hederagenin molecules. (A) DMPC:Cholesterol at a molar ratio of 0.75:0.25, (B) DMPC/Cholesterol/α-hederin at 0.67:0.23:0.1, (C) DMPC/Cholesterol/hederagenin at 0.67:0.23:0.1.

Local separation of sterols and phospholipids in MLVs

To confirm the phase separation between cholesterol and the phospholipids in phospholipid bilayers induced by α-hederin or hederagenin, we used FRET assay. The energy transfer between donor (DHE) and acceptor (DPH-PC) is efficient when the distance between both molecules does not exceed 1-10 nm(Loura et al., 2010), so the formation of even nanodomains can be detected. A decrease in FRET efficiency reflects local separation of phospholipids from DHE. Because DHE behaves in the same way as cholesterol in membranes (Wustner, 2007), we can expect also separation of phospholipids and cholesterol.

Fig. 4 shows the FRET efficiency between DHE and DPH-PC (I_{430}/I_{371}) upon time and increasing α-hederin (A,C,E) or hederagenin (B,D,F) total lipid ratios. FRET efficiency was between 2-3 in DMPC:Chol (3:1) MLVs and was stable upon time.

For α-hederin, we observed a continuous decrease of the FRET efficiency upon time and concentration (Fig. 4A). After 3h of incubation, only the highest α-hederin:lipid ratio (1.2) induced a significant decrease (Fig. 4C). Longer incubation periods (24h) didn't have any further effect (Fig. 4E).

Conversely, hederagenin wasn't able to significantly reduce FRET efficiency at 3h, 24h (Fig. 4D,F) or even 48h (data not shown) regardless the molar ratios of hederagenin/lipids used.

Accordingly, upon addition of α-hederin, FRET efficiency decreases as a consequence of increase of the distance between the fluorophores (Wrenn et al., 2001;Loura et al., 2001).

FIGURE 4

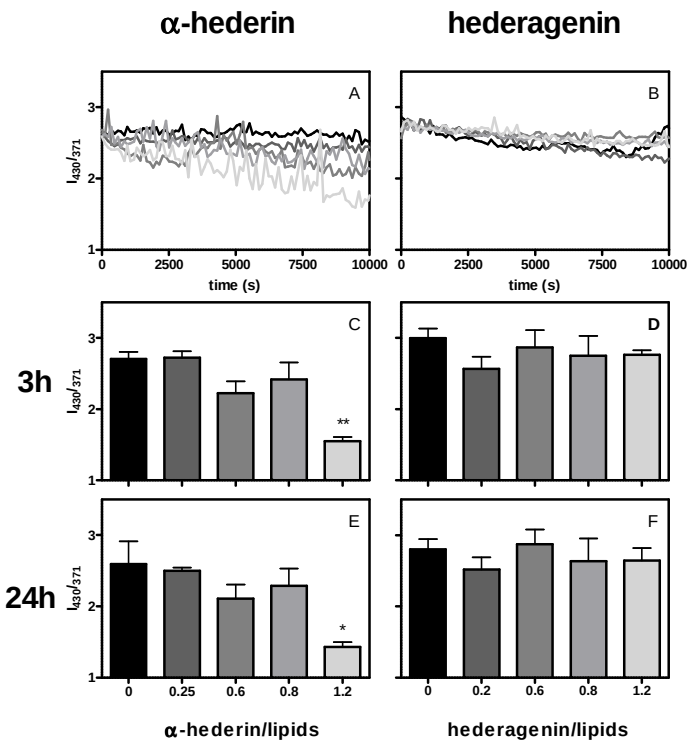

Effect of α-hederin (A,C,E) and hederagenin (B,D,F) on the fluorescence energy transfer efficiency betwen DHE and DPH-PC (I_{430}/I_{371}) for the control (black) and increasing compound/lipid ratios: 0.2, 0.6, 0.8 and 1.2 (increasingly brighter greys). FRET efficiency is represented upon 3h of incubation (A,B) and at two selected time points: 3h (C,D) and 24h (E,F). Concentration of MLVs was set to 50 µM. The experiments were performed at 25°C and the curves represent three independent experiments. Statistical analysis: (t-test) vs. control, *$p<0.05$, **$p<0.01$.

Visualization of phase separation in GUVs by fluorescence microscopy

To visualize the lipid domains, we took benefit from the resemblance of giant unilamellar vesicles to cell membranes in terms of their size and from fluorescence microscopy. GUVs were labeled with TR-DPPE (red) and NBD-DPPE (green), two markers with a large and small headgroup and known to partition in L_d and L_o phases, respectively (Fig. 5). TR-DPPE fluorescence (A,C) or TR-DPPE and NBD-DPPE fluorescence (B,D) were visualized. Data is illustrated for α-hederin at 10 µM (A,B) at different incubation periods. For hederagenin at 40 µM, GUVs presenting phase separation were illustrated at two incubation periods (4 and 48h) (C,D).

Following one GUV, no phase separation was observed until 2h of incubation with α-hederin (10 µM) (A,B). After 2h, fluorescent lipids became concentrated into small spots around the vesicle (see arrow). Later, after 2h15 - 2h20, the small spots fused into a tubular network around the vesicle. At the same time, parts of the membrane were deprived of TR-DPPE but still contained NBD-DPPE (the color of the vesicle changes from orange to green [Fig. 5B, 2h20]). Thereafter, TR-DPPE was accumulated on one or two poles of the vesicle, or it was concentrated in a belt around the vesicle. Finally at 2h40, a deformation of the vesicle into an oval form and formation of crystalline structures around the vesicle were observed. The concentration of fluorescent lipids within specific domains was confirmed by octadecylrhodamine (R18), another fluorescent probe (data not shown).

To visualize phase separation in more detail, we recorded a movie of GUVs marked with TR-DPPE. Resolution was lower but important features are visible (Movie S.1). The movie showed that once phase separation became visible, the process was relatively fast and needed only several minutes to be completed. Again, we observed the formation of a tubular network around the vesicle which collapsed and aggregated into several points (poles) on the vesicle.

Conversely to what was observed with α-hederin, hederagenin (40 µM) induced the formation of small round domains of accumulated fluorescent lipids in the membrane which did not fuse into larger aggregates (Fig 5C). The first domains appeared after 1-2h of incubation but the phenomenon became only important after longer incubation periods and higher concentrations compared to α-hederin.

FIGURE 5

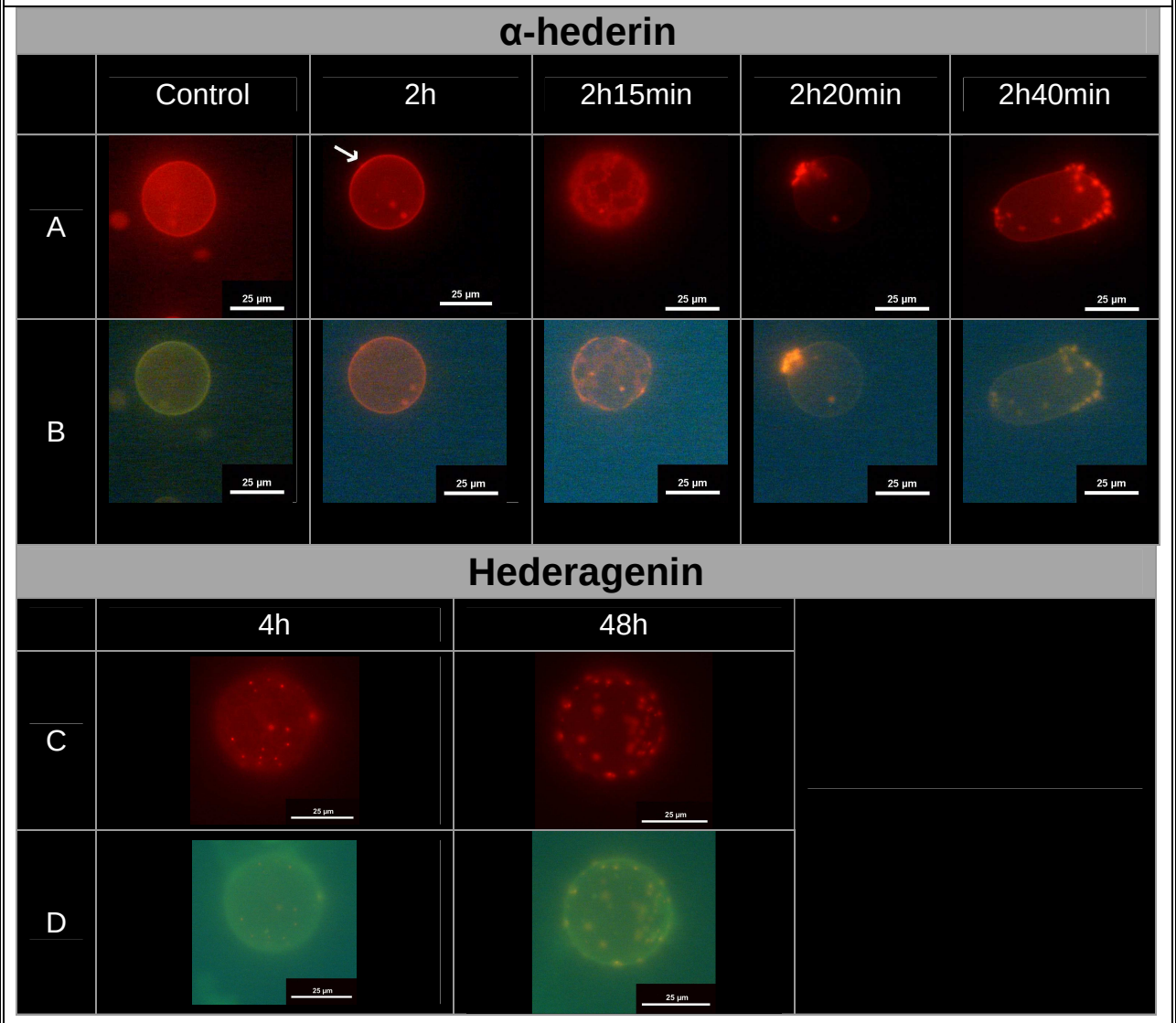

Effect of 10 µM α-hederin or 40 µM of hederagenin on GUV formed of DMPC:Chol (3:1) and marked by TR-DPPE and NBD-DPPE. One GUV was followed at different incubation times with 10 µM α-hederin (A,B). Phase separations induced by hederagenin (40 µM) on GUVs was illustrated after 4 and 48h of incubation (C,D). Lines A and C correspond to the fluorescence of TR-DPPE (red) and lines B and D to the fluorescence of TR-DPPE (red) and NBD-DPPE (green) simultaneously.

The quantification of these events (Fig. 6) pointed out that the most important feature observed on GUVs which have been incubated for 1 and 2h with 10 µM of α-hederin was phase separation (54.4 ± 13.3% and 65.7 ± 12.9%), followed by wrinkling and budding. With 40 µM of hederagenin, we observed 26.6 ± 1.8% of phase separation after 4h of incubation and 61.5 ±

1.5% after 48h. At a glance, phase separation induced by α-hederin was faster, domains were larger and the concentration required to induce phase separation was less important as compared to hederagenin.

FIGURE 6

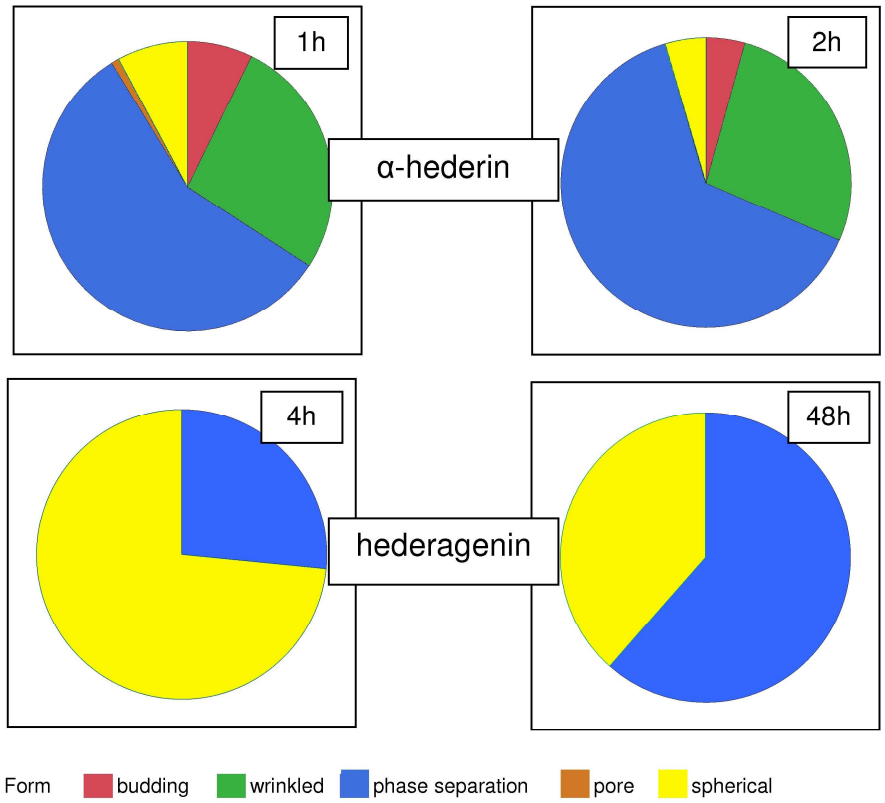

Percentage of GUVs incubated with 10 µM of α-hederin for 1 and 2h or with 40 µM of hederagenin for 4 and 48h and presenting different features (phase separation, budding, wrinkling, pore formation or a spherical shape).

Confocal microscopy of domain formation in GUV and permeability to dextran

To illustrate the changes induced by α-hederin on lamellar phases, we performed confocal microscopy of GUVs composed of DMPC/Chol (3:1, mol/mol) and labeled with TR-DPPE (red) and NBD-DPPE (green). In control membranes composed of DMPC and cholesterol (3:1, mol/mol) (Fig.7, control), we did not observe any visible macroscopic phase separation. This is typical for binary mixtures of phospholipids and cholesterol(Veatch and Keller, 2003) probably due to the fact that domains are in the nanometer range and too small to be detectable(Heberle et al., 2010). For GUVs incubated with α-hederin (10 µM), the formation of new domains was observed. We confirmed a time dependency of the processes induced by the saponin and

especially the initiation of domain formation (stage 2) as well as the appearance of domains accumulating mainly TR-DPPE (stage 3) and deprived of TR-DPPE (stages 4,5). The accumulation of TR-DPPE containing phase at one pole of the vesicle was observed in stage 5. The resting NBD-DPPE containing phase lost its coherence and the formation of large protuberations appeared. This phenomenon is more obvious in confocal microscopy than in fluorescence microscopy where the formation of NBD-DPPE containing "blebs" has not been observed. This might be due to the fact that the process of phase separation is slower in confocal microscopy sheets and is sometimes stopped because no more α-hederin is present in the solution (the volume in confocal incubation chambers is smaller and therefore the α-hederin/lipid ratio lower).

Domains induced by 40 µM of hederagenin after 48h of incubation were mainly enriched in TR-DPPE (Fig. 7, hederagenin).

FIGURE 7

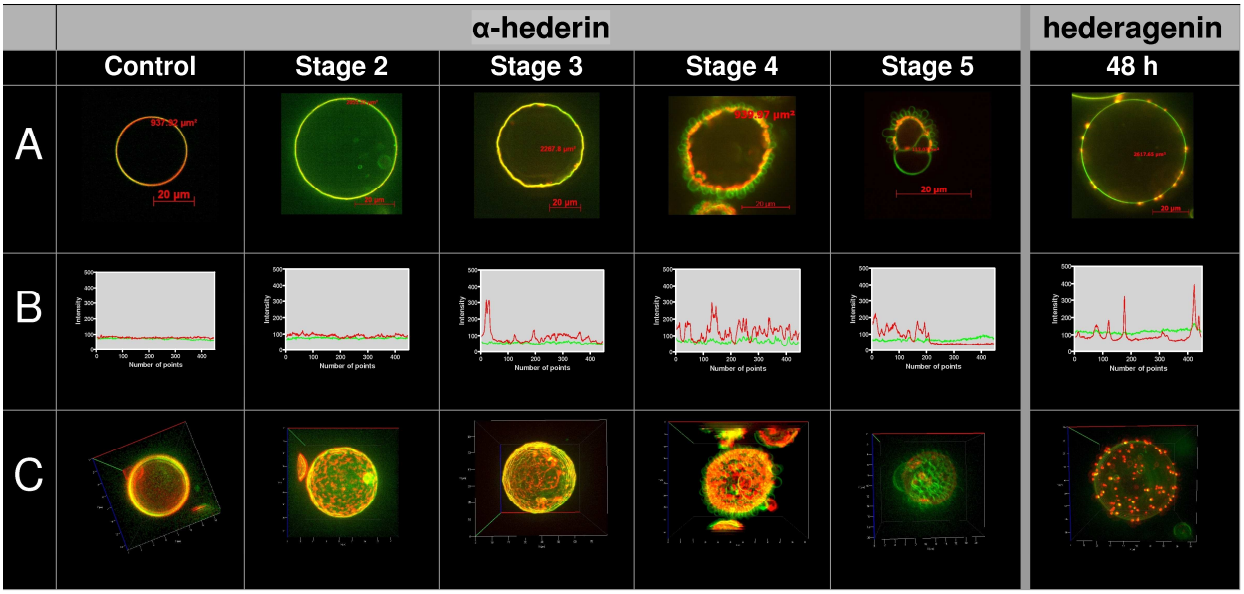

Effect of 10 µM α-hederin and 40 µM hederagenin on GUV formed of DMPC:Chol (3:1) and labeled with TR-DPPE and NBD-DPPE. (A) Confocal microscopy, cross-section at the axe of the vesicle; (B) Normalized fluorescence profile of vesicle contour for the same number of pixels; (C) 3D reconstruction of confocal images. We took images of GUVs at different stages of phase separation corresponding to fluorescence microscopy at the same incubation times.

To get insight of the consequences of these effects on membrane permeability, we followed permeation to FITC-dextran (4 kDa). At 10 µM of α-hederin, permeation to FITC-dextran was not observed for vesicles presenting budding (Fig. 8, budding). Moreover, vesicles presenting phase separation were not always permeabilized suggesting that permeabilization was a graded process (Fig.8, phase separation). Permeabilization was clearly time-dependent because at longer incubation times, GUVs were rather permeabilized.

To investigate if phase separation induced by hederagenin (40 µM) could be related to permeabilization, we observed GUVs after 48h of incubation. Permeation to FITC-dextran was only observed in vesicles presenting phase separation. This strongly suggests that both mechanisms are coupled.

FIGURE 8

α-hederin					
Control (90 min)	Budding (2min)	Phase separation (10min, 30min, 60min and 90min)			
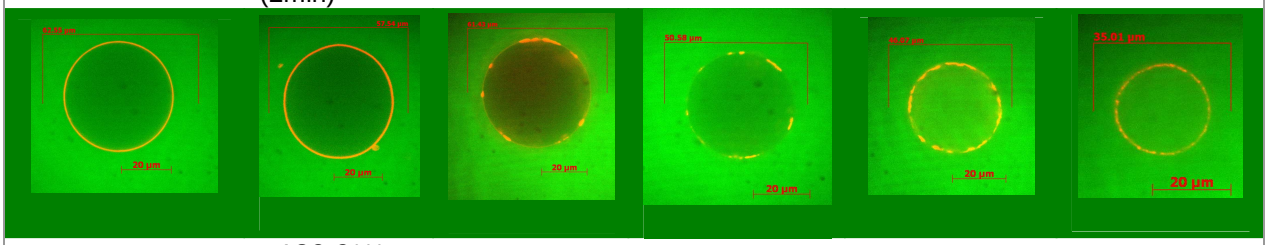					
121.2***± 5.6	120.9***± 5.4	175*** ± 3.7	61*** ± 2.9	N.S.	N.S.
hederagenin					
Control (48h)	Phase separation (48h)				
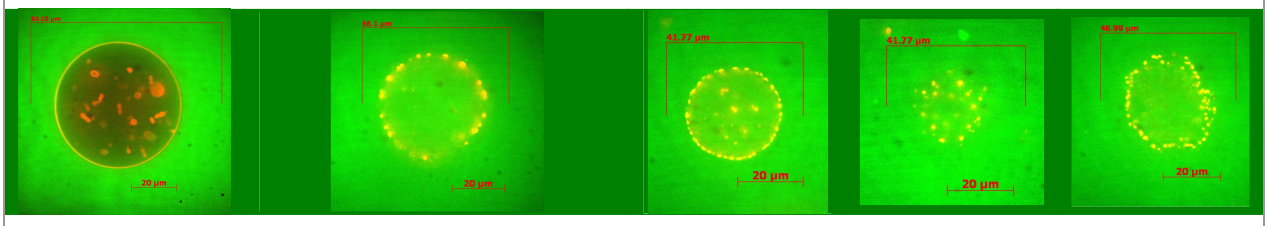					
221.1***± 2.8	N.S.	N.S.	N.S.	N.S.	

Permeation of GUVs with 10 µM of α-hederin at 2, 10, 30, 60 and 90min or 40 µM of hederagenin at 48h. GUVs present different features like phase separation or budding to FITC-dextran (4 kDa). Control contains 0.1% of DMSO. For each time point, the difference of normalized fluorescence between inside and outside of the vesicle was quantified. Statistical analysis (t-test) ***: $p<0.001$. N.S. means no significant difference.

Domain formation in supported planar bilayers

Figures 9, 10 and 11 show the effect of α-hederin on DMPC:Chol (3:1, mol/mol) SPBs. Prior to the injection of the molecule, SPBs were characterized in the presence of 1 % of DMSO showing no significant modification of the SPB due to the presence of the DMSO (Fig. 9A). Figure 9A shows a flat SPB covering 85% of the surface with a step height of 5.2 ± 0.4 nm and a roughness (R_a) mean value of 0.3 nm. The injection of 10 µM of α-hederin didn't have any effect on the membrane (data not shown).

After injection of α-hederin to a final concentration of 20 µM (Fig. 9B), the appearance of several structures that protrude 6.5 ± 1.5 nm from the top of the SPB surface was clearly seen. The SPB covered 95 % of the image with a step height of 4.3 ± 0.6 nm and R_a mean value of 0.2 nm. Interestingly, after the injection of α-hederin, a lower domain appeared on the SPB surface as shown in the inset image (Fig. 9B). This domain was 0.61 ± 0.11 nm lower than the top of the SPB (see arrows). Furthermore the decrease in the thickness of the bilayer together with the increase in the covering of the mica surface suggests that α-hederin interacts with the SPB decreasing lateral forces between lipid molecules.

FIGURE 9

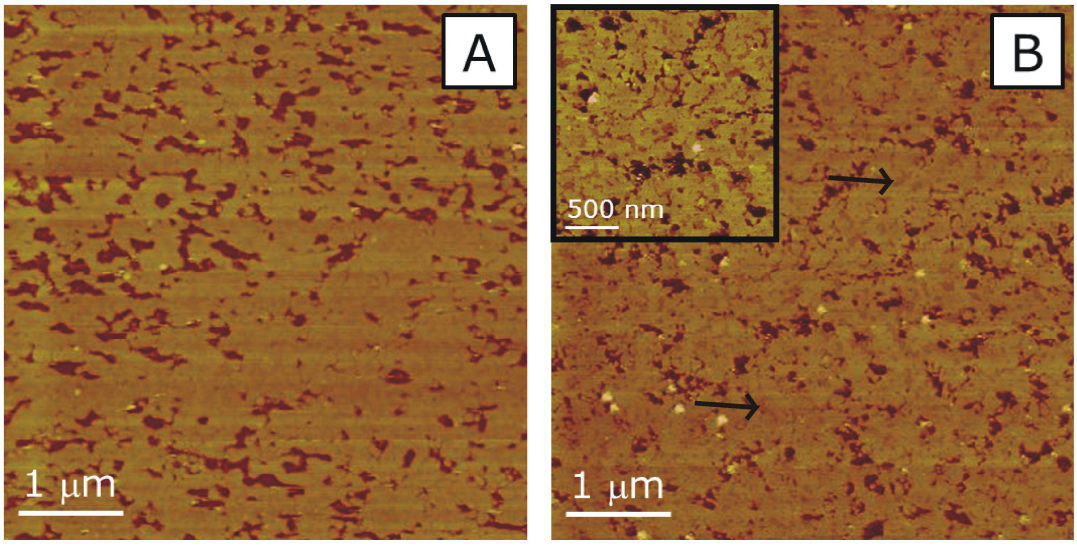

(A) SPB of DMPC:Chol (3:1, mol/mol) in presence of 1% DMSO; B) the same SPB 30 min after injection of α-hederin to a final concentration of 20 µM. Inset, zoom image from (B). The black arrows represent the new lower domain which was formed. Z-scale bar was 20 nm.

To a better understanding of how α-hederin interacts with SPB, we studied the interaction at a higher concentration of the molecule (40µM) (Fig. 10,11). Figure 10A shows a SPB of DMPC:Chol (3:1, mol/mol) covering nearly 99% of the image and with similar features than the SPB presented in Figure 9A. After injection of α-hederin to a final concentration of 40 µM (Fig. 10B-10D), we observed the appearance of small domains, presenting an increasing size and height. At the end of incubation (Fig. 10D), domains presented a worm-like shape and the height value of these domains was about 40 nm, reflecting a transformation of the original bilayer structure (4nm) into a new mesophase. Parallel to the formation of domains, we observed an increasing numbers of holes in the bilayer (red arrows). These holes became larger with incubation time. However, we didn't show a complete solubilization of the bilayer.

At a glance, we observed the formation of new domains in a concentration dependent manner. At small concentrations, the covering of the mica surface is increased and lateral forces seem to decrease. At higher concentrations, the formation of larger holes and accumulation of lipid material into worm-like aggregates is observed.

FIGURE 10

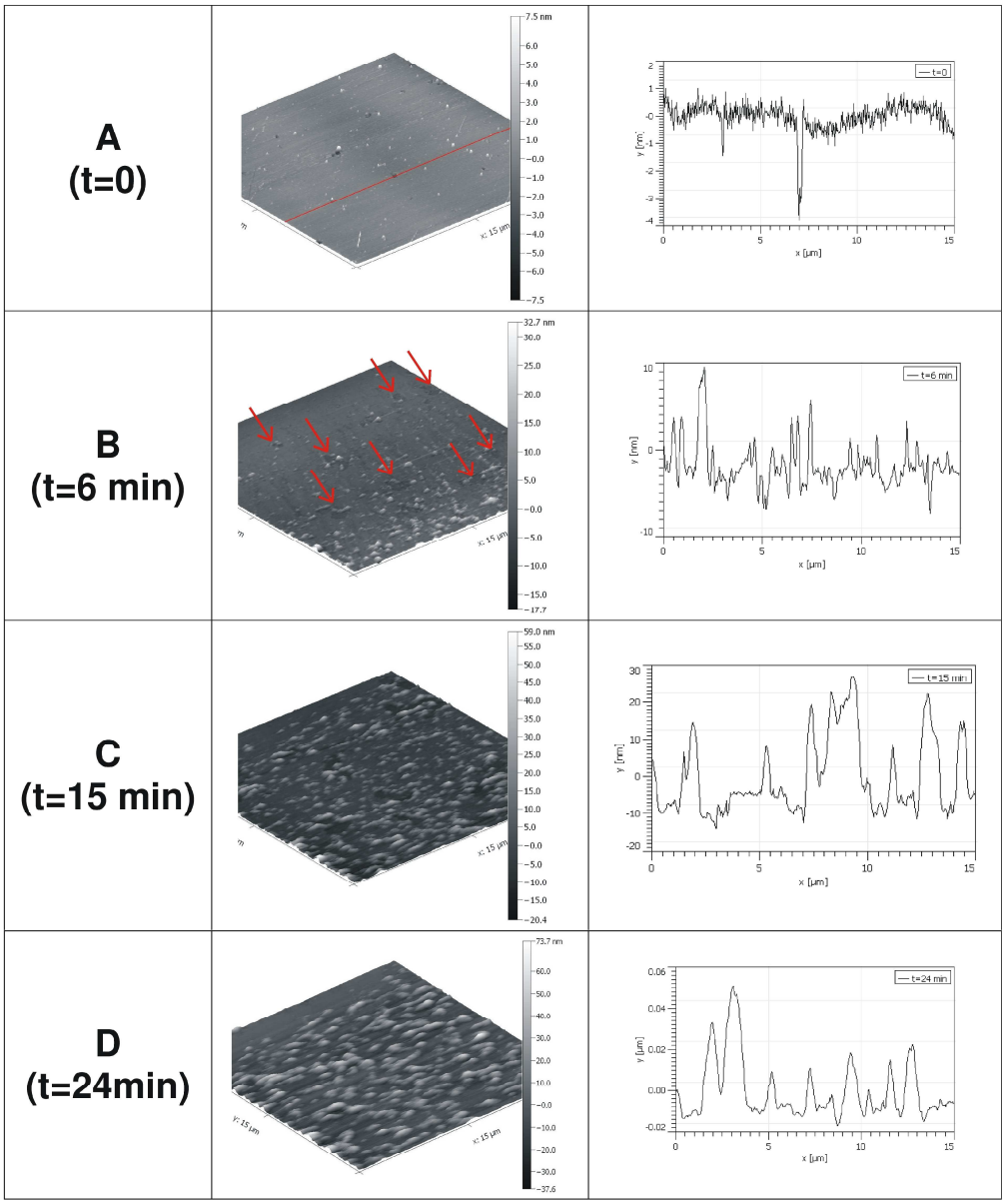

Left column: 3D reconstruction of AFM raw data of SPB composed of DMPC:Chol (3:1, mol/mol). Right column: Texture profiles corresponding to the red line in the first AFM sheet (positioned at 9,48 µm from the left edge). The red arrows indicate the holes induced by α-hederin. The SPB was incubated with 40 µM of α-hederin for t = 0 min (A), 6 min (B), 15 min (C) and 24 min (D). Z-scale bar indicates the height difference between the highest and lowest value.

Discussion

Lipid phase separation has become an important concept in membrane organization. Cholesterol is one of the main lipids characterizing lipid domains and rafts. We previously showed that the formation of lateral saponin/sterol domains induced by α-hederin would lead to increased transbilayer curvature and toroidal pores (Lorent et al., 2013). In this work, we characterized the ability of α-hederin to induce lateral phase separation in a monolayer (Big Layer Method) or bilayer (MLV, GUV and SPB) models composed of DMPC and cholesterol. In GUV and SPB, small lipid domains evolve into worm-like structures able to fuse into tubular aggregates. In GUV, they form a network which further collapses. The newly formed phase accumulates preferentially at one or two poles of the vesicle. We highlighted the critical role of the saponin concentration as well as the importance of the presence of a sugar chain on the aglycone. With hederagenin, the domain formation is less marked and higher concentrations and incubation periods are required to observe lipid domains. Moreover, domains induced by hederagenin keep a small round shape conversely to those observed with α-hederin. Nevertheless, both molecules were able to induce permeation of GUVs to dextran-FITC in the same time-frame they induced phase separation, which suggests that both processes are linked.

Several mechanisms could be involved to explain the ability of α-hederin and hederagenin to induce phase separation. Phase separation in lamellar phases is mainly driven by an increase of the line tension (λ) between domains and the surrounding phase (Baumgart et al., 2007;Blanchette et al., 2008;Kharakoz et al., 1993) whereas repulsive electrostatic forces between domains and curvature tend to reduce it (Sriram et al., 2012). In a binary model composed of DMPC and cholesterol, a nanoscopic phase separation below the resolution limit of an optical microscope is expected (Loura et al., 2001;de Almeida et al., 2009). Mismatch between different intrinsic curvatures of L_o and L_d domains would create elastic interactions at phase boundaries which reduce line tension and so inhibit macroscopic phase separation (Meinhardt et al., 2013). Another critical parameter which opposes lipid phase separation is the entropy of lipid mixing. Lateral lipid distribution is dominated by the entropy of lipid mixing in absence of preferred lipid interactions in a stationary system (Tian and Baumgart, 2009). However, high affinity of the exogeneous agent to one specific lipid component is probably enough to explain

lipid phase separation despite the loss of entropy. This is exactly what we showed with α-hederin and hederagenin which have a high affinity for DHE in aqueous solution and induce a change in its spectral properties suggesting aggregation.

The lipid phase separation induced by α-hederin and hederagenin is followed by the formation of new lipid mesophases. This is supported by ^{31}P-NMR spectroscopy we performed (Lorent et al., 2013) and which showed the appearance of a hexagonal or isotropic pattern when MLV had been incubated with α-hederin and hederagenin, respectively. The hexagonal pattern is in accordance with the observed highly curved tubular structures (Zimmerberg and Kozlov, 2006) induced by α-hederin and the isotropic pattern could correspond to the small round domains observed with hederagenin. Characterization of the newly formed domains by α-hederin has been done by AFM. Results demonstrated a time-dependent increase in the grain size and height suggesting the accumulation of membrane material into these domains. The height of the domains overcomes largely the original bilayer thickness (from 4 nm to 40 nm) which agrees with the transformation of the bilayer into a non-bilayer mesophase.

The new structures present a higher intrinsic curvature than the original bilayer (Zimmerberg and Kozlov, 2006). The increased membrane curvature in α-hederin/lipid aggregates can be explained by the 3D molecular structure of the molecule. α-Hederin is composed of two hydrophilic sugar units which point into one direction compared to its rigid triterpenic hydrophobic ring. The alignment of α-hederin molecules in the membrane would therefore lead to positive curvature into one direction of the membrane plane, which would favor the formation of the tubular mesophase (Lorent et al., 2013). Hederagenin, because of its sterol like shape should induce the formation of negative curved structures(Chen and Rand, 1997). The formation of preferentially inverted micelles has also been proposed for another pentacyclic triterpenic acid, ursolic acid (Prades et al., 2011). Because hederagenin does not present sugars which point into one direction, association of these molecules should induce inverted spherical structures.

The molecular compositions of the new lipid phases are unknown but three main observations suggest the presence of phospholipids. First, the new phases still contain TR-DPPE (a marked phospholipid) as evidenced by confocal microscopy. Second, we monitor a signal in ^{31}P-NMR characteristic of phospholipids (Lorent et al., 2013). Third, molecular modeling shows that α-hederin and hederagenin should be able to bind to phospholipids and cholesterol

simultaneously and form a ternary complex. This agrees with data reported for another saponin, α-tomatine (Keukens et al., 1995). A cooperative process between lipids is thought to be the driving factor in bilayer/inverted hexagonal phase transitions (Caffrey, 1985;Rappolt et al., 2003). In our bilayer system, cooperative aggregation of DMPC, cholesterol and α-hederin/hederagenin molecules could most probably lead to the new lipid mesophases.

Another important feature of this work is the importance of the sugar chain for phase separation as demonstrated by FRET, fluorescence and confocal microscopy. Hederagenin, lacking two sugar units was not able to induce phase separation of DHE and DPH-PC in MLV even after 48h of incubation. In GUVs, the speed of domain formation was largely reduced and we did not observe fusion of domains into worm like structures in contrary to what was observed with α-hederin. It seems therefore that the kinetics of domain formation and the shape of these domains are highly dependent on the sugar units. Several studies suggested that the formation of saponin enriched domains in the membrane depends on hydrophilic sugar-sugar interactions between saponin molecules (Keukens et al., 1995;Armah et al., 1999). These sugar-sugar interactions could therefore be important, but were not the only driving force in domain formation because hederagenin was able to induce domains in GUVs. Van der Waals attractions between the hydrophobic rings of the sapogenin and the sterol (or the acyl chains of phospholipids) should therefore be enough to induce aggregation of lipid molecules in membranes. This is also supported by the fact that hederagenin was able to induce aggregates with DHE in aqueous solution.

Regarding the permeabilization mechanism induced by α-hederin and hederagenin, we first focussed on α-hederin. We showed that at 10 µM, the saponin was able to induce membrane permeabilization and budding. Permeabilization is gradual as demonstrated by following the permeation of GUV to FITC-dextran (4 kDa) or by characterizing the SPBs using AFM (the size of membrane holes increased with time). Interestingly, we showed in another study that α-hederin at 40 µM induced immediate membrane permeabilization and macroscopic pore formation but no budding(Lorent et al., 2013). The concentration of α-hederin is hence critical for lipid phase separation, budding and membrane permeabilization. This could be related to the amphiphilic character of the saponin. Saponins are known to have surfactant activity and they reduce progressively the surface tension of water in a concentration dependent matter until their CMC

(Romussi et al., 1980;Bottger et al., 2012;Xiong et al., 2008;Mitra and Dungan, 1997;Mitra and Dungan, 2001). The CMC of α-hederin is supposed to be close to 13 µM (Bottger et al., 2012).

Based on this data, we develop a new model for α-hederin/membrane interaction based on the CMC (Scheme 1). Before any addition of α-hederin, nanoscopic domains enriched in cholesterol would exist in the DMPC/Chol bilayer (Scheme 1A). Below the CMC (at 10 µM), α-hederin monomers would insert into the external monolayer close to these domains (Scheme 1B) and induce a rapid increase of the area difference between the outer and inner monolayer which could lead to the induction of positive membrane curvature leading to immediate budding (Scheme 1C) (Zimmerberg and Kozlov, 2006). This has also been shown for other detergents with positive intrinsic molecular curvature (Staneva et al., 2005). At longer incubation periods, cooperative association of α-hederin/cholesterol and DMPC could lead to the formation of curved domains in the membrane whose size increases with time and which further develop into a tubular or hexagonal phase (Scheme 1D). This aggregation is accelerated by the presence of a sugar chain at C3 and could be responsible for the development of membrane defects (as seen by AFM) and gradual permeabilization of the membrane. Above the CMC (at 40 µM), micelles and other types of amphiphilic aggregates could be formed in aqueous solution as demonstrated with other saponins (Dai et al., 2013;Mitra and Dungan, 1997). When micelles would interact with membranes, they could directly deliver an increased local concentration of α-hederin molecules to the membrane surface and therefore favor the direct formation of macroscopic pores which could explain why α-hederin permeabilizes quasi instantaneously the GUVs at 40 µM but needs more than 1h at 10 µM (Lorent et al., 2013). This agrees with the data lately reported for glycyrrhizin (Sakamoto et al., 2013).

FIGURE 12

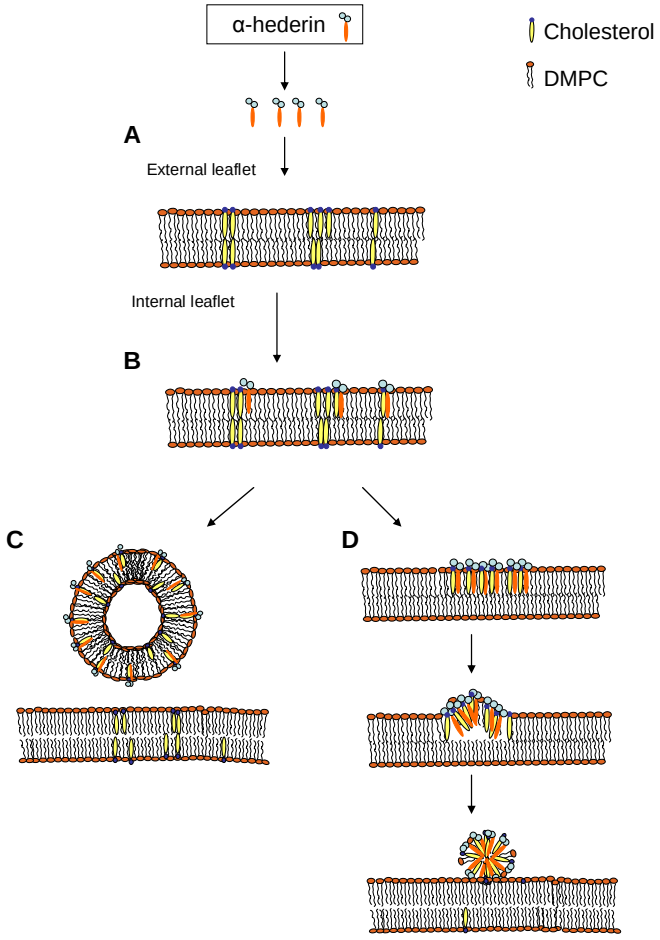

Model showing phase separation induced by α-hederin in a DMPC/Chol bilayer. Before addition of α-hederin, cholesterol nanodomains exist in the bilayer (A). After addition, α-hederin binds to the external bilayer and nanodomains (B) and induces immediate budding (C) due to the fast area difference induced between outer and inner membrane. After higher incubation periods, we observe coalescence of nanodomains into macroscopic domains. These domains transform into a new lipid mesophase presenting a worm-like shape (D).

Moving on the effect of the aglycone, hederagenin induced no budding at 40 µM. The induction of negative curvature to the external monolayer would be in accordance with this result. Membrane permeabilization and phase separation were observed after 48h in vesicles where phase separation was ongoing. Aggregation of lipids into domains and the formation of a new lipid mesophase could in this case also favor the formation of membrane defects and permeabilization(Correia et al., 2012;Hallock et al., 2003). It is not clear if the interaction of hederagenin with the membrane depends on the formation of hederagenin-aggregates/micelles in

the solution. Low concentrations of hederagenin didn't show any effect on membranes. It might be possible that only aggregates of triterpenic acids have an effect on the membrane as it has been suggested for madecassic and asiatic acid (Stephenson et al., 2008).

The possible biological consequences of the proposed membrane interactions are numerous. In addition to the previously described rapid permeabilization mechanism induced by α-hederin at concentrations above the CMC which was based on the formation of toroidal pores and induction of positive membrane curvature, a second "slower" permeabilization mechanism based on phase separation could be observed for triterpenic acids and saponins. It might be possible that the proposed permeabilization mechanism is responsible for hemolysis and cancer cell lysis of some triterpenic acids and saponins, a process which would strongly depend upon the concentration (Segal et al., 1966;Segal et al., 1974;Gauthier et al., 2009).

Regarding the effects on phase separation, it has been shown in biological membranes that the lateral organization of cholesterol influences membrane protein and drug activity. This has become a subject of great interest (George and Wu, 2012). Specific interaction of some saponins with cholesterol led to an effect on lipid rafts and the induction of the extrinsic apoptotic pathway (Li et al., 2005;Xu et al., 2009;Yi et al., 2009). Accumulation of α-hederin/hederagenin in the cellular membrane could lead to the unspecific activation of membrane proteins localized in rafts. The induction of apoptosis trough caspase-8 activation by α-hederin might happen through activation of death receptors which are known to reside in lipid rafts (George and Wu, 2012;Choi et al., 2008).

The interaction mechanism we established could allow us to synthesize new triterpenoids able to induce phase separation, activation of death receptors and apoptosis. Changing the three dimensional shape of saponins and the presence or the orientation of sugar moieties could lead to compounds which would be able to preferentially induce apoptosis but not hemolysis (Chwalek et al., 2006).

Acknowledgement

Special thanks to Henri Burhin and Christian Bailly for suggestions about polymers and providing the PDMS for the electroformation chamber. This work has been funded by the FNRS

(Fonds national de la récherche scientifique, contract number 3.4.588.10 and 3.4.578.12) and the Université catholique de Louvain by the Bourse du patrimoine.

.

3.1.3. Effects of α-hederin on model membranes displaying lateral phase separation containing cholesterol or not (**article 3, in preparation**)

Authors : Joseph Lorent[1,2], Claude Poleunis[3], Vincent Duprés[3], Laurence Lins[4], Robert Brasseur[4], Joelle Quetin-Leclercq[2] and Marie-Paule Mingeot-Leclercq[1*]

[1]Université catholique de Louvain, Louvain Drug Research Institute, Cellular and Molecular Pharmacology, UCL B1.73.05, avenue E. Mounier 73, B-1200 Bruxelles, Belgium.

[2]Université catholique de Louvain, Louvain Drug Research Institute, Pharmacognosy, UCL B1.72.03, avenue E. Mounier 72, B-1200 Bruxelles, Belgium.

[3]Université catholique de Louvain, Institute of Condensed Matter and Nanosciences, Bio and soft matter, UCL L7.04.01, Croix du Sud 1, 1348 Louvain-La-Neuve

[4]Centre de Biophysique Moléculaire Numérique, ULg Agro-BioTech Gembloux, Passage des Déportés, 2, B- 5030 Gembloux, Belgium

Subject and background : The aim of this work is to study the mechanisms by which α-hederin is able to influence the lateral phase separation in membranes containing cholesterol or not. We wanted to know if saponins and cholesterol really colocalize in membranes and how the saponin is able to insert into the membrane. For this purpose, we used Tof-SIMS (Time of flight-secondary ion monitoring), a mass spectrometric method allowing the creation of two-dimensional images (maximum resolution of 50 nm) of supported planar bilayers and giving for each pixel a mass spectra. At the moment, we were only able to establish data on membranes composed of DOPC/ DPPC (1:1).

Introduction

In previous chapters, we introduced the concept of lateral phase separation and rafts in biological membranes (see 2.2.2.2. and 2.2.5.1.). We showed that α-hederin was able to induce lateral phase separation and the transformation of bilayers into a tubular mesophase in a model composed of DMPC/Cholesterol (3:1, mol/mol) and presenting nanoscopic phase separation (see 3.1.2.). Unfortunately, this binary model was not useful for giving us information on how α-hederin inserts into the membrane and interacts with the cholesterol enriched liquid organized (L_o) phase (see 2.2.4) and the liquid crystalline (L_d) phase. It has been proposed in a molecular dynamics study that dioscin, a monodesmosidic saponin would first insert into the L_d phase and later interact with the cholesterol enriched L_o phase (Lin and Wang, 2010).

Therefore, to investigate thoroughly the mechanisms by which α-hederin is able to interact with lipid rafts and influence lipid phase separation, we used two different membrane models displaying lipid phase separation in the macroscopic range. Both models, when investigated by Tof-SIMS and AFM, present the advantage that they allow us to gain information about eventual co-localization of the saponin with membrane constituents and preferential interaction of α-hederin with a specific lamellar phase.

First, a binary DOPC/DPPC (1:1, mol/mol) model, composed of two phospholipids with a low and a high melting point respectively, displays a macroscopic gel/liquid crystalline phase coexistence (S_o/L_d) (see 2.2.5.2.). This model was used to investigate the effects on phase separation in the absence of cholesterol. On a biological point of view, this model does not really mimic cholesterol enriched membrane rafts and the L_o phase. Despite this drawback, the model is interesting to test if the saponin has a cholesterol-like effect and inhibits a gel/liquid phase separation.

Second, the effects of the saponin will be further tested on a ternary DOPC/DPPC/Cholesterol (1:1:1, molar ratio) model, displaying macroscopic liquid crystalline/liquid ordered phase separation (L_o/L_d). The liquid ordered phase which is mainly composed of DPPC and cholesterol molecules is similar to lipid rafts in cells because it contains in addition to cholesterol, a saturated phospholipid. However, in biological membranes, macroscopic phase separation is mostly not present. Different theories have been put forward to explain this phenomenon like the presence of line-active glycerophospholipids, the effects of

increased curvature in these domains which reduces line tension or the interactions of lipids with the cytoskeleton (Sonnino and Prinetti, 2013).

Materials and methods

LUVs and GUVs preparation

LUVs and GUVs have been prepared as described in 3.1.2.

Preparation and incubation of SPBs for AFM and Tof-SIMS (Time of flight-secondary ion monitoring)

Supported planar bilayers (SPBs) were prepared as follows. Briefly, multilamellar vesicles (MLV) of 1 mM in 10 mM TRIS.HCL at pH=7.4 and 20 mM $CaCl_2$ were spread on freshly cleaved mica and incubated at 45°C for 1h. After incubation, SPBs were washed 5 times with a 10 mM TRIS.HCl buffer solution without $CaCl_2$. SPBs were then incubated for 1h with α-hederin at 10 µM or 0.1% DMSO at 37°C. After incubation, SPBs were washed 6 times with distilled water. These samples can be analyzed by AFM (Giocondi et al., 2010). For Tof-SIMS analysis, SPBs were further plunge-frozen in liquid nitrogen and freeze-dried over night. Tof-SIMS was used to gather information about the chemical composition of domains and to decipher an eventual colocalization of α-hederin with one of the membrane constituents in SPB (Popov et al., 2008;Mazzucchelli et al., 2008).

Laurdan fluorescence spectroscopy

We used Laurdan fluorescence to detect phase separation in LUVs. The technique has been described in detail in chapter (3.2.).

Results

Decrease of phase separation induced by α-hederin in LUV composed of DOPC/DPPC (1:1)

A high GP_{ex} value can be associated with a high bilayer packing and a low polarity of the interfacial area of the membrane. A low GP_{ex} value reflects the opposite. An increase of Laurdans' GP_{ex} upon excitation wavelength at constant temperature reflects a lateral phase separation. A constant value reflects a gel phase whereby a decreasing value indicates a fluid phase.

In DOPC/DPPC (1:1) membranes (Fig. 1), we observed increasing GP_{ex} values upon excitation wavelength at temperatures ranging from 5 to 30°C. Above this temperature, the membrane was in a fluid state. This corresponds to data previously obtained on the same membrane model (see 3.2., Figure 3).

α-Hederin was able to reduce the slope of the GP_{ex} excitation function suggesting an inhibition of lateral phase separation. It also increased the GP_{ex} values of the membrane, especially those taken in the liquid crystalline state. This has also been observed in membranes composed of only dimyristoylphosphatidylcholine (see 3.1.1., Figure 8). This could be associated with the cholesterol-like effect of the triterpenoid ring structure that α-hederin could exert.

FIGURE 1

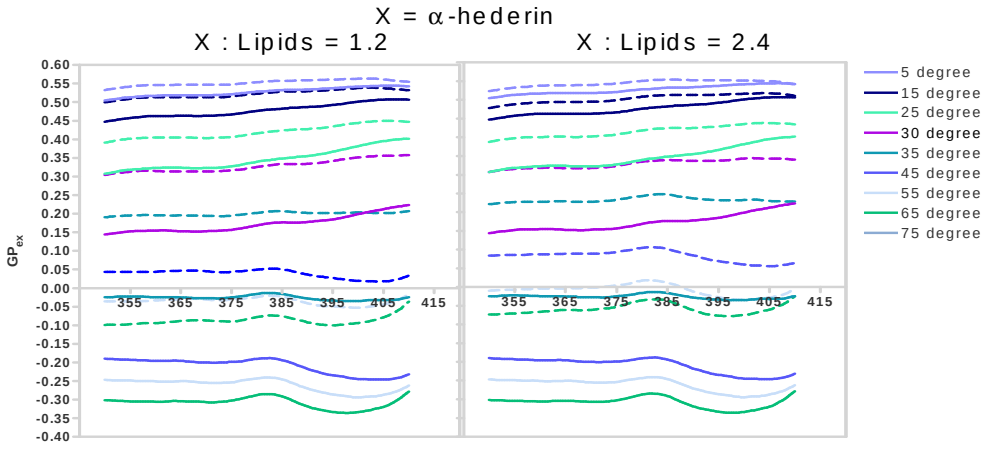

Laurdan spectroscopy

GP_{ex} upon increasing excitation wavelength and temperature in LUV composed of DOPC:DPPC (1:1). LUV have been preincubated for 1h at 37°C in the presence of α-hederin at a compound lipid ratio of 1.2 (left panel) and 2.4 (right panel). Full lines (control), dashed line (incubated)

Decrease of lateral phase separation in SPB composed of DOPC/DPPC (1:1, mol/mol) as evidenced by AFM

We observed a clear phase separation in DOPC/DPPC (1:1, mol/mol) membranes (Fig. 2A). Incubation of these membranes at 37°C for 1h with 10µM of α-hederin led to a considerable decrease in size of DPPC domains. (Fig. 2B). Phase separation became less evident.

FIGURE 2

(A) **(B)**

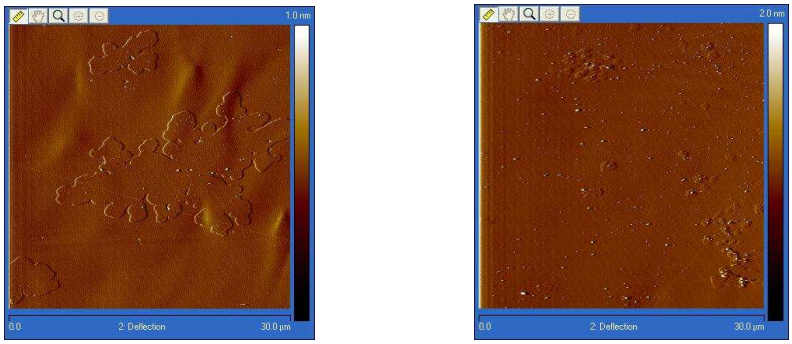

Deflection AFM images (30x30nm)

SPB on mica composed of DOPC:DPPC (1 :1) (A) or DOPC:DPPC (1:1) bilayer incubated for 1h at 37°C with 10 µM of α-hederin (B)

Decrease of lateral phase separation in SPB composed of DOPC/DPPC (1:1, mol/mol) as evidenced by Tof-SIMS

Tof-SIMS confirmed the results of AFM and Laurdan by which α-hederin reduced lateral phase separation. In the control, DOPC and DPPC signal where separated in domains of micrometric size, corresponding to the size of domains observed in AFM (Fig. 3A,B,C). After 1h of incubation at 37°C with 10 µM of α-hederin (Fig. 3D,E,F), size of domains was reduced and intensity signals of DOPC and DPPC were less separated. Unfortunately, no α-hederin could be detected when the SPB was washed twice, suggesting that the molecule is bound to the membrane by equilibrium binding as it has been suggested for digitonin in absence of cholesterol (Nishikawa et al., 1984).

FIGURE 3

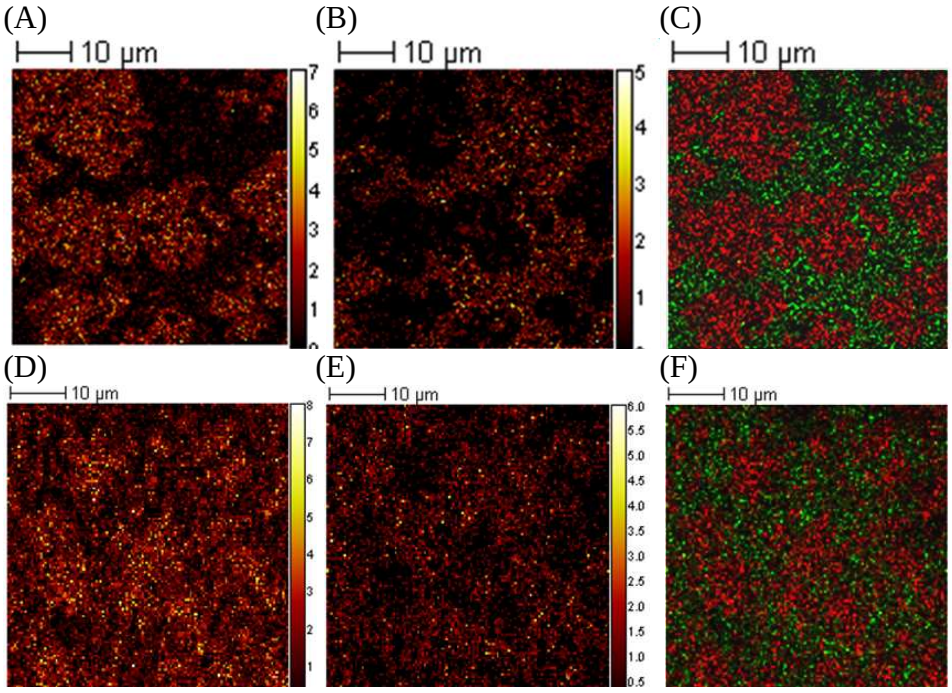

Tof-SIMs (2D intensity spectra, negative mode)
SPB on mica composed of DOPC:DPPC (1:1) and incubated with α-hederin. Control (A,B,C); 1h of incubation with α-hederin at 37°C (D,E,F). (A,D) DPPC, (B,E) DOPC, (C,F) DPPC (red) and DOPC (green)

Discussion

We have seen by using three complementary methods (Laurdan, AFM and Tof-SIMS) that α-hederin was able to suppress lateral phase separation in a model composed of DOPC:DPPC (1:1). The mechanism which was proposed is based on the ability of α-hederin to induce erosion at the borders of the membrane domains. This is in agreement with a Monte Carlo simulation on a DOPC:DPPC monolayer (data not shown, big monolayer method, see 3.1.2. and 3.2.). A similar behaviour was obtained with surfactin and glycyrrhizin (see 3.2. and general conclusions) (Sakamoto et al., 2013). α-hederin is hence able to reorganize lateral heterogeneity of lipids in a membrane, even when no cholesterol is present. This could lead to interesting activities on cell membranes where cholesterol is absent like in bacterias.

3.1.4. Apoptotic and non-apoptotic cell death in monocytes induced by α-hederin and hederagenin in a cholesterol dependent manner (**article 4, in preparation**)

Authors: Joseph Lorent[1,2], Marthe Abouzi[1], Farida Akabi[1], Joelle Quetin-Leclercq[2] and Marie-Paule Mingeot-Leclercq[1*]

[1]Université catholique de Louvain, Louvain Drug Research Institute, Cellular and Molecular Pharmacology, UCL B1.73.05, avenue E. Mounier 73, B-1200 Bruxelles, Belgium.

[2]Université catholique de Louvain, Louvain Drug Research Institute, Pharmacognosy, UCL B1.72.03, avenue E. Mounier 72, B-1200 Bruxelles, Belgium.

Subject and background : α-hederin and its aglycon, hederagenin, have shown activity on several cancer cells. They induce cell death by apoptosis and non-apoptotic cell death. An inhibition of α-hederin induced cell death was observed when cells were depleted in cholesterol (see 3.1.1.). We wanted in this part of our work investigate the apoptotic and non-apoptotic part of α-hederin induced cell death and explore the importance of membrane cholesterol for both effects. We also investigated the importance of the sugar chain for cell death and discussed possible mechanisms involved.

INTRODUCTION

Apoptosis can be distinguished from other cell deaths because of its distinctive morphological features. It is characterized by an intact plasma cell membrane where phosphatidylserine is externalized, the appearance of blebs, reduction of cytoplasmic volume, condensation of chromatin and fragmentation of the nucleus. After the induction of apoptosis, cells *in vitro* often undergo a further morphological change and their plasma membrane looses its coherence. This advanced stage of cell death is called late or secondary apoptosis (Kroemer et al., 2009).

Apoptosis is induced via two main pathways, the intrinsic and extrinsic pathway (Jin and El Deiry, 2005). The intrinsic pathway depends mainly on the disruption of the external mitochondrial membrane and the release of proapoptotic proteins into the cytoplasm. The extrinsic pathway is driven by the activation of death receptors present on the cell membrane (Galluzzi et al., 2012).

Saponins are able to induce apoptosis, and non-apoptotic cell death in cancer cells (Choi et al., 2008;Chwalek et al., 2006;Gerkens et al., 2007;Kim et al., 2008;Swamy et al., 2003). A non-apoptotic cell death described for monodesmosidic triterpenoid saponins presenting a sugar moiety at C3 was cytolysis. It is characterized by the lysis of the plasma membrane induced by the saponin (Gauthier et al., 2009;Wassler et al., 1987;Ohsaki et al., 2005). In addition to cytolysis, oleanane type saponins are able to induce apoptosis (Gauthier et al., 2009), which makes them interesting candidates for cancer therapy because their pleiotropic effect should make them less suspectible against resistance mechanisms (Kwon et al., 2008).

α-Hederin is an oleanane type saponin able to induce cell death via apoptosis and membrane lysis (Gauthier et al., 2009). The increase of extracellular Ca^{2+} influx and cytosolic ROS species was critical for apoptosis (Choi et al., 2008;Swamy and Huat, 2003). In addition, the saponin was also able to induce caspase-8 activation (Choi et al., 2008), suggesting the activation of the extrinsic pathway and death receptors (Dickens et al., 2012). The formation of membrane defects was observed in cancer cells by electron microscopy even after short incubation times (Danloy et al., 1994). The release of calcein-acetoxymethylester from the cytoplasm of cancer cells incubated with α-hederin confirmed the perforation of the plasma membrane (Gauthier et al., 2009).

Because cholesterol plays a critical role for both the alteration of cancer cells and hemolysis (Shany et al., 1974) induced by saponins, the characterization of the interaction between α-hederin and cholesterol is a key for the understanding of the mechanisms involved in saponin induced cell death. Cholesterol is an important constituent of the membrane influencing lipid dynamics. It is also a constituent of membrane rafts, lateral functional membrane domains (Lingwood and Simons, 2010) where death receptors are located. Their disorganization can lead to the induction of apoptosis via the extrinsic pathway, as it has been shown for ginsenoside Rh2 and avicins (Yi et al., 2009;Xu et al., 2009). It is likely that α-hederin could be able to influence lateral sterol organization in cells because it has been shown, that the compound and to a smaller extend, hederagenin, were able to induce lateral phase separation in a GUV raft model (see 3.1.2.). The aggregation and fusion of lipid rafts could lead to the activation of membrane receptors present in rafts (Garcia-Saez et al., 2011).

We therefore wanted to elucidate the role of cholesterol in apoptosis and non apoptotic cell death induced by α-hederin in cancer cells. We used U937 and THP-1 cells, two monocytic cell lines, one is cholesterol auxotroph (U937) (Billheimer et al., 1987) and the other is able to synthesize its own cholesterol (THP-1) (Kritharides et al., 1998). We also wanted to establish the importance of the sugar chain for saponin induced cell death.

MATERIAL AND METHODS

Materials

α-hederin and hederagenin (HPLC quality) were purchased from Extrasynthèse, (Genay, France). The compounds were dissolved in ethanol. After evaporation of the solvent, the residue was resolubilized in RPMI media (containing 0,1% of DMSO) in an ultrasonic bath for 5 min. Corresponding controls were used. Cells were purchased from ATCC. RPMI medium was ordered by Life technologies, Paisley, UK. The bicinchoninic (BCA) protein assay was purchased from Thermo scientific (Rockford, USA). Methyl-β-cyclodextrin (MβCD), DAPI, acridine orange and ethidium bromide were ordered from Sigma-Aldrich (St. Louis, MO). Amplex® red cholesterol assay kit was purchased from Invitrogen (Paisley, Scotland, UK). All other reagents were ordered from E. Merck AG (Darmstadt, Germany).

Cell culture, cholesterol depletion and incubation with α-hederin and hederagenin

Cells were cultivated in RMPI medium supplemented with 10% foetal calf serum in 95% air and 5% CO2. For cholesterol depletion, cells (10^6 cells/ml) were harvested and incubated for 2.5h in fresh RPMI medium supplemented with 1mg/ml BSA and 5 mM methyl-β-cyclodextrin (MβCD). Cell counting was performed in a Burker chamber. After this incubation, cells were washed 3 times with RPMI medium. At this time, a part of the cells were quantified for their cholesterol, phospholipid and protein contents. For cholesterol and phospholipid quantification, cellular lipids were first extracted by a protocol described earlier (Gamble et al., 1978) and further quantified with the Amplex® red cholesterol assay and phosphorus assay (Bartlett, 1985). Proteins of cells were quantified by the BCA protein assay kit. The other part of cells was incubated with increasing concentrations of α-hederin.

Determination of cell death

Cell death was quantified by the trypan blue exclusion assay using a phase contrast microscope and results were expressed in % of total cells (Tennant, 1964).

Determination of apoptotic/non-apoptotic cell death

As previously described, we used DAPI assay to quantify apoptosis (Servais et al., 2005). Briefly, cells presenting a fragmented and condensed nucleus were counted as apoptotic. A total of 500 cells was counted.

To distinguish between living, death cells and early and late apoptosis, we used the acridine orange/ethidium bromide (AO/EB) assay (Hathaway et al., 1964). After incubation, cells were harvested and washed in PBS medium. They were then put in contact with the AO/EB solution and directly observed in fluorescence microscopy. Death cells with defect membranes presented always EB influx and apoptotic cells had a fragmented nucleus. A total number of 200 cells were counted. Early apoptosis was defined as cells with fragmented nucleus and no EB influx. Late apoptotic cells presented also EB influx and were counted as death cells.

RESULTS

Depletion of cholesterol by MβCD in two monocytic cell lines

MβCD was very efficient in depleting the cholesterol/protein and cholesterol/phospholipid ratio U937 and THP-1 plasma membranes (Table 1). The total lipid amount was not influenced by MβCD (data not shown). The cholesterol amount of non-depleted cells corresponded almost to values reported in literature (De Pace and Esfahani, 1987;Wang et al., 2007b).

Table 1 : Ratios of cholesterol/proteins and cholesterol/phospholipids in U937 and THP-1 non-depleted and cholesterol depleted cells

		Non-depleted	**Depleted**
U937	Cholesterol/proteins	13.13 ± 1.30 µg/mg	4.49 ± 0.24 µg/mg
	Cholesterol/phospholipids	150.9 ± 14.98 µg/µM	40.26 ± 2.16 µg/µM
THP-1	Cholesterol/proteins	11.29 ± 0.39 µg/mg	6.54 ± 0.72 µg/mg
	Cholesterol/phospholipids	129.93 ± 4.17 µg/µM	60.07 ± 6.67 µg/µM

Cell death induced by α-hederin in cholesterol depleted and non-depleted cells as determined by Trypan Blue assay

Cell death was rapidly observed in U937 and THP-1 at the highest concentrations investigated (Fig. 1A,C). After only 2h of incubation, 25 µM of α-hederin induced 62 ± 5.2 % of cell death in U937 cells and 46.6 ± 6.1 % after 4h in THP-1 cells. Cell death was concentration and cell dependent. U937 cells were more sensitive to α-hederin induced cell death than THP-1.

Depletion of cholesterol by MβCD effectively reduced α-hederin induced cell death in U937 and THP-1 cells (Fig. 1B,D). In U937, cell death was inhibited at least for 18 h and in THP-1 cells for at least 30h.

FIGURE 1

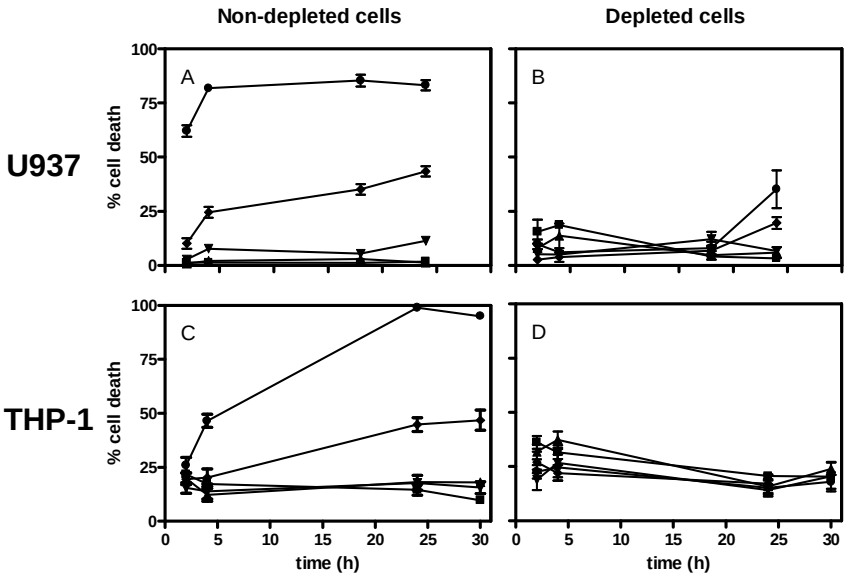

Trypan blue assay

U937 (A,B) and THP-1 (C,D) non-depleted (A,C) or depleted (B,D) in cholesterol. Cells were incubated with increasing concentrations of α-hederin: Control (■), 10 µM (▲), 15 µM (▼), 20 µM (♦) and 25 µM (●). Three independent experiments were performed

Apoptosis induced by α-hederin in cholesterol depleted and non-depleted cells as determined by DAPI and AO/EB assay

Fragmentation of nuclei, which corresponded to total apoptosis was determined by DAPI assay. It was induced in a concentration- and time dependent manner in U937 (Fig. 2A,C,D) and THP-1 cells (Fig. 2E,F). In both cells, a maximum of apoptosis could be observed at concentrations around 20 µM. At higher concentrations, the number of DAPI positive cells decreased.

In all the conditions investigated, depletion of cholesterol reduced apoptosis but did not completely suppress it (Fig. 2C,D,E,F).

FIGURE 2

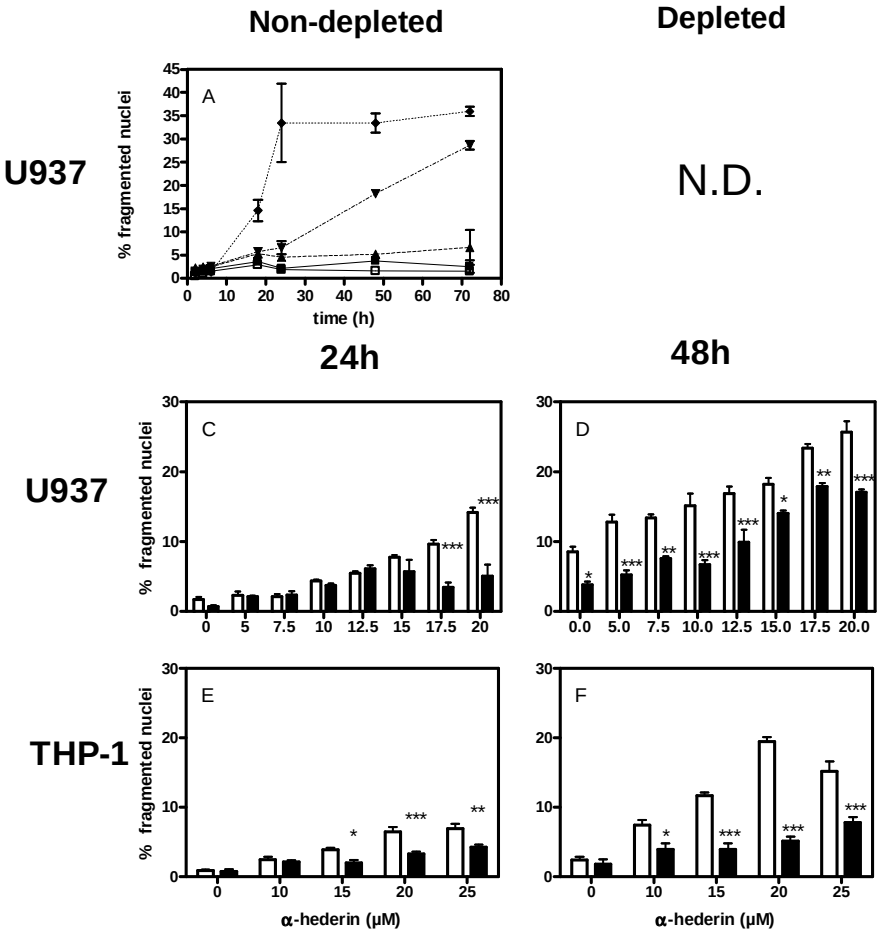

DAPI assay

U937 (A,B,C) and THP-1 (D,E) cells. Panel A, time course of apoptosis induced by α-hederin: Control (■), 10 µM (▲), 15 µM (▼), 20 µM (♦) and 40 µM (□). Panel C,D,E and F, apoptosis of depleted (black bars) or non-depleted (white bars) cells incubated for 24 (C,E) and 48h (D,F) with increasing concentrations of α-hederin. Statistical analysis: One way ANOVA; Symbols : *=depleted vs. non-depleted cells, one symbol: $p<0.05$, two symbols: $p<0.01$, three symbols: $p<0.001$

By monitoring closer the time dependency of apoptosis and total cell death induced by α-hederin in U937 cells (Fig. 3), we observed the first signs of apoptosis at 18h of incubation for non-depleted cells. Cell death (cells presenting defect membranes) was induced long before the appearence of apoptosis. It reached about 40% after 4h of incubation with 20 µM of α-hederin in

non-depleted cells. Depletion in cholesterol delayed apoptosis induction (for depleted cells, apoptosis appeared only after 24h of incubation). Cell death was also reduced in depleted cells which confirmed the results obtained with the trypan blue assay (Fig. 1, A).

FIGURE 3

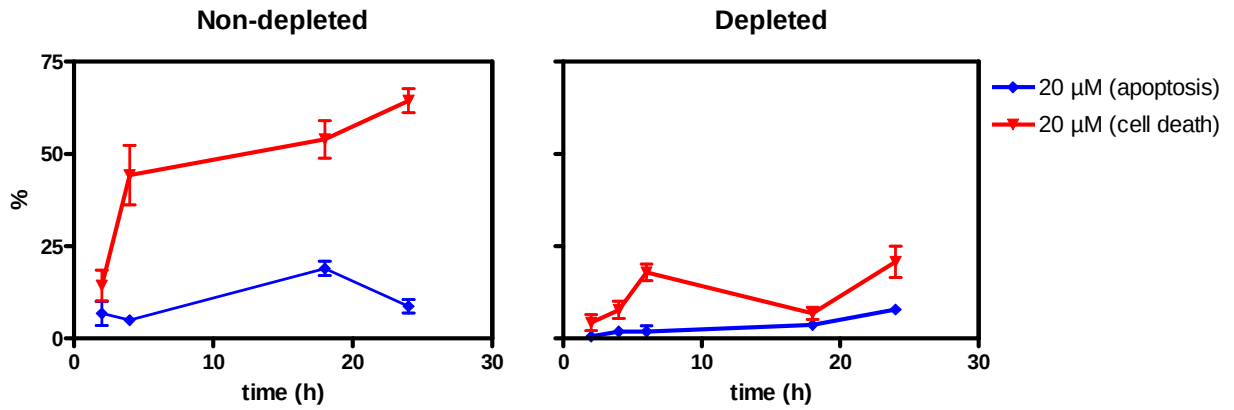

AO/EB assay

U937 cells depleted or not in cholesterol and incubated with α-hederin. Apoptosis in blue (♦) and total cell death in red (▼).

Importance of sugar chain for apoptosis and non-apoptotic cell death

To go further and investigate the critical role of sugars for induction of apoptosis and non-apoptotic cell death (Fig. 4), we compared the effects induced by α-hederin (A,C) and hederagenin (B,D) using AO/EB assay. Both compounds induced a time- and concentration dependent cell death in U937 cells.

Apoptosis was induced most efficiently at 20 µM of α-hederin which confirms previous results obtained using DAPI (Fig. 2A). On the contrary to what was observed with DAPI assay, we observed also a portion of fragmented nuclei at 2h and 4h of incubation for 40 µM of α-hederin (17,6 ± 3.8 % and 12.7 ± 1.5 % respectively). For the same concentration and incubation periods, we reached a total cell death of 81 ± 6.5 % and 92.6 ± 2.3 %, respectively. But we have to verify if this early cell death is really related to apoptosis.

Analysing the effect of hederagenin, the aglycone induced a slower cell death in U937 cells than α-hederin. Apoptosis became significant only after 24h of incubation at 40 µM of the compound. A slight increase of total cell death was only observed for 48h of incubation.

FIGURE 4

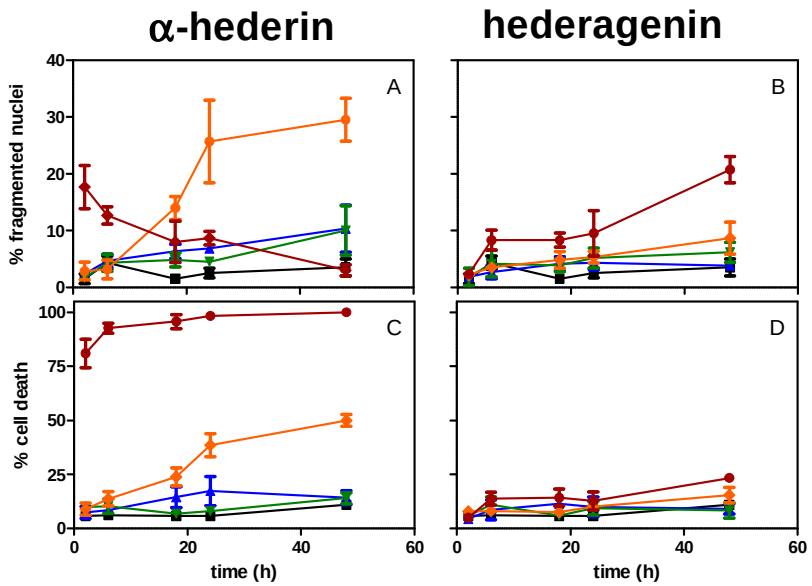

E

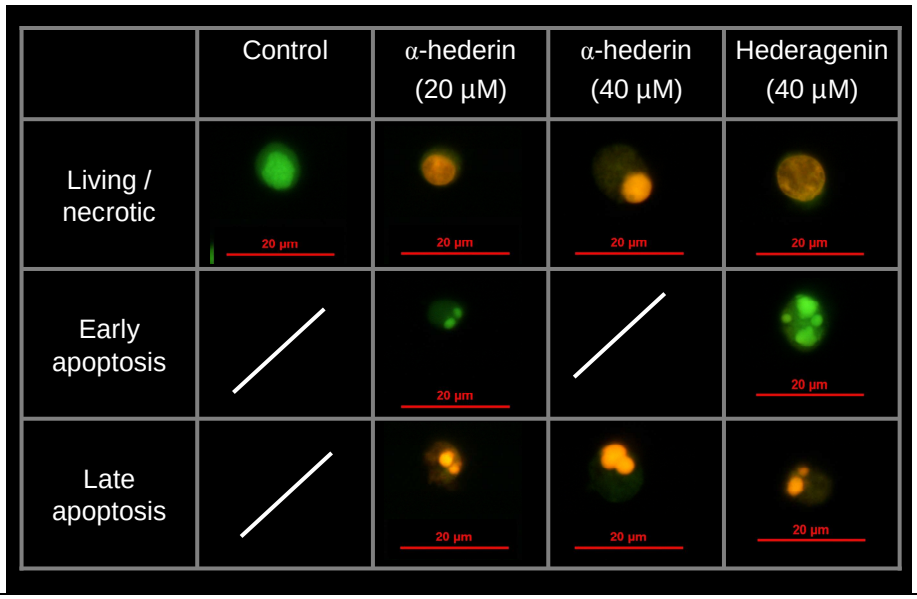

AO/EB assay

U937 cells incubated for 2, 6, 18, 24 and 48h with α-hederin (A,C) or hederagenin (B,D). Control (■, black), 10 µM (▲, blue), 15 µM (▼, green), 20 µM (♦, orange) and 40 µM (●, red). Images of cells (AO/EB) incubated for 48h with 0.1% of DMSO (Control), 20 or 40 M of α-hederin or 40 µM of hederagenin (E).

To have more insights into the morphological features of nuclei in cell death induced by both compounds, we took pictures after 48h of incubation (Fig. 4E). We observed that higher concentrations of α-hederin (40 µM) induced an increased condensation of the nuclei compared

to lower concentrations (20 µM) or hederagenin at 40 µM. This condensation of the nucleus is already observed after 2h of incubation with 40 µM of α-hederin (data not shown). Early and late apoptosis were characterized by the typical fragmentation of the nuclei for after incubation with 20 µM of α-hederin and 40 µM of hederagenin. At 40 µM of α-hederin, late apoptosis was difficult to differentiate from non-apoptotic cell death because fragmentation of the nuclei was most often uncomplete.

Moving on the mechanism involved in apoptosis induced by α-hederin and hederagenin and the role of caspases in cell death, we used the pan-caspase inhibitor Q-VD-OPh (Fig. 5). Apoptosis induced by α-hederin and hederagenin after 48h was inhibited by this inhibitor (Fig. 5A), suggesting an implication of caspases (Fig. 5A). In contrast, no effective inhibition of non-apoptotic cell death was observed (Fig. 5B). Cells characterized by late apoptosis (Fig. 5A, bars without patterns) were transformed into cells where no cell fragmentation, but ethidium bromide influx occurred when Q-VD-OPh was added. This was also true for camptothecin. α-hederin induced apoptosis was also partially inhibited by Ac-DEVD-CHO, a caspase-3 inhibitor (data not shown).

FIGURE 5

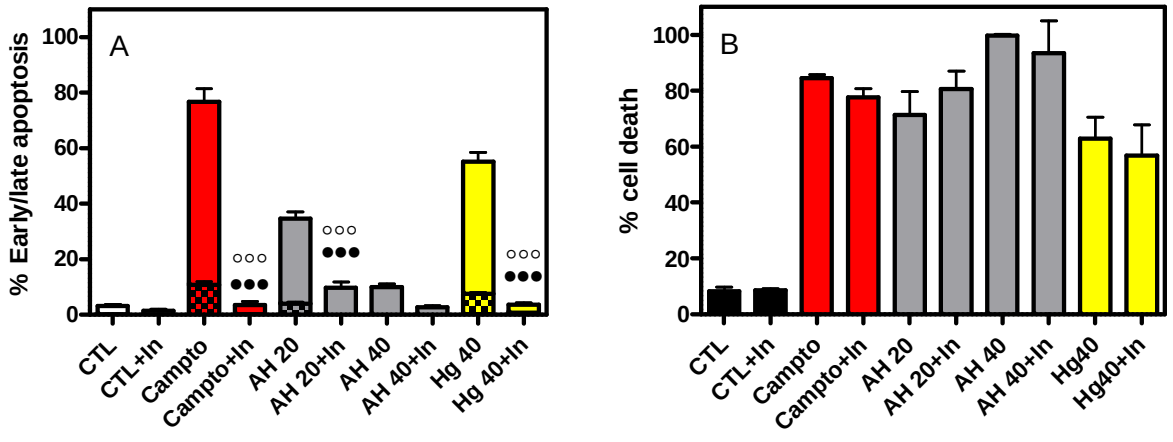

AO/EB assay

U937 cells incubated 48h with camptothecine (Campto, red), α-hederin (AH, grey), hederagenin (Hg, yellow) with or without pan-caspase inhibitor Q-Vd-OPh (Inh). (A) Early (squared bar)/late (not squared bar) apoptosis and (B) necrosis. CTL is the control. Statistical analysis: One way ANOVA; symbols : ●= Early apoptosis ± inhibitor ○=Late apoptosis ± inhibitor; three symbols: $p<0.001$

Discussion

So far, we can conclude that non apoptotic cell death and apoptosis by α-hederin is concentration and cholesterol-dependent. At 20 µM of α-hederin, we observed a maximum of apoptosis in U937 and THP-1 cells. Beyond this concentration, the cell death switched to non apoptotic cell death. Total cell death induced by α-hederin did not depend on apoptosis because non-apoptotic cell death is induced before any apoptosis appeared. Especially high saponin concentrations induced the non-apoptotic cell death.

Several hypotheses could be suggested to explain the cholesterol dependency of cell death induced by α-hederin.

First, the inhibition of rapid non-apoptotic cell death in cholesterol depleted cells at high saponin concentrations is probably due to an inhibition of pore formation by the saponin. Cholesterol dependent pore formation was shown in GUVs and LUVs and depended on the membrane curvature induced by the saponin (Lorent et al., 2013).

Second, the decrease and the delay of apoptosis in depleted cells could result from two main pathways.

(i) Depletion of cholesterol could decrease pore formation and so decrease extracellular Ca^{2+}-influx and inhibit the opening of the mitochondrial transition pore and further rupture of the outer mitochondrial membrane (Choi et al., 2008). Therefore, this would inhibit the formation of caspase-9 and the intrinsic pathway.

(ii) The extrinsic pathway could also play a role. In cancer cells, depletion of membrane cholesterol by MβCD inhibited activation of death receptors by avicin D (Xu et al., 2009). α-Hederin might be able to induce cell death via fusion of lipid rafts, activation of death receptors and caspase-8. Activation of death receptors via coalescence or disruption of lipid rafts has also been shown for other saponins and cholesterol binding toxins (Yi et al., 2009;Garcia-Saez et al., 2011). The induction of phase separation in GUVs mimicking nanoscopic raft domains by α-hederin supports this hypothesis (see 3.1.2.).

We further wanted to point out the importance of the sugar chain in cell death induction. Regarding the structure of the saponin, we showed that the presence of the sugar chain was critical for rapid cell death induction but didn’t seem necessary for cell death induction at longer incubation periods. Without the sugar chain, there was no rapid non-apoptotic cell death observed

whatever the concentrations. This can probably be put into relationship with the results obtained in GUV at high concentration, where an immediate permeation to dextran at 4 kDa was observed with α-hederin whereas the effect with hederagenin became only evident at 48h of incubation (Lorent et al., 2013). Induction of cell death required larger incubation periods and higher concentrations with hederagenin compared to α-hederin.

Regarding the importance of caspases, they are critical for apoptosis induced by the saponin and its genin. Unfortunately, at this stage, we are unable to answer to the question if activation of caspase-8 is really related to the induction of death receptors (Choi et al., 2008) (see 5.1.1.4.).

3.2. Effects of surfactin on membrane models displaying lipid phase separation (article 5, BBA – Biomembranes 1828, 2013)

Authors : Magali Deleu[1°], Joseph Lorent[2°], Laurence Lins[3], Robert Brasseur[3] Nathalie Braun[4], Karim El Kirat[4], Tommy Nylander[5], Yves F. Dufrêne[4] and Marie- Paule Mingeot-Leclercq[2]

[1] Université de Liège - Gembloux Agro-Bio Tech, Unité de Chimie Biologique Industrielle, Passage des Déportés, 2, B-5030 Gembloux, Belgium

[2] Université catholique de Louvain, Louvain Drug Research Institute, Cellular and Molecular Pharmacology, Avenue E. Mounier 73, B1.73.05, B-1200, Brussels, Belgium

[3]Université de Liège - Gembloux Agro-Bio Tech, Centre de Biophysique Moléculaire Numérique, Passage des Déportés, 2, B-5030 Gembloux, Belgium

[4] Université catholique de Louvain, Institute of Condensed Matter and Nanosciences, Bio and Soft Matter, Croix du Sud 1, L7.04.01, B-1348 Louvain-la-Neuve, Belgium

[5] Lund University, Center for Chemistry and Chemical Engineering, Physical Chemistry, 1S-221 00 Lund, Sweden

° Equal First author

Subject and background : The permeabilizing activity of surfactin has been described mainly as a detergent-like mechanism (see 2.7.). But despite this activity, which seems to depend on its CMC, we observed that the molecule is able to inhibit lateral phase separation in a supported planar bilayer composed of DOPC:DPPC at concentrations below its CMC. This article elucidates possible routes explaining this special behaviour in relation with its permeablizing activity and its affinity for DOPC.

Biochimica et Biophysica Acta 1828 (2013) 801–815

Contents lists available at SciVerse ScienceDirect

Biochimica et Biophysica Acta

journal homepage: www.elsevier.com/locate/bbamem

Effects of surfactin on membrane models displaying lipid phase separation

Magali Deleu [a,*,1], Joseph Lorent [b,1], Laurence Lins [c], Robert Brasseur [c], Nathalie Braun [d], Karim El Kirat [d], Tommy Nylander [e], Yves F. Dufrêne [d], Marie- Paule Mingeot-Leclercq [b]

[a] Université de Liège, Gembloux Agro-Bio Tech, Unité de Chimie Biologique Industrielle, Passage des Déportés, 2, B-5030 Gembloux, Belgium
[b] Université Catholique de Louvain, Louvain Drug Research Institute, Cellular and Molecular Pharmacology, Avenue E. Mounier 73, B1.73.05, B-1200, Brussels, Belgium
[c] Université de Liège, Gembloux Agro-Bio Tech, Centre de Biophysique Moléculaire Numérique, Passage des Déportés, 2, B-5030 Gembloux, Belgium
[d] Université Catholique de Louvain, Institute of Condensed Matter and Nanosciences, Bio and Soft Matter, Croix du Sud 1, L7.04.01, B-1348 Louvain-la-Neuve, Belgium
[e] Lund University, Center for Chemistry and Chemical Engineering, Physical Chemistry, 1S-221 00 Lund, Sweden

ARTICLE INFO

Article history:
Received 20 July 2012
Received in revised form 19 October 2012
Accepted 5 November 2012
Available online 14 November 2012

Keywords:
Surfactin
Membrane interaction
Phase coexistence
Laurdan and DPH fluorescence
Ellipsometry
AFM

ABSTRACT

Surfactin, a bacterial amphiphilic lipopeptide is attracting more and more attention in view of its bioactive properties which are in relation with its ability to interact with lipids of biological membranes. In this work, we investigated the effect of surfactin on membrane structure using model of membranes, vesicles as well as supported bilayers, presenting coexistence of fluid-disordered (DOPC) and gel (DPPC) phases. A range of complementary methods was used including AFM, ellipsometry, dynamic light scattering, fluorescence measurements of Laurdan, DPH, calcein release, and octadecylrhodamine B dequenching. Our findings demonstrated that surfactin concentration is critical for its effect on the membrane. The results suggest that the presence of rigid domains can play an essential role in the first step of surfactin insertion and that surfactin interacts both with the membrane polar heads and the acyl chain region. A mechanism for the surfactin lipid membrane interaction, consisting of three sequential structural and morphological changes, is proposed. At concentrations below the CMC, surfactin inserted at the boundary between gel and fluid lipid domains, inhibited phase separation and stiffened the bilayer without global morphological change of liposomes. At concentrations close to CMC, surfactin solubilized the fluid phospholipid phase and increased order in the remainder of the lipid bilayer. At higher surfactin concentrations, both the fluid and the rigid bilayer structures were dissolved into mixed micelles and other structures presenting a wide size distribution.

1. Introduction

Surfactin, a bacterial lipopeptide [1,2] has a structure consisting of a cyclic heptapeptide headgroup with the sequence Glu-Leu-D-Leu-Val-Asp-D-Leu-Leu linked to a C_{13-15} β-hydroxy fatty acid by a lactone bond. The β-hydroxy fatty acid chain of the homologues C13 and C15 are branched (isopropyl group at the chain end) while the one of the homologue C14 is linear. The two negatively-charged amino acids, which form a polar head opposite to the five lipophilic amino acids, and the hydrocarbon side chain account for the amphiphilic nature of surfactin and its strong surfactant properties [3,4]. Surfactin is attracting more and more attention in view of its many interesting bioactive properties. These include the lipopeptides potential as antiviral [5,6], antimycoplasma [7] and antibacterial agent [8–10] as well as its capacity as anti-adhesive agent against pathogenic bacteria [11], insecticide [12], antihypercholesterolemia agent [13], inflammation suppressor [14] and plant defense elicitor [15]. However it has also been reported to have hemolytic [16] and apoptotic [17] properties. It is generally accepted that these properties are directly related to the interaction of surfactin with the lipid component of the biological membranes, which eventually leads to membrane destabilization [18–23]. Surfactin interaction with the membrane is highly dependent on the surfactin concentration [20,23–26]. Shen et al. [26] have suggested the need for a threshold concentration of surfactin in the bilayer for its solubilization. Several studies have shown that sensitivity of model membranes to surfactin is dependent on their lipid composition [24–31], and also on lipid organization (i.e. the physical state) [22]. Surfactin exhibits an enhanced binding to solid ordered domains-containing vesicles [22]. Carillo et al. [28] have also suggested that dipalmitoylphosphatidylcholine (DPPC), forming a gel phase in synthetic bilayers, acts as a promoter of surfactin-induced leakage. On the contrary, cholesterol and POPE attenuate the membrane-perturbing effect of surfactin. Most of these earlier studies have considered very simple biomimetic membrane systems with single phospholipid. Only both of them [22,28] have tackled the question of the effect of surfactin on mixtures of lipids which are more realistic models.

Regarding the role played by lipid domains for cell physiology, we investigated the effect of surfactin on the lateral heterogeneity of bilayers.

* Corresponding author. Tel.: +32 81 62 26 52; fax: +32 81 62 22 31.
E-mail address: magali.deleu@ulg.ac.be (M. Deleu).
[1] Co-first author.

0005-2736/$ – see front matter © 2012 Elsevier B.V. All rights reserved.
http://dx.doi.org/10.1016/j.bbamem.2012.11.007

Indeed, the more rigid lipid domains (ordered phase Lo) within cell membranes are suggested to participate as platforms [32] for many processes like signal transduction, disease pathogenesis and intracellular sorting [33,34].

The present study therefore aims to reveal the effect of surfactin on the lipid phase coexistence and especially on the coexistence of gel (DPPC) and disordered liquid (Ld) (dioleoylphosphatidylcholine DOPC) phases, which so far has not been addressed. For this purpose, we used Laurdan fluorescence technique and atomic force microscopy. Further information on the influence of surfactin insertion onto the transversal organization of the bilayer was obtained by DPH and Laurdan fluorescence measurements. As model for segregated bilayer system we used a 1:1 mol/mol DPPC:DOPC mixture, which is known to be segregated into microscopic domains of different fluidity [24,35]. Surfactin concentration known to have different effects on model membrane destabilization [20,23,25,36] is considered in this study. The interaction was quantified with ellipsometry and the experimental results, supported by molecular modeling, are used to reveal the modes of interaction and preferred location of surfactin at the microscopic and molecular level. Consequences of these microscopic and molecular effects on the macroscopic behavior of the lipid vesicles are investigated by size, fusion and permeability measurements. Implications of our results on the biological activity of surfactin are discussed.

2. Materials and methods

2.1. Materials

Dipalmitoylphosphatidylcholine (DPPC), dioleoylphosphatidylcholine (DOPC), β-D-dodecyl maltoside and calcein were purchased from Sigma (St. Louis, MO). The self-quenched fluorescent probe calcein was purified as described in detail previously [37]. Briefly, calcein was dissolved in 6 N NaOH and subjected to size-exclusion chromatography through a Sephadex® LH-20 column. The final concentration of the calcein solution in 20 mM Tris–HCl was 73 mM with an osmolality of 404 mOsm/kg (measured by the freezing point technique, using a Knauer osmometer automatic (Berlin, Germany). DPH (1,6-diphenyl-1,3,5-hexatriene), Laurdan (6-dodecanoyl-2-dimethyl-aminonaphtalene) and octadecylrhodamine B (R_{18}) were purchased from Molecular Probes (Invitrogen, Carlsbad, CA). Surfactin was produced by fermentation of *B. subtilis* S499 and isolated as described in detail previously [38]. The primary structure and purity of surfactin (>95%) were ascertained by analytical RP-HPLC (Vydack 10 μm C18 column, 0.46×25 cm, Vydack, Hesperia, CA), amino acid analysis, and MALDI-TOF mass spectrometry measurements (Ultraflex TOF, Bruckner, Karlsruhe, Germany). The surfactin mixture, 95.4% pure, was composed of surfactin-C13, -C14 and -C15 (0.3:1:1 mol/mol/mol). The homologues C13 and C15 comprise a branched β-hydroxy fatty acid chain (isopropyl group at the chain end) with 13 or 15 carbon atoms and the homologue C14 encloses a linear β-hydroxy fatty acid chain with 14 carbon atoms. All other products (grade 1) were purchased from Sigma-Aldrich (St-Louis, MO).

2.2. Preparation of liposomes

Liposomes were prepared from a mixture of DOPC:DPPC (1:1). For this purpose, the lipids were dissolved in chloroform:methanol (2:1, v:v) in a round bottomed flask. The solvent was evaporated under vacuum (Rotavapor R Buchi RE-111, Buchi, Flawil, Switzerland) to obtain a thin lipid film, which was dried overnight in a vacuum dessicator to remove remaining solvent. The dry lipid film was hydrated for 1 h with Tris 10 mM and NaCl 150 mM at pH 8.5 and 37 °C in a nitrogen atmosphere. This suspension was submitted to five cycles of freezing/thawing to obtain multilamellar vesicles (MLV). Depending on the type of experiment to be performed, this suspension was either sonicated to yield small unilamellar vesicles (SUV) [39] or extruded to produce large unilamellar vesicles (LUV) of 100 nm diameter [37]. The actual phospholipid content of each preparation was determined by phosphorus assay [40] and the concentration of liposomes was adjusted for each type of experiment.

2.3. Preparation of supported phospholipid bilayers (SPBs)

For surface analysis by atomic force microscopy, we prepared supported lipid bilayers using the vesicle fusion method [41]. DOPC and DPPC were dissolved in chloroform at 1 mM final concentration. An equimolar mixture of these two lipids was then evaporated under nitrogen and dried in a dessicator under vacuum for 2 h. Multilamellar vesicles (MLV) were obtained by resuspending the lipidic dried film in calcium-containing buffer (10 mM Tris, 150 mM NaCl and 3 mM $CaCl_2$ at pH 8.5) at 1 mM final lipid concentration. To obtain small unilamellar vesicles (SUV), the suspension was sonicated to clarity (4 cycles of 2 min) using a 500 W probe sonicator (Fisher Bioblock Scientific, France; 35% of the maximal power; 13 mm probe diameter) while keeping the suspension in an ice bath. The liposomal suspension was then filtered on 0.2 μm nylon filters (Whatman Inc., USA) to remove titanium particles coming from the sonicator tip. Freshly cleaved mica squares (16 mm^2) were glued onto steel sample pucks (Veeco Metrology LLC, Santa Barbara, CA) using Epotek 377 (Gentec Benelux, Waterloo, Belgium). Two milliliters of the SUV suspension were then deposited onto the mica samples and the SUVs were allowed to adsorb and fuse on the solid surface for 1 h at 60 °C. Subsequently, the sample was rinsed five times with Tris 10 mM and NaCl 150 mM at pH 8.5 to eliminate calcium and non-adsorbed vesicles. The samples were then slowly cooled to room temperature.

For ellipsometry investigations, supported lipid bilayers were formed *in situ* in the ellipsometer cuvette by co-adsorption of phospholipids (DOPC or DPPC) with β-D-dodecyl maltoside on hydrophilic silicon–silicon oxide surfaces as described by Vacklin [42]. A typical procedure for bilayer formation contains six stages: adsorption from a 6:1 (w/w%) mixture of β-D-dodecyl maltoside and the requisite phospholipid at a concentration of 0.114 g/l, followed by extensive dilution (rinsing) with 10 mM Tris and 150 mM NaCl at pH 7.4 buffer, and two readsorption steps from 10 and 100 times more dilute phospholipid/maltoside solutions respectively, each followed by rinsing.

2.4. Isothermal titration calorimetry

Critical micellar concentration (CMC) was determined using isothermal titration calorimetry (ITC) on a VP-ITC Microcalorimeter (Microcal, Northampton USA) at both pH 7.4 and 8.5 in 10 mM Tris and 150 mM NaCl buffer into milliQ water (Millipore Co., Milford, MA) at 25 °C. The CMC was determined by calorimetric dilution experiments [19]. The injection syringe was filled with a micellar solution of surfactin (0.3 mM or 0.08 mM). The sequential injection (6 μL) of the micellar solution into the 1.4565 mL calorimeter mixing cell containing only buffer, which was stirred at a speed of 305 rpm, lead to disintegration of the micelles into surfactin monomers until the concentration in the cell approaches the CMC. At this point, micelles were no longer dissociated. The disintegration process produced a heat of demicellization that is then measured by the calorimeter. The typical profile of the heat generated versus addition of the micellar surfactin stock solution was sigmoidal and the CMC was determined from the inflection point.

Prior to each analysis all solutions were degassed using a sonicator bath. The heats linked to buffer injection were determined by injecting buffer into buffer and substracted from the heats determined in the experiments. All measurements were repeated two times with two different surfactin solutions. Data were processed by using the software Origin 7 (Originlab, Northampton, USA).

2.5. Ellipsometry

Measurements of surface excess values and thickness of supported DPPC or DOPC bilayers in absence or in presence of increasing concentration of surfactin were performed by ellipsometry. Ellipsometry is based on monitoring of amplitude, ψ, and phase, Δ, changes of the compounds of polarized light upon reflection. The rate of data collection, with a time resolution of about 2 s, is fast enough for kinetic studies of lipid and surfactant adsorption. The instrument used was a Rudolph Research null-ellipsometer, model 43606-200E, equipped with a xenon arc lamp (Osram XBO 75 W/2) as a light source (λ = 250–1000 nm).

All measurements were performed with a light-source wavelength of 401.5 nm and with an angle of incidence of 68°. The 5 ml cuvette was thermostated at 25.0 °C ± 0.1 °C, and agitation of the solution in the cuvette was performed with a magnetic stirrer at about 300 rpm. The ellipsometric angles ψ and Δ were used to compute the complex reflection amplitude ratio ρ:

$$\rho = \left|r_p/r_s\right| \exp\left(\delta_{rp} - \delta_{rs}\right) = \tan\psi \exp(i\Delta) \quad (1)$$

where r_s and r_p are the reflection coefficients for s- and p-polarizations and δ_{rp} and δ_{rs} represent their phase shifts upon reflection.

In a typical ellipsometry experiment, the measurement was performed on silicon wafer (50 mm × 10 mm) slides pre-treated as described by Tiberg and Landgren [43] and pre-equilibrated overnight in a 10 mM Tris and 150 mM NaCl buffer at pH 7.4. Oxide layers were first characterized by four-zone measurements in air and in water after an equilibration period of 30 min, recording 6 minima in each zone as described in details by Landgren and Jönsson [44]. The substrate optical parameters were on average found to be n_2 (Si) = 5.50–0.25i and n_1 (SiO_2) = 1.49, and d_1 = 270–300 Å. After changing the cuvette content with 10 mM Tris and 150 mM NaCl buffer at pH 7.4 and an equilibration time of 30 min, supported lipid bilayers were formed as described above. The changes in ψ and Δ were monitored as a function of time at each stage of bilayer formation until only a very small change resulted from rinsing. At this point, surfactin stock solution in dimethylsulfoxide (DMSO) (1–10 mM) was added (1–40 μL) and the change in ellipsometric angles typically monitored over a period of 8–24 h. The volume of DMSO injected into the cuvette containing the buffer 10 mM Tris and 150 mM NaCl at pH 7.4 is below 1% of the total volume and has no influence on the measured parameters. The recorded ψ, and Δ values was evaluated assuming four-layer optical model where each layer is homogenous and assuming homogenous planar layers, using a numerical procedure originally devised by McCrackin et al. [45] as described by Tiberg and Landgren [43], and Landgren and Jönsson [44]. The obtained thickness, d, and refractive index, n, of the adsorbed layer can then be used to calculate the surface excess (Γ) according to de Feijter:

$$\Gamma = [(n - n_0)/(dn/dc)]d \quad (2)$$

where n_0 is the refractive indexes of the bulk solvent, and dn/dc is the refractive index increment of the adsorbing specie, for which a value of 0.148 [46] was used.

The accuracy in the thickness determination is rather high (30–35%) for small adsorbed amount (Γ < 1.0 mg/m^2), decreasing rapidly to values around 2–7% for Γ > 1.0 mg/m^2. The error in adsorbed amount is much smaller: 15% for Γ < 1.0 mg/m^2 and 0.5–2% for Γ > 1.0 mg/m^2. This is due to the fact that for low adsorbed amount, thin layers, and low optical contrasts, the refractive index of the layer and the layer thickness are coupled, due to limits of the resolution of the instrument, and it is therefore only possible to determine the adsorbed amount [47].

2.6. Laurdan generalized polarization

To gain information on lipid phase (gel, liquid-disordered and coexisting phases) as well as on transition temperature between gel and liquid-disordered phases, we used Laurdan, a polarity sensitive probe, located at the glycerol backbone of the bilayer with the lauric acid tail anchored in the phospholipid acyl chain region [48,49].

This probe doesn't show any preferential partitioning between gel and fluid phases and is considered to have uniform distribution between the inner and outer leaflets of a bilayer [49,50]. The intensity of Laurdan fluorescence is high in the visible range and is highly sensitive to the local environmental with limited scattering effects [51]. The emission spectral shift of Laurdan fluorescence mostly results from phase changes within the membrane, making it useful for discriminating between membrane phases.

Upon excitation, the dipole moment of Laurdan increases noticeably and water molecules in the vicinity of the probe reorient around this new dipole. When the membrane is in a fluid phase, the reorientation rate is faster than the emission process and, consequently, a red-shift is observed in the emission spectrum of Laurdan. When the bilayer packing increases, a part of the water molecules is excluded from the bilayer and the dipolar relaxation of the remaining water molecules is slower, leading to a fluorescent spectrum which is significantly less shifted to the red.

The steady state fluorescence parameter known as the excitation generalized polarization quantitatively relates these spectral changes by taking into account the relative fluorescence intensities of the blue and red edge regions of the emission spectra [48,49]. Excitation Generalized Polarization (GP_{ex}) was calculated using Eq. (3):

$$GP_{ex} = (I_{440} - I_{490})/(I_{440} + I_{490}) \quad (3)$$

were I_{440} and I_{490} are the fluorescence intensities at emission wavelengths of 440 nm (gel phase) and 490 nm (liquid-disordered phase), respectively.

The presence of coexisting phases is reflected by the increase of GP_{ex} upon increasing excitation wavelengths from 340 to 410. The opposite is observed when phospholipids are in the fluid-phase. When the phospholipids are in the gel phase, the GP_{ex} values don't show any change with increasing excitation wavelengths. Experiments were performed at increasing temperatures (from 5 °C to 65 °C). Monitoring GP_{ex} values as a function of temperature, also allowed to determine T_m. An adjustment to a Hill function (4) was performed:

$$GP_{ex} = GP_{ex}{}^2 + \left(GP_{ex}{}^1 - GP_{ex}{}^2\right)/\left(1 + \exp^{m\cdot(T_m - T)}\right) \quad (4)$$

where $GP_{ex}{}^1$ and $GP_{ex}{}^2$ are the maximum and minimum values of GP_{ex}, T_m, the melting temperature of the composition studied and m, the Hill coefficient. λ_{exc} was 340 nm and λ_{em} were 440 nm and 490 nm. The slope at mid-point (T_m) was calculated by the first derivative of GP_{ex} function at temperature T_m (Eq. (5)) (see [52]):

$$(dGP_{exc}/dT)_{T_m} = \left[\left(GP_{ex}{}^1 - GP_{ex}{}^2\right)\cdot m\cdot \ln 10\right]/4. \quad (5)$$

Fluorescence determinations were carried out using a thermostated Perkin-Elmer LS55 luminescence spectrometer. The lipid concentration of LUV was adjusted to 50 μM with Tris 10 mM and NaCl 150 mM at pH 8.5. Laurdan was added from a 5×10^{-3} M stock solution of DMF to give a lipid:probe ratio of 300. Surfactin was added to LUV to a final concentration of 3, 15, 25 and 100 μM and incubated under continuous agitation at 37 °C out of light for 60 min.

2.7. Atomic force microscopy

Visualization of the nanoscale effect of surfactin on membrane surface was performed using supported bilayers [41] monitored with commercial AFM (NanoScope IV MultiMode AFM, Veeco Metrology LLC, Santa Barbara, CA) equipped with a 12 μm×12 μm scanner (E-scanner). AFM images were obtained in contact mode at room temperature (23–25 °C) in Tris buffer (10 mM Tris and 150 mM NaCl at pH 8.5). All images were recorded using oxide-sharpened microfabricated Si_3N_4 cantilevers (Microlevers, Veeco Metrology LLC, Santa Barbara, CA) with spring constant of 0.01 N/m (manufacturer specified), with a minimal applied force (<500 pN) and at a scan rate of 5–6 Hz.

2.8. Molecular modeling

The "Big Monolayer" (BM) method proceeds in two steps: (i) Calculation of paired interactions between the molecules and (ii) Construction of a grid of 200×200 molecules, taking the molar ratios into account.

The first step is derived from the hypermatrix method described elsewhere [53,54]. The molecules of the system studied (surfactin, DPPC, DOPC) are first oriented at the interface, taking their hydrophobic and hydrophilic centers into account [55]. For each pair of molecules (surfactin/DPPC, surfactin/DOPC, surfactin/surfactin, DPPC/DPPC, DOPC/DOPC, and DOPC/DPPC), the interaction energies (sum of electrostatic, Van der Waals, and hydrophobic energies) are calculated for a large number of positions, resulting from translations and rotations of one molecule toward the other. In this study, we let the molecules undergo 36 rotations around themselves in steps of 10°. For each of these positions, horizontal and vertical translations are carried out on a distance of 10 and 5 Å with a step of 0.5 and 0.25 Å, respectively. For all those positions, an additional tilt of −10° to +10° by step of 0.5° is further applied. The total number of relative positions tested is thus more than 23,400,000 (36×36×21×21×41). For each pair of molecules, the statistical Boltzmann energy is considered. The latter is calculated taking into account a Boltzmann statistics corresponding to the sum of the interaction energy of each relative position tested multiplied by the probability of the position. This interaction energy matrix is then used in the second step.

The second step consists in the construction and minimization of the system using the interaction matrix calculated in step 1. A grid of 40,000 (200×200) molecules, initially positioned at random, is constructed and the energy of the system is calculated. The energy of one molecule is equal to the sum of the energies with its 24 closest neighbors in the grid. Random permutations are made and the energy of the new configuration is calculated. By a Monte Carlo procedure, this new configuration is kept or not, as a function of the energy difference between the two states. For a grid of 40,000 molecules, one calculation step consists in 40,000 permutations. 50,000 to 100,000 steps are carried out. For the molecules at the border of the grid, the molecules at the opposite border are considered as their closest neighbors, avoiding border limits.

The preferential interactions and phase separation between the molecules studied are visualized by representing each molecule type by a colored point and all the points are represented on the grid.

2.9. Diphenylhexatriene fluorescence polarization

The lipid dynamics and cooperative behavior of acyl lipid chains can be monitored by following the degree of polarization of diphenylhexatriene (DPH), a dye which probes the hydrophobic core of the membrane [56–58]. Anisotropy values (r) were determined as shown in Eq. (6):

$$r = (I_{VV} - G \cdot I_{VH})/(I_{VV} + 2 \cdot G \cdot I_{VH}) \quad (6)$$

where I_{VV} is the fluorescence intensity when angle between polarizers is 0°, I_{VH} is the fluorescence intensity when angle between polarizers is 90°, and G is an inherent factor to the fluorometer used.

T_m can be determined by monitoring anisotropy values as a function of temperature and adjustment to a Hill Eq. (7) as:

$$r = r_2 + (r_1 - r_2)/\left(1 + \exp^{m\cdot(T_m - T)}\right) \quad (7)$$

where r_1 and r_2 are the maximum and minimum values of anisotropy, T_m the melting temperature of the composition studied, and m the slope of the transition that gives information about the cooperativity of the process. The slope at T_m was calculated with the Eq. (6), which is the first derivative of the Hill equation at mid-point [52].

$$(dr/dT)_{T_m} = [(r_1 - r_2)\cdot m \cdot \ln 10]/4. \quad (8)$$

DPH was dissolved to a final concentration of 100 μM in tetrahydrofuran and added to the chloroform solution containing the lipids at a molar ratio of 300:1 (lipid:DPH) during the initial stage of preparing the vesicles (LUV) as described above. The total phospholipid concentration was adjusted to a final value of 50 μM with 10 mM Tris and 150 mM NaCl at pH 8.5. Surfactin (3, 15, 25 and 100 μM) was incubated for 60 min at 37 °C with LUV under darkness. Anisotropy (r) of samples was determined as a function of the temperature. All fluorescence determinations were performed using an LS 55 fluorescence spectrophotometer with λ_{exc} and λ_{em} of 381 nm and 426 nm, respectively.

2.10. Calcein release

Changes in the membrane permeability were followed as described by Weinstein [59]. Leakage of entrapped, self-quenched fluorescent probe, calcein, from liposomes can be monitored by the fluorescence increase as a consequence of the dilution of the probe. In these experiments the dried lipid films were hydrated with a solution of purified calcein (73 mM) in Tris 10 mM, buffer pH 8.5, which had an osmolarity of 404 mOsm/kg. The unencapsulated dye was removed from the LUV dispersion by the mini-column centrifugation technique [60]. The liposomes were diluted to a final lipid concentration of 5 μM in an isoosmotic Tris buffer (Tris 10 mM and NaCl 188 mM) pH 8.5 and equilibrated for 10 min at 25 °C. Thereafter, values were recorded for 30 s before addition of surfactin at increasing final concentrations of 3, 15, 25 or 100 μM. After the addition of surfactin, the fluorescence intensities were continuously recorded as a function of time (up to 500 s). The percentage of calcein released was determined as $[(F_t - F_{contr})/(F_{tot} - F_{contr})]\times 100$, where F_t is the fluorescence signal measured at a time t in the presence of surfactin, F_{contr} is the fluorescence signal measured at the same time t for control liposomes, and F_{tot} is the total fluorescence signal obtained after complete disruption of the liposomes by 0.02% Triton X-100. Values were fitted to a biexponential function

$$\%\,calcein\,released = y^1_{max}\left(1 - \exp^{(-k_1 t)}\right) + y^2_{max}\left(1 - \exp^{(-k_2 t)}\right) \quad (9)$$

where y^1_{max} and y^2_{max} are the maximum releases in percent due to the 1st and 2nd release mechanism respectively. k_1 and k_2 are the release constants in/s of the first and second release mechanism, respectively. t is the time in s. $t^1{}_{1/2}$ and $t^2{}_{1/2}$ are defined as the time periods for which R_{18} calcein release is doubled, respectively to the mechanism. They can be derived from $t_{1/2} = \ln 2/k$.

All fluorescence determinations were performed at 25 °C on a Perkin Elmer LS 30 Fluorescence Spectrophotometer (Perkin-Elmer Ltd., Beaconsfield, U.K.) using λ_{exc} of 472 nm and a λ_{em} of 516 nm.

2.11. Dynamic light scattering

The apparent average diameter of liposomes was estimated by dynamic light scattering using a Malvern Zetasizer Nano ZS® (Malvern Instruments, Ltd., Worcestershire, U.K.). The liposome concentration was set at 50 μM in buffer (Tris 10 mM and NaCl 150 mM at pH 8.5). Surfactin was added to liposomes at different concentrations (3, 15, 25, 75 or 100 μM). Just after mixing, dynamic light scattering was measured at an angle of 90° with monodisperse latex particles of 100 and 800 nm diameters as control. Data were analyzed using both unimodal and size distribution analysis modes to determine the mean diameter and the size distribution profile of LUVs in presence of surfactin, respectively.

2.12. Fluorescence dequenching of octadecylrhodamine B

The fusion of lipid vesicles was determined by measuring the dequenching of the fluorescence of octadecylrhodamine B chloride (R_{18}) [61]. The fluorescence of this lipid-soluble probe is self-quenched at high membrane concentration and any decrease of its surface density is therefore associated with a commensurate increase of the fluorescence intensity of the preparation [61]. Labeled LUV liposomes were obtained by incorporating R_{18} in the dry lipid film at a molar ratio of 5.7% with respect to the total lipids. The liposomes were diluted to a concentration of 10 μM in the buffer solution (Tris 10 mM and NaCl 150 mM at pH 8.5). These labeled liposomes were mixed with unlabelled LUV liposomes (adjusted to the same concentration) at a ratio of 1:4. Liposomes were equilibrated for 10 min at 25 °C. Fluorescence intensities were then recorded for 30 s before addition of surfactin at increasing concentrations (3, 15, 25 and 100 μM). Fluorescence was followed at room temperature during 200 s, using a λ_{exc} of 560 nm and a λ_{em} of 590 nm (Perkin-Elmer LS-30, Perkin-Elmer Ltd, Beaconsfield, UK). Results were expressed as percentage of R_{18} dequenching defined as $[(F_t - F_{contr})/(F_{tot} - F_{contr})] \times 100$, where F_t is the fluorescence signal measured at time t in the presence of surfactin, F_{contr} is the fluorescence signal measured at the same time t for control liposomes, and F_{tot} is the total fluorescence signal obtained after complete disruption of the liposomes by 0.02% Triton X-100. Values were fitted to an exponential function:

$$\%R_{18}\,dequenching = y_{max}\left(1 - \exp^{(-kt)}\right) \quad (10)$$

where y_{max} is the maximum dequenching achieved, k is the dequenching speed constant (in/s) and t the time in s. $t_{1/2}$ is defined as the time period for which R_{18} dequenching is doubled. It can be derived from $t_{1/2} = \ln 2/k$.

3. Results and discussion

3.1. Critical micellar concentration of surfactin

It is well-known that the effect of surfactin on membranes is very dependent on the concentration [20,23–26]. Since surfactin is known to self-assembly into micelles, the first step of our study was to determine the critical micellar concentration (CMC) of the used sample of surfactin, by means of isothermal titration calorimetry. Fig. 1A shows the typical heat flow as a result of successive injections of 6 μL of surfactin 0.08 mM in a Tris 10 mM and NaCl 150 mM at pH 7.4 and 25 °C. The corresponding molar heat of demicellization ($\delta h_i/\delta n_{surf}$) as a function of surfactin concentration is shown on Fig. 1B. As the injections were performed, the absolute value of $\delta h_i/\delta n_{surf}$ decreased as the concentration of surfactin in the cell increased. This is consequence of the fact that since there is increasing number of surfactant molecules in the solution, the energy released upon break-up of the micelles decreases until it finally approaches zero at CMC. The CMC value, defined at the inflection point of the sigmoidal curve, was 2.95 ± 0.55 μM. At pH 8.5, CMC was determined to be 12.85 ± 0.05 μM. This value is higher than the value of 7.5 μM reported by Heerklotz and Seelig [19] for similar conditions (Tris 10 mM and NaCl 100 mM at pH 8.5 and 25 °C). The differences between the values found in our study and these previous data can most likely be related to the different composition of surfactin homologous in the sample used as it is well known that surfactin acyl chain length greatly influences its capacity to self-assemble into micelles [16,18].

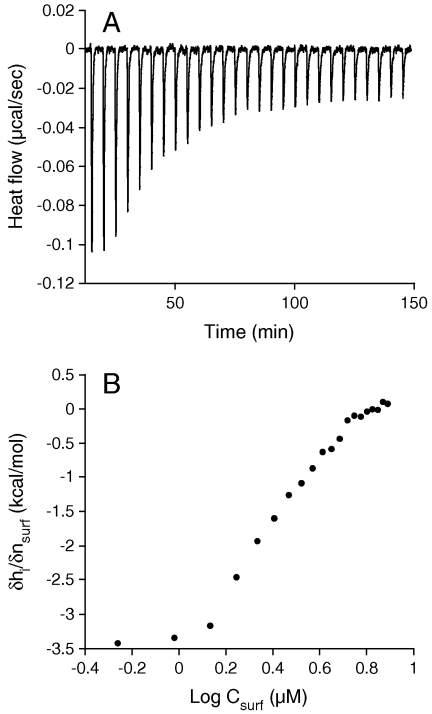

Fig. 1. CMC determination by ITC. (A) Heat flow per injection of 6 μL surfactin 0.08 mM into a 10 mM Tris and 150 mM NaCl buffer at pH 7.4 and 25 °C; and (B) Heat of injection per mole of surfactin injected versus the concentration logarithm of surfactin in the cell.

3.2. Integrity of supported phospholipid bilayers (SPBs)

In order to assess the integrity of a gel (DPPC) and a fluid (DOPC) phase lipid bilayers, the changes in thickness (d) and surface excess (Γ) of the supported DPPC or DOPC bilayer were recorded by null-ellipsometry. The effect of the sequentially increasing concentration of surfactin in the aqueous medium, at pH 7.4 was followed. Under these conditions, CMC was determined to 2.95 ± 0.55 μM at 25 °C. For each surfactin concentration, the steady state values of d and Γ obtained are reported relative to the initial values of pure SPBs (Fig. 2A and B).

The effect of surfactin on lipid bilayer was concentration dependent and was influenced by the physical state of the bilayer. Surfactin had no significant effect on both types of lipid bilayers DOPC and DPPC, at concentration lower than CMC (0.2 μM). At a concentration near the CMC (2 μM), the lipopeptide induced a low but significant decrease of both Γ and d of DOPC bilayer while it had no significant effect on DPPC bilayer. The decrease in Γ and d was more pronounced for DOPC above the CMC (10 μM). Total disintegration and removal of the DOPC bilayer was observed when the concentration of surfactin was ~6 times higher (20 μM) than CMC (Fig. 2A). At this surfactin concentration, the rate of the removal process was fast (Fig. 2C). Only 20 min were needed to totally take away the bilayer from the supporting surface. In the case of DPPC bilayer, the same concentration of surfactin (20 μM) didn't

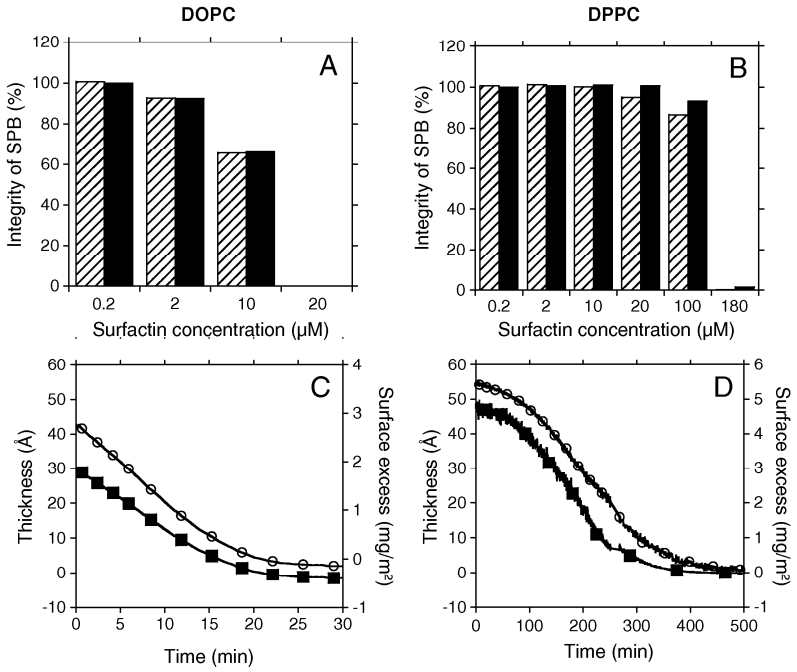

Fig. 2. Ellipsometry measurements. Top panels: Effect of surfactin concentration on supported phospholipid bilayers (SPB) integrity. Results are given in percent of bilayer thickness (striated bars) or surface excess (black bars) after addition of surfactin at different concentrations related to initial values of the pure SPB. (A) DOPC bilayer and (B) DPPC bilayer. Bottom: Time evolution of thickness (open symbols) and surface excess (closed symbols) after addition of surfactin at a critical concentration leading to a complete removal of the SPB: (C) DOPC bilayer — Final surfactin concentration in the medium = 20 μM and (D) DPPC bilayer — Final surfactin concentration in the medium = 180 μM.

influence Γ but a slight decrease of d was observed. The decrease in the bilayer thickness without removal of molecules from the supporting surface is in accordance with the model of surfactin insertion described by Heerklotz et al. [21]. In their model, surfactin molecule is rather deeply inserted into the bilayer, leading to an increasing tilt of the lipid acyl chains resulting to a decrease in the thickness. The deposited amount of DPPC bilayer was significantly decreased when 100 μM of surfactin (~33 times the CMC) was added. The complete removal of DPPC bilayer was observed when 180 μM (~60 times the CMC) of surfactin was injected (Fig. 2B). The requirement of a concentration much above the CMC to solubilize DPPC bilayer is in accordance with neutron reflectometry data obtained by Shen et al. [26]. It also took more than 300 min for the Γ and d values to reach zero (Fig. 2D). The rate of the DPPC solubilization was thus much slower than the corresponding process for DOPC.

Ellipsometry experiments clearly showed that lipid molecules in a fluid state (DOPC) are more easily solubilized by surfactin than molecules in a well-packed gel state (DPPC). The resistance of gel phases to detergent solubilization was previously described in literature for detergents (octylglucoside [62–64] or Triton X-100 [65,66]) as well as drugs like general volatile anesthetic (enflurane [67]) or lipopeptides (fengycin [68]).

3.3. Changes in bilayer packing and lipid phases induced by surfactin

The effect of surfactin concentration on lipid phases structure was investigated by monitoring the lipid phase-dependent emission spectral shift of Laurdan, which locates into the glycerol backbone region of phospholipid bilayer.

The Generalized Polarization (*GP*) makes it possible to distinguish between a mixed phase of coexisting domains, a homogeneous liquid-disordered phase and a gel phase [50]. Laurdan molecules surrounded by phospholipids in liquid-disordered and gel phases are excited in red band of the excitation spectrum. If phospholipids in gel phase are present, they mainly populate the red band of excitation, emitting with a blue spectrum and with a high *GP* value [50,69]. If no phospholipids are in the gel phase only relaxed molecules populate the red band, with a red-shifted emission spectrum and a low *GP* value. Thus, when the excitation is moved to larger wavelengths, the GP value decreases in the homogeneous liquid-disordered phase, while in bilayer composed of coexisting phases, the *GP* value increases. In gel phase, the *GP* value stays stable with the excitation wavelength [48]. Laurdan fluorescence has been monitored for liposomes composed of synthetic lipids as well as for cellular membranes [70,71] for investigating the effect of change in lipid composition (cholesterol or gangliosides e.g.) [72–74] or for characterizing effects of drugs (tamoxifen [75], propofol [76], fenitrothion [77], and phenothiazine derivatives [78] on lipid membrane organization.

The effect of surfactin on lipid phases in DOPC:DPPC (molar ratio 1:1) LUVs was investigated for surfactin concentrations lower, close and higher than CMC (3, 15, 25 and 100 μM) as function of increasing the temperature from 5 °C to 65 °C. The recorded data obtained at selected temperatures (5 °C, 25 °C, 35 °C and 55 °C) are shown (Fig. 3). Data obtained at 15 °C, 45° and 65 °C are illustrated in supplementary material. Based on these data, GP_{ex} was calculated and plotted as a function of increasing surfactin concentrations and excitation wavelengths (Fig. 3).

At 5 °C (Fig. 3A), values of GP_{ex} were around +0.4 to +0.5 with a slight increase of GP_{ex} with excitation wavelengths suggesting a high level of bilayer packing and lipid-coexisting phases. Surfactin addition at a concentration of 3 to 25 μM slightly increased the GP_{ex} values reflecting a more ordered environment at the same time as it decreased the effect of increasing excitation wavelengths on GP_{ex}, suggesting the presence of a gel phase. At 25 °C (Fig. 3B), as expected, GP_{ex} values were lower (+0.1 to +0.4) suggesting a less ordered environment.

The presence of co-existing phases was clearly observed, where DPPC gel domains were inserted in a DOPC fluid matrix. Global GP_{ex} values increased with surfactin concentrations below or close to the CMC and decreased with high surfactin concentrations, which means some ordering of the lipid phase at surfactin concentrations from 3 to 25 μM and disordering at higher concentrations (100 μM). The phase behavior tends to shift from co-existing phases towards a gel phase, as observed from the GP_{ex} values that became more and more independent of the wavelength at increasing concentrations. At 35 °C (Fig. 3C), the lipids were in fluid phase with GP_{ex} values around −0.1. A marked increase of GP_{ex} (values reached +0.3/+0.4) was observed upon increasing surfactin concentrations (from 3 to 15–25 μM), suggesting an ordering effect of surfactin with increase of packing of phospholipids. In parallel, GP_{ex} values slightly increased with the excitation wavelengths, reflecting formation of coexisting phases. The GP_{ex} was reduced at higher surfactin concentrations (100 μM) to values in the range of 0/−0.1. Simultaneously, the GP_{ex} slightly decreased with increasing excitation wavelengths, especially for wavelengths higher than 385 nm, confirming a fluidification effect of surfactin at this concentration. At higher temperatures (55 °C) (Fig. 3D), the lipids were clearly in fluid phases with GP_{ex} values around −0.2/−0.3 and increasing the surfactin concentrations didn't significantly affect lipid phase behavior.

In summary, at room temperature (25 °C), surfactin inhibited lipid-phase co-existence at concentrations close to CMC and increased GP_{ex} values, suggesting high ordering. At higher surfactin concentrations, the effect on ordering was decreased.

3.4. Nanoscale morphological changes of SPBs due to surfactin interaction

We used AFM to visualize at a nanoscale the effect of surfactin concentrations on domain formation as well as on any other morphological changes of mixed DOPC:DPPC (1:1; mol/mol) bilayers. Three defined concentrations (3 μM, 15 μM and 1 mM), i.e. below, near and far above the CMC, were selected. As shown in Fig. 4 (at time t = 0 min), the topographic image obtained for a native DOPC:DPPC (1:1 mol/mol) bilayer revealed the coexistence of two phases, the lighter and darker levels corresponding to DPPC- and DOPC-enriched phases respectively [79,80]. The step height measured between the two phases was 1.1 ± 0.1 nm and resulted from a difference in the thickness and mechanical properties of the DOPC and DPPC films [81].

Incubation of DOPC:DPPC (1:1 mol/mol) bilayers with surfactin at a concentration lower than the CMC (3 μM) caused a time-dependent erosion of the DPPC domains (Fig. 4A). It appears that the erosion phenomenon proceeds essentially at the boundary between the gel and fluid phases, thereby resulting in the disruption of the tight molecular packing of DPPC. This behavior is reminiscent of that observed with the drug azithromycin [79] and with the non-ionic detergent Triton X-100 at low concentration (half the CMC) [65]. According to Francius et al. [24], surfactin C14 at the same concentration has no effect on DOPC: DPPC bilayers. It indicates that the mixture of surfactins has a higher penetration activity than the pure surfactin C14. The high proportion of surfactin C15 that has been shown to be the most active on erythrocyte membranes [18] is likely to increase the effect of the surfactin mixture. The higher hydrophobicity but also the *iso* structure of the C15 β-hydroxy fatty acid chain can explain the higher activity of this homologue.

Notably, a very different behavior was noted near the CMC (15 μM; Fig. 4B). Twenty minutes after injection, the DPPC domains appeared to be considerably higher. The new DPPC domain height was 5.4 ± 0.2 nm, which corresponds to the thickness of a DPPC bilayer and thus indicates complete removal of the DOPC-fluid phase. At longer incubation times, a few holes appeared inside the remaining DPPC patches (see arrow in

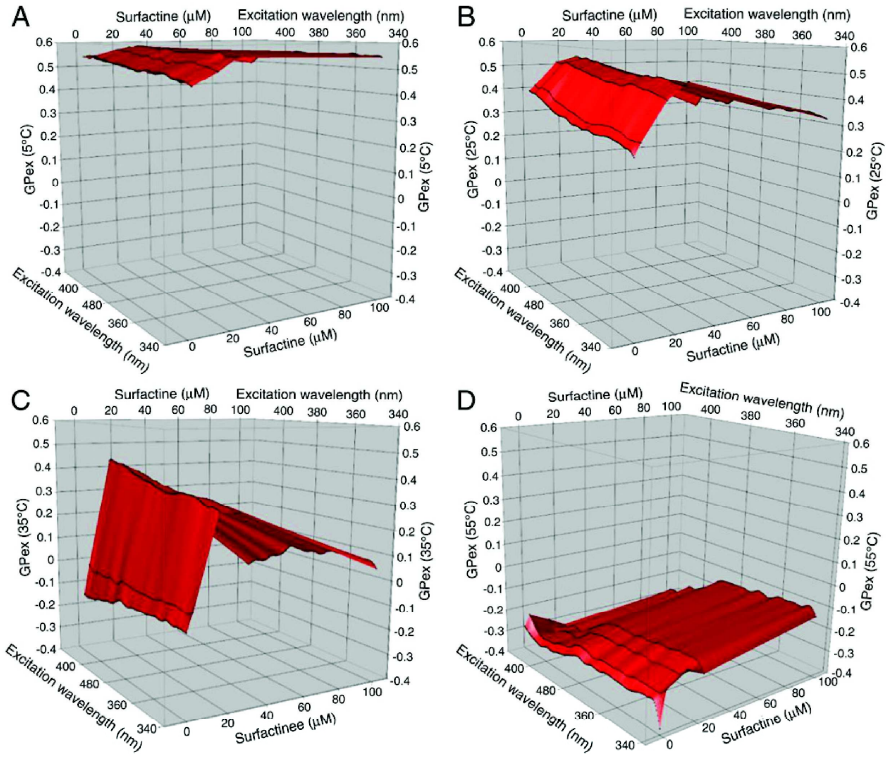

Fig. 3. Excitation generalized polarization (GP_{ex}) of Laurdan in DOPC:DPPC (1:1) in function of excitation wavelengths (from 340 nm to 410 nm) in absence and presence of increasing concentrations of surfactin (3, 15, 25, and 100 μM) at 5 °C (A), 25 °C (B), 35 °C (C), and 55 °C (D) in 10 mM Tris and 150 mM NaCl buffer at pH 8.5.

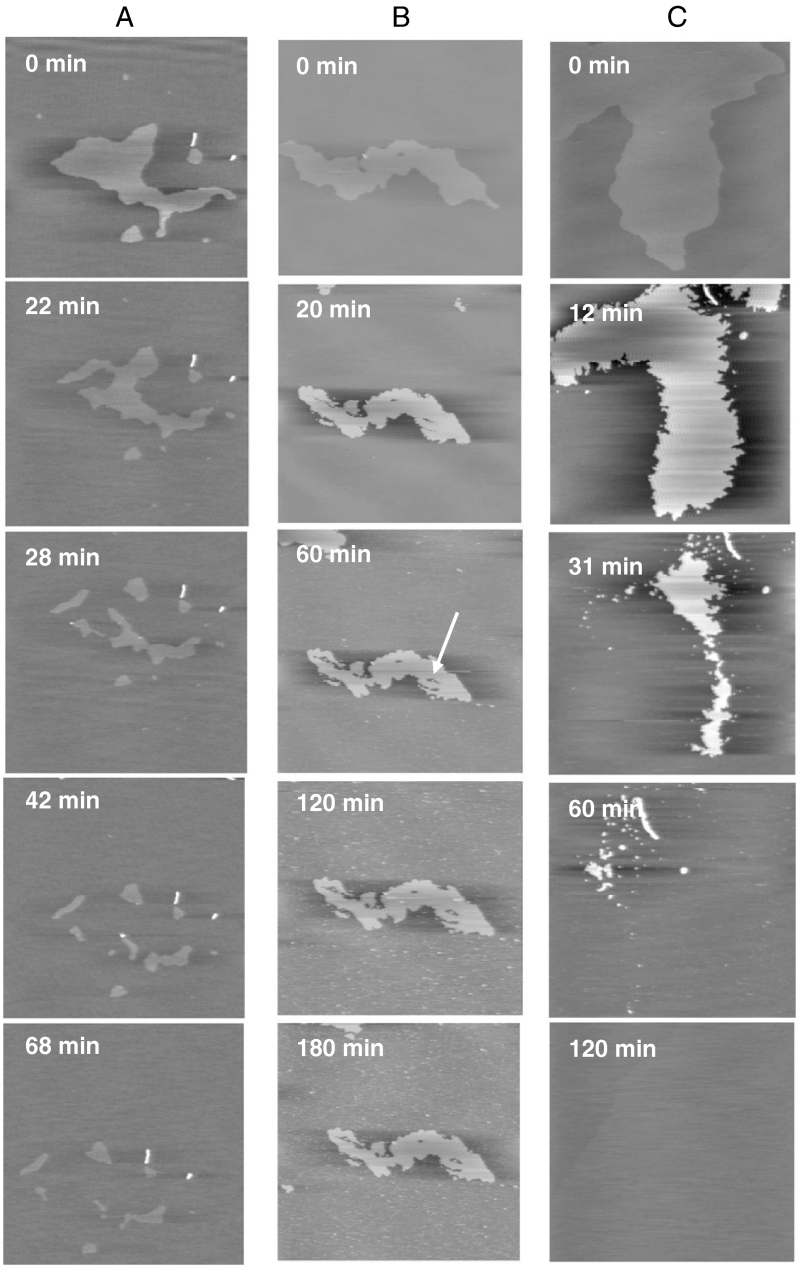

Fig. 4. AFM topographic images of a DOPC:DPPC (1:1) bilayer recorded in 10 mM Tris and 150 mM NaCl buffer at pH 8.5 (0 min) and at increasing incubation times (A) below the CMC (3 μM) (image size: 10 μm×10 μm and z-range: 5 nm), (B) near the CMC (15 μM) (image size: at 0 min: 15 μm×15 μm, after 0 min: 20 μm×20 μm and z-range: 10 nm) and above the CMC (1 mM) (image size: 10 μm×10 μm and z-range: 10 nm).

Fig. 4B), while the general shape of the domains remained essentially unaltered. Moreover, numerous white particles are observed. It is likely to be a redeposition of mixed DOPC:surfactin micelles on the mica surface [24]. These results are also very similar to those observed with Triton X-100 at a concentration 2 times greater than the CMC [65], thus indicating that surfactin, near the CMC, is able to solubilize the DOPC-fluid phase in a detergent-like manner. Finally, our results fitted well with the quantitative model reported by Keller et al. [64] which reported that order-preferring lipids like DPPC are "resistant" regardless of the presence of a second, fluid-phase lipid, like DOPC, for the action of a membrane solubilizer.

At much larger concentrations (1 mM), the DOPC-fluid phase seems to be completely removed and also the remaining DPPC domains were progressively eroded (see images recorded at 12 and 31 min; Fig. 4C) and disappeared after 60 min. No redeposition of mixed micelles or continuous bilayer was observed as was the case for octyl glucoside surfactant [82]. The dispersion of mixed DOPC:DPPC:surfactin micelles containing a high concentration of surfactin would be a stable colloidal

system in our conditions. Hence, compared with the previous situation, it appears that the detergent effect of surfactin is stronger when the concentration is well above the CMC since both DOPC and DPPC were solubilized.

AFM studies clearly revealed three major steps involved in the effect of surfactin on mixed lipid bilayers (i) erosion of DPPC domains, (ii) DOPC solubilization with removal of fluid phase and redeposition of DOPC:surfactin micelles, and (iii), erosion and disappearance of DPPC domains and dispersion of DOPC:DPPC:surfactin micelles.

3.5. Lateral distribution of surfactin within a modeled DOPC:DPPC monolayer

The effect of surfactin on the domain coexistence is confirmed by modeling the lateral distribution of surfactin within a DOPC:DPPC (1:1 mol:mol) monolayer at 25 °C. In absence of surfactin, the coexistence of segregated rounded-shape domains is observed in accordance with AFM results (Fig. 5A). For the two proportions studied (lipid:surfactin 2:0.1 and 2:0.3), surfactin molecules are localized at the boundaries between DOPC and DPPC domains (Fig. 5B and C). At higher surfactin molar ratios (Fig. 5C), an obvious changes in the shape of DOPC domains is observed suggesting that surfactin affects more strongly the fluid phase, in accordance with AFM data that, as discussed above, clearly showed a preferential solubilization of fluid lipid phase at higher surfactin concentration.

3.6. Changes in thermotropic behavior of DOPC:DPPC vesicles induced by surfactin

We determined the thermotropic effect of surfactin on both the interfacial and the hydrophobic core regions of the membrane of liposomes (DOPC:DPPC; 1:1; mol:mol) in order to further understand the nature of effect of surfactin on lipid phases observed by Laurdan fluorescence spectroscopy and visualized by AFM. For this purpose we measured the changes in GP_{ex} of the Laurdan and the fluorescence anisotropy of DPH upon temperature increase.

As previously reported for synthetic lipids (e.g. DOPC:DPPC), we clearly showed the appearance of gel and liquid phases with a defined T_m. The characteristic shape of the plot of GP_{ex} as well as fluorescence anisotropy (r) versus temperature is sigmoidal (Fig. 6), with (i) a plateau of high GP_{ex} or anisotropy values at temperatures below T_m, (ii) another plateau of low GP_{ex} or anisotropy values at temperature above T_m, and (iii) a sharp transition of GP_{ex} or anisotropy values in a short range of temperatures for which the inflexion point corresponds to T_m. The temperature dependence of Laurdan GP_{ex} as well as of DPH anisotropy provides additional information both on the apparent transition temperature and on the extent of cooperativity [83].

The GP_{ex} versus temperature is clearly dependent on the concentration of surfactin (Fig. 6A; Table 1). At 3 μM, surfactin induced a significant increase of T_m from 28.8 °C to 34.4 °C. The shift is even larger when adding a higher concentration of surfactin (15 μM) with a T_m of 39.0 °C. Above the CMC (25 μM), no further increase of T_m (38.7 °C) was recorded. At higher concentration (100 μM), T_m (29.2 °C) was similar to that of the control sample without surfactin. The highest cooperativity of the thermal transition, as determined from the slope of the steepest part of the curves in Fig. 6 (Table 1), was observed for surfactin concentrations close to CMC (15 μM). At this concentration, surfactin seems to induce a rigidifying effect both below and above T_m. For the highest concentration of surfactin (100 μM), a marked change of the trend of the curve was observed, especially at temperature above T_m, with a huge increase of GP_{ex}, reflecting an ordering effect of the interfacial region.

The DPH-steady state fluorescence anisotropy also reflected a significant increase of the T_m values from 26.6 °C to 30.2 °C (Fig. 6B; Table 1) after addition of 3 μM of surfactin. Again, the maximal increase in T_m was observed at surfactin concentration close to CMC with a T_m of 37.3 °C at 15 μM of surfactin. At 25 μM of surfactin, T_m slightly decreased to reach 34.5 °C. At the highest surfactin concentration (100 μM), the T_m value was similar (26.4 °C) to that of the surfactin free samples. For concentrations between 3 and 25 μM, both below and above T_m, a rigidifying effect was monitored.

At temperatures between 20 and 40 °C and at concentrations lower, equal or slightly higher than CMC, surfactin induced an almost similar effect on the hydrocarbon chain region (reflected by the DPH-steady state fluorescence anisotropy) as on the membrane polar surface region (as judged from the GP_{ex} data). Under these conditions and when the lipid composition is such that it mimics lipid domains found in biological membranes, surfactin was able to shift the phospholipid phase transition to higher temperature. When DOPC is solubilized from the lipid bilayer at surfactin concentrations around the CMC, one would expect that the cooperativity and transition temperature would increase as the bilayer system formed would be mostly composed of DPPC. This is exactly what we observed and what Juhastz et al. [84] reported when they decreased DOPC:DPPC ratio. In fact the transition temperature of DPPC is 41 °C which corresponds almost to value (39.0 °C) we obtained in presence of 15 μM of surfactin. Promotion of the ordered domains was also reported [85] when Triton X-100 was added to DPPC:Chol:SM vesicles i.e. when cholesterol (Chol) and sphingomyelin (SM) were present to mimic lipid domains found in biological membranes (lipid rafts), suggesting the interest of the binary lipid mixture we selected. In contrast, at conditions where DOPC was solubilized, suppressing the existence of domains, surfactin tended to shift the gel-to-liquid crystalline "melting" temperature of lipids to lower temperatures, close to value obtained for control liposomes. This behavior observed for surfactin concentrations above CMC, was similar to the effect of non-ionic detergent like Triton X-100 described by Goni et al. [86] and the effect of surfactin, on DPPC alone reported by Grau et al. [30].

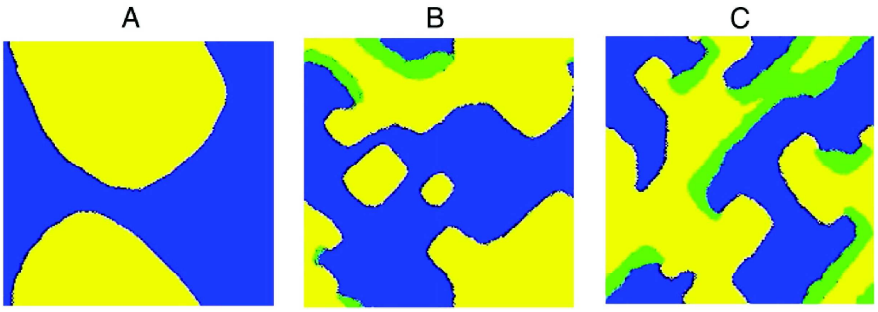

Fig. 5. Monolayer grid of 200×200 lipids calculated by the BM procedure (see Materials and methods). Each pixel represents a molecule. Blue: DPPC molecule; yellow: DOPC molecule; green: surfactin molecule. (A) DOPC:DPPC at 1:1 molar ratio, (B) DOPC:DPPC:surfactin at 1:1:0.1 molar ratio, and (C) DOPC:DPPC/surfactin at 1:1:0.3 molar ratio.

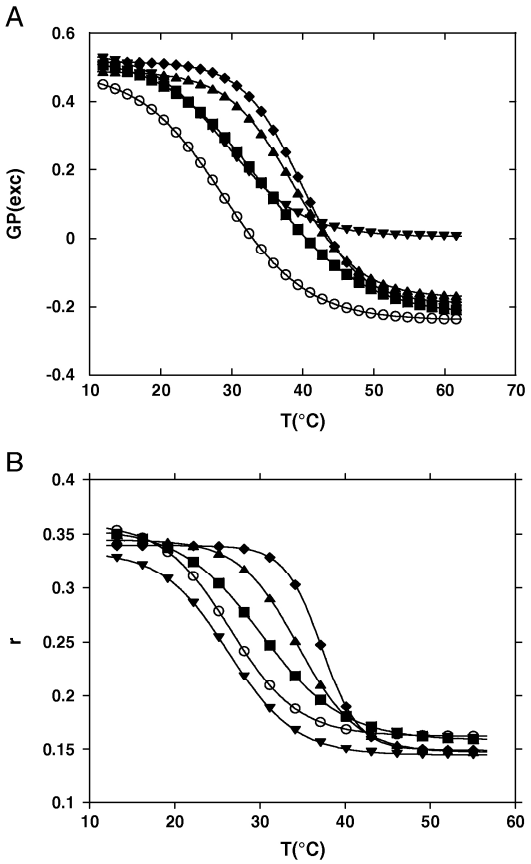

Fig. 6. Temperature-dependent Generalized Polarization (GP_{ex}) of fluorescence of Laurdan (A) and temperature-dependent fluorescence anisotropy (r) of DPH (B) in LUVs prepared from DOPC:DPPC (1:1) in 10 mM Tris and 150 mM NaCl buffer at pH 8.5 [○]. Increasing surfactin concentrations, (3 μM [■], 15 μM [◆], 25 μM [▲] and 100 μM [▼]) were added. The excitation wavelengths were 340 and 381 nm for Laurdan and DPH, respectively. The emission wavelengths were 440 and 490 nm (Laurdan) and 426 nm (DPH).

We can conclude that under conditions where lipid domains are formed, both the generalized polarization and anisotropy studies showed a marked increase of T_m induced by surfactin. The effect is very dependent on the surfactin concentration and the maximum effect was obtained for concentrations close to the CMC. For higher surfactin concentrations, when DOPC was solubilized, a clear decrease of T_m was observed.

3.7. Membrane permeability of liposomes induced by surfactin

We have previously discussed how surfactin greatly affected the organization of the lipids in supported lipid bilayers as well as in vesicles. Highly relevant from a biological activity point of view is to know if surfactin is able to induce, in our model of lipids forming phase coexistence, membrane permeabilization. For this purpose, calcein was encapsulated at a self-quenching concentration within liposomes of DOPC:DPPC (1:1 mol:mol) [59]. Surfactin was added after 30 s of recording. The best fitting of the results was obtained with a biexponential function, suggesting permeabilization took place through two processes. At the lowest concentration of surfactin investigated (3 μM), we observed a slow but steady release which reached around 75% of the maximal membrane permeabilization after 500 s (Fig. 7, Table in supplementary data). The release could involve two processes, the first one presenting a $t^1_{1/2}$ of 157.2 s and contributing to 57.5% of the absolute release, and a second one showing a $t^2_{1/2}$ of 24.9 s and contributing to 25.9% of the absolute release (Table in supplementary data). At concentrations closer to the CMC (15 and 25 μM), around 80% of calcein was released within the first 100 s (Fig. 7). The contribution of the first process to the total release of calcein became less important ~40% for 15 μM and 13.1% for 25 μM whereas the second mechanism prevailed. An increased rate of calcein release was observed upon concentration ($t^2_{1/2}$ of 12.7 and 9.8 for 15 and 25 μM, respectively) (Table in supplementary data). At concentration exceeding largely the CMC (100 μM), the release was instantaneous with the maximal release observed within the first 15 s (Fig. 7). The first process did not significantly contribute to the permeabilization, but the second one increased further in speed ($t^2_{1/2}$ of 4.8).

Below the CMC, the first release process could be governed by the insertion and accumulation of the amphiphilic molecules into the membrane. At concentrations close to or beyond the CMC, release was complete. At concentrations exceeding largely the CMC, the release was almost instantaneous. This could be due to the complete solubilisation of phospholipid vesicles and the formation of mixed micelles composed of phospholipids and surfactin, corresponding to the second release process. This behavior is close to what has been observed with Triton X-100 [87].

From a lipid self-assembly point of view, the partial membrane permeabilization induced by membrane-interacting peptides could result from two mechanisms (i) some vesicles in the population release all their aqueous contents (all-or-none mechanism), while the rest maintains the barrier intact [88], or (ii) virtually all vesicles gradually released the dye (graded mechanism) and this process is followed by an annealing process that prevents further leakage [20]. The latter mechanism is in agreement with a bilayer-couple mechanism where strain inducing leakage arises from a selective increase in the area requirement of the outer (but not the inner) leaflet by surfactin. Transient membrane failures would allow some surfactin and lipid to redistribute within membrane followed by some release of calcein from the vesicle interior. The driving force for leakage would then be reduced and the membrane would anneal and restore its integrity. Further studies aiming to

Table 1
Transition temperature and minimum slope values obtained from non-linear regression of curves from Fig. 6A and B. Comparison of values has been performed by a one-way ANOVA test. Asterisks indicate a significant difference to the control.

Surfactin concentrations	Laurdan generalized polarization		DPH anisotropy	
	$T_m \pm$ SD (°C)	Min. slope (dGP_{ex}/dT_m) ± SD	$T_m \pm$ S	Min. slope (dr/dT_m) ± SD
Control	28.8 ± 0.3	−0.031 ± 0.0005	26.6 ± 0.9	−0.013 ± 0.0004
3 μM	34.4* ± 4.9	−0.032 ± 0.0033	30.2** ± 0.3	−0.010* ± 0.0002
15 μM	39.0*** ± 2.2	−0.041 ± 0.0180	37.3*** ± 0.8	−0.022*** ± 0.0011
25 μM	38.7*** ± 1.0	−0.037 ± 0.0008	34.5*** ± 1.5	−0.015 ± 0.0009
100 μM	29.2 ± 0.5	−0.026 ± 0.0013	26.4 ± 0.9	−0.012 ± 0.0007

* $p<0.05$.
** $p<0.01$.
*** $p<0.001$.

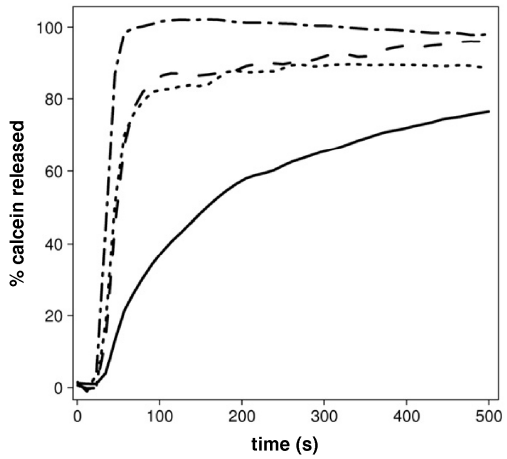

Fig. 7. Release of calcein from DOPC:DPPC (1:1) liposomes, upon addition (at t = 30s) of increasing concentrations of surfactin (3 μM [——], 15 μM [- - -], 25 μM [·····] and 100 μM [- · -]) in 10 mM Tris and 188 mM NaCl buffer at pH 8.5 and 25 °C. The recording was made for 500 s. The ordinate shows the amount of calcein released in the presence of surfactin as a percentage of the total amount released by 0.02% Triton X-100.

monitor the fluorescence lifetime of entrapped calcein as well as to visualize dye influx into individual GUVs should be done to decipher between all-or-none and graded mechanisms [88].

3.8. Fusion of LUV lipid bilayers induced by surfactin

Transient membrane discontinuities induced by surfactin insertion could be related to the propensity of membrane to fuse as reported for peptides derived from the membrane-proximal external region of HIV-1Gp41 [89]. Fusion of lipidic phase particles, e.g. vesicles, can be monitored by following the dequenching of octadecylthodamine B (R_{18}) fluorescence [61]. Aggregation of vesicles or other processes that reduce the local concentration of the fluorescent probe within the lipid bilayer could also lead to increase of fluorescence. Triton X-100 above its CMC was used as a reference for 100% dequenching since it has been shown to induce membrane fusion followed by complete solubilization of R_{18} into micelles [90].

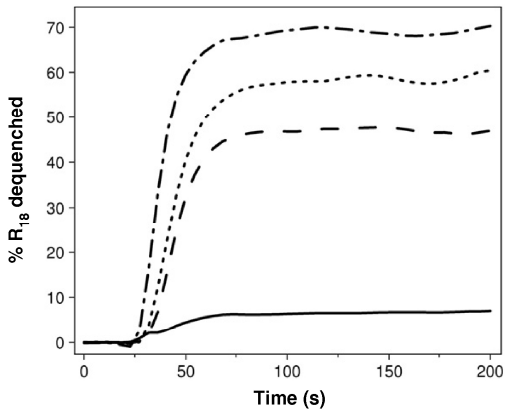

Fig. 8. Dequenching of octadecylrhodamine B (R_{18}) as a percentage of the total amount released by 0.02% Triton X-100 after addition of surfactin (t = 30s). Liposomes of DOPC:DPPC (1:1) were incubated for 200 s at 25 °C in the presence of increasing concentrations in surfactin (3 μM [——], 15 μM [- - -], 25 μM [·····] and 100 μM [- · -]) in 10 mM Tris and 150 mM NaCl buffer at pH 8.5 and 25 °C.

The values of R_{18} dequenching we observed upon addition of surfactin to DOPC:DPPC (1:1 mol:mol) vesicles are best fitted to a mono-exponential function upon time, which suggests that one primary mechanism leads to R_{18} dequenching. For surfactin concentrations below the CMC, we observed only a very small dequenching of R_{18} (max 6.8%) (Table in supplementary data) suggesting no major effect on the aggregation state of lipid dispersion (Fig. 8). Dequenching became important at CMC and for instance, at 15 μM of surfactin, it reached 47.6% that induced by Triton X-100. At 25 μM of surfactin, dequenching increased by another 12% compared to 15 μM. Further increase of surfactin concentration (100 μM) induced a faster but still partial dequenching (68.8%) [61].

However, it should be noted that many factors could influence the recorded dequenching. In particular, the dequenching properties of octadecylrhodamine can be affected by changes in lipid composition due to preferential effect of surfactin on DOPC.

3.9. Size of liposomes

To provide further insight on the relation between dequenching and vesicle aggregation/fusion, we followed the apparent size and homogeneity of the liposomes preparation incubated with surfactin, by means of dynamic light scattering, to monitor the morphological changes of DOPC:DPPC (1:1 mol:mol) vesicles induced by surfactin (Fig. 9).

Addition of 3, 15, 25 or 50 μM surfactin didn't change the DOPC:DPPC vesicle size significantly (~100 nm). At higher concentrations (75 and 100 μM) of surfactin, two main populations were observed, one with a very small mean diameter (around 10 nm) and the other with an average diameter ranging from 200 to 300 nm, suggesting the existence of fused liposomes [91].

The very small structures observed at 75 and 100 μM probably reflect mixed micelles of lipids and surfactin [19,23,25]. Indeed, surfactin should provide a solubilization of the liposome to mixed-micelles at concentrations above the CMC (25 μM) [92,93]. Once surfactin concentration within the bilayer reached a critical surfactin:lipid ratio (depending also of the lipid density and composition), surfactin molecules with their relatively large polar head compared to their small apolar chain section is expected to distort the bilayer structure. In this respect, surfactin should act as a surfactant able to solubilize phospholipid molecules.

At 25 μM, a population of small size should have been observed. However, it must be kept in mind that one limitation of dynamic light scattering technique is that results can be dominated by a small fraction of a larger species that gives a higher scattering intensity. The presence of fused vesicles or lipid aggregates can prevent the observation of individual micelles. Furthermore, since the diameters of the particles are calculated from the determined diffusion constants using Stoke–Einstein equation, which assumes spherical aggregates, the appearance of non-spherical structures would affect the calculated values of the particle diameter. Although the time-dependence of liposome solubilization by surfactin has been reported by Liu et al. [25], we found that the particle size and distribution stayed the same throughout 150 min under the conditions we used and for surfactin concentrations below 50 μM (data not shown).

At subsolubilizing concentration and based on the results from studies of surfactant induced phospholipid vesicle fusion [94], surfactin should be able to induce vesicle growth well above CMC (75 and 100 μM). Such a process has been suggested to involve surfactant-induced vesicle opening into disks stabilized on the edges by surfactants and followed by fusion of these disks if electrostatic repulsions are reduced [95]. Such a mechanism could explain the results of our dynamic light scattering data. It should also be noted that assembly of mixed lipid-surfactin micelles into a network has been reported by Boettcher et al. [96], and this also could explain the presence of larger size aggregates.

In conclusion, the results from the dynamic light scattering measurements of the mean apparent diameter of liposomes incubated with surfactin at concentrations above CMC revealed the appearance

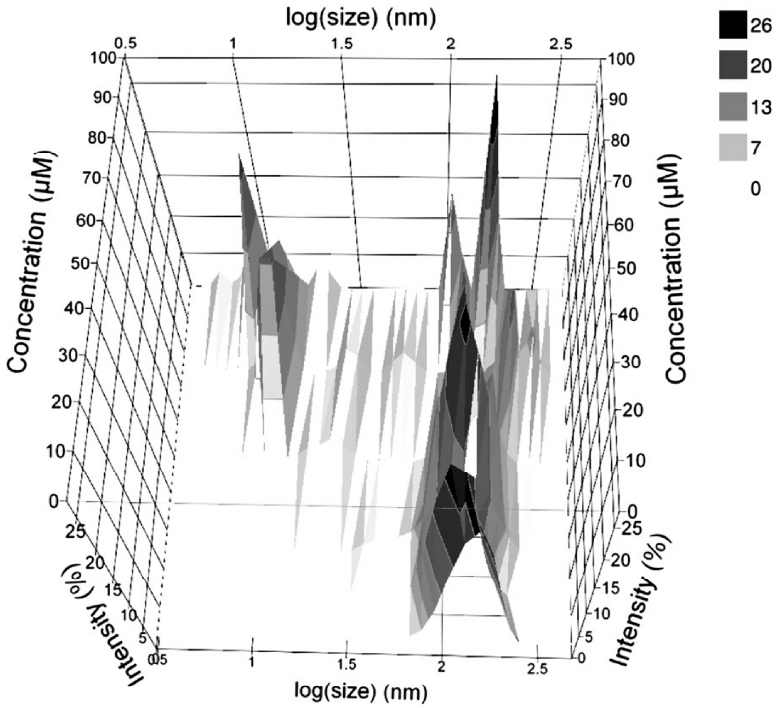

Fig. 9. Size distribution of intensity (%) upon increasing surfactin concentrations (μM) to DOPC:DPPC (1:1) vesicles in 10 mM Tris and 150 mM NaCl buffer at pH 8.5 and 25 °C. Five different levels of gray represent different limits of intensity in percent. 0% [□], 7% [▨], 13% [▩], 20% [■] and 26%[■].

of very small structures, which are probably micelles, as well as larger structures, which could be aggregated micelles, fused liposomes or disks.

4. General discussion and conclusion

The molecular mechanism of membrane permeabilization by surfactin still remained an open question. Several viewpoints have been discussed in literature and various methods have been used to investigate this process. Most of the membrane models applied in the previous studies were composed by a single lipid and hence far from real biological membranes containing domains of different lipid phases.

In the present study, DOPC:DPPC bilayers displaying coexistence of fluid and gel domains were exploited to better understand the effect of surfactin on structural changes of biological membranes. For this purpose the effect of surfactin on lipid phases and lipid fluidity in relation to membrane integrity at the nano- and macroscopic scale was analyzed. We explored both the organization and the dynamics of DOPC:DPPC vesicles in presence of surfactin taking advantages of an array of complementary methods including Laurdan and DPH fluorescence, AFM and ellipsometry, release of calcein entrapped at self-quenching concentrations within liposomes, and dequenching of octadecylrhodamine B fluorescence.

All our observations showed that the consequences of the surfactin interaction with the membrane were highly dependent on the surfactin concentration, which confirmed previous results obtained by Francius et al. [24] and Liu et al. [25] and suggesting a detergent-like process.

A model consisting of three steps of structural and morphological changes occurring during the solubilization process and depending on the surfactin concentration can be proposed (Fig. 10) on the basis of our own and previously published findings.

First, at concentration below CMC (3 μM; Fig. 10A), binding of surfactin to the boundary between gel and fluid domains is likely to occur as suggested by AFM imaging of supported lipid bilayer domains. Data obtained by molecular modeling for two surfactin:lipid molar ratios are in accordance with this hypothesis.

The surfactin insertion at this stage makes the bilayer slightly more rigid, an effect similar to that of cholesterol [36], i.e. an increase of van der Waals interactions promotes the membrane ordering of the fluid phase. The insertion of surfactin at the boundary between DPPC and DOPC could also explain the erosion process as revealed by AFM. Liposome size was not affected by this low concentration of surfactin whereas around 85% of calcein was released. The latter observation could result from the asymmetric location of surfactin in the outer leaflet of the lipid bilayer, as the flip-flop of surfactin from the outer to the inner lipid leaflet has been reported to be limited [21,26], due to the molecular shape of surfactin. This could induce some transient perturbations leading to limited calcein release without global structural changes of the bilayer. This would correspond to the first release mechanism characterized by $t^{1}_{½}$ and $y^{1}_{max.}$

As the concentration of surfactin is increased close to CMC (15 μM at 25° C; Fig. 10B), an immediate solubilization of the fluid phase occurs. Most of DOPC molecules are solubilized and removed by surfactin and will presumably form mixed micelles. DPPC rigid domains are maintained at this surfactin concentration. This may result from unfavorable interactions between detergent and order-preferring lipid in the gel domains.

By this arrangement, surfactin induces a high ordering effect with enhancement of one gel phase, as reflected by Laurdan studies at 25 °C, probably reflecting the remaining DPPC domains. Regarding the effect on membrane permeability and as explained before, the increase in surface tension between the outer and inner leaflet as well as the curvature strain [20], due to asymmetric distribution of surfactin between inner and outer leaflet and the subsequent reorganization of lipids, were probably responsible for the membrane permeability induced by the lipopeptide

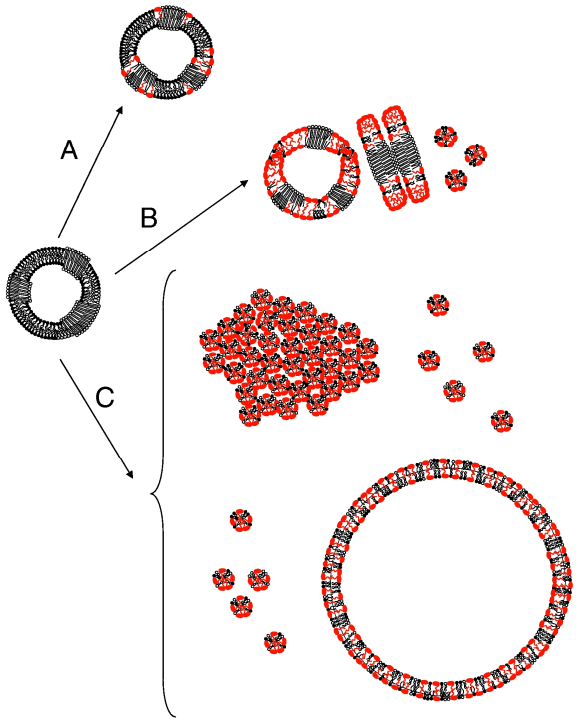

Fig. 10. Schematic model of destructuring effect of surfactin on bilayer composed by fluid and rigid domains. Surfactin concentration (A) below the CMC, (B) near the CMC, (C) well above CMC. Surfactin in red, DOPC in black and DPPC in white.

[19]. The rapid lipid fusion and the absence of effect on the liposome size could be explained by changing the lipid vesicles morphology into disks or reshaped vesicles containing surfactin and phospholipid (Fig. 10B). This could further lead to a release of calcein and might be considered as the second process contributing to calcein release and characterized by $t^2_{1/2}$ and y^2_{max}. The existence of bilayered disk-like structures is consistent with cryo-TEM observations of Kell et al. [23] and Boettcher et al. [96].

For high surfactin concentrations (≫CMC; Fig. 10C), all the results clearly demonstrated a solubilization effect of surfactin on fluid as well as on rigid bilayers. This effect is accompanied by a marked impact on liposome size and membrane permeability. A total destabilization of the lipid bilayer occurs with a direct formation of mixed DOPC-and/or DPPC-surfactin micelles. Large particles are also formed. They can be (i) mixed micelles organized in a large network assembly (Fig. 10C top picture), in accordance with cryo-TEM images shown by Boettcher et al. [96] and/or (ii) remodeled fluid supramolecular entities with diverse morphologies (spherical (Fig. 10C bottom picture) or aspherical vesicles, open vesicles, long cylindrical micelles…) such as described by Elsayed and Cevc [97]. The second hypothesis suggests that surfactin at high concentration promotes highly curved lipid layers favoring the formation of fusion intermediates such as those suggested by Zemel et al. [98] for amphipathic peptide.

The influence of the lipid bilayer state on the solubilization by detergents is physiologically significant because tightly packed liquid ordered macro- and microdomains exist in biological membranes. These domains, believed to be rich in lipids with high phase transition temperatures, tend to be tightly packed and form liquid-ordered phase. Ellipsometry results, obtained on separated DPPC and DOPC bilayers, suggest that surfactin interacts with both bilayers in a different way. The condensed nature of the DPPC bilayer will lead to much slower diffusion rate of surfactin in the plane of the bilayer interface. DOPC bilayer on the other hand should have a lower lateral pressure than DPPC and it is also like to expose more of the hydrocarbon region to the solution. Both factors make it more favorable for surfactin binding and/or for less restricted diffusion of surfactin. This can explain the lower required surfactin concentration for the onset of fluid matrix solubilization. However, the preferential eroding action of surfactin at the boundary between DOPC and DPPC shown by AFM and molecular modeling suggests that rigid domains can play an essential role in the first step of the solubilization mechanism. Our findings are in agreement with the results from Henry et al.'s study [22], which has shown that surfactin exhibits an enhanced binding to solid ordered domains-containing vesicles and with Carillo et al.'s results [28] which suggest that DPPC acts as a promoter of surfactin-induced leakage.

Besides the effect of surfactin in the lateral plane of phospholipid bilayer, change induced by surfactin in the transversal plane of phospholipids was explored by studying the interaction of this lipopeptide with the polar head group region and hydrophobic core of phospholipids bilayer. We clearly showed the ability of surfactin, at concentrations lower or close to CMC and temperatures between 20 and 40 °C, to make the membrane regions, where Laurdan and DPH were located, more rigid with a marked increase of T_m. This is a consequence of the amphiphilic properties of surfactin and in agreement with previous studies [19]. The latter has reported that surfactin both interacts at the membrane interface and core as observed for non-ionic detergents. For concentrations much higher than CMC, we demonstrated an increase of order at the interfacial region above *Tm* whereas, within the hydrophobic core, surfactin induced a slight decrease of ordering, both below and above CMC. Our results are also in accordance with previous observations made by Fourier-transform infrared spectroscopy that reported on the incorporation of surfactin into POPC membranes [28]. The authors have shown a strong dehydration of the phospholipid C═O groups, related to a decrease in hydrogen bonding of water to the C═O groups and water penetration into the polar head group region of the membrane and hence, an ordering effect as confirmed by our Laurdan results.

In conclusion, our results give insights on the effects of a lipopeptide like surfactin, on the structure and phase behavior of model membranes composed of domain forming lipids, using Laurdan fluorescence in parallel to complementary methods such as AFM and ellipsometry. They gave rise to both a better understanding of the interaction between surfactin and lipid membrane and some insight into the molecular mechanisms leading to the biological activity of surfactin. Our findings demonstrate the crucial importance of surfactin concentration in the mechanism of membrane solubilization. However, it has to be kept in mind that solubilization is a continuous process which is also dependent on the initial aggregate size, on the transition kinetics [97] as well as on the surfactant/lipid ratio [19]. More generally, our results highlight the close relationship between the physical structure of the lipid bilayer and its association with surfactin. By affecting the lipid dynamics, surfactin could also influence the function of membrane proteins which are believed to be regulated by the phase behavior of the surrounding lipid bilayer [32].

Acknowledgements

This work was supported by the National Foundation for Scientific Research (FNRS), the Université Catholique de Louvain (Fonds Spéciaux de Recherche, Action de Recherche concertée), the Federal Office for Scientific, Technical and Cultural Affairs (Interuniversity Poles of Attraction Programme) and the Région Wallonne. R.B., Y.F.D. L.L. and M.D. are Research Director and Research Associates of the FNRS, respectively. The authors thank Marité Cardenas for theoretical and technical support for ellipsometry measurements.

Appendix A. Supplementary data

Supplementary data to this article can be found online at http://dx.doi.org/10.1016/j.bbamem.2012.11.007.

References

[1] K. Arima, A. Kakinuma, G. Tamura, Surfactin, a crystalline peptidelipid surfactant produced by *Bacillus subtilis*: isolation, characterization and its inhibition of fibrin clot formation, Biochem. Biophys. Res. Commun. 31 (1968) 488–494.

[2] A. Kakinuma, G. Tamura, K. Arima, Wetting of fibrin plate and apparent promotion of fibrinolysis by surfactin, a new bacterial peptidelipid surfactant, Experientia 24 (1968) 1120–1121.

[3] J.M. Bonmatin, M. Genest, H. Labbe, M. Ptak, Solution three-dimensional structure of surfactin: a cyclic lipopeptide studied by ^{1}H-NMR, distance geometry, and molecular dynamics, Biopolymers 34 (1994) 975–986.

[4] P. Tsan, L. Volpon, F. Besson, J.M. Lancelin, Structure and dynamics of surfactin studied by NMR in micellar media, J. Am. Chem. Soc. 129 (2007) 1968–1977.

[5] M. Kracht, H. Rokos, M. Ozel, M. Kowall, G. Pauli, J. Vater, Antiviral and hemolytic activities of surfactin isoforms and their methyl ester derivatives, J. Antibiot. Tokyo 52 (1999) 613–619.

[6] D. Vollenbroich, M. Ozel, J. Vater, R.M. Kamp, G. Pauli, Mechanism of inactivation of enveloped viruses by the biosurfactant surfactin from *Bacillus subtilis*, Biologicals 25 (1997) 289–297.

[7] D. Vollenbroich, G. Pauli, M. Ozel, J. Vater, Antimycoplasma properties and application in cell culture of surfactin, a lipopeptide antibiotic from *Bacillus subtilis*, Appl. Environ. Microbiol. 63 (1997) 44–49.

[8] A.W. Bernheimer, L.S. Avigad, Nature and properties of a cytolytic agent produced by *Bacillus subtilis*, J. Gen. Microbiol. 61 (1970) 361–369.

[9] X. Huang, Z. Wei, G. Zhao, X. Gao, S. Yang, Y. Cui, Optimization of sterilization of *Escherichia coli* in milk by surfactin and fengycin using a response surface method, Curr. Microbiol. 56 (2008) 376–381.

[10] N. Tsukagoshi, G. Tamura, K. Arima, A novel protoplast-bursting factor (surfactin) obtained from *Bacillus subtilis* IAM 1213. II. The interaction of surfactin with bacterial membranes and lipids, Biochim. Biophys. Acta 196 (1970) 211–214.

[11] A.E. Zeraik, M. Nitschke, Biosurfactants as agents to reduce adhesion of pathogenic bacteria to polystyrene surfaces: effect of temperature and hydrophobicity, Curr. Microbiol. 61 (2010) 554–559.

[12] L.K. Assie, M. Deleu, L. Arnaud, M. Paquot, P. Thonart, C. Gaspar, E. Haubruge, Insecticide activity of surfactins and iturins from a biopesticide *Bacillus subtilis* Cohn (S499 strain), Meded. Rijksuniv. Gent Fak. Landbouwkd. Toegep. Biol. Wet. 67 (2002) 647–655.

[13] Y. Imai, T. Sugino, A. Fujita, A. Kakinuma, Hypocholesterolimic effect of surfactin, a novel bacterial peptide lipid, J. Takeda Res. Lab. 30 (1971) 728–734.

[14] D.H. Kim, K.W. Yu, E.A. Bae, H.J. Park, J.W. Choi, Metabolism of kalopanaxsaponin B and H by human intestinal bacteria and antidiabetic activity of their metabolites, Biol. Pharm. Bull. 21 (1998) 360–365.

[15] M. Ongena, G. Henry, A. Adam, E. Jourdan, P. Thonart, Insights into the plant defense mechanisms induced by *Bacillus* lipopeptides, Biol. Plant–Microb. Interactions 7 (2010) 1–5.

[16] S. Dufour, M. Deleu, K. Nott, B. Wathelet, P. Thonart, M. Paquot, Hemolytic activity of new linear surfactin analogs in relation to their physico-chemical properties, Biochim. Biophys. Acta 1726 (2005) 87–95.

[17] X.H. Cao, S.S. Zhao, D.Y. Liu, Z. Wang, L.L. Niu, L.H. Hou, C.L. Wang, ROS-Ca^{2+} is associated with mitochondria permeability transition pore involved in surfactin-induced MCF-7 cells apoptosis, Chem. Biol. Interact. 190 (2011) 16–27.

[18] M. Deleu, H. Bouffioux, H. Razafindralambo, M. Paquot, C. Hbid, Ph. Thonart, Ph. Jacques, R. Brasseur, Interaction of surfactin with membranes: a computational approach, Langmuir 19 (2003) 3377–3385.

[19] H. Heerklotz, J. Seelig, Detergent-like action of the antibiotic peptide surfactin on lipid membranes, Biophys. J. 81 (2001) 1547–1554.

[20] H. Heerklotz, J. Seelig, Leakage and lysis of lipid membranes induced by the lipopeptide surfactin, Eur. Biophys. J. 36 (2007) 305–314.

[21] H. Heerklotz, A. Tsamaloukas, K. Kita-Tokarczyk, P. Strunz, T. Gutberlet, Structural, volumetric, and thermodynamic characterization of a micellar sphere-to-rod transition, J. Am. Chem. Soc. 126 (2004) 16544–16552.

[22] G. Henry, M. Deleu, E. Jourdan, P. Thonart, M. Ongena, The bacterial lipopeptide surfactin targets the lipid fraction of the plant plasma membrane to trigger immune-related defence responses, Cell. Microbiol. 13 (2011) 1824–1837.

[23] H. Kell, J.F. Holzwarth, C. Boettcher, R.K. Heenan, J. Vater, Physicochemical studies of the interaction of the lipoheptapeptide surfactin with lipid bilayers of L-alpha-dimyristoyl phosphatidylcholine, Biophys. Chem. 128 (2007) 114–124.

[24] G. Francius, S. Dufour, M. Deleu, M. Paquot, M.P. Mingeot-Leclercq, Y.F. Dufrene, Nanoscale membrane activity of surfactins: influence of geometry, charge and hydrophobicity, Biochim. Biophys. Acta 1778 (2008) 2058–2068.

[25] J. Liu, A. Zou, B. Mu, Toluidine blue: aggregation properties and distribution behavior in surfactin micelle solution, Colloids Surf. B Biointerfaces 75 (2010) 496–500.

[26] H.H. Shen, R.K. Thomas, J. Penfold, G. Fragneto, Destruction and solubilization of supported phospholipid bilayers on silica by the biosurfactant surfactin, Langmuir 26 (2010) 7334–7342.

[27] O. Bouffioux, A. Berquand, M. Eeman, M. Paquot, Y.F. Dufrene, R. Brasseur, M. Deleu, Molecular organization of surfactin-phospholipid monolayers: effect of phospholipid chain length and polar head, Biochim. Biophys. Acta 1768 (2007) 1758–1768.

[28] C. Carrillo, J.A. Teruel, F.J. Aranda, A. Ortiz, Molecular mechanism of membrane permeabilization by the peptide antibiotic surfactin, Biochim. Biophys. Acta 1611 (2003) 91–97.

[29] M. Eeman, A. Berquand, Y.F. Dufrene, M. Paquot, S. Dufour, M. Deleu, Penetration of surfactin into phospholipid monolayers: nanoscale interfacial organization, Langmuir 22 (2006) 11337–11345.

[30] A. Grau, J.C. Gomez Fernandez, F. Peypoux, A. Ortiz, A study on the interactions of surfactin with phospholipid vesicles, Biochim. Biophys. Acta 1418 (1999) 307–319.

[31] R. Maget-Dana, M. Ptak, Interactions of surfactin with membrane models, Biophys. J. 68 (1995) 1937–1943.

[32] K. Simons, W.L. Vaz, Model systems, lipid rafts, and cell membranes, Annu. Rev. Biophys. Biomol. Struct. 33 (2004) 269–295.

[33] L.A. Bagatolli, J.H. Ipsen, A.C. Simonsen, O.G. Mouritsen, An outlook on organization of lipids in membranes: searching for a realistic connection with the organization of biological membranes, Prog. Lipid Res. 49 (2010) 378–389.

[34] J. Juhasz, J.H. Davis, F.J. Sharom, Fluorescent probe partitioning in giant unilamellar vesicles of 'lipid raft' mixtures, Biochem. J. 430 (2010) 415–423.

[35] M.L. Schmidt, L. Ziani, M. Boudreau, J.H. Davis, Phase equilibria in DOPC/DPPC: conversion from gel to subgel in two component mixtures, J. Chem. Phys. 131 (Nov 2009) 175103.

[36] S. Buchoux, J. Lai-Kee-Him, M. Garnier, P. Tsan, F. Besson, A. Brisson, E.J. Dufourc, Surfactin-triggered small vesicle formation of negatively charged membranes: a novel membrane-lysis mechanism, Biophys. J. 95 (2008) 3840–3849.

[37] F. Van Bambeke, M.P. Mingeot-Leclercq, A. Schanck, R. Brasseur, P.M. Tulkens, Alterations in membrane permeability induced by aminoglycoside antibiotics: studies on liposomes and cultured cells, Eur. J. Pharmacol. 247 (1993) 155–168.

[38] H. Razafindralambo, M. Paquot, C. Hbid, P. Jacques, J. Destain, P. Thonart, Purification of antifungal lipopeptides by reversed-phase high-performance liquid chromatography, J. Chromatogr. 639 (1993) 81–85.

[39] J.P. Montenez, F. Van Bambeke, J. Piret, R. Brasseur, P.M. Tulkens, M.P. Mingeot-Leclercq, Interactions of macrolide antibiotics (Erythromycin A, roxithromycin, erythromycylamine [Dirithromycin], and azithromycin) with phospholipids: computer-aided conformational analysis and studies on acellular and cell culture models, Toxicol. Appl. Pharmacol. 156 (1999) 129–140.

[40] G.R. Bartlett, Colorimetric assay methods for free and phosphorylated glyceric acids, J. Biol. Chem. 234 (1959) 469–471.

[41] M.P. Mingeot-Leclercq, M. Deleu, R. Brasseur, Y.F. Dufrêne, Atomic force microscopy of supported lipid bilayers, Nat. Protoc. 3 (2008) 1654–1659.

[42] H.P. Vacklin, F. Tiberg, R.K. Thomas, Formation of supported phospholipid bilayers via co-adsorption with beta-D-dodecyl maltoside, Biochim. Biophys. Acta 1668 (2005) 17–24.

[43] F. Tiberg, M. Landgren, Characterization of thin nonionic surfactant films at the silica/water interface by means of ellipsometry, Langmuir 9 (1993) 927–932.

[44] M. Landgren, B. Jönsson, Determination of the optical properties of Si/SiO* surfaces by means of ellipsometry, using different ambient media, J. Phys. Chem. 97 (1993) 1656–1660.

[45] F.L. McCrackin, E. Passaglia, R.R. Stromberg, H.L. Steinberg, Measurement of the thickness and refractive index of very thin films and the optical properties of surfaces by ellipsometry, J. Res. Natl. Bur. Stand. Sect. A 67A (1963) 363–377.

[46] H.P. Vacklin, F. Tiberg, G. Fragneto, R.K. Thomas, Phospholipase A2 hydrolysis of supported phospholipid bilayers: a neutron reflectivity and ellipsometry study, Biochemistry 44 (2005) 2811–2821.

[47] P.A. Cuypers, J.W. Corsel, M.P. Janssen, J.M. Kop, W.T. Hermens, H.C. Hemker, The adsorption of prothrombin to phosphatidylserine multilayers quantitated by ellipsometry, J. Biol. Chem. 258 (1983) 2426–2431.

[48] T. Parasassi, G. De Stasio, G. Ravagnan, R.M. Rusch, E. Gratton, Quantitation of lipid phases in phospholipid vesicles by the generalized polarization of Laurdan fluorescence, Biophys. J. 60 (1991) 179–189.

[49] T. Parasassi, E. Gratton, Membrane lipid domains and dynamics as detected by Laurdan fluorescence, J. Fluoresc. 5 (1995) 59–69.

[50] L.A. Bagatolli, E. Gratton, Direct observation of lipid domains in free-standing bilayers using two-photon excitation fluorescence microscopy, J. Fluoresc. 11 (2001) 141–161.

[51] W. Yu, P.T. So, T. French, E. Gratton, Fluorescence generalized polarization of cell membranes: a two-photon scanning microscopy approach, Biophys. J. 70 (1996) 626–636.

[52] J. Giraldo, N.M. Vivas, E. Vila, A. Badia, Assessing the (a)symmetry of concentration–effect curves: empirical versus mechanistic models, Pharmacol. Ther. 95 (2002) 21–45.

[53] R. Brasseur, J.A. Killian, B. De Kruijff, J.M. Ruysschaert, Conformational analysis of gramicidin–gramicidin interactions at the air/water interface suggests that gramicidin aggregates into tube-like structures similar as found in the gramicidin-induced hexagonal HII phase, Biochim. Biophys. Acta 903 (1987) 11–17.

[54] L. Lins, A. Thomas-Soumarmon, T. Pillot, J. Vandekerchkhove, M. Rosseneu, R. Brasseur, Molecular determinants of the interaction between the C-terminal domain of Alzheimer's beta-amyloid peptide and apolipoprotein E alpha-helices, J. Neurochem. 73 (1999) 758–769.

[55] R. Brasseur, TAMMO: theoretical analysis of membrane molecular organisation. in: Molecular Description of Biological Membrane Components by Computer-aided Conformational Analysis, Brasser Edt, I and II, CRC Press, Boca Raton, Fla, 1990, pp. 203–219.

[56] R.D. Kaiser, E. London, Location of diphenylhexatriene (DPH) and its derivatives within membranes: comparison of different fluorescence quenching analyses of membrane depth, Biochemistry 37 (1998) 8180–8190.

[57] B.R. Lentz, Use of fluorescent probes to monitor molecular order and motions within liposome bilayers, Chem. Phys. Lipids 64 (1993) 99–116.

[58] M. Shinitzky, Y. Barenholz, Fluidity parameters of lipid regions determined by fluorescence polarization, Biochim. Biophys. Acta 515 (1978) 367–394.

[59] J.N. Weinstein, S. Yoshikami, P. Henkart, R. Blumenthal, W.A. Hagins, Liposome–cell interaction: transfer and intracellular release of a trapped fluorescent marker, Science 195 (1977) 489–492.
[60] P.I. Lelkes, Methodogical aspects dealing with stability measurements of liposomes in vitro using the carboxyfluorescein assay, in: Liposome Technology, Gregoriadis Edts, 3, CRC Press, 1984, pp. 225–246.
[61] D. Hoekstra, T. de Boer, K. Klappe, J. Wilschut, Fluorescence method for measuring the kinetics of fusion between biological membranes, Biochemistry 23 (1984) 5675–5681.
[62] M.L. Jackson, B.J. Litman, Rhodopsin–phospholipid reconstitution by dialysis removal of octyl glucoside, Biochemistry 21 (1982) 5601–5608.
[63] M.L. Jackson, C.F. Schmidt, D. Lichtenberg, B.J. Litman, A.D. Albert, Solubilization of phosphatidylcholine bilayers by octyl glucoside, Biochemistry 21 (1982) 4576–4582.
[64] S. Keller, A. Tsamaloukas, H. Heerklotz, A quantitative model describing the selective solubilization of membrane domains, J. Am. Chem. Soc. 127 (2005) 11469–11476.
[65] S. Morandat, K. El Kirat, Membrane resistance to Triton X-100 explored by real-time atomic force microscopy, Langmuir 22 (2006) 5786–5791.
[66] E. Schnitzer, D. Lichtenberg, M.M. Kozlov, Temperature-dependence of the solubilization of dipalmitoylphosphatidylcholine (DPPC) by the non-ionic surfactant Triton X-100, kinetic and structural aspects, Chem. Phys. Lipids 126 (2003) 55–76.
[67] N. Hauet, F. Artzner, F. Boucher, C. Grabielle-Madelmont, I. Cloutier, G. Keller, P. Lesieur, D. Durand, M. Paternostre, Interaction between artificial membranes and enflurane, a general volatile anesthetic: DPPC–enflurane interaction, Biophys. J. 84 (2003) 3123–3137.
[68] M. Deleu, M. Paquot, T. Nylander, Effect of fengycin, a lipopeptide produced by *Bacillus subtilis*, on model biomembranes, Biophys. J. 94 (2008) 2667–2679.
[69] T. Parasassi, G. Ravagnan, R.M. Rusch, E. Gratton, Modulation and dynamics of phase properties in phospholipid mixtures detected by Laurdan fluorescence, Photochem. Photobiol. 57 (1993) 403–410.
[70] G. Balogh, G. Maulucci, I. Gombos, I. Horvath, Z. Torok, M. Peter, E. Fodor, T. Pali, S. Benko, T. Parasassi, M. De Spirito, J.L. Harwood, L. Vigh, Heat stress causes spatially-distinct membrane re-modelling in K562 leukemia cells, PLoS One 6 (2011) e21182.
[71] K. Gaus, E. Gratton, E.P. Kable, A.S. Jones, I. Gelissen, L. Kritharides, W. Jessup, Visualizing lipid structure and raft domains in living cells with two-photon microscopy, Proc. Natl. Acad. Sci. U. S. A. 100 (2003) 15554–15559.
[72] L.A. Bagatolli, S.A. Sanchez, T. Hazlett, E. Gratton, Giant vesicles, Laurdan, and two-photon fluorescence microscopy: evidence of lipid lateral separation in bilayers, Methods Enzymol. 360 (2003) 481–500.
[73] C. Dietrich, L.A. Bagatolli, Z.N. Volovyk, N.L. Thompson, M. Levi, K. Jacobson, E. Gratton, Lipid rafts reconstituted in model membranes, Biophys. J. 80 (2001) 1417–1428.
[74] K.K. Halling, B. Ramstedt, J.H. Nystrom, J.P. Slotte, T.K. Nyholm, Cholesterol interactions with fluid-phase phospholipids: effect on the lateral organization of the bilayer, Biophys. J. 95 (2008) 3861–3871.
[75] M. Engelk, P. Bojarski, R. Bloss, H. Diehl, Tamoxifen perturbs lipid bilayer order and permeability: comparison of DSC, fluorescence anisotropy, Laurdan generalized polarization and carboxyfluorescein leakage studies, Biophys. Chem. 90 (2001) 157–173.
[76] S.V. Balasubramanian, R.B. Campbell, R.M. Straubinger, Propofol, a general anesthetic, promotes the formation of fluid phase domains in model membranes, Chem. Phys. Lipids 114 (2002) 35–44.
[77] M.R. Gonzalez-Baro, H. Garda, R. Pollero, Effect of fenitrothion on dipalmitoyl and 1-palmitoyl-2-oleoylphosphatidylcholine bilayers, Biochim. Biophys. Acta 1468 (2000) 304–310.
[78] A.B. Hendrich, K. Michalak, O. Wesolowska, Phase separation is induced by phenothiazine derivatives in phospholipid/sphingomyelin/cholesterol mixtures containing low levels of cholesterol and sphingomyelin, Biophys. Chem. 130 (2007) 32–40.
[79] A. Berquand, M.P. Mingeot-Leclercq, Y.F. Dufrene, Real-time imaging of drug–membrane interactions by atomic force microscopy, Biochim. Biophys. Acta 1664 (2004) 198–205.
[80] M.C. Giocondi, L. Pacheco, P.E. Milhiet, C. Le Grimellec, Temperature dependence of the topology of supported dimirystoyl–distearoyl phosphatidylcholine bilayers, Ultramicroscopy 86 (2001) 151–157.
[81] Y.F. Dufrene, A. van der Wal, W. Norde, P.G. Rouxhet, X-ray photoelectron spectroscopy analysis of whole cells and isolated cell walls of Gram-positive bacteria: comparison with biochemical analysis, J. Bacteriol. 179 (1997) 1023–1028.
[82] S. Morandat, K. El Kirat, Solubilization of supported lipid membranes by octyl glucoside observed by time-lapse atomic force microscopy, Colloids Surf. B Biointerfaces 55 (2007) 179–184.
[83] S. Mukherjee, A. Chattopadhyay, Monitoring the organization and dynamics of bovine hippocampal membranes utilizing Laurdan generalized polarization, Biochim. Biophys. Acta 1714 (2005) 43–55.
[84] J. Juhasz, J.H. Davis, F.J. Sharom, Fluorescent probe partitioning in GUVs of binary phospholipid mixtures: implications for interpreting phase behavior, Biochim. Biophys. Acta 1818 (2012) 19–26.
[85] H. Heerklotz, Triton promotes domain formation in lipid raft mixtures, Biophys. J. 83 (2002) 2693–2701.
[86] F.M. Goni, M.A. Urbaneja, J.L. Arrondo, A. Alonso, A.A. Durrani, D. Chapman, The interaction of phosphatidylcholine bilayers with Triton X-100, Eur. J. Biochem. 160 (1986) 659–665.
[87] G.M. Alder, W.M. Arnold, C.L. Bashford, A.F. Drake, C.A. Pasternak, U. Zimmermann, Divalent cation-sensitive pores formed by natural and synthetic melittin and by Triton X-100, Biochim. Biophys. Acta 1061 (1991) 111–120.
[88] H. Patel, C. Tscheka, K. Edwards, G. Karlsson, H. Heerklotz, All-or-none membrane permeabilization by fengycin-type lipopeptides from *Bacillus subtilis* QST713, Biochim. Biophys. Acta 1808 (2011) 2000–2008.
[89] B. Apellaniz, S. Nir, J.L. Nieva, Distinct mechanisms of lipid bilayer perturbation induced by peptides derived from the membrane-proximal external region of HIV-1 gp41, Biochemistry 48 (2009) 5320–5331.
[90] T. Buranda, Y. Wu, D. Perez, A. Chigaev, L.A. Sklar, Real-time partitioning of octadecyl rhodamine B into bead-supported lipid bilayer membranes revealing quantitative differences in saturable binding sites in DOPC and 1:1:1 DOPC/SM/cholesterol membranes, J. Phys. Chem. B 114 (2010) 1336–1349.
[91] F. Van Bambeke, P.M. Tulkens, R. Brasseur, M.P. Mingeot-Leclercq, Aminoglycoside antibiotics induce aggregation but not fusion of negatively-charged liposomes, Eur. J. Pharmacol. 289 (1995) 321–333.
[92] A. De la Maza, J.L. Parra, Vesicle–micelle structural transition of phosphatidylcholine bilayers and Triton X-100, Biochem. J. 303 (1994) 907–914.
[93] U. Kragh-Hansen, M. le Maire, J.V. Moller, The mechanism of detergent solubilization of liposomes and protein-containing membranes, Biophys. J. 75 (1998) 2932–2946.
[94] M. Silvander, K. Edwards, A method to detect leakage of DNA intercalators through liposome membranes, Anal. Biochem. 242 (1996) 40–44.
[95] K. Edwards, J. Gustafsson, M. Almgren, G. Karlsson, Solubilization of lecithin vesicles by a cationic surfactant — intermediate structures in the vesicle micelle transition observed by cryo-transmission electron microscopy, J. Colloid Interface Sci. 161 (1993) 299–309.
[96] C. Boettcher, H. Kell, J.F. Holzwarth, J. Vater, Flexible loops of thread-like micelles are formed upon interaction of L-alpha-dimyristoyl-phosphatidylcholine with the biosurfactant surfactin as revealed by cryo-electron tomography, Biophys. Chem. 149 (2010) 22–27.
[97] M.M. Elsayed, G. Cevc, The vesicle-to-micelle transformation of phospholipid-cholate mixed aggregates: a state of the art analysis including membrane curvature effects, Biochim. Biophys. Acta 1808 (2011) 140–153.
[98] A. Zemel, A. Ben Shaul, S. May, Modulation of the spontaneous curvature and bending rigidity of lipid membranes by interfacially adsorbed amphipathic peptides, J. Phys. Chem. B 112 (2008) 6988–6996.

4. Conclusions and Discussion

In this part, we will summarize data we obtained and suggest a general conclusion about the mechanisms by which α-hederin and its aglycon hederagenin as well as surfactin, three amphiphilic compounds, interact with membranes. We will further discuss (i) the influences of the membrane model on their activity, (ii) the parameters which influence activity on cells and (iii) the role of the amphiphile's molecular structure on their activity.

4.1. Membrane interactions of α-hederin, hederagenin and surfactin

α-Hederin, hederagenin and surfactin have shown several interesting activities on membranes. In this part, we will integrate all data we obtained with the goal to establish a general conclusion about the interaction mechanisms with membranes of the analyzed compounds.

4.1.1. Mechanism involved in the interaction of α-hederin with membranes

Several mechanisms by which monodesmosidic triterpenoid saponins interact and permeabilize membranes have been proposed (2.4.5.). Based on these permeabilization models and the new data we obtained (see 3.1.1., 3.1.2. and 3.1.3.), we are able to propose a new general mechanism of membrane interation for α-hederin and similar monodesmosidic triterpenoid saponins (Figure 33). We can divide the interactions into four main activities/parts: (A) insertion into the membrane and interaction with domains enriched in cholesterol, (B) formation of buds out of the membrane, (C) lateral phase separation and formation of a new mesophase, (D) pore formation. The activity depended largely on the saponin concentration. A change of activity towards GUVs was seen around the CMC of α-hederin.

At concentrations below its CMC, monomers should first interact with the membrane components and bind to cholesterol enriched nanodomains (Figure 33,A). This will have consequences on phospholipid mobility (see 3.1.1., GP_{ex} of Laurdan) and create an area difference and curvature strain between the outer and inner monolayers which leads to budding (Figure 33,B). At longer incubation periods, a cooperative aggregation of α-hederin,

phospholipids and cholesterol leads to phase separation (Figure 33,C). The induction of positive curvature by α-hederin in the newly formed domains leads to a continuing transformation of these domains into a tubular phase which could induce transient defects in the membrane. Those could be responsible for the slow dextran release observed (see 3.1.2. and 2.3.3.3.). Hence, it is not excluded that the permeation to dextran is due to transient pores which allow gradually small quantities of dextran to influx (see 2.3.3.1.) or toroidal pores (see 2.3.3.2.) whose size increases with time and which are too small in the beginning to let the dextran molecules pass through (see discussion 3.1.1.).

At concentrations above the CMC, α-hederin aggregates should deliver increased concentrations of molecules close to the nanodomains and allow rapid interaction with cholesterol and phospholipids to induce pore formation (Figure 33,D). Pore formation is also based on the curvature induction by the saponin (3.1.1.). Nevertheless, the CMC of α-hederin has to be reconfirmed by another assay (see 5.1.1.1.), but obtained data and the results of Bottger and coll. support these conclusions (Bottger et al., 2012). CMC dependent activity has recently been suggested for glycyrrhizin, another monodesmosidic saponin (Sakamoto et al., 2013).

The membrane interactions proposed should be valid for cellular activity as well. It was shown that fast plasma membrane lysis was mainly obtained at concentrations > 20µM (~slightly higher than its CMC). The importance of membrane cholesterol for α-hederin induced membrane lysis was also proven (3.1.4.). Consequences of membrane interactions for cells will be discussed later (4.3.).

FIGURE 33

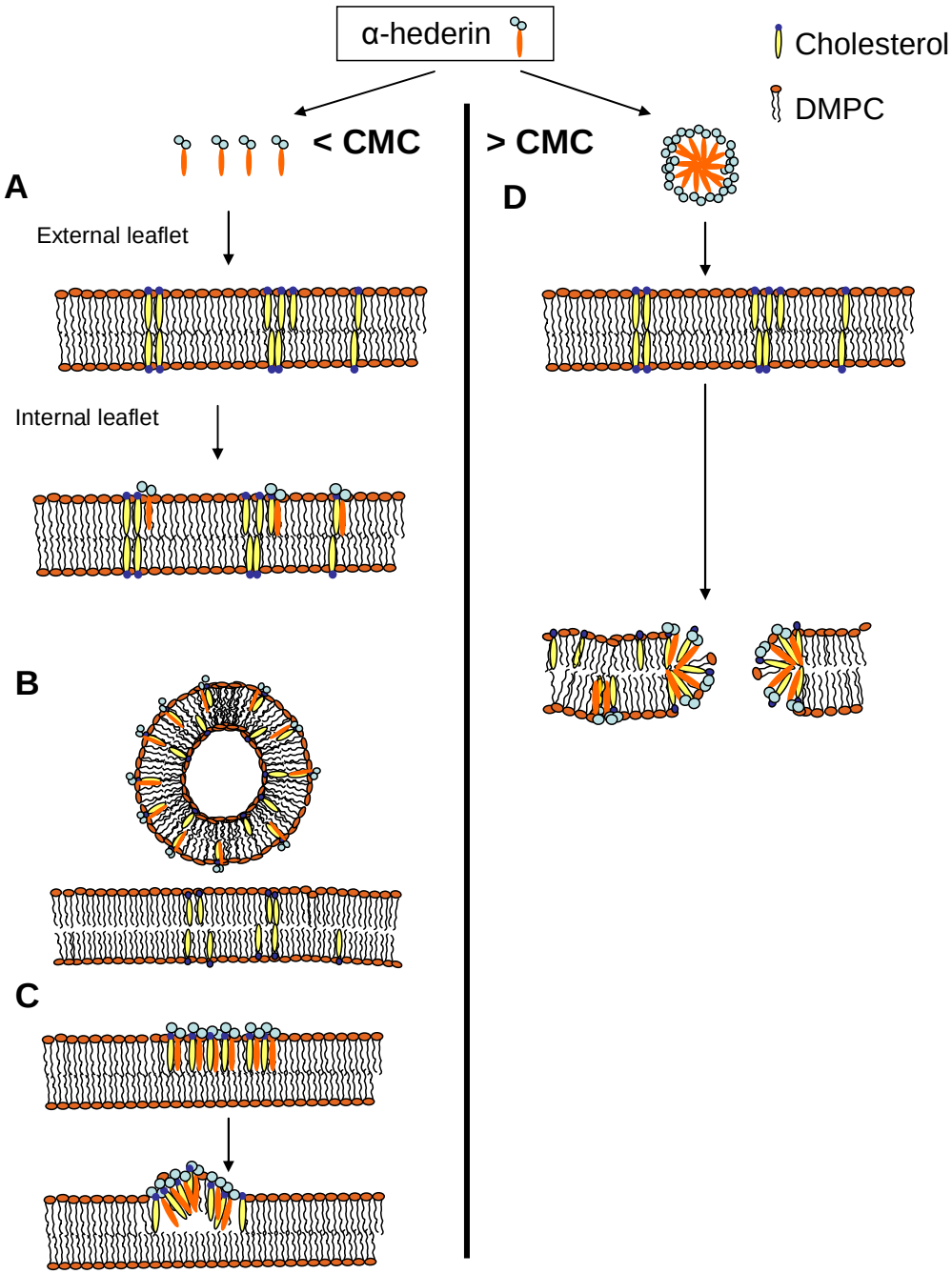

Proposed interaction mechanism between α-hederin and lipid membranes containing cholesterol.

At concentrations below the CMC, α-hederin monomers insert into the membrane, interact with cholesterol nanodomains (A) and induce budding (B), lateral phase separation and transformation into a new mesophase (C). At concentrations beyond the CMC, α-hederin aggregates interact with cholesterol rich domains to induce mainly pore formation (D)

In a membrane model presenting lateral phase separation but no cholesterol, the molecule was able to inhibit lateral phase separation at small concentrations (3.1.3.). The molecule could therefore present linactant activity in the absence of cholesterol. Linactants can be regarded as two-dimensional surface active agents, which insert at the phase boundary, reduce line tension between different phases and thereby inhibit lateral phase separation (Trabelsi et al., 2008). These molecules are thought to be an important factor in cellular membranes and would help to inhibit macroscopic phase separation (Sriram et al., 2012). Because mammal plasma membranes contain all cholesterol, this effect should not be observed in mammal cells, but the effect could play a role for interaction with membranes lacking cholesterol like bacterias.

4.1.2. Interaction mechanisms of hederagenin with membranes

Our results show that hederagenin was not able to induce budding. At high concentrations (40 µM) and very long incubation periods (48h), we observed formation of small circular domains in GUV. These domains (see 3.1.2.) could correspond to the small isotropic peak observed in ^{31}P-NMR of MLV (see 3.1.1.). Regarding the small hydrophilic head of the triterpenic structure, these domains should correspond to inverse structures. But it is not excluded that hederagenin forms also normal structures with phospholipids. Compared to α-hederin, the absence of a sugar chain at C3 and sugar-sugar interactions could decrease the rate of domain for hederagenin.

In parallel to the formation of domains we observed also permeabilization of GUVs. The rearrangement of the membrane into a new mesophase has probably consequences for membrane permeability. The formation of transient defects near the phase boundaries could be responsible for permeabilization (Figure 34 and see 2.3.3.3.). This would correspond to a new permeabilization mechanism for triterpenic acids, which would be less dependent on the induction of positive curvature strain.

It is further difficult to say whether the activity of hederagenin depends on self-aggregation. It is not clear if the inflexion point obtained with the DHE assay (see 3.1.2., discussion) corresponds really to its CMC (because there is no CMC value in the litterature to

compare). Nevertheless, asiatic and madecassic acid, two triterpenic acids, showed no activity towards cancer cells below their CMC (Rafat et al., 2008).

FIGURE 34

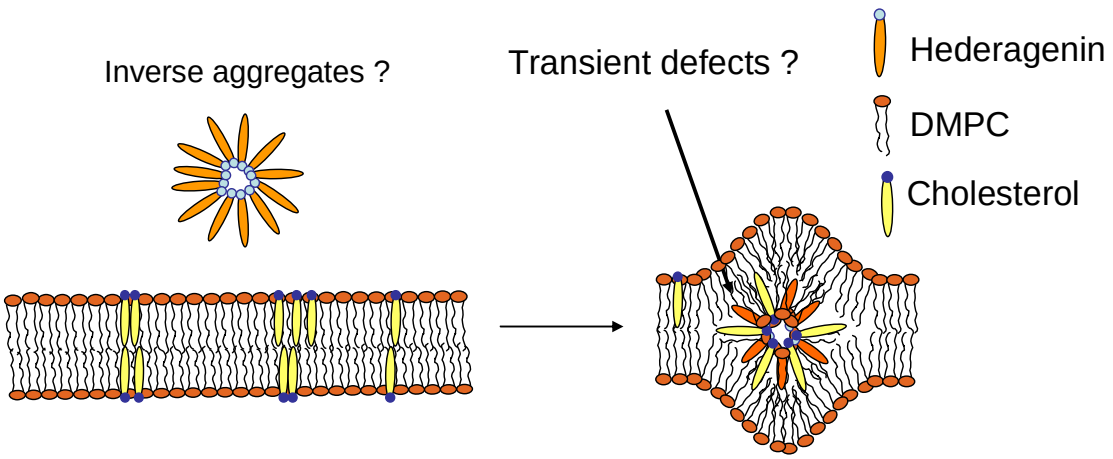

Hypothetical interaction mechanism of hederagenin with membranes

4.1.3. Surfactin-membrane interactions

Concerning surfactin, we showed that the molecule is able to inhibit lateral phase separation, change lipid dynamics and induce permeabilization by two main mechanisms (see 3.2.). Membrane interaction was clearly CMC dependent. AFM and ellipsometry (see 3.2., Figures 2,4) supported this conclusion.

Below its CMC, the linactant activity of the molecule was the most important and we monitored a reduction of phospholipid mobility. We also observed a gradual calcein release corresponding to transient defects and no lipid demixing or membrane reaarrangements.

Beyond its CMC, the molecule induced an increase of phospholipid mobility, lipid demixing and the formation of mixed micellar aggregates preferentially with the lipid in the liquid crystalline state (DOPC). Permeabilization was instantaneous. This is in agreement with conclusions from Heerklotz and Seelig, who showed that the amphiphile/lipid ratio to obtain solubilization depended on $K_p.CMC$ (K_p is the partition constant of surfactin between liposomes and the solution (Heerklotz and Seelig, 2001).

Permeabilization is hence not dependent on the rearrangement of the membrane at higher concentrations and surfactin can exert the permeabilizing effect at subsolubilizing concentrations.

4.2. Influences of the membrane-model on the activity of amphiphiles

The results we obtained show that observed effects depend on lipid composition of the membrane model and the membrane model itself. We will discuss in this part why the amphiphiles behave differently towards different models.

4.2.1. Influence of the lipid composition

Interaction of amphiphiles with membranes is highly dependent on the lipid composition of the membrane model. In a bilayer composed of DOPC:DPPC, α-hederin and surfactin are able to inhibit macroscopic phase separation (see 3.1.3. and 3.2.). The inhibition of phase separation in a model composed of two immiscible lipids has also been shown for glycyrrhizin, a monodesmosidic saponin, at concentrations below its CMC (Sakamoto et al., 2013). This activity can most probably be attributed to their linactant activity (see 4.1.).

Conversely, in membrane models containing cholesterol (DMPC:Chol [3:1]), α-hederin induces macroscopic phase separation and permeabilization. This effect could be attributed to its preferential binding to cholesterol and was largely discussed in 3.1.1. and 3.1.2.

The proportion of zwitterionic and negatively charged phospholipids, modifying the resulting membrane potential can also influence the membrane activity of the amphiphile. Surfactin is known to interact differently with anionic phospholipids, which could increase its specificity towards bacteria, characterized by high proportions of anionic phospholipids. In these membranes, the induction of electrostatic repulsions between lipids and amphiphiles increased the lytic activity (Buchoux et al., 2008).

4.2.2. Influence of membrane models

Comparing the activity on different membrane models, we observed that the same amphiphile concentration had sometimes different effects on different models.

First of all, the presence of dimethylsulfoxide (DMSO) as a cosolvent in the solution, might increase the permeability of membrane models. It has been shown that the molecule induces transient water pores in cells and model membranes (He et al., 2012;Gurtovenko and Anwar, 2007). However, in our experimental conditions, this is unlikely because DMSO at 0.1-1% v/v had no permeabilizing effect on the membrane models we investigated, so this activity could be excluded.

In GUVs the activity of saponins seems to depend on the CMC whereby activity on LUVs is mainly influenced by the effective saponin/lipid ratio. This should be due to the fact, that concentration of total lipids in the GUV model is very small. The activity is therefore influenced by the concentration of the molecule and its ability to self aggregate (its CMC).

In LUVs and MLVs, the total lipid amount is much higher than in the GUV model. The activity depends in these models not only on the ability of the amphiphile to form micelles (CMC) but also on the effective amphiphile/lipid ratio. When the total amount of amphiphiles is much smaller than lipids (even if concentration is above its CMC), the effect will be minimal. The amphiphiles present in the solution will most probably partition into the liposomes and concentration in the solution will decrease rapidly below its CMC (Lichtenberg et al., 2000).

The effect on *in silico* monolayers did not always correlate with AFM or the results on GUVs. We have to keep in mind that the “Big monolayer” method can only predict preferential association of a molecule in a two-dimensional manner. It does not consider curvature effects, line tension and long range lateral dipole moments, which are known to play an important role in domain formation (Seul and Andelman, 1995). The model is also limited to bimolecular interactions and is not able to simulate the formation of ternary complexes, which has been proposed for α-hederin, cholesterol and DMPC. Nevertheless, the model gave interesting clues on how saponins and surfactin could insert into membranes and influence phase separation.

4.3. Membrane activities of α-hederin and hederagenin on biological cells

The lytic mechanisms we proposed for artificial membranes (see 4.1.1. and 4.1.2.) should be extended for membranes of erythrocytes and cancer cells. However, it is not excluded that interactions with the cytoskeleton or membrane proteins might amplify or attenuate the pore forming activity or the effect on phase separation. Moreover, the artificial membrane models used were only composed of a few lipids, hence the presence of thousand of different lipid species in biological membranes might further complicate membrane interactions.

α-Hederin has been shown to be very active on monocytic leukemia cells (see 3.1.4.). Cell death was not only induced by membrane lysis, but also by apoptosis. Its triterpenic aglycone, hederagenin also showed apoptogenic activity, but no rapid membrane lysis suggesting different mechanisms for apoptosis and cell death due to membrane lysis. An extensive discussion on how both molecules should be able to induce apoptosis has been done in (3.1.4.).

Regarding the relevance of our work, we have to push forward several questions which might influence the activity on cells like (i) the importance of the concentration (ii) the time-dependency, (iii) the role of the cell medium, (iv) the cell-type dependence, (v) the stability of the compound.

It may be possible that activity of α-hederin on cancer cells is also CMC dependent (see 4.1.1.). This could be similar for hederagenin (see 4.1.2.), since other triterpenic acids have shown to be active only at concentrations beyond their CMC (Rafat et al., 2008). α-Hederin might be able to induce lateral phase separation mainly at concentrations below its CMC and induce the extrinsic apoptotic pathway (see 3.1.4.). At concentrations largely above its CMC, α-hederin should induce mainly membrane lysis.

The time to induce cytotoxicity was lower with α-hederin than with hederagenin. It might be possible that the rate to develop transient defects in the plasma membrane is decreased in the absence of sugar units. This would explain the delay of cytotoxicity observed with hederagenin and would correspond to the interaction model we developed in 4.1.1. and 4.1.2. for both molecules. However, at this stage we cannot exclude an effect on phase separation (and a possible activation of death receptors) which was also influenced by the sugar units.

The concentration to induce membrane lysis in cells was higher than in GUVs. The reason might be that α-hederin activity is influenced by both the media and the foetal calf serum (FCS)

in the incubation solution, as it has been suggested by Danloy et al. (Danloy et al., 1994). α - Hederin would be able to bind to BSA, present in the FCS. The serum contains also a non-neglectable concentration of cholesterol, which could interact directly with the saponin and the triterpenic acid to form insoluble aggregates (see 3.1.1. and 3.1.2.).

Regarding the influence of the cell type, it has been shown on several cells that the cytotoxicity of α-hederin towards cancer cells is higher compared to normal cells (Swamy and Huat, 2003). The suggested explanation was that α-hederin could act specifically on some cancer cells probably because they have increased cholesterol contents in their plasma membrane compared to normal cells (discussion in 3.1.1. and 3.1.4.). At this point, it is impossible to conclude that this selectivity is really related to an increased cholesterol concentration in these cancer cells or rather to other changes in metabolism or membrane structure. For example it has been shown that ceramides play an important role in cancer proliferation (Saddoughi and Ogretmen, 2013). Changing the amount of membrane ceramides could influence membranes and thereby change saponin activity. In fact, any change in membrane composition influencing the membrane dynamics, the capacity to form rafts or other membrane parameters could modify the activity of saponins. It has been shown that displacement of cholesterol from phospholipids by "membrane intercalators" increased lytic activity of saponins (Lange et al., 2005;Lange et al., 2009).

Finally, the presence of glycosidases within the membrane might also influence saponin activity. The hydrolysis of saponin into its sapogenin could reduce the cytolytic effect observed. The presence of glycosidases conferred some resistance to α-tomatine activity against fungi (Morrissey and Osbourn, 1999;Bouarab et al., 2002).

4.4. Structure-activity relationship on the amphiphilic activity

To gain futher understanding on the importance of the molecular structure for amphiphile-membrane interactions, we will enlarge in this chapter the results of analyzed molecules with data obtained on similar compounds in litterature.

4.4.1. α-Hederin and derivatives

As we pointed out in chapter 3.1.1., the three-dimensional molecular structure of α-hederin was very important for its interactions with membranes. The induction of positive curvature depended on the sugar chain present on C3. The form of induced lateral domains changed also with the structure of the molecule (3.1.2.). We are aware that the three-dimensional molecular structure given by Chemdraw 3D does not reflect real molecular modeling. Nevertheless, the 3D-structures obtained by molecular modeling (see 3.1.2.) were almost identical to those given by Chemdraw 3D.

The structure-activity relationships for hemolysis and cytotoxicity were studied for some hederagenin diglycosides (Chwalek et al., 2006), but It has been shown that there was no direct link between these activities. In this study, the importance of the branching and the nature of the sugar moieties on the aglycone was pointed out. The (1→2) branching between α-L-arabinose present on the C3 of the aglycon and other sugars gave the most efficient compounds regarding hemolysis and cytotoxicity. Compared to other sugars, the presence of a rhamnose linked to the arabinose residue in the (1→2) configuration, increased more the hemolytic and cytotoxicic activity. Some authors suggested, that the presence of a more hydrophobic sugar would increase the activity of the saponin (maybe due to a facilitated insertion of the molecule into the membrane) (Chwalek et al., 2006;Wang et al., 2007b).

Increasing the number of sugars at the α-hederin disaccharide moiety increased further the cytotoxicity of the compounds, which supports a curvature driven lysis mechanism in cells (Bang et al., 2008).

The lysis mechanism should also be valid for other monodesmosidic saponins presenting a sugar moiety at C3 because the number of sugars increased in most cases the hemolytic activity (see Figure 23).

Regarding the hydrophobic portion of the saponin, hemolytic activity has been intensively discussed for saponins (see Figure 23). For α-hederin, when the triterpenic acid was esterified, hemolytic activity generally increased, which points out the importance for hydrophobicity of this part of the molecule (Chwalek et al., 2006).

4.4.2. Surfactin

The structure of the lipopeptide surfactin contains a polar head which is negatively charged. The peptide ring would adopt a “horse-saddle” conformation in solution with the two anionic residues forming a claw (Bonmatin et al., 1992). Its conformation should therefore depend on the ionic strength and pH. We worked mainly at a pH of 8.5 because the lipopeptide was more soluble. Our studies and the results of Heerklotz and coll. (Heerklotz and Seelig, 2001) suggested a detergent-like, CMC dependent mechanism. The CMC itself depended of the pH of the solution and decreased rapidly upon decreasing pH. Surfactin activity was enhanced in membranes containing negatively charged lipids and by increasing the charge of the lipopeptide (Buchoux et al., 2008;Francius et al., 2008). Without its acyl chain, surfactin would not be able to insert into the membrane (Eeman et al., 2006). An increase in the length of the acyl chain increased also the capacity to solubilize membranes composed of DOPC and DPPC (Francius et al., 2008).

4.5. Similarities and differences between membrane activities of α-hederin and surfactin

Our experiments show that despite their structural differences, surfactine, α-hederin and even hederagenin displayed typical features of amphiphiles and amphiphile-membrane interactions which have been intensively discussed. The main similarities of α-hederin and surfactin activity can be summarized as follows: (i) integration into the membrane facilitated by a lipophilic part of the molecule (ii) preferential interaction with (a) specific membrane lipid(s), (iii) induction of positive membrane curvature, (iv) abilities to self-aggregate, (v) differences in kinetics of permeabilization below and beyond their CMC, (vi) suppression of lateral phase separation in a DOPC:DPPC model, (vii) interaction with LUVs in a manner that induces populations of different sizes and new mesophases, (viii) change in membrane dynamics and order at hydrophilic heads and lipophilic tails, (ix) ability to permeabilize membranes, (x) induction of apoptosis most probably by a membrane dependent mechanism.

Nonetheless, there exist important differences in their mode of action. The most importants are the (i) permeabilizing activity of α-hederin which depends on cholesterol whereas that of surfactine is enhanced by fluid phase and negatively charged lipids and (ii) their activities on membrane order. Surfactin increased membrane order until its CMC and than decreased it. This behaviour was not observed with α-hederin.

Conversely to α-hederin and surfactin, hederagenin has a less important amphiphilic character because of its small hydrophilic headgroup. Permeabilization was only induced at very high concentrations and incubation times. It might be possible that this mechanism is only based on the formation of a new mesophase with cholesterol and phospholipids and less on the induction of potitive curvature strain and the formation of toroidal pores.

5. Perspectives

A lot of questions arise from our results. To obtain a more detailed understanding of α-hederin, hederagenin and surfactin activity, other experiments have to be performed.

This chapter is divided into two parts. In the first part, we will discuss short term perspectives about ongoing and future experiments. In the second part, we will try to answer in a long term perspective if the tested amphiphiles could be interesting drug candidates and what general lessons can be taken from this study.

5.1. Short term perspectives - future and ongoing studies

We made a lot of interesting studies which haven't yet been integrated into publications or into the previous chapters of this thesis because they are at this stage, too preliminary. Therefore some experiments have to be completed or done in the next future. They are briefly described hereunder.

5.1.1. α-Hederin and hederagenin

5.1.1.1.Determination of self-aggregating properties

The self aggregating properties and the CMC of both compounds should be investigated to confirm the hypothesis of their role in the modes of action on membranes. This could be done by measurements of surface tension, isothermal titration calorimetry or the use of other fluorescent probes like pyrene.

We looked by DLS if α-hederin was able to form aggregates in the solution above a certain concentration. The behaviour seems to change at ~ 15 µM (10 mM TRIS-HCl at pH=7.4) as predicted by the DHE experiments. Unfortunately the polydispersity index of the results is very high and so the results do not allow a final conclusion. This could possibly be due to the formation of one-dimensional aggregates, which are known for their high polydispersity (2.4.4.2.3.). The form of aggregates should be determined by cryo-TEM.

5.1.1.2.Interaction with membranes

It should be interesting to test the used amphiphiles on a ternary membrane model containing sphingomyelin, cholesterol and an unsaturated phospholipid. This model mimics better the molecular composition of lipid rafts in cells and presents macroscopic phase separation. It should give further information, if the molecule might be able to influence the hydrogen bond network, which is formed between the sphingomyelin molecules (Sonnino and Prinetti, 2013).

The completion of the Tof-SIMS experiments should provide interesting information on how the molecules are able to interact with cholesterol in supported planar membranes (see 3.1.3.). A similar approach on cells has been attempted for hederacolchiside A1 by Mazzucchelli and coll. (see 2.4.7.1.). However, they were not able to prove colocalization of cholesterol and the saponin for small incubation periods (Mazzucchelli et al., 2008). The advantage of SPBs compared to cells is that all molecules are known. The mass resolution can therefore be diminished, which increases the lateral resolution of the 2D image (Benabdellah et al., 2010).

In a similar approach, it could be possible to monitor sterol rich domains by incorporating DHE in GUVs and observe them by multiphoton microscopy (Garvik et al., 2009). This should give confidence about the effects of saponins or triterpenoids regarding sterol distribution in membranes. A similar approach could be done on cells (see 5.1.1.4.)

5.1.1.3.Determination of composition and structure of the new induced mesophases

We have shown the formation of a new mesophase by ^{31}P-NMR and DLS in MLVs and LUVs that have been incubated with α-hederin. Incubation of highly concentrated MLVs composed of DMPC/Chol (3:1) led to the formation of a macroscopic phase separation in the sample and a new flocculated phase which was less dense (see 3.1.1.). We supposed that this phase corresponded to the newly induced worm-like structures observed in SPBs and GUVs (see 3.1.2.).

We analyzed by mass spectrometry (direct injection in an Atmospheric pressure chemical ionization source (APCI) on a LCQAD-30000 mass spectrometer equipped with an Ion-Trap analyzer in positive and negative ionization mode) the different macroscopic phases which have been obtained. In a first attempt, we could confirm the presence of DMPC, cholesterol and α-hederin in the newly formed phase. This means that this phase is also composed of all three constituents as it has been suggested (3.1.2.). We haven't until yet an idea of the proportions of

all three components in both phases because the formation of many different types of aggregates between all three components makes the analysis of the mass spectra difficult. Nonetheless, we should be able to complete interpretation of the mass spectra soon which could be integrated in 3.1.2.

The use of cryogenic transmission electron microscopy (Cryo-Tem) should allow to vizualize the 3D shape of the structures which have been formed when DMPC:Chol (3:1) liposomes (LUVs and MLVs) were incubated with α-hederin or hederagenin (see 3.1.1. and 3.1.2.). It is not sure that we will obtain the same structures we obtained on SPBs (see 3.1.2.) because the curvature of LUVs is higher than that of SPBs (see 8.1.2). The determination of the shape of aggregates could eventually also determine if the saponin is a good candidate for the formation of nanoparticles (see 5.4.3.).

5.1.1.4.Investigations on cellular activity

To make progress in deciphering the cellular activity of α-hederin and hederagenin, we are testing the activity of both compounds in delipidated media to reduce possible interactions with cholesterol. Because U937 cells are not able to synthesize their own cholesterol, cells once depleted in cholesterol should keep the low amount of membrane cholesterol upon time. Preliminary results showed a more important cell death inhibition for U937 cells, which have been depleted for cholesterol and further incubated with α-hederin in delipidated media. The depletion of membrane cholesterol seems also to inhibit apoptosis induction by hederagenin but results have to be confirmed.

To prove a direct interaction of α-hederin or hederagenin with cholesterol in cells, we could add cholesterol to the incubation media and observe if there would be a change of cytotoxicity.

The activity on lateral membrane organization, lipid rafts and death receptors in cancer cells should also be investigated. Reorganization of lipid rafts in cells can be visualized by multiphoton microscopy of Laurdan (Yi et al., 2009) or DHE (McIntosh et al., 2003) in living cells. These methods have been shown to be more reliable than the use of specific antibodies or toxins which bind to raft constituents, because there is no risk of lipid cross-linking and the induction of artifacts which could ressemble rafts (Owen et al., 2007).

Activation of death receptors can be determined by activation of caspase-8 (see 2.4.8.3.4.1.). The addition of specific caspase-8 inhibitors like Z-IETD-FMK or a western blot of caspase-8 should give information about the importance of this enzyme in cell death. The visualization of death receptors in cells and their aggregation and colocalization with lipid rafts which would precede their activation can be visualized by specific antibodies (Yi et al., 2009).

5.1.2. Surfactin

There exist a huge number of studies treating the permeabilizing activity of this compound (Kracht et al., 1999;Heerklotz and Seelig, 2001;Dufour et al., 2005;Francius et al., 2008;Heerklotz and Seelig, 2007;Carrillo et al., 2003;Eeman et al., 2006;Ostroumova et al., 2010). Nevertheless, the activity on phase separation, regarding the enormous possible implications (see 3.5.), should be investigated more deeply. For this purpose, similar studies which have been proposed for α-hederin or hederagenin could be carried out (5.1.1.).

5.2. Long term perspectives

At the end of our work, we keep in mind two main questions: (i) are α-hederin, hederagenin and surfactin good drug candidates ? and (ii) what general lessons can we take from this study for future studies on amphiphiles ?

5.2.1. Are α-hederin, hederagenin and surfactin good drug-candidates ?

To be a valuable drug candidate a molecule must obey certain pharmacological and pharmacokinetic conditions. We will discuss these issues to obtain an idea if it is really worth to pursue studies on these molecules.

5.2.1.1.Pharmacodynamic and toxicological considerations

The major limitation of saponins in general and α-hederin for intravenous administration is their hemolytic effect (see 2.4.7.). If molecules will pass through the blood stream, their toxic potential should limit their pharmacological use. At this stage, we have to question if the

benefit/risk balance is high enough to consider future studies. For cancer studies, the benefit is always high compared to the risk, because the outcome of cancer is mostly death. α-Hederin has only been tested once for its antitumor activity, but the results seem promising. The molecule, tested at 15 mg/kg (i.p.) on colon 26- or 3LL Lewis lung carcinoma bearing mice, was as effective as cisplatin at 3 mg/kg and no weight loss or evidence of toxicity was observed in healthy mice (Park et al., 2001). Conversely, because of its toxic potential, the molecule should not be used for other pharmacological purposes.

The integration of the saponin into nanoparticles could probably increase the therapeutic index of the molecules by reducing hemolysis and increasing cytotoxicity towards cancer cells (Hu et al., 2010). If α-hederin is able to form nanoparticles by itself or with cholesterol and other phospholipids should be further investigated.

Hederagenin could be an interesting candidate for cancer therapy because it has shown cytotoxic potential towards cancer cells but no induction of hemolysis (Gauthier et al., 2009). However, the molecule was not cytotoxic in various studies but this could be related to small incubation periods investigated (the molecule showed its activity only after long incubation periods, see 3.1.4.). The question remains if hederagenin will be active on cancer cells *in vivo*. Other triterpenic acids like ursolic or betulinic acid have been intensively studied *in vivo* on different cancers and are known for their therapeutic potential (Patlolla and Rao, 2012;Mullauer et al., 2010;Shanmugam et al., 2013;Zuco et al., 2002;Prasad et al., 2012). Both compounds are highly cytotoxic, induced cell death by several pathways after long incubation times and betulinic acid showed selective cytotoxicity towards cancer cells (Zuco et al., 2002;Xavier et al., 2013). Triterpenoid acids are therefore promising anticancer agents.

Surfactin could be possibly used as antibacterial or anticancer agent *in vivo*. Unfortunately it has shown high hemolytic activity (Kracht et al., 1999;Dufour et al., 2005) which should limit its use as antiinfective agent. Daptomycin constitutes already an effective lipopeptide antibiotic which has a lower hemolytic potential than surfactin (Straus and Hancock, 2006). Until now, there exists no *in vivo* study in humans about the anticancer potential of surfactin. It is therefore impossible to predict whether there would be an interesting compound. Currently, the molecule seems to be an interesting candidate to fight plant infections. The producer of surfactin, *Bacillus*

subtilis is a promising bacteria cultivated to prevent plant diseases (Stein, 2005;Toure et al., 2004).

5.2.1.2.Pharmacokinetic considerations

Several pharmacokinetic studies on saponins exist but to our knowledge there exist no study dealing with the pharmacokinetics of α-hederin. As a general rule, a molecule is considered as an interesting candidate for oral administration if it follows the Lipinsky rules (a molecular mass < 500 Da, hydrogen donors < 5, hydrogen acceptors < 10, $\log_{10}$ of octanol/water partition coefficient [log P] < 5). α-Hederin has a molecular mass of 750.9 Da, 7 H-bond donors, 12 H-bond acceptors and a theoretical log P of 3.6 (calculated by PubChem Compound). Except for its lipophilicity, all parameters which define a "good" drug candidate for oral administration are out of range. But even the Lipinsky rules do not consider the possibility of self-aggregation (or aggregation with other compounds), which could significantly change its absorption behaviour. We also cannot exclude the possibility that the molecule will be absorbed by active transport in lipid micelles. Active transport has been suggested for some saponins but in general their bioavailability was low (Yu et al., 2012). On the contrary, digoxin, a cardiotonic heteroside already in use for a long time against cardiac insufficiency showed a very good biodisponibility (70-80%) in humans and the molecule was resorbed by passive diffusion (Iisalo, 1977).

The oral biodisponibility could also be changed by the presence of microbial glucosidases in the gut flora. This has been shown in a phase I study for asiaticoside which is completely transformed into asiatic acid in the gut (Grimaldi et al., 1990). α-Hederin could be cleaved into δ-hederin or hederagenin and be administrated as a hederagenin pro-drug (Yu et al., 2012). Regarding interaction with other compounds after oral administration, saponins could influence their resorption, due to their surfactant and self-aggregating properties (Bruneton, 2009).

All these factors make it very difficult to predict the biodisponibility of α-hederin.

Nonetheless, regarding intravenous administration of saponins, it has been shown that several monodesmosidic saponins showed a favorable intravenous pharmacokinetic profile with low clearance and long half lifes (Patel et al., 2012). Intravenous injection is very common for anticancer compounds and could be applied for α-hederin, but hemolysis has to be avoided.

Hederagenin has a molecular weight of 472,6 Da, 3 H-bond donors, 4 H-bond acceptors and a theoretical log P of 6.8 (calculated by PubChem Compound). Except its high lipophilicity, the molecule could be a good theoretical candidate for oral administration. There exists no pharmacokinetic study about hederagenin. Other triterpenic acids, like ursolic acid have already been used by oral administration in rats but showed moderate oral biodisponibility (Shanmugam et al., 2013) while betulinic acid showed even a high oral biodisponibility in humans (Smith et al., 2007). The low solubility of triterpenic acids is a problem in intravenous administration. This could be circumvented by integration into liposomes. A liposomal form of intravenously administrated ursolic acid showed interesting results in a clinical study (Shanmugam et al., 2013). Therefore, triterpenic acids seem by pharmacokinetic considerations very promising compounds for cancer treatment.

To our knowledge no pharmacokinetic study of surfactin was published. Other lipopetides like daptomycin, which are already in clinical use have a well known pharmacokinetic profile. It has been approved by the European medecines agency and registered under the name of cubicin. Daptomycin is injected in its dissolved form intravenously. Because of their high molecular weight, lipopeptides are generally not absorbed after oral administration.

5.2.2. What general lessons can we take from this study for future investigations on amphiphiles ?

We have to be aware for future pharmacological studies, that amphiphiles behave often in similar ways (see 4.5.) and that their three-dimensional structure and charge will have major implications on their activity. The capacity to self-aggregate and form a new mesophase should always be taken into consideration for quite all types of molecules. It has been shown that even molecules which do not possess a strong amphiphilic character like triterpenic or bile acids are able to form aggregates or micelles in solution (Rafat et al., 2008;Sayyed-Ahmad et al., 2010). Self-aggregation can change completely the behaviour of compounds towards ligands making the determination of the CMC of a compound (or solubility for molecules which form infinite aggregates, see 2.2.1.2) a prerequisite for pharmacological investigations.

A possible interaction of amphiphilic compounds with biological membranes should never be excluded. A lot of pharmacodynamic and pharmacokinetic properties are guided through their membrane interactions.

However, we have shown in this thesis, that molecules presenting an amphiphilic character may be very interesting compounds with various activities towards lipid membranes. The isolation of new original substances from plants and other natural resources should help to develop molecules with specific activities towards membranes of cancer cells or infectious agents. Understanding their membrane interactions should allow us to make chemical modifications of the molecules which enhance their specificity.

6. Bibliography

Reference List

1. Abe,H., H.Konishi, H.Komiya, and S.Arichi. 1981. Effects of saikosaponins on biological membranes. 3. Ultrastructural studies on effects of saikosaponins on the cell surface. *Planta Med.* 42:356-363.

2. Afrose,S., M.S.Hossain, T.Maki, and H.Tsujii. 2009. Karaya root saponin exerts a hypocholesterolemic response in rats fed a high-cholesterol diet. *Nutr. Res.* 29:350-354.

3. Ahyayauch,H., M.Bennouna, A.Alonso, and F.M.Goni. 2010. Detergent effects on membranes at subsolubilizing concentrations: transmembrane lipid motion, bilayer permeabilization, and vesicle lysis/reassembly are independent phenomena. *Langmuir* 26:7307-7313.

4. Akiyama,T., S.Takagi, U.Sankawa, S.Inari, and H.Saito. 1980. Saponin-Cholesterol Interaction in the Multibilayers of Egg-Yolk Lecithin As Studied by Deuterium Nuclear Magnetic-Resonance - Digitonin and Its Analogs. *Biochemistry* 19:1904-1911.

5. Almgren,M. 2000. Mixed micelles and other structures in the solubilization of bilayer lipid membranes by surfactants. *Biochim. Biophys. Acta - Biomembranes* 1508:146-163.

6. Amara-Mokrane,Y.A., M.P.Lehucher-Michel, G.Balansard, G.Dumenil, and A.Botta. 1996. Protective effects of alpha-hederin, chlorophyllin and ascorbic acid towards the induction of micronuclei by doxorubicin in cultured human lymphocytes. *Mutagenesis* 11:161-167.

7. Angelini,T.E., M.Roper, R.Kolter, D.A.Weitz, and M.P.Brenner. 2009. Bacillus subtilis spreads by surfing on waves of surfactant. *Proc. Natl. Acad. Sci. U. S. A* 106:18109-18113.

8. Angelova,M.I., S.Soléau, Ph.Méléard, J.F.Faucon, and P.Bothorel. 1992. Preparation of giant vesicles by external AC electric fields. Kinetics and applications. *Progress in colloid and Polymer science* 89:127-131.

9. Arias,M., J.C.Quijano, V.Haridas, J.U.Gutterman, and V.V.Lemeshko. 2010. Red blood cell permeabilization by hypotonic treatments, saponin, and anticancer avicins. *Biochim. Biophys. Acta - Biomembranes* 1798:1189-1196.

10. Arima,K., A.Kakinuma, and G.Tamura. 1968. Surfactin, a crystalline peptidelipid surfactant produced by Bacillus subtilis: Isolation, characterization and its inhibition of fibrin clot formation. *Biochemical and Biophysical Research Communications* 31:488-494.

11. Armah,C.N., A.R.Mackie, C.Roy, K.Price, A.E.Osbourn, P.Bowyer, and S.Ladha. 1999. The membrane-permeabilizing effect of avenacin A-1 involves the reorganization of bilayer cholesterol. *Biophys. J.* 76:281-290.

12. Ashworth,L.A. and C.Green. 1966. Plasma membranes: phospholipid and sterol content. *Science* 151:210-211.

13. Assa,Y., S.Shany, B.Gestetner, Y.Tencer, Y.Birk, and A.Bondi. 1973. Interaction of alfalfa saponins with components of the erythrocyte membrane in hemolysis. *Biochim. Biophys. Acta - Biomembranes* 307:83-91.

14. Bagatolli,L.A., J.H.Ipsen, A.C.Simonsen, and O.G.Mouritsen. 2010. An outlook on organization of lipids in membranes: searching for a realistic connection with the organization of biological membranes. *Prog. Lipid Res.* 49:378-389.

15. Balakrishnan,S., S.Varughese, and A.P.Deshpande. 2006. Micellar characterisation of saponin from Sapindus mukorossi. *Tenside Surfactants Detergents* 43:262-268.

16. Bang,S.C., H.H.Seo, H.R.Shin, K.C.Lee, l.T.Hoang, and S.H.Jung. 2008. A convenient preparation of a disaccharide motif and its role in the cytotoxicity of the triterpenoid saponin, alpha-hederin. *Arch. Pharm. Res.* 31:555-561.

17. Bangham,A.D., R.W.Horne, A.M.Glauert, J.T.Dingle, and J.A.Lucy. 1962. Action of saponin on biological cell membranes. *Nature* 196:952-955.

18. Barros,L.F., T.Kanaseki, R.Sabirov, S.Morishima, J.Castro, C.X.Bittner, E.Maeno, Y.Ando-Akatsuka, and Y.Okada. 2003. Apoptotic and necrotic blebs in epithelial cells display similar neck diameters but different kinase dependency. *Cell Death. Differ.* 10:687-697.

19. Bartlett,G.R. 1985. Citation Classic - Phosphorus Assay in Column Chromatography. *Current Contents/Life Sciences*16.

20. Bashkirov,P.V., S.A.Akimov, A.I.Evseev, S.L.Schmid, J.Zimmerberg, and V.A.Frolov. 2008. GTPase cycle of dynamin is coupled to membrane squeeze and release, leading to spontaneous fission. *Cell* 135:1276-1286.

21. Baumann,E., G.Stoya, A.Volkner, W.Richter, C.Lemke, and W.Linss. 2000. Hemolysis of human erythrocytes with saponin affects the membrane structure. *Acta Histochemica* 102:21-35.

22. Baumgart,T., G.Hunt, E.R.Farkas, W.W.Webb, and G.W.Feigenson. 2007. Fluorescence probe partitioning between Lo/Ld phases in lipid membranes. *Biochim. Biophys. Acta* 1768:2182-2194.

23. Bayer,M., P.Proksch, I.Felsner, H.Brenden, Z.Kohne, R.Walli, T.N.Duong, C.Gotz, J.Krutmann, and S.Grether-Beck. 2011. Photoprotection against UVAR: effective triterpenoids require a lipid raft stabilizing chemical structure. *Exp. Dermatol.* 20:955-958.

24. Becher,A., J.H.White, and R.A.McIlhinney. 2001. The gamma-aminobutyric acid receptor B, but not the metabotropic glutamate receptor type-1, associates with lipid rafts in the rat cerebellum. *J. Neurochem.* 79:787-795.

25. Becher,P. 1983. Hydrophile-lipophile balance: History and recent developments. *Journal of Dispersion science and Technology* 5:577-585.

26. Bechinger,B. and K.Lohner. 2006. Detergent-like actions of linear amphipathic cationic antimicrobial peptides. *Biochim. Biophys. Acta - Biomembranes* 1758:1529-1539.

27. Benabdellah,F., A.Seyer, L.Quinton, D.Touboul, A.Brunelle, and O.Laprevote. 2010. Mass spectrometry imaging of rat brain sections: nanomolar sensitivity with MALDI versus nanometer resolution by TOF-SIMS. *Anal. Bioanal. Chem.* 396:151-162.

28. Billheimer,J.T., D.Chamoun, and M.Esfahani. 1987. Defective 3-ketosteroid reductase activity in a human monocyte-like cell line. *J. Lipid Res.* 28:704-709.

29. Blanchette,C.D., W.C.Lin, C.A.Orme, T.V.Ratto, and M.L.Longo. 2008. Domain nucleation rates and interfacial line tensions in supported bilayers of ternary mixtures containing galactosylceramide. *Biophys. J.* 94:2691-2697.

30. Bonmatin,J.M., M.Genest, M.C.Petit, E.Gincel, J.P.Simorre, B.Cornet, X.Gallet, A.Caille, H.Labbe, F.Vovelle, and . 1992. Progress in multidimensional NMR investigations of peptide and protein 3-D structures in solution. From structure to functional aspects. *Biochimie* 74:825-836.

31. Bottger,S., K.Hofmann, and M.F.Melzig. 2012. Saponins can perturb biologic membranes and reduce the surface tension of aqueous solutions: a correlation? *Bioorg. Med. Chem.* 20:2822-2828.

32. Bouarab,K., R.Melton, J.Peart, D.Baulcombe, and A.Osbourn. 2002. A saponin-detoxifying enzyme mediates suppression of plant defences. *Nature* 418:889-892.

33. Brasseur,R. 1990. TAMMO: Theoretical analysis of membrane molecular organization. *In* Molecular description of biological membrane components by computer-aided conformational analysis. R.Brasseur, editor. CRC press, Boca Raton.

34. Brasseur,R., J.A.Killian, B.de Kruijff, and J.M.Ruysschaert. 1987. Conformational analysis of gramicidin-gramicidin interactions at the air/water interface suggests that gramicidin aggregates into tube-like structures similar as found in the gramicidin-induced hexagonal HII phase. *Biochim. Biophys. Acta* 903:11-17.

35. British standard institute. Nanoparticles - Vocabulary. PAS 71:2011, 1-28. 2011. British standard institute.

36. Brown,D.A. and J.K.Rose. 1992. Sorting of GPI-anchored proteins to glycolipid-enriched membrane subdomains during transport to the apical cell surface. *Cell* 68:533-544.

37. Bruneton,J. 2009. Pharmacognosie, Phytochimie, Plantes médicinales. Lavoisier.

38. Buchoux,S., J.Lai-Kee-Him, M.Garnier, P.Tsan, F.Besson, A.Brisson, and E.J.Dufourc. 2008. Surfactin-triggered small vesicle formation of negatively charged membranes: a novel membrane-lysis mechanism. *Biophys. J.* 95:3840-3849.

39. Bun,S.S., R.Elias, B.Baghdikian, J.Ciccolini, E.Ollivier, and G.Balansard. 2008. Alpha-hederin potentiates 5-FU antitumor activity in human colon adenocarcinoma cells. *Phytother. Res.* 22:1299-1302.

40. Caffrey,M. 1985. Kinetics and mechanism of the lamellar gel/lamellar liquid-crystal and lamellar/inverted hexagonal phase transition in phosphatidylethanolamine: a real-time X-ray diffraction study using synchrotron radiation. *Biochemistry* 24:4826-4844.

41. Cao,F., W.Ouyang, and Y.Wang. 2010. [Preparation of O/W ginseng saponins-based nanoemulsion and its amplified immune response]. *Zhongguo Zhong. Yao Za Zhi.* 35:439-443.

42. Cao,X., A.H.Wang, R.Z.Jiao, C.L.Wang, D.Z.Mao, L.Yan, and B.Zeng. 2009. Surfactin induces apoptosis and G(2)/M arrest in human breast cancer MCF-7 cells through cell cycle factor regulation. *Cell Biochem. Biophys.* 55:163-171.

43. Cao,X.H., S.S.Zhao, D.Y.Liu, Z.Wang, L.L.Niu, L.H.Hou, and C.L.Wang. 2011. ROS-Ca(2+) is associated with mitochondria permeability transition pore involved in surfactin-induced MCF-7 cells apoptosis. *Chem. Biol. Interact.* 190:16-27.

44. Carrillo,C., J.A.Teruel, F.J.Aranda, and A.Ortiz. 2003. Molecular mechanism of membrane permeabilization by the peptide antibiotic surfactin. *Biochim. Biophys. Acta - Biomembranes* 1611:91-97.

45. Cerneus,D.P., E.Ueffing, G.Posthuma, G.J.Strous, and A.van der Ende. 1993. Detergent insolubility of alkaline phosphatase during biosynthetic transport and endocytosis. Role of cholesterol. *J. Biol. Chem.* 268:3150-3155.

46. Chaigne-Delalande,B., J.F.Moreau, and P.Legembre. 2008. Rewinding the DISC. *Arch. Immunol. Ther. Exp. (Warsz.)* 56:9-14.

47. Chang,C.H. and E.I.Franses. 1995. Adsorption dynamics of surfactants at the air/water interface: a critical review of mathematical models, data, and mechanisms. *Colloids and Surfaces A: Physicochemical and Engineering Aspects* 100:1-45.

48. Chen,Z. and R.P.Rand. 1997. The influence of cholesterol on phospholipid membrane curvature and bending elasticity. *Biophys. J.* 73:267-276.

49. Cheng,G., Y.Zhang, X.Zhang, H.F.Tang, W.D.Cao, D.K.Gao, and X.L.Wang. 2006. Tubeimoside V (1), a new cyclic bisdesmoside from tubers of Bolbostemma paniculatum, functions by inducing apoptosis in human glioblastoma U87MG cells. *Bioorg. Med. Chem. Lett.* 16:4575-4580.

50. Cheng,K.H., J.Virtanen, and P.Somerharju. 1999. Fluorescence studies of dehydroergosterol in phosphatidylethanolamine/phosphatidylcholine bilayers. *Biophys. J.* 77:3108-3119.

51. Choi,J.H., H.W.Lee, H.J.Park, S.H.Kim, and K.T.Lee. 2008. Kalopanaxsaponin A induces apoptosis in human leukemia U937 cells through extracellular Ca2+ influx and caspase-8 dependent pathways. *Food Chem. Toxicol.* 46:3486-3492.

52. Chong,P.L. 1994. Evidence for regular distribution of sterols in liquid crystalline phosphatidylcholine bilayers. *Proc. Natl. Acad. Sci. U. S. A* 91:10069-10073.

53. Chu,P. and S.Sadullah. 2009. The current role of amphotericin B lipid complex in managing systemic fungal infections. *Curr. Med. Res. Opin.* 25:3011-3020.

54. Chwalek,M., N.Lalun, H.Bobichon, K.Ple, and L.Voutquenne-Nazabadioko. 2006. Structure-activity relationships of some hederagenin diglycosides: haemolysis, cytotoxicity and apoptosis induction. *Biochim. Biophys. Acta - General Subjects* 1760:1418-1427.

55. Ciechomska,I.A. and A.M.Tolkovsky. 2007. Non-autophagic GFP-LC3 puncta induced by saponin and other detergents. *Autophagy.* 3:586-590.

56. Clausell,A., M.Garcia-Subirats, M.Pujol, M.A.Busquets, F.Rabanal, and Y.Cajal. 2007. Gram-negative outer and inner membrane models: insertion of cyclic cationic lipopeptides. *J. Phys. Chem. B* 111:551-563.

57. Coleman,J.J., I.Okoli, G.P.Tegos, E.B.Holson, F.F.Wagner, M.R.Hamblin, and E.Mylonakis. 2010. Characterization of plant-derived saponin natural products against Candida albicans. *ACS Chem. Biol.* 5:321-332.

58. Correia,R.F., M.I.Viseu, T.J.Prazeres, and J.M.Martinho. 2012. Spontaneous vesicles, disks, threadlike and spherical micelles found in the solubilization of DMPC liposomes by the detergent DTAC. *J. Colloid Interface Sci.* 379:56-63.

59. Cullis,P.R. and B.de Kruijff. 1978. The polymorphic phase behaviour of phosphatidylethanolamines of natural and synthetic origin. A 31P NMR study. *Biochim. Biophys. Acta* 513:31-42.

60. Dai,X., X.Shi, Q.Yin, H.Ding, and Y.Qiao. 2013. Multiscale study on the interaction mechanism between ginsenoside biosurfactant and saikosaponin a. *J. Colloid Interface Sci.* 396:165-172.

61. Daines,A.M., B.W.Greatrex, C.M.Hayman, S.M.Hook, W.T.McBurney, T.Rades, P.M.Rendle, and I.M.Sims. 2009. Mannosylated saponins based on oleanolic and glycyrrhizic acids. Towards synthetic colloidal antigen delivery systems. *Bioorganic & Medicinal Chemistry* 17:5207-5218.

62. Danielli,J.F. and H.Davson. 1935. A contribution to the theory of permeability of thin films. *Journal of cellular and comparative physiology* 5:495-508.

63. Danloy,S., J.Quetin-Leclercq, P.Coucke, M.C.Pauw-Gillet, R.Elias, G.Balansard, L.Angenot, and R.Bassleer. 1994. Effects of alpha-hederin, a saponin extracted from Hedera helix, on cells cultured in vitro. *Planta Med.* 60:45-49.

64. de Almeida,R.F., A.Fedorov, and M.Prieto. 2003. Sphingomyelin/phosphatidylcholine/cholesterol phase diagram: boundaries and composition of lipid rafts. *Biophys. J.* 85:2406-2416.

65. de Almeida,R.F., L.M.Loura, and M.Prieto. 2009. Membrane lipid domains and rafts: current applications of fluorescence lifetime spectroscopy and imaging. *Chem. Phys. Lipids* 157:61-77.

66. de Kruijff,B. 1997. Lipid polymorphism and biomembrane function. *Curr. Opin. Chem. Biol* 1:564-569.

67. De Pace,D.M. and M.Esfahani. 1987. The effects of cholesterol depletion on cellular morphology. *Anat. Rec.* 219:135-143.

68. de Ven,H.V., L.Van Dyck, W.Weyenberg, L.Maes, and A.Ludwig. 2010. Nanosuspensions of chemically modified saponins: reduction of hemolytic side effects and potential tool in drug targeting strategy. *J. Control Release* 148:e122-e123.

69. Deleu,M., J.Lorent, L.Lins, R.Brasseur, N.Braun, K.El Kirat, T.Nylander, Y.F.Dufrene, and M.P.Mingeot-Leclercq. 2013. Effects of surfactin on membrane models displaying lipid phase separation. *Biochim. Biophys. Acta* 1828:801-815.

70. Demana,P.H., N.M.Davies, S.Hook, and T.Rades. 2007. Analysis of Quil A-phospholipid mixtures using drift spectroscopy. *International Journal of Pharmaceutics* 342:49-61.

71. Demana,P.H., N.M.Davies, U.Vosgerau, and T.Rades. 2004. Pseudo-ternary phase diagrams of aqueous mixtures of Quil A, cholesterol and phospholipid prepared by the lipid-film hydration method. *International Journal of Pharmaceutics* 270:229-239.

72. Dennis,E.A. 1986. Micellization and solubilization of phospholipids by surfactants. *Adv. Colloid Interface Sci.* 26:155-175.

73. Desai,J.D. and I.M.Banat. 1997. Microbial production of surfactants and their commercial potential. *Microbiol. Mol. Biol. Rev.* 61:47-64.

74. Desmond,E. and S.Gribaldo. 2009. Phylogenomics of sterol synthesis: insights into the origin, evolution, and diversity of a key eukaryotic feature. *Genome Biol. Evol.* 1:364-381.

75. Detmers,P.A., S.Patel, M.Hernandez, J.Montenegro, J.M.Lisnock, B.Pikounis, M.Steiner, D.Kim, C.Sparrow, Y.S.Chao, and S.D.Wright. 2000. A target for cholesterol absorption inhibitors in the enterocyte brush border membrane. *Biochim. Biophys. Acta - Molecular and Cell Biology of Lipids* 1486:243-252.

76. Dickens,L.S., I.R.Powley, M.A.Hughes, and M.MacFarlane. 2012. The 'complexities' of life and death: death receptor signalling platforms. *Exp. Cell Res.* 318:1269-1277.

77. Domenech,O., G.Francius, P.M.Tulkens, F.Van Bambeke, Y.Dufrene, and M.P.Mingeot-Leclercq. 2009. Interactions of oritavancin, a new lipoglycopeptide derived from vancomycin, with phospholipid bilayers: Effect on membrane permeability and nanoscale lipid membrane organization. *Biochim. Biophys. Acta* 1788:1832-1840.

78. Dufour,S., M.Deleu, K.Nott, B.Wathelet, P.Thonart, and M.Paquot. 2005. Hemolytic activity of new linear surfactin analogs in relation to their physico-chemical properties. *Biochim. Biophys. Acta - General Subjects* 1726:87-95.

79. Eeman,M., A.Berquand, Y.F.Dufrene, M.Paquot, S.Dufour, and M.Deleu. 2006. Penetration of surfactin into phospholipid monolayers: nanoscale interfacial organization. *Langmuir* 22:11337-11345.

80. Elias,P.M., D.S.Friend, and J.Goerke. 1979. Membrane sterol heterogeneity. Freeze-fracture detection with saponins and filipin. *J. Histochem. Cytochem.* 27:1247-1260.

81. Elias,P.M., J.Goerke, D.S.Friend, and B.E.Brown. 1978. Freeze-fracture identification of sterol-digitonin complexes in cell and liposome membranes. *J. Cell Biol.* 78:577-596.

82. Ellington,A.A., M.Berhow, and K.W.Singletary. 2005. Induction of macroautophagy in human colon cancer cells by soybean B-group triterpenoid saponins. *Carcinogenesis* 26:159-167.

83. Epand,R.M. and R.F.Epand. 2009. Lipid domains in bacterial membranes and the action of antimicrobial agents. *Biochim. Biophys. Acta* 1788:289-294.

84. Epand,R.M., S.Rotem, A.Mor, B.Berno, and R.F.Epand. 2008. Bacterial membranes as predictors of antimicrobial potency. *J. Am. Chem. Soc.* 130:14346-14352.

85. Erbes,J., G.Rapp, and R.Winter. 1996. Kinetics and mechanisms of lamellar and non-lamellar phase transitions in aqueous lipid dispersions. *In* Progress in Biotechnology High Pressure Bioscience and Biotechnology Proceedings of the International Conference on High Pressure Bioscience and Biotechnology. R.H.and, editor. Elsevier, 181-4.

86. Evans,E. and D.Needham. 1986. Giant vesicle bilayers composed of mixtures of lipids, cholesterol and polypeptides. Thermomechanical and (mutual) adherence properties. *Faraday Discuss. Chem. Soc.*267-280.

87. Fontell,K. 1992. Some aspects on the cubic phases in surfactant and surfactant-like lipid systems. *Advances in Colloid and Interface Science* 41:127-147.

88. Francis,G., Z.Kerem, H.P.Makkar, and K.Becker. 2002. The biological action of saponins in animal systems: a review. *Br. J. Nutr.* 88:587-605.

89. Francius,G., S.Dufour, M.Deleu, M.Paquot, M.P.Mingeot-Leclercq, and Y.F.Dufrene. 2008. Nanoscale membrane activity of surfactins: influence of geometry, charge and hydrophobicity. *Biochim. Biophys. Acta - Biomembranes* 1778:2058-2068.

90. Friedrichson,T. and T.V.Kurzchalia. 1998. Microdomains of GPI-anchored proteins in living cells revealed by crosslinking. *Nature* 394:802-805.

91. Fukuda,K., H.Utsumi, S.Soda, J.Shoji, and A.Hamada. 1987. Specific interaction of arabinose residue in ginsenoside with egg phosphatidylcholine vesicles. *Biochim. Biophys. Acta - Biomembranes* 900:267-274.

92. Gajate,C. and F.Mollinedo. 2011. Lipid rafts and Fas/CD95 signaling in cancer chemotherapy. *Recent Pat Anticancer Drug Discov.* 6:274-283.

93. Galluzzi,L., I.Vitale, J.M.Abrams, E.S.Alnemri, E.H.Baehrecke, M.V.Blagosklonny, T.M.Dawson, V.L.Dawson, W.S.El Deiry, S.Fulda, E.Gottlieb, D.R.Green, M.O.Hengartner, O.Kepp, R.A.Knight, S.Kumar, S.A.Lipton, X.Lu, F.Madeo, W.Malorni, P.Mehlen, G.Nunez, M.E.Peter, M.Piacentini, D.C.Rubinsztein, Y.Shi, H.U.Simon, P.Vandenabeele, E.White, J.Yuan, B.Zhivotovsky, G.Melino, and G.Kroemer. 2012. Molecular definitions of cell death subroutines: recommendations of the Nomenclature Committee on Cell Death 2012. *Cell Death. Differ.* 19:107-120.

94. Gamble,W., M.Vaughan, H.S.Kruth, and J.Avigan. 1978. Procedure for determination of free and total cholesterol in micro- or nanogram amounts suitable for studies with cultured cells. *J. Lipid Res.* 19:1068-1070.

95. Gang,H.Z., J.F.Liu, and B.Z.Mu. 2011. Molecular dynamics study of surfactin monolayer at the air/water interface. *J. Phys. Chem. B* 115:12770-12777.

96. Gao,J., X.Li, G.Gu, B.Sun, M.Cui, M.Ji, and H.X.Lou. 2011. Efficient synthesis of trisaccharide saponins and their tumor cell killing effects through oncotic necrosis. *Bioorg. Med. Chem. Lett.* 21:622-627.

97. Garcia-Saez,A.J., S.B.Buschhorn, H.Keller, G.Anderluh, K.Simons, and P.Schwille. 2011. Oligomerization and pore formation by equinatoxin II inhibit endocytosis and lead to plasma membrane reorganization. *J. Biol Chem.* 286:37768-37777.

98. Garvik,O., P.Benediktson, A.C.Simonsen, J.H.Ipsen, and D.Wustner. 2009. The fluorescent cholesterol analog dehydroergosterol induces liquid-ordered domains in model membranes. *Chem. Phys. Lipids* 159:114-118.

99. Gauthier,C., J.Legault, K.Girard-Lalancette, V.Mshvildadze, and A.Pichette. 2009. Haemolytic activity, cytotoxicity and membrane cell permeabilization of semi-synthetic and natural lupane- and oleanane-type saponins. *Bioorg. Med. Chem.* 17:2002-2008.

100. Gawrisch,K. 2005. The dynamics of membrane lipids. *In* The structure of biological membranes. P.L.Yeagle, editor. CRC Press LLC, Boca Raton. 147-71.

101. George,K.S. and S.Wu. 2012. Lipid raft: A floating island of death or survival. *Toxicol. Appl. Pharmacol.* 259:311-319.

102. Gepdiremen,A., V.Mshvildadze, H.Suleyman, and R.Elias. 2005. Acute anti-inflammatory activity of four saponins isolated from ivy: alpha-hederin, hederasaponin-C, hederacolchiside-E and hederacolchiside-F in carrageenan-induced rat paw edema. *Phytomedicine.* 12:440-444.

103. Gerkens,P.C., R.Dobson, N.Tabatadze, V.Mshviladzade, R.Elias, O.J.Peulen, O.M.Jolois, and M.C.Pauw-Gillet. 2007. Apoptosis and cytolysis induced by giganteosides and hederacolchisides in HL-60 cells. *Anticancer Res.* 27:2529-2534.

104. Giessen,T.W. and M.A.Marahiel. 2012. Ribosome-independent biosynthesis of biologically active peptides: Application of synthetic biology to generate structural diversity. *FEBS Lett.* 586:2065-2075.

105. Gilabert-Oriol,R., K.Mergel, M.Thakur, B.von Mallinckrodt, M.F.Melzig, H.Fuchs, and A.Weng. 2013. Real-time analysis of membrane permeabilizing effects of oleanane saponins. *Bioorg. Med Chem.* 21:2387-2395.

106. Giocondi,M.C., D.Yamamoto, E.Lesniewska, P.E.Milhiet, T.Ando, and G.C.Le. 2010. Surface topography of membrane domains. *Biochim. Biophys. Acta* 1798:703-718.

107. Gogelein,H. and A.Huby. 1984. Interaction of saponin and digitonin with black lipid membranes and lipid monolayers. *Biochim. Biophys. Acta - Biomembranes* 773:32-38.

108. Gorter,E. and F.Grendel. 1925. On bimolecular layers of lipoids on the chromocytes of the blood. *J. Exp. Med.* 41:439-443.

109. Grimaldi,R., F.De Ponti, L.D'Angelo, M.Caravaggi, G.Guidi, S.Lecchini, G.M.Frigo, and A.Crema. 1990. Pharmacokinetics of the total triterpenic fraction of Centella asiatica after single and multiple administrations to healthy volunteers. A new assay for asiatic acid. *J. Ethnopharmacol.* 28:235-241.

110. Guan,F., Y.Shan, X.Zhao, D.Zhang, M.Wang, F.Peng, B.Xia, and X.Feng. 2011. Apoptosis and membrane permeabilisation induced by macranthoside B on HL-60 cells. *Nat. Prod. Res.* 25:332-340.

111. Gulcin,I., V.Mshvildadze, A.Gepdiremen, and R.Elias. 2004. Antioxidant activity of saponins isolated from ivy: alpha-hederin, hederasaponin-C, hederacolchiside-E and hederacolchiside-F. *Planta Med.* 70:561-563.

112. Guo,L.Y., E.J.Joo, K.H.Son, S.J.Jeon, S.Jang, E.M.Shin, H.Y.Zhou, and Y.S.Kim. 2009. Cimiside E arrests cell cycle and induces cell apoptosis in gastric cancer cells. *Arch. Pharm. Res.* 32:1385-1392.

113. Gurtovenko,A.A. and J.Anwar. 2007. Ion transport through chemically induced pores in protein-free phospholipid membranes. *J. Phys. Chem. B* 111:13379-13382.

114. Hallock,K.J., D.K.Lee, and A.Ramamoorthy. 2003. MSI-78, an analogue of the magainin antimicrobial peptides, disrupts lipid bilayer structure via positive curvature strain. *Biophys. J.* 84:3052-3060.

115. Ham,Y.M., J.H.Lim, H.K.Na, J.S.Choi, B.D.Park, H.Yim, and S.K.Lee. 2006. Ginsenoside-Rh2-induced mitochondrial depolarization and apoptosis are associated with reactive oxygen species- and Ca2+-mediated c-Jun NH2-terminal kinase 1 activation in HeLa cells. *J. Pharmacol. Exp. Ther.* 319:1276-1285.

116. Haney,E.F., S.Nathoo, H.J.Vogel, and E.J.Prenner. 2010. Induction of non-lamellar lipid phases by antimicrobial peptides: a potential link to mode of action. *Chem. Phys. Lipids* 163:82-93.

117. Harada,S. 2005. The broad anti-viral agent glycyrrhizin directly modulates the fluidity of plasma membrane and HIV-1 envelope. *Biochem. J.* 392:191-199.

118. Haridas,V., X.Li, T.Mizumachi, M.Higuchi, V.V.Lemeshko, M.Colombini, and J.U.Gutterman. 2007. Avicins, a novel plant-derived metabolite lowers energy metabolism in tumor cells by targeting the outer mitochondrial membrane. *Mitochondrion.* 7:234-240.

119. Hase,J., K.Kobashi, K.Mitsui, T.Namba, M.Yoshizaki, and T.Tomimori. 1981. The structure-hemolysis relationship of oleanolic acid derivatives and inhibition of the saponin-induced hemolysis with sapogenins. *J. Pharmacobiodyn.* 4:833-837.

120. Haslam,R.M. and W.Klyne. 1953. The precipitation of 3beta-hydroxysteroids by digitonin. *Biochem. J.* 55:340-346.

121. Haslewood,G.A. 1947. Digitonides of steroid ketones. *Biochem. J.* 41:xli.

122. Hathaway,W.E., L.A.Newby, and J.H.Githens. 1964. The acridine orange viability test applied to bone marrow cells. I. Correlation with trypan blue exclusion and eosin dye exclusion and tissue culture transformation. *Blood* 23:517-525.

123. Haworth,R.A. and D.R.Hunter. 1979. The Ca2+-induced membrane transition in mitochondria. II. Nature of the Ca2+ trigger site. *Arch. Biochem. Biophys.* 195:460-467.

124. He,F., W.Liu, S.Zheng, L.Zhou, B.Ye, and Z.Qi. 2012. Ion transport through dimethyl sulfoxide (DMSO) induced transient water pores in cell membranes. *Mol. Membr. Biol* 29:107-113.

125. Heberle,F.A., J.Wu, S.L.Goh, R.S.Petruzielo, and G.W.Feigenson. 2010. Comparison of three ternary lipid bilayer mixtures: FRET and ESR reveal nanodomains. *Biophys. J.* 99:3309-3318.

126. Heerklotz,H. 2001. Membrane stress and permeabilization induced by asymmetric incorporation of compounds. *Biophys. J.* 81:184-195.

127. Heerklotz,H. and J.Seelig. 2001. Detergent-like action of the antibiotic peptide surfactin on lipid membranes. *Biophys. J.* 81:1547-1554.

128. Heerklotz,H. and J.Seelig. 2007. Leakage and lysis of lipid membranes induced by the lipopeptide surfactin. *Eur. Biophys. J.* 36:305-314.

129. Heffer-Lauc,M., B.Viljetic, K.Vajn, R.L.Schnaar, and G.Lauc. 2007. Effects of detergents on the redistribution of gangliosides and GPI-anchored proteins in brain tissue sections. *J. Histochem. Cytochem.* 55:805-812.

130. Heiner,A.L., E.Gibbons, J.L.Fairbourn, L.J.Gonzalez, C.O.McLemore, T.J.Brueseke, A.M.Judd, and J.D.Bell. 2008. Effects of cholesterol on physical properties of human erythrocyte membranes: impact on susceptibility to hydrolysis by secretory phospholipase A2. *Biophys. J.* 94:3084-3093.

131. Helfrich,W. 1973. Elastic properties of lipid bilayers: theory and possible experiments. *Z. Naturforsch. C.* 28:693-703.

132. Hope,M.J., M.B.Bally, G.Webb, and P.R.Cullis. 1985. Production of Large Unilamellar Vesicles by A Rapid Extrusion Procedure - Characterization of Size Distribution, Trapped Volume and Ability to Maintain A Membrane-Potential. *Biochimica et Biophysica Acta* 812:55-65.

133. Hu,K.F., S.Berenjian, R.Larsson, J.Gullbo, P.Nygren, T.Lovgren, and B.Morein. 2010. Nanoparticulate Quillaja saponin induces apoptosis in human leukemia cell lines with a high therapeutic index. *International Journal of Nanomedicine* 5:51-62.

134. Hu,M., K.Konoki, and K.Tachibana. 1996. Cholesterol-independent membrane disruption caused by triterpenoid saponins. *Biochim. Biophys. Acta - Biomembranes* 1299:252-258.

135. Hunter,D.R. and R.A.Haworth. 1979a. The Ca2+-induced membrane transition in mitochondria. I. The protective mechanisms. *Arch. Biochem. Biophys.* 195:453-459.

136. Hunter,D.R. and R.A.Haworth. 1979b. The Ca2+-induced membrane transition in mitochondria. III. Transitional Ca2+ release. *Arch. Biochem. Biophys.* 195:468-477.

137. Hur,G.H., C.R.Vickery, and M.D.Burkart. 2012. Explorations of catalytic domains in non-ribosomal peptide synthetase enzymology. *Nat. Prod. Rep.* 29:1074-1098.

138. Hwang,Y.S., K.K.Park, and W.Y.Chung. 2012. Kalopanaxsaponin A inhibits the invasion of human oral squamous cell carcinoma by reducing metalloproteinase-9 mRNA stability and protein trafficking. *Biol Pharm Bull* 35:289-300.

139. Iisalo,E. 1977. Clinical pharmacokinetics of digoxin. *Clin. Pharmacokinet.* 2:1-16.

140. Ilangumaran,S. and D.C.Hoessli. 1998. Effects of cholesterol depletion by cyclodextrin on the sphingolipid microdomains of the plasma membrane. *Biochem. J.* 335 (Pt 2):433-440.

141. Inamitsu,T. and I.Ohtsuki. 1984. Characterization of ATP-dependent Ca2+ uptake by canine brain microsomes with saponin. *Eur. J. Biochem.* 145:115-121.

142. Ioffe,D.V. 1986. Sterols as complex-forming species. *Russian chemical reviews* 55:333-349.

143. Ishida,H., Y.Hirota, and H.Nakazawa. 1993. Effect of sub-skinning concentrations of saponin on intracellular Ca2+ and plasma membrane fluidity in cultured cardiac cells. *Biochim. Biophys. Acta - Biomembranes* 1145:58-62.

144. Israelachvili,J.N. 1976. Theory of self-assembly of hydrocarbon amphiphiles into micelles and bilayers. *Journal of Chemical society, Farady transactions* 72:1525-1568.

145. Israelachvili,J.N. 2011. Intermolecular and Surface Forces. Academic Press, Elsevier, Amsterdam.

146. Israelachvili,J.N., D.J.Mitchell, and B.W.Ninham. 1977. Theory of self-assembly of lipid bilayers and vesicles. *Biochim. Biophys. Acta - Biomembranes* 470:185-201.

147. Jacobson,K., O.G.Mouritsen, and R.G.W.Anderson. 2007. Lipid rafts: at a crossroad between cell biology and physics. *Nature Cell Biology* 9:7-14.

148. Jeong,S.I., B.Zhou, J.B.Bae, N.S.Kim, S.G.Kim, J.Kwon, D.K.Kim, T.Y.Shin, H.Jeon, J.P.Lim, H.Kim, H.K.Kim, and C.H.Oh. 2008. Apoptosis-inducing effect of akebia saponin D from the roots of Dipsacus asper Wall in U937 cells. *Arch. Pharm. Res.* 31:1399-1404.

149. Jian,H.L., X.X.Liao, L.W.Zhu, W.M.Zhang, and J.X.Jiang. 2011. Synergism and foaming properties in binary mixtures of a biosurfactant derived from Camellia oleifera Abel and synthetic surfactants. *J. Colloid Interface Sci.* 359:487-492.

150. Jiang,Y.S., Z.X.Jin, H.Umehara, and T.Ota. 2010. Cholesterol-dependent induction of dendrite formation by ginsenoside Rh2 in cultured melanoma cells. *Int. J. Mol. Med.* 26:787-793.

151. Jin,J.O., V.V.Shastina, S.W.Shin, Q.Xu, J.I.Park, V.A.Rasskazov, S.A.Avilov, S.N.Fedorov, V.A.Stonik, and J.Y.Kwak. 2009. Differential effects of triterpene glycosides, frondoside A and cucumarioside A2-2 isolated from sea cucumbers on caspase activation and apoptosis of human leukemia cells. *FEBS Lett.* 583:697-702.

152. Jin,Z. and W.S.El Deiry. 2005. Overview of cell death signaling pathways. *Cancer Biol. Ther.* 4:139-163.

153. John,K., S.Schreiber, J.Kubelt, A.Herrmann, and P.Muller. 2002. Transbilayer movement of phospholipids at the main phase transition of lipid membranes: implications for rapid flip-flop in biological membranes. *Biophys. J.* 83:3315-3323.

154. Jokela,J., L.Oftedal, L.Herfindal, P.Permi, M.Wahlsten, S.O.Doskeland, and K.Sivonen. 2012. Anabaenolysins, novel cytolytic lipopeptides from benthic Anabaena cyanobacteria. *PLoS. One.* 7:e41222.

155. Jones,P.J., D.E.MacDougall, F.Ntanios, and C.A.Vanstone. 1997. Dietary phytosterols as cholesterol-lowering agents in humans. *Can. J. Physiol Pharmacol.* 75:217-227.

156. Juhasz,J., J.H.Davis, and F.J.Sharom. 2010. Fluorescent probe partitioning in giant unilamellar vesicles of 'lipid raft' mixtures. *Biochem. J.* 430:415-423.

157. Jung,H.J., C.O.Lee, K.T.Lee, J.Choi, and H.J.Park. 2004. Structure-activity relationship of oleanane disaccharides isolated from Akebia quinata versus cytotoxicity against cancer cells and NO inhibition. *Biol. Pharm. Bull.* 27:744-747.

158. Kanatomo,S., S.Nagai, K.Ohki, and Y.Yasuda. 1995. Study on surfactin, a cyclic depsipeptide. I. Isolation and structure of eight surfactin analogs produced by Bacillus natto KMD 2311. *Yakugaku Zasshi* 115:756-764.

159. Karatekin,E., O.Sandre, H.Guitouni, N.Borghi, P.H.Puech, and F.Brochard-Wyart. 2003. Cascades of transient pores in giant vesicles: line tension and transport. *Biophys. J.* 84:1734-1749.

160. Kersten,G.F. and D.J.Crommelin. 1995. Liposomes and ISCOMS as vaccine formulations. *Biochim. Biophys. Acta - Rev. on Biomembranes* 1241:117-138.

161. Keukens,E.A., T.de Vrije, C.van den Boom, P.de Waard, H.H.Plasman, F.Thiel, V.Chupin, W.M.Jongen, and B.de Kruijff. 1995. Molecular basis of glycoalkaloid induced membrane disruption. *Biochim. Biophys. Acta - Biomembranes* 1240:216-228.

162. Kharakoz,D.P., A.Colotto, K.Lohner, and P.Laggner. 1993. Fluid-gel interphase line tension and density fluctuations in dipalmitoylphosphatidylcholine multilamellar vesicles: an ultrasonic study. *Journal of Physical Chemistry B* 97:9844-9851.

163. Kim,D.W., K.H.Bang, Y.H.Rhee, K.T.Lee, and H.J.Park. 1998. Growth inhibitory activities of kalopanaxsaponins A and I against human pathogenic fungi. *Arch. Pharm. Res.* 21:688-691.

164. Kim,d.Y., M.W.Park, H.D.Yuan, H.J.Lee, S.H.Kim, and S.H.Chung. 2009. Compound K induces apoptosis via CAMK-IV/AMPK pathways in HT-29 colon cancer cells. *J. Agric. Food Chem.* 57:10573-10578.

165. Kim,J.Y., C.Y.Choi, and H.G.Jeong. 2005. Involvement of cytokines in the hepatic metallothionein expression by alpha-hederin. *Planta Med.* 71:743-747.

166. Kim,M.O., D.O.Moon, Y.H.Choi, D.Y.Shin, H.S.Kang, B.T.Choi, J.D.Lee, W.Li, and G.Y.Kim. 2008a. Platycodin D induces apoptosis and decreases telomerase activity in human leukemia cells. *Cancer Lett.* 261:98-107.

167. Kim,S.Y., J.Y.Kim, S.H.Kim, H.J.Bae, H.Yi, S.H.Yoon, B.S.Koo, M.Kwon, J.Y.Cho, C.E.Lee, and S.Hong. 2007. Surfactin from Bacillus subtilis displays anti-proliferative effect via apoptosis induction, cell cycle arrest and survival signaling suppression. *FEBS Lett.* 581:865-871.

168. Kim,Y.J., H.C.Kwon, H.Ko, J.H.Park, H.Y.Kim, J.H.Yoo, and H.O.Yang. 2008b. Anti-tumor activity of the ginsenoside Rk1 in human hepatocellular carcinoma cells through inhibition of telomerase activity and induction of apoptosis. *Biol. Pharm. Bull.* 31:826-830.

169. Kim,Y.H. 1997. Studies on components of Patrinia scabiosaefolia. *Saengyak Hakhoechi* 28:93-98.

170. King,F.W., S.Fong, C.Griffin, M.Shoemaker, R.Staub, Y.L.Zhang, I.Cohen, and E.Shtivelman. 2009. Timosaponin AIII is preferentially cytotoxic to tumor cells through inhibition of mTOR and induction of ER stress. *PLoS. One.* 4:e7283.

171. Kleinschmidt,J.H. and L.K.Tamm. 2002. Structural transitions in short-chain lipid assemblies studied by (31)P-NMR spectroscopy. *Biophys. J.* 83:994-1003.

172. Knobler,C.M. and R.C.Desai. 1992. Phase transitions in monolayers. *Annu. Rev. Phys. Chem.* 43:207-236.

173. Ko,H., Y.J.Kim, J.S.Park, J.H.Park, and H.O.Yang. 2009. Autophagy inhibition enhances apoptosis induced by ginsenoside Rk1 in hepatocellular carcinoma cells. *Biosci. Biotechnol. Biochem.* 73:2183-2189.

174. Kostetsky,E.Y., N.M.Sanina, A.N.Mazeika, A.V.Tsybulsky, N.S.Vorobyeva, and V.L.Shnyrov. 2011. Tubular immunostimulating complex based on cucumarioside A2-2 and monogalactosyldiacylglycerol from marine macrophytes. *J. Nanobiotechnology.* 9:35.

175. Kowaltowski,A.J., R.F.Castilho, and A.E.Vercesi. 1996. Opening of the mitochondrial permeability transition pore by uncoupling or inorganic phosphate in the presence of Ca2+ is dependent on mitochondrial-generated reactive oxygen species. *FEBS Lett.* 378:150-152.

176. Kracht,M., H.Rokos, M.Ozel, M.Kowall, G.Pauli, and J.Vater. 1999. Antiviral and hemolytic activities of surfactin isoforms and their methyl ester derivatives. *J. Antibiot. (Tokyo)* 52:613-619.

177. Kragh-Hansen,U., M.le Maire, and J.V.Moller. 1998. The mechanism of detergent solubilization of liposomes and protein-containing membranes. *Biophys. J.* 75:2932-2946.

178. Kritharides,L., A.Christian, G.Stoudt, D.Morel, and G.H.Rothblat. 1998. Cholesterol metabolism and efflux in human THP-1 macrophages. *Arterioscler. Thromb. Vasc. Biol* 18:1589-1599.

179. Kroemer,G., L.Galluzzi, P.Vandenabeele, J.Abrams, E.S.Alnemri, E.H.Baehrecke, M.V.Blagosklonny, W.S.El Deiry, P.Golstein, D.R.Green, M.Hengartner, R.A.Knight, S.Kumar, S.A.Lipton, W.Malorni, G.Nunez, M.E.Peter, J.Tschopp, J.Yuan, M.Piacentini, B.Zhivotovsky, and G.Melino. 2009. Classification of cell death: recommendations of the Nomenclature Committee on Cell Death 2009. *Cell Death Differ.* 16:3-11.

180. Kumar,A., M.Kumar, T.Y.Park, M.H.Park, T.Takemoto, T.Terado, M.Kitano, and H.Kimura. 2009. Molecular mechanisms of ginsenoside Rp1-mediated growth arrest and apoptosis. *Int. J. Mol. Med.* 24:381-386.

181. Kumar,V.V. 1991. Complementary molecular shapes and additivity of the packing parameter of lipids. *Proc. Natl. Acad. Sci. U. S. A* 88:444-448.

182. Kumara,S.S. and B.T.Huat. 2001. Extraction, isolation and characterisation of antitumor principle, alpha-hederin, from the seeds of Nigella sativa. *Planta Med.* 67:29-32.

183. Kwon,H.Y., E.H.Kim, S.W.Kim, S.N.Kim, J.D.Park, and D.K.Rhee. 2008. Selective toxicity of ginsenoside Rg3 on multidrug resistant cells by membrane fluidity modulation. *Arch. Pharm. Res.* 31:171-177.

184. Ladbrooke,B.D., R.M.Williams, and D.Chapman. 1968. Studies on lecithin-cholesterol-water interactions by differential scanning calorimetry and X-ray diffraction. *Biochim. Biophys. Acta - Biomembranes* 150:333-340.

185. Ladokhin,A.S. and S.H.White. 2001. 'Detergent-like' permeabilization of anionic lipid vesicles by melittin. *Biochim. Biophys. Acta - Biomembranes* 1514:253-260.

186. Lafleur,M., M.Bloom, E.F.Eikenberry, S.M.Gruner, Y.Han, and P.R.Cullis. 1996. Correlation between lipid plane curvature and lipid chain order. *Biophys. J.* 70:2747-2757.

187. Lange,Y., J.Ye, M.E.Duban, and T.L.Steck. 2009. Activation of membrane cholesterol by 63 amphipaths. *Biochemistry* 48:8505-8515.

188. Lange,Y., J.Ye, and T.L.Steck. 2005. Activation of membrane cholesterol by displacement from phospholipids. *J. Biol Chem.* 280:36126-36131.

189. Launikonis,B.S. and D.G.Stephenson. 1999. Effects of beta-escin and saponin on the transverse-tubular system and sarcoplasmic reticulum membranes of rat and toad skeletal muscle. *Pflugers Archiv-European Journal of Physiology* 437:955-965.

190. Lavaud,C., L.Voutquenne, G.Massiot, L.Le Men-Olivier, and C.Delaude. 1995. Triterpenoid saponins from Smelophyllum capense (Sapindaceae). *Bull. Soc. R. Sci. Liege* 63:455-463.

191. Lee,J.C., C.L.Su, L.L.Chen, and S.J.Won. 2009. Formosanin C-induced apoptosis requires activation of caspase-2 and change of mitochondrial membrane potential. *Cancer Sci.* 100:503-513.

192. Lee,K.T., I.C.Sohn, H.J.Park, D.W.Kim, G.O.Jung, and K.Y.Park. 2000. Essential moiety for antimutagenic and cytotoxic activity of hederagenin monodesmosides and bisdesmosides isolated from the stem bark of Kalopanax pictus. *Planta Med.* 66:329-332.

193. Lee,R.C., F.Despa, X.Tang, I.Titushkin, and M.Cho. 2006. Direct observation of the p188 mediated membrane sealing with atomic force microscopy. *Molecular and Cellular Biomechanics* 3:185-186.

194. Legembre,P., S.Daburon, P.Moreau, F.Ichas, F.de Giorgi, J.F.Moreau, and J.L.Taupin. 2005. Amplification of Fas-mediated apoptosis in type II cells via microdomain recruitment. *Mol. Cell Biol.* 25:6811-6820.

195. Lemeshko,V.V., V.Haridas, J.C.Quijano Perez, and J.U.Gutterman. 2006. Avicins, natural anticancer saponins, permeabilize mitochondrial membranes. *Arch. Biochem. Biophys.* 454:114-122.

196. Lenne,P.F., L.Wawrezinieck, F.Conchonaud, O.Wurtz, A.Boned, X.J.Guo, H.Rigneault, H.T.He, and D.Marguet. 2006. Dynamic molecular confinement in the plasma membrane by microdomains and the cytoskeleton meshwork. *EMBO J.* 25:3245-3256.

197. Lentz,B.R., D.A.Barrow, and M.Hoechli. 1980. Cholesterol-phosphatidylcholine interactions in multilamellar vesicles. *Biochemistry* 19:1943-1954.

198. Leslie,M. 2011. Mysteries of the cell. Do lipid rafts exist? *Science* 334:1046-1047.

199. Leung,Y.M., Y.J.Ou, C.Y.Kwan, and T.T.Loh. 1997. Specific interaction between tetrandrine and Quillaja saponins in promoting permeabilization of plasma membrane in human leukemic HL-60 cells. *Biochim. Biophys. Acta - Biomembranes* 1325:318-328.

200. Levin,S. and R.Korenstein. 1991. Membrane fluctuations in erythrocytes are linked to MgATP-dependent dynamic assembly of the membrane skeleton. *Biophys. J.* 60:733-737.

201. Lewis,R.N. and R.N.McElhaney. 2000. Surface charge markedly attenuates the nonlamellar phase-forming propensities of lipid bilayer membranes: calorimetric and (31)P-nuclear magnetic resonance studies of mixtures of cationic, anionic, and zwitterionic lipids. *Biophys. J.* 79:1455-1464.

202. Lewis,R.N.A.H. and R.N.McElhaney. 2005. The mesomorphic phase behaviour of lipid bilayers. *In* The structure of biological membranes. P.L.Yeagle, editor. CRC Press, 53-120.

203. Li,D.W., J.E.Hyun, C.S.Jeong, Y.S.Kim, and E.B.Lee. 2003. Antiinflammatory activity of alpha-hederin methyl ester from the alkaline hydrolysate of the butanol fraction of Kalopanax pictus bark extract. *Biol Pharm Bull* 26:429-433.

204. Li,X.X., B.Davis, V.Haridas, J.U.Gutterman, and M.Colombini. 2005. Proapoptotic triterpene electrophiles (avicins) form channels in membranes: cholesterol dependence. *Biophys. J.* 88:2577-2584.

205. Li,Y.C., M.J.Park, S.K.Ye, C.W.Kim, and Y.N.Kim. 2006. Elevated levels of cholesterol-rich lipid rafts in cancer cells are correlated with apoptosis sensitivity induced by cholesterol-depleting agents. *Am. J. Pathol.* 168:1107-1118.

206. Lichtenberg,D., E.Opatowski, and M.M.Kozlov. 2000. Phase boundaries in mixtures of membrane-forming amphiphiles and micelle-forming amphiphiles. *Biochim. Biophys. Acta - Biomembranes* 1508:1-19.

207. Lichtenberg,D., R.J.Robson, and E.A.Dennis. 1983. Solubilization of phospholipids by detergents. Structural and kinetic aspects. *Biochim. Biophys. Acta - Rev. on Biomembranes* 737:285-304.

208. Lichtenthaler,H.K. 1999. The 1-deoxy-D-xylulose-5-phosphate pathway of isoprenoid biosynthesis in plants. *Annu. Rev. Plant Physiol Plant Mol. Biol* 50:47-65.

209. Lin,F. and R.Wang. 2010. Hemolytic mechanism of dioscin proposed by molecular dynamics simulations. *J. Mol. Model.* 16:107-118.

210. Lin,H., X.Zhang, G.Cheng, H.F.Tang, W.Zhang, H.N.Zhen, J.X.Cheng, B.L.Liu, W.D.Cao, W.P.Dong, and P.Wang. 2008. Apoptosis induced by ardipusilloside III through BAD dephosphorylation and cleavage in human glioblastoma U251MG cells. *Apoptosis.* 13:247-257.

211. Lin,X., L.Ma, S.B.Racette, C.L.Anderson Spearie, and R.E.Ostlund, Jr. 2009. Phytosterol glycosides reduce cholesterol absorption in humans. *Am. J. Physiol Gastrointest. Liver Physiol* 296:G931-G935.

212. Lingwood,D., J.Ries, P.Schwille, and K.Simons. 2008. Plasma membranes are poised for activation of raft phase coalescence at physiological temperature. *Proc. Natl. Acad. Sci. U. S. A* 105:10005-10010.

213. Lingwood,D. and K.Simons. 2010. Lipid Rafts As a Membrane-Organizing Principle. *Science* 327:46-50.

214. Lins,L., A.Thomas-Soumarmon, T.Pillot, J.Vandekerchkhove, M.Rosseneu, and R.Brasseur. 1999. Molecular determinants of the interaction between the C-terminal domain of Alzheimer's beta-amyloid peptide and apolipoprotein E alpha-helices. *J. Neurochem.* 73:758-769.

215. Liu,G.Y., X.Bu, H.Yan, and W.W.Jia. 2007. 20S-protopanaxadiol-induced programmed cell death in glioma cells through caspase-dependent and -independent pathways. *J. Nat. Prod.* 70:259-264.

216. Liu,W., X.F.Huang, Q.Qi, Q.S.Dai, L.Yang, F.F.Nie, N.Lu, D.D.Gong, L.Y.Kong, and Q.L.Guo. 2009. Asparanin A induces G(2)/M cell cycle arrest and apoptosis in human hepatocellular carcinoma HepG2 cells. *Biochem. Biophys. Res. Commun.* 381:700-705.

217. Liu,Y., G.Yang, X.Bu, G.Liu, J.Ding, P.Li, and W.Jia. 2011. Cell-type-specific regulation of raft-associated Akt signaling. *Cell Death Dis.* 2:e145.

218. Liu,Z.Q., X.Y.Luo, Y.X.Sun, Y.P.Chen, and Z.C.Wang. 2002. Can ginsenosides protect human erythrocytes against free-radical-induced hemolysis? *Biochim. Biophys. Acta - General Subjects* 1572:58-66.

219. Lohner,K. 2009. New strategies for novel antibiotics: peptides targeting bacterial cell membranes. *Gen. Physiol Biophys.* 28:105-116.

220. Lohner,K., E.Staudegger, E.J.Prenner, R.N.Lewis, M.Kriechbaum, G.Degovics, and R.N.McElhaney. 1999. Effect of staphylococcal delta-lysin on the thermotropic phase behavior and vesicle morphology of dimyristoylphosphatidylcholine lipid bilayer model membranes. Differential scanning calorimetric, 31P nuclear magnetic resonance and Fourier transform infrared spectroscopic, and X-ray diffraction studies. *Biochemistry* 38:16514-16528.

221. London,E. 2005. How principles of domain formation in model membranes may explain ambiguities concerning lipid raft formation in cells. *Biochim. Biophys. Acta-Molecular Cell Research* 1746:203-220.

222. Lorent,J., C.S.Le Duff, J.Quetin-Leclercq, and M.P.Mingeot-Leclercq. 2013. Induction of Highly Curved Structures in Relation to Membrane Permeabilization and Budding by the Triterpenoid Saponins, alpha- and delta-Hederin. *J. Biol Chem.* 288:14000-14017.

223. Lösche,M. 1983. A Fluorescence Microscopic Study Concerning the Phase Diagram of Phospholipids. *Ber. Bundes. Phys. Chem.* 87:848-852.

224. Loura,L.M., A.Fedorov, and M.Prieto. 2001. Fluid-fluid membrane microheterogeneity: a fluorescence resonance energy transfer study. *Biophys. J.* 80:776-788.

225. Loura,L.M., F.Fernandes, and M.Prieto. 2010. Membrane microheterogeneity: Forster resonance energy transfer characterization of lateral membrane domains. *Eur. Biophys. J.* 39:589-607.

226. Loura,L.M. and M.Prieto. 1997. Dehydroergosterol structural organization in aqueous medium and in a model system of membranes. *Biophys. J.* 72:2226-2236.

227. Luzzati,V. 1997. Biological significance of lipid polymorphism: the cubic phases. *Curr. Opin. Struct. Biol* 7:661-668.

228. Madsen,H.B., P.Ifversen, F.Madsen, B.Brodin, I.Hausser, and H.M.Nielsen. 2009. In Vitro Cutaneous Application of ISCOMs on Human Skin Enhances Delivery of Hydrophobic Model Compounds Through the Stratum Corneum. *Aaps Journal* 11:728-739.

229. Mahapatro,A. and D.K.Singh. 2011. Biodegradable nanoparticles are excellent vehicle for site directed in-vivo delivery of drugs and vaccines. *J. Nanobiotechnology.* 9:55.

230. Majester-Savornin,B., R.Elias, A.M.Diaz-Lanza, G.Balansard, M.Gasquet, and F.Delmas. 1991. Saponins of the ivy plant, Hedera helix, and their leishmanicidic activity. *Planta Med.* 57:260-262.

231. Man,S., W.Gao, Y.Zhang, L.Huang, and C.Liu. 2010. Chemical study and medical application of saponins as anti-cancer agents. *Fitoterapia* 81:703-714.

232. Mandal,S.M., A.E.A.D.Barbosa, and O.L.Franco. 2013. Lipopeptides in microbial infection control: Scope and reality for industry. *Biotechnology Advances* 31:338-345.

233. Marsh,D. 1996. Intrinsic curvature in normal and inverted lipid structures and in membranes. *Biophys. J.* 70:2248-2255.

234. Matsumoto,K., J.Kusaka, A.Nishibori, and H.Hara. 2006. Lipid domains in bacterial membranes. *Mol. Microbiol.* 61:1110-1117.

235. Mazzucchelli,G.D., N.A.Cellier, V.Mshviladzade, R.Elias, Y.H.Shim, D.Touboul, L.Quinton, A.Brunelle, O.Laprevote, E.A.De Pauw, and M.C.Pauw-Gillet. 2008. Pores formation on cell membranes by hederacolchiside A1 leads to a rapid release of proteins for cytosolic subproteome analysis. *J. Proteome. Res.* 7:1683-1692.

236. McIntosh,A.L., A.M.Gallegos, B.P.Atshaves, S.M.Storey, D.Kannoju, and F.Schroeder. 2003. Fluorescence and multiphoton imaging resolve unique structural forms of sterol in membranes of living cells. *J. Biol Chem.* 278:6384-6403.

237. McMullen,T.P., C.Vilcheze, R.N.McElhaney, and R.Bittman. 1995. Differential scanning calorimetric study of the effect of sterol side chain length and structure on dipalmitoylphosphatidylcholine thermotropic phase behavior. *Biophys. J.* 69:169-176.

238. McMullen,T.P.W., R.N.A.H.Lewis, and R.N.McElhaney. 2004. Cholesterol phospholipid interactions, the liquid-ordered phase and lipid rafts in model and biological membranes. *Current Opinion in Colloid & Interface Science* 8:459-468.

239. Mehta,S.K., S.Sharma, N.Mehta, and S.S.Cameotra. 2010. Biomimetic amphiphiles: properties and potential use. *Adv. Exp. Med. Biol.* 672:102-120.

240. Meinhardt,S., R.L.Vink, and F.Schmid. 2013. Monolayer curvature stabilizes nanoscale raft domains in mixed lipid bilayers. *Proc. Natl. Acad. Sci. U. S. A* 110:4476-4481.

241. Meleard,P., C.Gerbeaud, T.Pott, L.Fernandez-Puente, I.Bivas, M.D.Mitov, J.Dufourcq, and P.Bothorel. 1997. Bending elasticities of model membranes: influences of temperature and sterol content. *Biophys. J.* 72:2616-2629.

242. Meyer Bodansky. 1929. The effect of hydrogen ion concentration on saponin hemolysis. *J. Biol. Chem.* 82:567-577.

243. Mitra,S. and S.R.Dungan. 1997. Micellar properties of quillaja saponin. 1. Effects of temperature, salt, and pH on solution properties. *Journal of Agricultural and Food Chemistry* 45:1587-1595.

244. Mitra,S. and S.R.Dungan. 2000. Micellar properties of quillaja saponin. 2. Effect of solubilized cholesterol on solution properties. *Colloids and Surfaces B-Biointerfaces* 17:117-133.

245. Mitra,S. and S.R.Dungan. 2001. Cholesterol solubilization in aqueous micellar solutions of quillaja saponin, bile salts, or nonionic surfactants. *J. Agric. Food Chem.* 49:384-394.

246. Mizuno,N., J.Varkey, N.C.Kegulian, B.G.Hegde, N.Cheng, R.Langen, and A.C.Steven. 2012. Remodeling of lipid vesicles into cylindrical micelles by alpha-synuclein in an extended alpha-helical conformation. *J. Biol. Chem.* 287:29301-29311.

247. Montero,J., A.Morales, L.Llacuna, J.M.Lluis, O.Terrones, G.Basanez, B.Antonsson, J.Prieto, C.Garcia-Ruiz, A.Colell, and J.C.Fernandez-Checa. 2008. Mitochondrial cholesterol contributes to chemotherapy resistance in hepatocellular carcinoma. *Cancer Res.* 68:5246-5256.

248. Morehouse,L.A., F.W.Bangerter, M.P.DeNinno, P.B.Inskeep, P.A.McCarthy, J.L.Pettini, Y.E.Savoy, E.D.Sugarman, R.W.Wilkins, T.C.Wilson, H.A.Woody, L.M.Zaccaro, and C.E.Chandler. 1999. Comparison of synthetic saponin cholesterol absorption inhibitors in rabbits: evidence for a non-stoichiometric, intestinal mechanism of action. *J. Lipid Res.* 40:464-474.

249. Morrissey,J.P. and A.E.Osbourn. 1999. Fungal resistance to plant antibiotics as a mechanism of pathogenesis. *Microbiol. Mol. Biol Rev.* 63:708-724.

250. Moulin-Traffort,J., A.Favel, R.Elias, and P.Regli. 1998. Study of the action of alpha-hederin on the ultrastructure of Candida albicans. *Mycoses* 41:411-416.

251. Muhr,P., W.Likussar, and M.SchubertZsilavecz. 1996. Structure investigation and proton and carbon-13 assignments of digitonin and cholesterol using multidimensional NMR techniques. *Magnetic Resonance in Chemistry* 34:137-142.

252. Mullauer,F.B., J.H.Kessler, and J.P.Medema. 2010. Betulinic acid, a natural compound with potent anticancer effects. *Anticancer Drugs* 21:215-227.

253. Myschik,J., D.G.Lendemans, W.T.McBurney, P.H.Demana, S.Hook, and T.Rades. 2006. On the preparation, microscopic investigation and application of ISCOMs. *Micron.* 37:724-734.

254. Nag,S.A., J.J.Qin, W.Wang, M.H.Wang, H.Wang, and R.Zhang. 2012. Ginsenosides as Anticancer Agents: In vitro and in vivo Activities, Structure-Activity Relationships, and Molecular Mechanisms of Action. *Front Pharmacol.* 3:25.

255. Nanjundan,M. and F.Possmayer. 2001. Pulmonary lipid phosphate phosphohydrolase in plasma membrane signalling platforms. *Biochem. J.* 358:637-646.

256. Naruse,M., H.Suetomo, T.Matsubara, T.Sato, H.Yanagawa, M.Hoshi, and M.Matsumoto. 2010. Acrosome reaction-related steroidal saponin, Co-ARIS, from the starfish induces structural changes in microdomains. *Dev. Biol* 347:147-153.

257. Nazari,M., M.Kurdi, and H.Heerklotz. 2012. Classifying surfactants with respect to their effect on lipid membrane order. *Biophys. J.* 102:498-506.

258. Nes,W.D. 2011. Biosynthesis of cholesterol and other sterols. *Chem. Rev.* 111:6423-6451.

259. Nielsen,J.K., T.Nagao, H.Okabe, and T.Shinoda. 2010. Resistance in the plant, Barbarea vulgaris, and counter-adaptations in flea beetles mediated by saponins. *J. Chem. Ecol.* 36:277-285.

260. Nishikawa,M., S.Nojima, T.Akiyama, U.Sankawa, and K.Inoue. 1984. Interaction of Digitonin and Its Analogs with Membrane Cholesterol. *Journal of Biochemistry* 96:1231-1239.

261. Niu,Y.P., L.M.Wu, Y.L.Jiang, W.X.Wang, and L.D.Li. 2008. Beta-escin, a natural triterpenoid saponin from Chinese horse chestnut seeds, depresses HL-60 human leukaemia cell proliferation and induces apoptosis. *J. Pharm. Pharmacol.* 60:1213-1220.

262. Oftedal,L., L.Myhren, J.Jokela, G.Gausdal, K.Sivonen, S.O.Doskeland, and L.Herfindal. 2012. The lipopeptide toxins anabaenolysin A and B target biological membranes in a cholesterol-dependent manner. *Biochim. Biophys. Acta - Biomembranes* 1818:3000-3009.

263. Ohsaki,Y., T.Maeda, and T.Fujimoto. 2005. Fixation and permeabilization protocol is critical for the immunolabeling of lipid droplet proteins. *Histochem. Cell Biol.* 124:445-452.

264. Okunade,A.L., M.P.Elvin-Lewis, and W.H.Lewis. 2004. Natural antimycobacterial metabolites: current status. *Phytochemistry* 65:1017-1032.

265. Ostroumova,O.S., V.V.Malev, M.G.Ilin, and L.V.Schagina. 2010. Surfactin activity depends on the membrane dipole potential. *Langmuir* 26:15092-15097.

266. Ota,T., K.Fujikawa-yamamoto, Z.P.Zong, M.Yamazaki, S.Odashima, I.Kitagawa, H.Abe, and S.Arichi. 1987. Plant-glycoside modulation of cell surface related to control of differentiation in cultured B16 melanoma cells. *Cancer Res.* 47:3863-3867.

267. Owen,D.M., M.A.Neil, P.M.French, and A.I.Magee. 2007. Optical techniques for imaging membrane lipid microdomains in living cells. *Semin. Cell Dev. Biol* 18:591-598.

268. Ozel,M., S.Hoglund, H.R.Gelderblom, and B.Morein. 1989. Quaternary structure of the immunostimulating complex (iscom). *J. Ultrastruct. Mol. Struct. Res.* 102:240-248.

269. Pallas,N.R. and B.A.Pethica. 1985. Liquid-expanded to liquid-condensed transition in lipid monolayers at the air/water interface. *Langmuir* 1:509-513.

270. Pallas,N.R. and B.A.Pethica. 1987. The liquid–vapour transition in monolayers of n-pentadecanoic acid at the air/water interface. *Journal of the Chemical society, Faraday transactions I* 83:585-590.

271. Papadopoulou,K., R.E.Melton, M.Leggett, M.J.Daniels, and A.E.Osbourn. 1999. Compromised disease resistance in saponin-deficient plants. *Proc. Natl. Acad. Sci. U. S. A* 96:12923-12928.

272. Parasassi,T., M.Loiero, M.Raimondi, G.Ravagnan, and E.Gratton. 1993. Absence of lipid gel-phase domains in seven mammalian cell lines and in four primary cell types. *Biochim. Biophys. Acta - Biomembranes* 1153:143-154.

273. Park,E.K., E.J.Lee, S.H.Lee, K.H.Koo, J.Y.Sung, E.H.Hwang, J.H.Park, C.W.Kim, K.C.Jeong, B.K.Park, and Y.N.Kim. 2010. Induction of apoptosis by the ginsenoside Rh2 by internalization of lipid rafts and caveolae and inactivation of Akt. *Br. J. Pharmacol.* 160:1212-1223.

274. Park,H.J., S.H.Kwon, J.H.Lee, K.H.Lee, K.Miyamoto, and K.T.Lee. 2001. Kalopanaxsaponin A is a basic saponin structure for the anti-tumor activity of hederagenin monodesmosides. *Planta Med* 67:118-121.

275. Park,S.Y., J.H.Kim, Y.J.Lee, S.J.Lee, and Y.Kim. 2013. Surfactin suppresses TPA-induced breast cancer cell invasion through the inhibition of MMP-9 expression. *Int. J. Oncol.* 42:287-296.

276. Parker,A., K.Miles, K.H.Cheng, and J.Huang. 2004. Lateral distribution of cholesterol in dioleoylphosphatidylcholine lipid bilayers: cholesterol-phospholipid interactions at high cholesterol limit. *Biophys. J.* 86:1532-1544.

277. Patel,D.N., H.S.Lin, and H.L.Koh. 2012. Quantification of ginsenosides Rh4 and Rk3 in rat plasma by liquid chromatography-tandem mass spectrometry: application to a pre-clinical pharmacokinetic study. *J. Mass Spectrom.* 47:1510-1517.

278. Patlolla,J.M. and C.V.Rao. 2012. Triterpenoids for cancer prevention and treatment: current status and future prospects. *Curr. Pharm Biotechnol.* 13:147-155.

279. Patra,S.K. 2008. Dissecting lipid raft facilitated cell signaling pathways in cancer. *Biochim. Biophys. Acta - Rev. on Cancer* 1785:182-206.

280. Pillion,D.J., J.A.Amsden, C.R.Kensil, and J.Recchia. 1996. Structure-function relationship among Quillaja saponins serving as excipients for nasal and ocular delivery of insulin. *J. Pharm. Sci.* 85:518-524.

281. Ponder,E. 1953. The kinetics of progressive reactions in systems containing saponin, digitonin, and sodium taurocholate. *J. Gen. Physiol* 36:723-732.

282. Popov,A.M. 2003. Comparative study of the effect of different sterols and triterpenoids on permeability of model lipid membranes. *Zh. Evol. Biokhim. Fiziol.* 39:244-249.

283. Popov,J., D.Vobornik, O.Coban, E.Keating, D.Miller, J.Francis, N.O.Petersen, and L.J.Johnston. 2008. Chemical mapping of ceramide distribution in sphingomyelin-rich domains in monolayers. *Langmuir* 24:13502-13508.

284. Prades,J., O.Vogler, R.Alemany, M.Gomez-Florit, S.S.Funari, V.Ruiz-Gutierrez, and F.Barcelo. 2011. Plant pentacyclic triterpenic acids as modulators of lipid membrane physical properties. *Biochim. Biophys. Acta - Biomembranes* 1808:752-760.

285. Prasad,S., V.R.Yadav, B.Sung, S.Reuter, R.Kannappan, A.Deorukhkar, P.Diagaradjane, C.Wei, V.Baladandayuthapani, S.Krishnan, S.Guha, and B.B.Aggarwal. 2012. Ursolic acid inhibits growth and metastasis of human colorectal cancer in an orthotopic nude mouse model by targeting multiple cell signaling pathways: chemosensitization with capecitabine. *Clin. Cancer Res.* 18:4942-4953.

286. Prenner,E.J., R.N.Lewis, K.C.Neuman, S.M.Gruner, L.H.Kondejewski, R.S.Hodges, and R.N.McElhaney. 1997. Nonlamellar phases induced by the interaction of gramicidin S with lipid bilayers. A possible relationship to membrane-disrupting activity. *Biochemistry* 36:7906-7916.

287. Raaijmakers,J.M., B.De, I, O.Nybroe, and M.Ongena. 2010. Natural functions of lipopeptides from Bacillus and Pseudomonas: more than surfactants and antibiotics. *FEMS Microbiol. Rev.* 34:1037-1062.

288. Rafat,M., K.W.Fong, A.Goldsipe, B.C.Stephenson, S.T.Coradetti, T.G.Sambandan, A.J.Sinskey, and C.Rha. 2008. Association (micellization) and partitioning of aglycon triterpenoids. *J. Colloid Interface Sci.* 325:324-330.

289. Raffa,V., O.Vittorio, C.Riggio, and A.Cuschieri. 2010. Progress in nanotechnology for healthcare. *Minim. Invasive. Ther. Allied Technol.* 19:127-135.

290. Raju,J. and R.P.Bird. 2007. Diosgenin, a naturally occurring steroid [corrected] saponin suppresses 3-hydroxy-3-methylglutaryl CoA reductase expression and induces apoptosis in HCT-116 human colon carcinoma cells. *Cancer Lett.* 255:194-204.

291. Ramadurai,S., A.Holt, V.Krasnikov, G.van den Bogaart, J.A.Killian, and B.Poolman. 2009. Lateral diffusion of membrane proteins. *J. Am. Chem. Soc.* 131:12650-12656.

292. Rappolt,M., A.Hickel, F.Bringezu, and K.Lohner. 2003. Mechanism of the lamellar/inverse hexagonal phase transition examined by high resolution x-ray diffraction. *Biophys. J.* 84:3111-3122.

293. Riedl,S., D.Zweytick, and K.Lohner. 2011. Membrane-active host defense peptides--challenges and perspectives for the development of novel anticancer drugs. *Chem. Phys. Lipids* 164:766-781.

294. Roddick,J.G. 1979. Complex formation between solanaceous steroidal glycoalkaloids and free sterols in vitro. *Phytochemistry* 18:1467-1470.

295. Rog,T., M.Pasenkiewicz-Gierula, I.Vattulainen, and M.Karttunen. 2009. Ordering effects of cholesterol and its analogues. *Biochim. Biophys. Acta - Biomembranes* 1788:97-121.

296. Romussi,G., S.Cafaggi, and G.Bignardi. 1980. Hemolytic action and surface activity of triterpene saponins from Anchusa officinalis L. Part 21: On the costituents of Boraginaceae. *Pharmazie* 35:498-499.

297. Rosen,M.J. 1978. Surfactants and Interfacial Phenomenon. Wiley, New York.

298. Ruckenstein,E. and A.Bhakta. 1994. Clustering and its effects on adsorption. *Langmuir* 10:2694-2698.

299. Ruckenstein,E. and B.Q.Li. 1995. A surface equation of state based on clustering of surfactant molecules of insoluble monolayers. *Langmuir* 11:3510-3515.

300. Saddoughi,S.A. and B.Ogretmen. 2013. Diverse functions of ceramide in cancer cell death and proliferation. *Adv. Cancer Res.* 117:37-58.

301. Sakamoto,S., H.Nakahara, T.Uto, Y.Shoyama, and O.Shibata. 2013. Investigation of interfacial behavior of glycyrrhizin with a lipid raft model via a Langmuir monolayer study. *Biochim. Biophys. Acta - Biomembranes* 1828:1271-1283.

302. Sakuma,Y., T.Taniguchi, and M.Imai. 2010. Pore formation in a binary giant vesicle induced by cone-shaped lipids. *Biophys. J.* 99:472-479.

303. Sandstrom,M.C., L.M.Ickenstein, L.D.Mayer, and K.Edwards. 2005. Effects of lipid segregation and lysolipid dissociation on drug release from thermosensitive liposomes. *Journal of Controlled Release* 107:131-142.

304. Sano,K., S.Sanada, Y.Ida, and J.Shoji. 1991. Studies on the constituents of the bark of Kalopanax pictus Nakai. *Chem. Pharm. Bull.* 39:865-870.

305. Sarnthein-Graf,C. and C.La Mesa. 2004. Association of saponins in water and water-gelatine mixtures. *Thermochimica Acta* 418:79-84.

306. Sayyed-Ahmad,A., L.M.Lichtenberger, and A.A.Gorfe. 2010. Structure and dynamics of cholic acid and dodecylphosphocholine-cholic acid aggregates. *Langmuir* 26:13407-13414.

307. Scholz,M., M.Lipinski, M.Leupold, H.Luftmann, L.Harig, R.Ofir, R.Fischer, D.Prufer, and K.J.Muller. 2009. Methyl jasmonate induced accumulation of kalopanaxsaponin I in Nigella sativa. *Phytochemistry* 70:517-522.

308. Schroeder,A., D.A.Heller, M.M.Winslow, J.E.Dahlman, G.W.Pratt, R.Langer, T.Jacks, and D.G.Anderson. 2012. Treating metastatic cancer with nanotechnology. *Nat. Rev. Cancer* 12:39-50.

309. Schroeder,F. 1984. Fluorescent sterols: probe molecules of membrane structure and function. *Prog. Lipid Res.* 23:97-113.

310. Schroeder,F., Y.Barenholz, E.Gratton, and T.E.Thompson. 1987. A fluorescence study of dehydroergosterol in phosphatidylcholine bilayer vesicles. *Biochemistry* 26:2441-2448.

311. Schroeder,R.J., S.N.Ahmed, Y.Zhu, E.London, and D.A.Brown. 1998. Cholesterol and sphingolipid enhance the Triton X-100 insolubility of glycosylphosphatidylinositol-anchored proteins by promoting the formation of detergent-insoluble ordered membrane domains. *J. Biol. Chem.* 273:1150-1157.

312. Seddon,J.M. 1990. Structure of the inverted hexagonal (HII) phase, and non-lamellar phase transitions of lipids. *Biochim. Biophys. Acta - Rev. on Biomembranes* 1031:1-69.

313. Seeman,P. 1967. Transient holes in the erythrocyte membrane during hypotonic hemolysis and stable holes in the membrane after lysis by saponin and lysolecithin. *J. Cell Biol.* 32:55-70.

314. Seeman,P., D.Cheng, and G.H.Iles. 1973. Structure of membrane holes in osmotic and saponin hemolysis. *J. Cell Biol.* 56:519-527.

315. Segal,R., M.Mansour, and D.V.Zaitschek. 1966. Effect of ester groups on the haemolytic action of some saponins and sapogenins. *Biochem. Pharmacol.* 15:1411-1416.

316. Segal,R. and I.Milo-Goldzweig. 1975. On the mechanism of saponin hemolysis. II. Inhibition of hemolysis by aldonolactones. *Biochem. Pharmacol.* 24:77-81.

317. Segal,R. and I.Milo-Goldzweig. 1978. The susceptibility of cholesterol-depleted erythrocytes to saponin and sapogenin hemolysis. *Biochim. Biophys. Acta - Biomembranes* 512:223-226.

318. Segal,R., I.Milo-Goldzweig, G.Kaplan, and E.Weisenberg. 1977. The protective action of glycyrrhizin against saponin toxicity. *Biochem. Pharmacol.* 26:643-645.

319. Segal,R. and E.Schlosser. 1975. Role of glycosidases in the membranlytic, antifungal action of Saponins. *Arch. Microbiol.* 104:147-150.

320. Segal,R., P.Shatkovsky, and I.Milo-Goldzweig. 1974. On the mechanism of saponin hemolysis--I. Hydrolysis of the glycosidic bond. *Biochem. Pharmacol.* 23:973-981.

321. Sehgal,P.B., G.G.Guo, M.Shah, V.Kumar, and K.Patel. 2002. Cytokine signaling: STATS in plasma membrane rafts. *J. Biol. Chem.* 277:12067-12074.

322. Sen,R. 2010. Surfactin: biosynthesis, genetics and potential applications. *Adv. Exp. Med. Biol.* 672:316-323.

323. Servais,H., P.Van Der Smissen, G.Thirion, G.Van der Essen, F.Van Bambeke, P.M.Tulkens, and M.P.Mingeot-Leclercq. 2005. Gentamicin-induced apoptosis in LLC-PK1 cells: involvement of lysosomes and mitochondria. *Toxicol. Appl. Pharmacol.* 206:321-333.

324. Seul,M. and D.Andelman. 1995. Domain shapes and patterns: the phenomenology of modulated phases. *Science* 267:476-483.

325. Seul,M. and M.J.Sammon. 1990. Competing interactions and domain-shape instabilities in a monomolecular film at an air-water interface. *Phys. Rev. Lett.* 64:1903-1906.

326. Shai,Y., A.Makovitzky, and D.Avrahami. 2006. Host defense peptides and lipopeptides: modes of action and potential candidates for the treatment of bacterial and fungal infections. *Curr. Protein Pept. Sci.* 7:479-486.

327. Shanmugam,M.K., X.Dai, A.P.Kumar, B.K.Tan, G.Sethi, and A.Bishayee. 2013. Ursolic acid in cancer prevention and treatment: Molecular targets, pharmacokinetics and clinical studies. *Biochem. Pharmacol.* 85:1579-1587.

328. Shany,S., A.W.Bernheimer, P.S.Grushoff, and K.S.Kim. 1974. Evidence for membrane cholesterol as the common binding site for cereolysin, streptolysin O and saponin. *Mol. Cell Biochem.* 3:179-186.

329. Sheetz,M.P. and S.J.Singer. 1974. Biological membranes as bilayer couples. A molecular mechanism of drug-erythrocyte interactions. *Proc. Natl. Acad. Sci. U. S. A* 71:4457-4461.

330. Shin,D.Y., G.Y.Kim, W.Li, B.T.Choi, N.D.Kim, H.S.Kang, and Y.H.Choi. 2009. Implication of intracellular ROS formation, caspase-3 activation and Egr-1 induction in platycodon D-induced apoptosis of U937 human leukemia cells. *Biomed. Pharmacother.* 63:86-94.

331. Sidhu,G.S. and D.G.Oakenfull. 1986. A mechanism for the hypocholesterolaemic activity of saponins. *Br. J. Nutr.* 55:643-649.

332. Siegel,D.P. 1986. Inverted micellar intermediates and the transitions between lamellar, cubic, and inverted hexagonal amphiphile phases. III. Isotropic and inverted cubic state formation via intermediates in transitions between L+¦ and HII phases. *Chemistry and Physics of Lipids* 42:279-301.

333. Siegel,D.P. 1999. The modified stalk mechanism of lamellar/inverted phase transitions and its implications for membrane fusion. *Biophys. J.* 76:291-313.

334. Siegel,D.P. and R.M.Epand. 1997. The mechanism of lamellar-to-inverted hexagonal phase transitions in phosphatidylethanolamine: implications for membrane fusion mechanisms. *Biophys. J.* 73:3089-3111.

335. Simons,K. and E.Ikonen. 1997. Functional rafts in cell membranes. *Nature* 387:569-572.

336. Simons,K. and W.L.Vaz. 2004. Model systems, lipid rafts, and cell membranes. *Annu. Rev. Biophys. Biomol. Struct.* 33:269-295.

337. Singer,S.J. and G.L.Nicolson. 1972. The fluid mosaic model of the structure of cell membranes. *Science* 175:720-731.

338. Sleep,J., D.Wilson, R.Simmons, and W.Gratzer. 1999. Elasticity of the red cell membrane and its relation to hemolytic disorders: an optical tweezers study. *Biophys. J.* 77:3085-3095.

339. Smith,P.F., A.Ogundele, A.Forrest, J.Wilton, K.Salzwedel, J.Doto, G.P.Allaway, and D.E.Martin. 2007. Phase I and II study of the safety, virologic effect, and pharmacokinetics/pharmacodynamics of single-dose 3-o-(3',3'-dimethylsuccinyl)betulinic acid (bevirimat) against human immunodeficiency virus infection. *Antimicrob. Agents Chemother.* 51:3574-3581.

340. Smyth,T.J.P., A.Perfumo, S.McClean, R.Marchant, and I.M.Bant. 2010. Isolation and Analysis of Lipopeptides and High Molecular Weight Biosurfactants. *In* Handbook of hydrocarbon and Lipid microbiology. Springer Verlag, Berlin. 3689-704.

341. Somerharju,P., J.A.Virtanen, K.H.Cheng, and M.Hermansson. 2009. The superlattice model of lateral organization of membranes and its implications on membrane lipid homeostasis. *Biochim. Biophys. Acta* 1788:12-23.

342. Song,S., L.Zhu, and W.Zhou. 2008. Simultaneous removal of phenanthrene and cadmium from contaminated soils by saponin, a plant-derived biosurfactant. *Environ. Pollut.* 156:1368-1370.

343. Song,X., L.Zang, and S.Hu. 2009. Amplified immune response by ginsenoside-based nanoparticles (ginsomes). *Vaccine* 27:2306-2311.

344. Sonnino,S. and A.Prinetti. 2013. Membrane domains and the "lipid raft" concept. *Curr. Med Chem.* 20:4-21.

345. Sriram,I., B.Singhana, T.R.Lee, and D.K.Schwartz. 2012. Line tension and line activity in mixed monolayers composed of aliphatic and terphenyl-containing surfactants. *Langmuir* 28:16294-16299.

346. Staneva,G., M.Seigneuret, K.Koumanov, G.Trugnan, and M.I.Angelova. 2005. Detergents induce raft-like domains budding and fission from giant unilamellar heterogeneous vesicles: a direct microscopy observation. *Chem. Phys. Lipids* 136:55-66.

347. Stanimirova,R., K.Marinova, S.Tcholakova, N.D.Denkov, S.Stoyanov, and E.Pelan. 2011. Surface rheology of saponin adsorption layers. *Langmuir* 27:12486-12498.

348. Staubach,S. and F.G.Hanisch. 2011. Lipid rafts: signaling and sorting platforms of cells and their roles in cancer. *Expert. Rev. Proteomics.* 8:263-277.

349. Stein,T. 2005. Bacillus subtilis antibiotics: structures, syntheses and specific functions. *Mol. Microbiol.* 56:845-857.

350. Stephenson,B.C., A.Goldsipe, and D.Blankschtein. 2008. Molecular dynamics simulation and thermodynamic modeling of the self-assembly of the triterpenoids asiatic acid and madecassic acid in aqueous solution. *J. Phys. Chem. B* 112:2357-2371.

351. Stine,K.J., R.K.Hercules, J.D.Duff, and B.W.Walker. 2006. Interaction of the glycoalkaloid tomatine with DMPC and sterol monolayers studied by surface pressure measurements and Brewster angle microscopy. *Journal of Physical Chemistry B* 110:22220-22229.

352. Stohlman,E.F. and M.I.Smith. 1934. Experimental saponin anemia in albino rats. *Public Health Reports* 49:751-753.

353. Straus,S.K. and R.E.Hancock. 2006. Mode of action of the new antibiotic for Gram-positive pathogens daptomycin: comparison with cationic antimicrobial peptides and lipopeptides. *Biochim. Biophys. Acta - Biomembranes* 1758:1215-1223.

354. Stuart,M.C. and E.J.Boekema. 2007. Two distinct mechanisms of vesicle-to-micelle and micelle-to-vesicle transition are mediated by the packing parameter of phospholipid-detergent systems. *Biochim. Biophys. Acta - Biomembranes* 1768:2681-2689.

355. Sudbrack,T.P., N.L.Archilha, R.Itri, and K.A.Riske. 2011. Observing the solubilization of lipid bilayers by detergents with optical microscopy of GUVs. *J. Phys. Chem. B* 115:269-277.

356. Sugar,I.P. and P.L.Chong. 2012. A statistical mechanical model of cholesterol/phospholipid mixtures: linking condensed complexes, superlattices, and the phase diagram. *J. Am. Chem. Soc.* 134:1164-1171.

357. Sun,H.X., Y.Xie, and Y.P.Ye. 2009. Advances in saponin-based adjuvants. *Vaccine* 27:1787-1796.

358. Sung,M.K., C.W.Kendall, and A.V.Rao. 1995. Effect of soybean saponins and gypsophila saponin on morphology of colon carcinoma cells in culture. *Food Chem. Toxicol.* 33:357-366.

359. Suzuki,K., K.Ritchie, E.Kajikawa, T.Fujiwara, and A.Kusumi. 2005. Rapid hop diffusion of a G-protein-coupled receptor in the plasma membrane as revealed by single-molecule techniques. *Biophys. J.* 88:3659-3680.

360. Swamy,S.M.K. and B.T.K.Huat. 2003. Intracellular glutathione depletion and reactive oxygen species generation are important in alpha-hederin-induced apoptosis of P388 cells. *Molecular and Cellular Biochemistry* 245:127-139.

361. Sy,L.K., S.C.Yan, C.N.Lok, R.Y.K.Man, and C.M.Che. 2008. Timosaponin A-III Induces Autophagy Preceding Mitochondria-Mediated Apoptosis in HeLa Cancer Cells. *Cancer Research* 68:10229-10237.

362. Tadros,M.M., N.S.Ghaly, and M.N.Moharib. 2008. Molluscicidal and schistosomicidal activities of a steroidal saponin containing fraction from Dracaena fragrans (L.). *J. Egypt. Soc. Parasitol.* 38:585-598.

363. Takechi,M., S.Shimada, and Y.Tanaka. 1992. Time course and inhibition of saponin-induced hemolysis. *Planta Med.* 58:128-130.

364. Takechi,M. and Y.Tanaka. 1995. Haemolytic time course differences between steroid and triterpenoid saponins. *Planta Med.* 61:76-77.

365. Takechi,M., C.Uno, and Y.Tanaka. 1996. Structure-activity relationships of synthetic saponins. *Phytochemistry* 41:121-123.

366. Tanaka,O., Y.Tamura, H.Masuda, and K.Mizutani. 1996. Application of saponins in foods and cosmetics: saponins of Mohave yucca and Sapindus mukurossi. *Adv. Exp. Med. Biol.* 405:1-11.

367. Taverna,E., E.Saba, J.Rowe, M.Francolini, F.Clementi, and P.Rosa. 2004. Role of lipid microdomains in P/Q-type calcium channel (Cav2.1) clustering and function in presynaptic membranes. *J. Biol. Chem.* 279:5127-5134.

368. Tchen,T.T. and K.Bloch. 1957. On the mechanism of enzymatic cyclization of squalene. *J. Biol. Chem.* 226:931-939.

369. Teixeira,V., M.J.Feio, and M.Bastos. 2012. Role of lipids in the interaction of antimicrobial peptides with membranes. *Prog. Lipid Res.* 51:149-177.

370. Tennant,J.R. 1964. Evaluation of the trypan blue technique for determintion of cell viability. *Transplantation* 2:685-694.

371. Thome,W. 1885. Flore von Deutschland, Österreich und der Schweiz. Gera, Zezschwitz, Gera.

372. Tian,A. and T.Baumgart. 2009. Sorting of lipids and proteins in membrane curvature gradients. *Biophys. J.* 96:2676-2688.

373. Tin,M.M., C.H.Cho, K.Chan, A.E.James, and J.K.Ko. 2007. Astragalus saponins induce growth inhibition and apoptosis in human colon cancer cells and tumor xenograft. *Carcinogenesis* 28:1347-1355.

374. Toure,Y., M.Ongena, P.Jacques, A.Guiro, and P.Thonart. 2004. Role of lipopeptides produced by Bacillus subtilis GA1 in the reduction of grey mould disease caused by Botrytis cinerea on apple. *J. Appl. Microbiol.* 96:1151-1160.

375. Trabelsi,S., S.Zhang, T.R.Lee, and D.K.Schwartz. 2008. Linactants: surfactant analogues in two dimensions. *Phys. Rev. Lett.* 100:037802.

376. Trump,B.F. and I.K.Berezesky. 1995. Calcium-mediated cell injury and cell death. *FASEB J.* 9:219-228.

377. Tsamaloukas,A., H.Szadkowska, and H.Heerklotz. 2006. Nonideal mixing in multicomponent lipid/detergent systems. *J. Phys. Condens. Matter* 18:S1125-S1138.

378. Valcarcel,C.A., S.M.Dalla, C.Potrich, I.Bernhart, M.Tejuca, D.Martinez, F.Pazos, M.E.Lanio, and G.Menestrina. 2001. Effects of lipid composition on membrane permeabilization by sticholysin I and II, two cytolysins of the sea anemone Stichodactyla helianthus. *Biophys. J.* 80:2761-2774.

379. van der Haar,A.W. 1912. Phytochemische Untersuchungen in der Familie der Araliaceae. I. Saponinartige Glykoside aus den Bl+ñttern von Polyscias nodosa und Hedera helix. *Arch. Pharm. Pharm. Med. Chem.* 250:560.

380. Van Dyck,S., G.Caulier, M.Todesco, P.Gerbaux, I.Fournier, M.Wisztorski, and P.Flammang. 2011. The triterpene glycosides of Holothuria forskali: usefulness and efficiency as a chemical defense mechanism against predatory fish. *J. Exp. Biol.* 214:1347-1356.

381. Van Echteld,C.J., B.de Kruijff, J.G.Mandersloot, and J.De Gier. 1981. Effects of lysophosphatidylcholines on phosphatidylcholine and phosphatidylcholine/cholesterol liposome systems as revealed by 31P-NMR, electron microscopy and permeability studies. *Biochim. Biophys. Acta - Biomembranes* 649:211-220.

382. van Meer,G. 2005. Cellular lipidomics. *EMBO J.* 24:3159-3165.

383. Veatch,S.L. and S.L.Keller. 2003. Separation of liquid phases in giant vesicles of ternary mixtures of phospholipids and cholesterol. *Biophys. J.* 85:3074-3083.

384. Verdier,M., C.Jayat, M.H.Ratinaud, and D.Troutaud. 2000. Optimization of cell permeabilization for multiparametric flow cytometric analysis with lectin staining. *Cytometry* 41:55-61.

385. Virtanen,J.A., K.H.Cheng, and P.Somerharju. 1998. Phospholipid composition of the mammalian red cell membrane can be rationalized by a superlattice model. *Proc. Natl. Acad. Sci. U. S. A* 95:4964-4969.

386. Virtanen,J.A., M.Ruonala, M.Vauhkonen, and P.Somerharju. 1995. Lateral organization of liquid-crystalline cholesterol-dimyristoylphosphatidylcholine bilayers. Evidence for domains with hexagonal and centered rectangular cholesterol superlattices. *Biochemistry* 34:11568-11581.

387. Vollhardt,D. and V.B.Fainerman. 2006. Progress in characterization of Langmuir monolayers by consideration of compressibility. *Adv. Colloid Interface Sci.* 127:83-97.

388. Voutquenne,L., C.Lavaud, G.Massiot, and L.Men-Olivier. 2002. Structure-activity relationships of haemolytic saponins. *Pharmaceutical Biology* 40:253-262.

389. Walker,B.W., N.Manhanke, and K.J.Stine. 2008. Comparison of the interaction of tomatine with mixed monolayers containing phospholipid, egg sphingomyelin, and sterols. *Biochim. Biophys. Acta - Biomembranes* 1778:2244-2257.

390. Wang,G., H.Chen, M.Huang, N.Wang, J.Zhang, Y.Zhang, G.Bai, W.F.Fong, M.Yang, and X.Yao. 2006. Methyl protodioscin induces G2/M cell cycle arrest and apoptosis in HepG2 liver cancer cells. *Cancer Lett.* 241:102-109.

391. Wang,G.X., D.X.Jiang, J.Li, J.Han, Y.T.Liu, and X.L.Liu. 2010. Anthelmintic activity of steroidal saponins from Dioscorea zingiberensis C. H. Wright against Dactylogyrus intermedius (Monogenea) in goldfish (Carassius auratus). *Parasitol. Res.* 107:1365-1371.

392. Wang,Y., C.M.Che, J.F.Chiu, and Q.Y.He. 2007a. Dioscin (saponin)-induced generation of reactive oxygen species through mitochondria dysfunction: a proteomic-based study. *J. Proteome Res.* 6:4703-4710.

393. Wang,Y., Z.Chen, Y.Liao, C.Mei, H.Peng, M.Wang, H.Guo, and H.Lu. 2007b. Angiotensin II increases the cholesterol content of foam cells via down-regulating the expression of ATP-binding cassette transporter A1. *Biochem. Biophys. Res. Commun.* 353:650-654.

394. Wang,Y., Y.Zhang, Z.Zhu, S.Zhu, Y.Li, M.Li, and B.Yu. 2007c. Exploration of the correlation between the structure, hemolytic activity, and cytotoxicity of steroid saponins. *Bioorg. Med. Chem.* 15:2528-2532.

395. Wassler,M., I.Jonasson, R.Persson, and E.Fries. 1987. Differential permeabilization of membranes by saponin treatment of isolated rat hepatocytes. Release of secretory proteins. *Biochem. J.* 247:407-415.

396. Wassler,M., J.Westman, and E.Fries. 1990. Permeabilization of hepatocytes by a saponin and the effects of dextran. *Eur. J. Cell Biol.* 51:252-258.

397. Williams,J.R. and H.Gong. 2007. Biological activities and syntheses of steroidal saponins: the shark-repelling pavoninins. *Lipids* 42:77-86.

398. Wrenn,S.P., M.Gudheti, A.N.Veleva, E.W.Kaler, and S.P.Lee. 2001. Characterization of model bile using fluorescence energy transfer from dehydroergosterol to dansylated lecithin. *J. Lipid Res.* 42:923-934.

399. Wustner,D. 2007. Fluorescent sterols as tools in membrane biophysics and cell biology. *Chem. Phys. Lipids* 146:1-25.

400. Xavier,C.P., C.F.Lima, D.F.Pedro, J.M.Wilson, K.Kristiansen, and C.Pereira-Wilson. 2013. Ursolic acid induces cell death and modulates autophagy through JNK pathway in apoptosis-resistant colorectal cancer cells. *J. Nutr. Biochem.* 24:706-712.

401. Xiao,J.X., G.Q.Huang, and S.H.Zhang. 2007a. Soyasaponins inhibit the proliferation of Hela cells by inducing apoptosis. *Exp. Toxicol. Pathol.* 59:35-42.

402. Xiao,J.X., G.Q.Huang, C.P.Zhu, D.D.Ren, and S.H.Zhang. 2007b. Morphological study on apoptosis Hela cells induced by soyasaponins. *Toxicol. In Vitro* 21:820-826.

403. Xiao,X., P.Bai, T.M.Bui Nguyen, J.Xiao, S.Liu, G.Yang, L.Hu, X.Chen, X.Zhang, J.Liu, and H.Wang. 2009. The antitumoral effect of Paris Saponin I associated with the induction of apoptosis through the mitochondrial pathway. *Mol. Cancer Ther.*

404. Xiong,J., J.Guo, L.Huang, B.Meng, and Q.Ping. 2008. Self-micelle formation and the incorporation of lipid in the formulation affect the intestinal absorption of Panax notoginseng. *Int. J. Pharm.* 360:191-196.

405. Xu,Z.X., T.Ding, V.Haridas, F.Connolly, and J.U.Gutterman. 2009. Avicin D, a plant triterpenoid, induces cell apoptosis by recruitment of Fas and downstream signaling molecules into lipid rafts. *PLoS. One.* 4:e8532.

406. Xu,Z.X., J.Liang, V.Haridas, A.Gaikwad, F.P.Connolly, G.B.Mills, and J.U.Gutterman. 2007. A plant triterpenoid, avicin D, induces autophagy by activation of AMP-activated protein kinase. *Cell Death and Differentiation* 14:1948-1957.

407. Yaghmur,A., B.Sartori, and M.Rappolt. 2011. The role of calcium in membrane condensation and spontaneous curvature variations in model lipidic systems. *Phys. Chem. Chem. Phys.* 13:3115-3125.

408. Yan,L.H., L.Z.Xu, J.Lin, S.L.Yang, and Y.L.Feng. 2009. Triterpenoid saponins from the stems of Clematis parviloba. *J. Asian Nat. Prod. Res.* 11:332-338.

409. Yi,J.S., H.J.Choo, B.R.Cho, H.M.Kim, Y.N.Kim, Y.M.Ham, and Y.G.Ko. 2009. Ginsenoside Rh2 induces ligand-independent Fas activation via lipid raft disruption. *Biochemical and Biophysical Research Communications* 385:154-159.

410. Yu,K., F.Chen, and C.Li. 2012. Absorption, disposition, and pharmacokinetics of saponins from Chinese medicinal herbs: what do we know and what do we need to know more? *Curr. Drug Metab* 13:577-598.

411. Zhang,C., B.Li, A.S.Gaikwad, V.Haridas, Z.Xu, J.U.Gutterman, and M.Duvic. 2008. Avicin D selectively induces apoptosis and downregulates p-STAT-3, bcl-2, and survivin in cutaneous T-cell lymphoma cells. *J. Invest Dermatol.* 128:2728-2735.

412. Zhang,D.F., H.Xu, B.B.Sun, J.Q.Li, Q.J.Zhou, H.L.Zhang, and A.F.Du. 2012. Adjuvant effect of ginsenoside-based nanoparticles (ginsomes) on the recombinant vaccine against Eimeria tenella in chickens. *Parasitol. Res.* 110:2445-2453.

413. Zhang,D.M., Y.Wang, M.K.Tang, Y.W.Chan, H.M.Lam, W.C.Ye, and K.P.Fung. 2007. Saxifragifolin B from Androsace umbellata induced apoptosis on human hepatoma cells. *Biochem. Biophys. Res. Commun.* 362:759-765.

414. Zhong,H.M., C.X.Chen, X.Tian, Y.X.Chui, and Y.Z.Chen. 2001. Triterpenoid saponins from Clematis tangutica. *Planta Med* 67:484-488.

415. Zhou,X.M., Y.L.Cao, and D.Q.Dou. 2006. Protective effect of ginsenoside-Re against cerebral ischemia/reperfusion damage in rats. *Biol. Pharm. Bull.* 29:2502-2505.

416. Zhuang,M., D.I.Oltean, I.Gomez, A.K.Pullikuth, M.Soberon, A.Bravo, and S.S.Gill. 2002. Heliothis virescens and Manduca sexta lipid rafts are involved in Cry1A toxin binding to the midgut epithelium and subsequent pore formation. *J. Biol. Chem.* 277:13863-13872.

417. Zimmerberg,J. and M.M.Kozlov. 2006. How proteins produce cellular membrane curvature. *Nat. Rev. Mol. Cell Biol.* 7:9-19.

418. Zuco,V., R.Supino, S.C.Righetti, L.Cleris, E.Marchesi, C.Gambacorti-Passerini, and F.Formelli. 2002. Selective cytotoxicity of betulinic acid on tumor cell lines, but not on normal cells. *Cancer Lett.* 175:17-25.